N° d'ordre : 2013-56 Année 2013

THÉSE

Présentée devant

L'ÉCOLE CENTRALE DE LYON

Pour obtenir le grade de **DOCTEUR**

Par

Fida MAJDOUB

(Ingénieur)

Spécialité : Mécanique
Ecole doctorale : Mécanique, Energétique, Génie civil, Acoustique (MEGA)

Innovative Measurement of Ultra-low Friction,

Analysis of dynamic free responses characterized by damped oscillatory motion

Soutenue le 11 Décembre 2013 devant le Jury composé de :

A. Akay	Professeur (Carnegie Mellon University, Pittsburgh, USA) (Bilkent University, Ankara, Turkey)	Rapporteur
A. Neville	Professeur (University of Leeds, England)	Rapporteur
A. Chateauminois	Professeur (École Supérieure de Physique et Chimie, France)	Examinateur
J.M. Martin	Professeur (École Centrale de Lyon)	Directeur de thèse
J. Perret-Liaudet	Maître de conférences, HDR (École Centrale de Lyon)	Directeur de thèse
M. Belin	Ingénieur de recherche (École Centrale de Lyon)	Invité
F. Jarnias	Ingénieur docteur (TOTAL, Solaize, France)	Invité

In the loving memory of my dad, Faisal

To my precious mom, Mona and my exceptional brother, Fadi

Acknowledgements

Many people have attributed in producing this thesis. Therefore, I have the pleasure to get this opportunity to thank each and every one of them.

First, I would like to thank the French Ministry of the National Education and Scientific Research for their financial support during the 3-years period of my Ph.D. at the laboratory of Tribology and Dynamical Systems (LTDS) of Ecole Centrale de Lyon (ECL). Also, I would like to thank the Carnot Institute I@L, France for partially financing this research.

Next and foremost, I would like to express my sincere gratitude to my supervisor Joël Perret-Liaudet, my co-supervisor Jean-Michel Martin and Michel Belin. Joël has been a vital source of ideas and inspiration. Also, it is a rare privilege to work with someone like Jean-Michel Martin in which I have benefited immensely from his vast experience in tribology. Michel has played as well an essential role in this research; he has been constantly helping me in the experimental work. Moreover, I would like to thank them for carefully reading and correcting my thesis manuscript.

I would like to extend my gratitude to Dr. M. Kano and his group from Kanagawa Industrial Technology Center in Japan for providing us with DLC-coated samples. I would like to thank as well TOTAL Research Centre of Solaize, France for the collaboration performed during this research.

Also, I would like to acknowledge Professors Adnan Akay and Anne Neville for giving me the honor to be the reporters of my thesis manuscript. I wish also to thank Professor Antoine Chateauminois for accepting to be the examiner of my Ph.D. defense. Moreover, I thank Dr. Frédéric Jarnias from TOTAL for his interest in this research work.

Most of all I am very grateful to all the people in the laboratory for making it such a fantastic place. In particular, I would like to thank my office colleagues Cecile, Flavien and Laura for their good spirit which has been a very important part of the good working atmosphere. Moreover, I would like to thank Maria-Isabel, Alain, Denis, Clotide, Elise, Fabrice, Emanuel, Juliette, Julien,…for the valuable discussions during the thesis. Also, I would like to thank other colleagues, Chaïma, Jao, Maha, Mohamadou, Mehdy, Christine, Paule, Catia, Modestino, Paula, Sophie, Sam, Sophia, Medard, Viet, Eloi, Olga, Cyrielle, Osseini, Imène, Simon, Thibault, Fabien, Gilles, Irene, Juliette, Simon, Salma, Thomas… for the moments shared during my stay at LTDS.

I would like to express my deepest gratitude to my mom Mona for all her ultimate sacrifices throughout these years. I would also wish to thank my brother Fadi for his unlimited support and my sister, Faten for her encouragements. I would never been able to accomplish my path without their infinite support. Also, I would like to thank my lovely nephew, Faisal and adorable nieces, Mona and Leen, for their incredible joy that nourishes my life with cheerful moments.

Last but not least, I would like to thank my fiancé Osman for fully supporting me during my Ph.D. thesis. He has been always there beside me through the great and hard time.

Fida Majdoub

Table of Contents

Résumé Etendu

Introduction 1

State of Art

A Novel Experimental Technique

Decaying law for the free oscillating response

Hysteresis Effect on the Friction Force

Conclusion

Scientific Production

Résumé Etendu

0 Résume Etendu

Introduction

Le frottement est défini par la force résistante au mouvement relatif des deux surfaces en contact. Sans le frottement, nous ne serions pas en mesure d'accomplir de nombreuses tâches essentielles dans nos activités quotidiennes comme tenir debout et marcher, se raser, s'habiller, se brosser les dents, arrêter une voiture, faire du feu en frottant deux bouts de bois, masser avec les mains, etc. Une vie sans frottement est certainement difficile à imaginer. Néanmoins, une vie à frottement contrôlé et maîtrisé est sans aucun doute un des buts ultimes de la technologie moderne.

Une partie importante de la recherche vise à contrôler et optimiser l'efficacité énergétique dans de nombreuses communautés scientifiques et industrielles. Ceci est essentiel non seulement pour préserver nos ressources énergétiques limitées, mais aussi pour éviter à notre planète des émissions dangereuses et éviter les dépenses économiques ultimes en défaveur des générations futures. La perte d'énergie est principalement due à des produits technologiques qui opèrent sur des sources d'énergie non renouvelables telles que le transport et les dispositifs robotiques. Ces produits génèrent de l'énergie mécanique sous forme du mouvement. Malheureusement, dès que le mouvement apparaît, le frottement intervient. En fait, les pertes d'énergie dues au frottement entre les composants mécaniques représentent la plus grande part du total des pertes énergétiques.

Récemment, le défi de la recherche a visé d'une part à réduire et maîtriser le frottement, mais aussi à observer l'existence de la friction quasi nulle (*near-zero friction*) entre deux surfaces solides en glissement relatif. Ce phénomène est défini par supra-glissement, c'est-à-dire un mouvement dans lequel le frottement est pratiquement nul ou de l'ordre de 10^{-4} à 10^{-3} et même plus bas.

Dans les cas où le frottement est impossible à ignorer, une loi de frottement optimale est nécessaire afin de concevoir le système. Bien que la théorie de frottement soit facile à comprendre, il est difficile d'avoir un modèle du frottement simulé. Plusieurs modèles de frottement sont définis par différentes fonctions non-linéaires comme les discontinuités, l'hystérésis et d'autres effets. Donc il faut bien choisir un modèle de frottement afin de respecter les propriétés du système.

Le travail présenté dans cette thèse porte sur une technique innovante capable de mesurer le frottement faible en glissant un pion sphérique sur un plan. Dans cette technique, le système est soumis à une excitation vibratoire qui produit un mouvement oscillatoire. Le frottement est alors évalué grâce à des réponses libres en déplacement et vitesse. Les propriétés tribologiques du contact sont très importantes pour ces mesures. En outre, le modèle de frottement est essentiel afin d'évaluer le coefficient frottement. En plus, le frottement dépend du tribosystème étudié. Plusieurs simulations numériques ont été réalisées afin de modéliser le système par une loi de frottement cohérente et ensuite comparer les réponses simulées avec les résultats expérimentaux.

Le manuscrit commence par une revue de l'état de l'art (chapitre 1). L'état de l'art présente brièvement l'histoire du frottement. Ensuite, nous étudions les différentes lois de frottement trouvées dans la littérature dans les deux états stable et variable. Enfin, le chapitre 1 se termine avec un aperçu général sur le frottement à l'échelle nanométrique, c'est à dire supra-glissement. Cette vaste étude nous permet d'interpréter les résultats numériques et expérimentaux présentés dans les chapitres suivants.

Dans le chapitre 2, la technique expérimentale est décrite. Ensuite, les résultats expérimentaux sont présentés dans deux parties différentes. Dans la première partie, différents contacts lubrifiés avec de l'acide oléique ou de glycérol sont testés. Cette partie vise à étudier l'effet de revêtements de type DLC (*Diamond-like carbon*) sur les surfaces acier / acier. Puis, nous montrons dans la deuxième partie les résultats expérimentaux de contacts acier / acier lubrifiés. Trois lubrifiants différents avec / sans additifs sont utilisés. Nous étudions l'effet de la température dans la deuxième partie expérimentale.

Dans le troisième chapitre, nous simulons un système dynamique décrit par une loi de frottement polynomiale. La loi de la décroissance de réponses oscillantes libres est analysée en utilisant différentes méthodes numériques. Enfin, nous présentons et discutons les résultats numériques qui permettent de spécifier le modèle de frottement et comparer les résultats numériques avec ceux des expériences.

Le chapitre 4 se concentre sur quelques tests expérimentaux afin étudier la force de frottement tangentielle mesurée. Ensuite, un système oscillant d'un degré de liberté unique induite par un modèle de frottement LuGre est analysé numériquement.

Enfin, la conclusion générale et les perspectives de cette thèse récapitulent les idées principales évoquées dans le manuscrit, les principaux résultats numériques et expérimentaux présentés tout au long dans les différents chapitres, et propose finalement des suggestions pour les travaux futurs.

0.1 Etat de l'art

0.1.1 Introduction

Il n'y a aucun doute ; l'homme a pensé au frottement et aux moyens qui aident à le réduire depuis longtemps, bien avant les révolutions industrielle et scientifique [1] et [2]. En effet, les premiers systèmes mécaniques ont été fabriqués de bois et pierre. Certains ont été lubrifiés par graisse animale. Ces systèmes ont été trouvés avant la période de 4000 avant J.C. Toutefois, avec la révolution industrielle est venue le développement des machines lourdement chargées et comportant des liaisons mécaniques plus que jamais complexes. Elle a ainsi introduit un besoin essentiel pour l'analyse sérieuse du frottement, de l'usure et de la lubrification. La maîtrise des pertes dues au frottement contribue non seulement à la durée de vie des éléments mais aussi à la fiabilité et la productivité des filières industrielles complètes.

Les premières études sur le frottement sont effectuées au XVème siècle par Leonardo da Vinci (1452-1519). Il s'est rendu compte de la vitalité de l'étude de frottement dans les systèmes mécaniques. Da Vinci a simplement déclaré deux lois de frottement. La première loi dit que la force de frottement est directement proportionnelle à la charge appliquée. Dans la deuxième loi, il a déclaré que la loi de frottement est indépendante sur la zone de contact appliqué. La figure 1 montre ses dessins de l'expérience réalisée sur des surfaces sèches utilisés afin de montrer que la force de frottement est indépendante de la surface de contact. En outre, il a observé que plusieurs matériaux se déplacent avec facilité et a conclu que le coefficient de frottement des matériaux lisses est plus faible. Il a également étudié d'autres sujets liés au frottement tels que l'usure et ses mécanismes, systèmes lubrifiés, engrenages, vérins à vis et roulements. Parmi ses investigations, Leonardo Da Vinci a étudié la relation entre le frottement et la musique. Il savait que la musique est produite par du frottement des sphères célestes. Son travail montre un progrès incroyable dans la technologie existante pendant sa période. Les observations de Da Vinci sont venues deux cents ans avant celles de Guillaume Amontons.

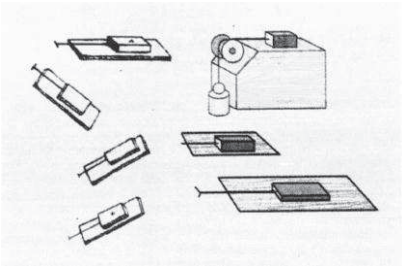

Figure 1. Un schéma des expériences de Leonardo Da Vinci.

Guillaume Amontons était parmi les pionniers qui ont émis les principes du frottement. Il a redécouvert les deux lois fondamentales trouvées précédemment par Leonardo Da Vinci [3].

Il s'est également rendu compte que le frottement vient de la rugosité de la surface. Il croyait que le frottement est utilisé pour soulever une surface par la rugosité, la déformation ou l'usure de l'autre surface. En s'appuyant sur des mesures de contacts secs sur différents matériaux, Amontons a réussi à étudier la production de chaleur et l'adhérence solide ainsi qu'à analyser l'effet de la rugosité de surface sur le frottement. Dans la Figure 2, Amontons trouve le principe d'évaluer le coefficient de frottement dans la plupart des tribomètres à l'aide de ressorts et de déplacements mesurés selon l'équation $F_{frottement} = \mu N$.

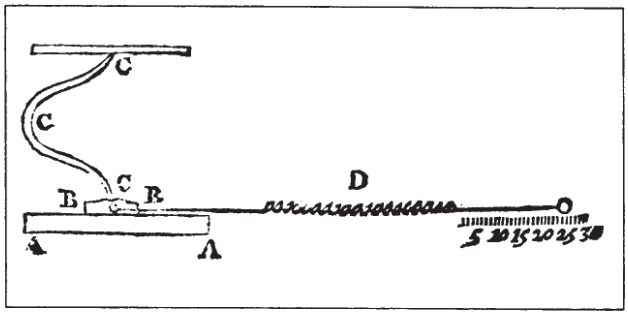

Figure 2. Le principe d'évaluer le frottement dans la plupart des tribomètres.

Néanmoins, la solution théorique du problème a été introduite par Euler en 1750 : il a défini le concept de frottement. Ces concepts de frottement existent toujours de nos jours dans de nombreuses applications d'ingénierie. La configuration la plus facile à comprendre est le frottement statique, qui consiste en un corps placé sur un plan incliné. Cette dernière étude a été réalisée par Leonardo da Vinci (1452-1519) (Figure 1) et Leonardo Euler (1707-1783). Euler a également distingué la différence entre frottement statique et dynamique et a représenté la rugosité de la surface comme un modèle pyramidal. Toutefois, le premier qui a réellement fait une distinction entre le frottement statique et dynamique a été John Andreas Von Segner (1704-1777).

Pendant la révolution industrielle, Coulomb a fait différentes expériences afin d'identifier les paramètres qui affectent le frottement pendant les conditions de glissement et roulement. Ces paramètres sont les propriétés des matériaux, le lubrifiant, le contact, la pression appliquée et aussi le temps de relaxation de contact avant l'expérience. Ses expériences ont confirmé les lois d'Amontons et ont également montré que le coefficient de frottement ne varie pas avec la vitesse de glissement. Cela lui a été attribué plus tardivement comme une troisième loi de frottement. Toutefois, cette loi n'est pas applicable pour les grandes surfaces. En effet, les lois Amontons-Coulomb de frottement sont applicables pour plusieurs combinaisons de matériaux et de géométries.

En 1954, Bowdon et Tabor ont expliqué physiquement les lois précédentes du frottement. Ils ont prouvé que la vraie zone de contact est faible par rapport à la zone de contact apparente. Ils ont également montré qu'avec l'augmentation de charge normale, les aspérités sont plus développées dans le contact. Celles-ci augmentent la surface de contact.

Les premiers travaux sur le frottement lubrifié ont été réalisés par Hirn en 1847 [4]. Il a étudié expérimentalement l'évolution du coefficient de frottement sous charge constante et vitesse

variable, dans les deux cas des contacts secs et lubrifiés. Pour le cas lubrifié, il a pu constater que le coefficient de frottement augmente proportionnellement à la vitesse ; un résultat rejeté par la communauté scientifique de l'époque en raison de son apparent conflit avec la troisième loi de frottement (pour un coefficient de frottement constant). Ces résultats ont cependant montré qu'une nouvelle analyse était nécessaire pour étudier les contacts entièrement lubrifiés.

Le comportement de frottement a été largement étudié pendant le XXème siècle. Dernièrement, l'intérêt pour le frottement dynamique a augmenté. Ainsi, il est très important d'avoir un modèle de frottement spécifique pour chaque système mécanique. Dans la section ci-dessous, nous allons présenter certains des modèles de frottement précédemment énumérés.

0.1.2 Modèles de frottement

Cette section présente un aperçu de certains modèles de frottement trouvés dans la littérature. Le modèle de frottement est divisé en deux catégories : la loi de frottement d'état stable et celle d'état variable.

Il est connu que le frottement est représenté par le coefficient de frottement noté μ. La force de frottement, F , présentée par :

$$F = \mu N \qquad (1)$$

N est la force normale exercée sur la masse, m, représentée dans la Figure 3. x et $\dot{x}$ sont respectivement le déplacement et la vitesse du système.

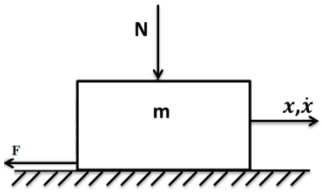

Figure 3. Système de masse, m décrite par une charge normale, N et une force de frottement F.

Les lois de frottement de l'état stable se composent de différents éléments afin de comprendre le comportement de frottement. Le frottement d'état stable, décrit comme une loi simple, peut caractériser les systèmes dynamiques ayant des réponses oscillantes libres. Le coefficient de frottement de ces modèles dépend uniquement de la vitesse instantanée relative et peut être désigné en tant que:

$$\mu = \mu(\dot{x}) \qquad (2)$$

Pendant le XVIIIème siècle, Coulomb a retravaillé sur le frottement découvert par Da Vinci, puis par Amontons pendant la période du XVIIème siècle. Le frottement de Coulomb dépend du mouvement du système. Cette loi dit que le frottement s'oppose au mouvement et que la force de frottement est indépendante de la vitesse et de la zone de contact. Le coefficient de frottement de Coulomb est représenté comme suit:

$$\mu(\dot{x}) = \mu_c sign(\dot{x}) \quad (3)$$

μ_c est la constante de frottement de Coulomb. Cette loi est utilisée pour modéliser de nombreux systèmes mécaniques [5].

En 1886, Reynolds a développé la théorie de l'hydrodynamique, dans lequel il a trouvé une équation pour la force de frottement lié à la viscosité du lubrifiant [6]. Cette loi correspond à un modèle de frottement visqueux [7]. Le coefficient de frottement visqueux est décrit comme suit:

$$\mu(\dot{x}) = \mu_v \dot{x} \quad (4)$$

μ_v est la constante de frottement visqueux.

Stribeck a établi sa fameuse courbe qui distingue trois différents régimes de lubrification [8]. Ce classement dépend de la façon dont le frottement varie en fonction de la viscosité η, la vitesse des surfaces U, et la charge normale P (voir Figure 4). Le premier régime est le régime de lubrification limite. L'épaisseur du film étant très petite, ce régime est caractérisé par un frottement très élevé, proche du frottement sec. La charge est supportée par les aspérités des surfaces qui sont en contact direct. Le deuxième régime est la lubrification mixte. La charge est supportée en partie par le contact des aspérités, ainsi que par le film lubrifiant. Dans ce régime, le coefficient de frottement est inférieur à celui du régime limite. A des grandes vitesses et faibles charges, le lubrifiant forme un film qui sépare complètement les deux surfaces en contact. Dans ce troisième régime, le coefficient de frottement est très faible. Dans les cas où la pression de contact est faible comme dans les contacts conformes, on distingue la lubrification hydrodynamique (HD) où le frottement augment de façon linéaire avec la vitesse des surfaces.

Pour des fortes pressions de contacts comme dans les contacts non conformes (par exemple roulement à billes), la lubrification est dite élasto-hydrodynamique (EHD) parce que les surfaces subit des déformations élastiques. De plus, la viscosité du lubrifiant dépend de la pression et de l'augmentation de température non négligeable dans le contact. Ce qui a précédé représente le point de vue classique de la lubrification. Cependant, ce point de vue peut être contesté dans les nouvelles applications qui incluent des contacts de taille nanométrique. Si on devait positionner ces applications sur la courbe de Stribeck, on se

trouverait à la frontière entre le régime de la lubrification élasto-hydrodynamique et celui de la lubrification mixte. Cette étude concerne la lubrification nanométrique où l'épaisseur du film lubrifiant est de quelques nanomètres seulement. Des effets moléculaires, principalement dus aux interactions lubrifiant/surfaces, sont susceptibles de se produire à cette échelle.

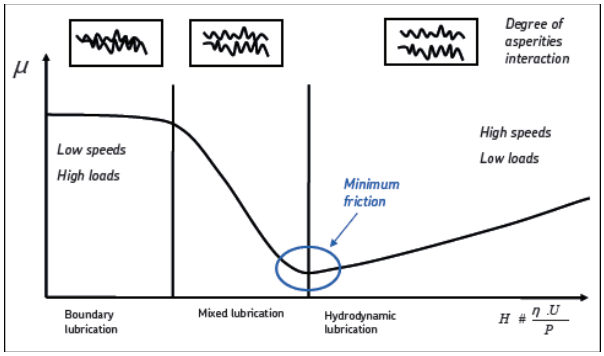

Figure 4. La courbe de Stribeck montrant les trois régimes classiques de la lubrification.

En 1990, Soom et Hess [8] ont effectué des expériences. Ils ont trouvé une relation entre le coefficient et la vitesse de contact pendant les régimes de lubrification complète et mixte. Puis, ils ont obtenu un modèle satisfaisant pour leurs résultats expérimentaux. Ce modèle combine à la fois la loi de Stribeck classique et la loi de Stribeck modifiée. Cette loi est représentée par l'équation suivante :

$$\mu = \frac{\mu_b}{1+c_1(\frac{\eta V}{\sqrt{WE}})^2} + c_2\frac{\eta V L}{W} \text{ for } V > 0 \qquad (5)$$

Récemment, la loi de frottement d'état variable est devenue de plus en plus intéressante afin de modéliser différents systèmes. Dans cette loi, le coefficient de frottement est défini en fonction de nombreux paramètres et mécanismes. Dans la suite de l'étude, on présentera quelques modèles de frottement d'état variable.

En 1968, Dahl a introduit un modèle de frottement [10]. Son but était de simuler un modèle de frottement adapté afin de contrôler les systèmes.

$$\frac{dF}{dx} = \sigma(1 - \frac{F}{F_c} sgn(\dot{x}))^{\alpha} \qquad (6)$$

x est le déplacement, F est la force de frottement et F_c est la force de frottement de Coulomb. σ est défini comme le coefficient de raideur et α comme le paramètre qui détermine la forme de la courbe contrainte-déformation. Le modèle Dahl permet d'obtenir une hystérésis [11].

Afin de mieux modéliser un système avec des surfaces irrégulières, Canudas de Wit et ses collègues ont développé un nouveau modèle de frottement, nommé le modèle de LuGre [12]. Cette loi de frottement est basée sur une variable interne, connu par la déviation des fibres. Ce modèle permet de décrire correctement la relation entre la vitesse de glissement relatif et la

force de frottement [13]. De plus, la force de frottement présente une hystérésis avec la vitesse de glissement.

En 1993, Haroy et Friedland [14] ont proposé un modèle de frottement basé sur l'hydrodynamique d'un palier lisse lubrifié. La force de frottement est simplifiée par l'équation suivante :

$$F = K_1(\varepsilon - \varepsilon_{tr})^2\Delta + \frac{K_2}{\sqrt{1-\varepsilon^2}}\dot{x} \qquad (7)$$

Dans la littérature, il existe rarement une loi de frottement qui peut modéliser un système avec le phénomène *"contact stress"*. Ainsi, Tan et son groupe ont trouvé un modèle de frottement dynamique [15]. Cette loi de frottement combine à la fois la viscosité et la distribution des contraintes. Ce modèle est défini par le coefficient de friction suivant :

$$\mu = \frac{\eta}{P}\frac{d\dot{x}}{dz} \qquad (8)$$

η est la viscosité du lubrifiant, P est la pression normale, $\dot{x}$ est la vitesse parallèle à l'effort de friction et z est la coordonnée ayant une direction perpendiculaire à la vitesse.

0.1.3 Frottement à l'échelle nanométrique

L'un des challenges de la tribologie est d'avoir un coefficient de frottement très faible. Certains chercheurs ont observé l'existence de frottement "quasi-nul" entre deux surfaces en glissement. C'est ce qu'on appelle le phénomène de Supra-glissement [16]. Le Supra-glissement est un régime du mouvement dans lequel le frottement est négligeable [17]. De nombreux savants ont étudié récemment des surfaces revêtues de couches de carbone amorphe (DLC). Les couches DLC sont souvent utilisées afin d'éviter l'usure grâce à leurs propriétés tribologiques excellentes. Elles sont très résistantes à l'usure abrasive et adhésive.

En 2003, Kano et al. [18] ont observé grâce à leurs expériences que les surfaces revêtues avec DLC lubrifiée par l'huile ester ont des valeurs très faibles de frottement. Deux ans plus tard, Kano et al. [19] ont examiné le frottement ultra-faible avec des surfaces revêtues avec un DLC lubrifié par glycérol mono-oléate (GMO). Ils ont effectué des expériences avec 3 contacts différents : acier/acier, a-C: H/acier et ta-C /acier. Puis, ils ont trouvé que le coefficient de frottement de ta-C/acier lubrifié avec d'huile de poly-alpha-oléfine (PAO) et GMO est plus faible que 0,02. Ces résultats sont présentés dans la Figure 5.

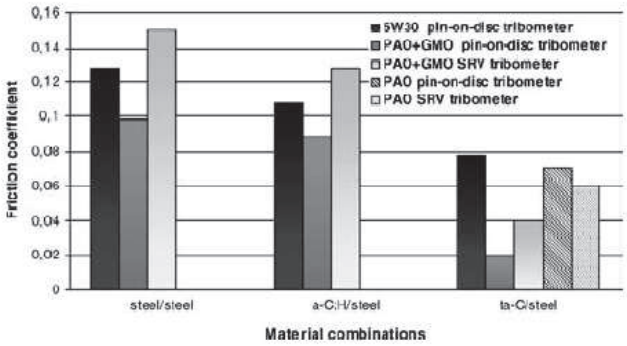

Figure 5. Comparaison entre 3 différents contacts: acier/acier, a-C:H/acier et ta-C/acier en utilisant différents tribomètres [20].

Au début de 2006, Kano et son groupe [21] ont fait une expérience en faisant glisser trois cylindres sur un disque rotatif en acier. Le disque rotatif a été revêtu par le carbone amorphe. Deux types de DLC ont été préparés pour le test: a-C: H par CVD et ta-C par PVD. Ils ont trouvé que le coefficient de frottement passe de 0,8 à 0,1

Jolly-Pottuz et al [20] ont utilisé le tribomètre du type “Cameron-Plint“ afin d’étudier les coefficients de frottement de l'acier/acier, ta-C/ta-C et a-C:H/a-C:H. Ces contacts sont lubrifiés par du glycérol pur. Les résultats montrent que le contact ta-C/ta-C présente un coefficient de frottement très faible d'environ 0.025, comparé à celui de a-C: H /a-C :H (0,10) et les contacts acier/acier (0,15) (voir Figure 6).

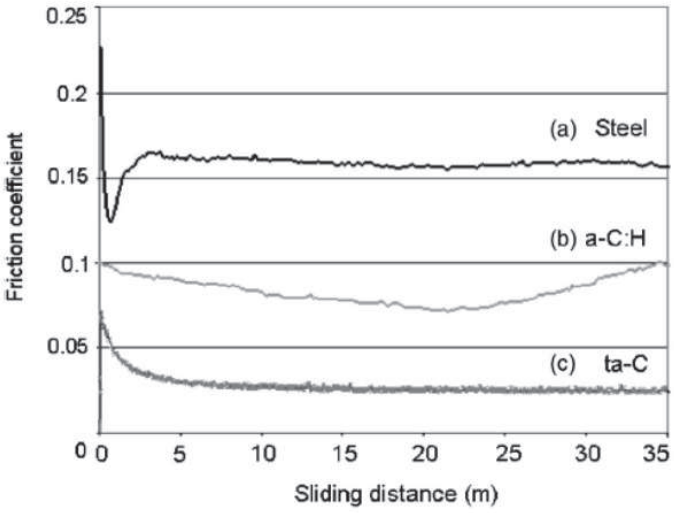

Figure 6. Le coefficient de frottement de différents contacts : (a) acier/acier, (b) a-C :H/a-C :H et (c)ta-C/ta-C lubrifiées pas le glycérol pur.

0.1.4 Conclusion

La connaissance de tous les modèles de frottement nous a apporté une compréhension importante du comportement de frottement en fonction de nombreux paramètres. Dans la partie suivante, nous allons présenter une nouvelle technique de mesure. Puis, quelques tribosystèmes seront testés en utilisant cette technique. Ensuite, certains modèles de frottement seront simulés avec le système mécanique. Le principal objectif de la thèse est de mettre en œuvre un nouveau modèle de frottement, approprié pour le système mécanique utilisé dans la nouvelle technique expérimentale.

0.2 Une nouvelle technique expérimentale

0.2.1 Introduction

Le frottement représente, de nos jours, un important challenge pour les communautés scientifiques et industrielles. Effectivement, le contrôle du frottement – et sa réduction, sont devenus un sujet majeur dans le contexte de la maîtrise de la consommation d'énergie. En effet, les tribomètres classiques mesurent directement le coefficient de frottement.

Récemment, Liang et Feeny [22, 23 et 24] ont présenté une méthode exacte qui permet l'estimation les coefficients de frottement Coulomb et visqueux. Ces paramètres sont identifiés grâce à la réponse vibratoire de déplacement ou de vitesse.

Afin d'appliquer la méthode présentée ci-dessus, une nouvelle technique de mesure de frottement a été développée [25]. Ce nouveau dispositif est décrit par ses performances afin de mesurer des coefficients de frottement faibles.

0.2.2 Description de la nouvelle technique

En 2010, un nouvel appareil appelé "tribomètre dynamique oscillant" ou aussi connu comme "tribomètre relaxant" [25 et 26] a été développé afin de mesurer le frottement cinématique entre deux surfaces. Le système mécanique est décrit par un système masse-ressort-amortisseur oscillant. Ce tribomètre permet l'évaluation de frottement sans mesurer la force tangentielle à l'interface. Dans la suite de cette section, nous allons tester plusieurs tribosystèmes et évaluer deux contributions du frottement : une première qui dépend de la vitesse, μ_1 et un autre qui ne dépend pas de la vitesse, μ_0. La Figure 7 montre le dispositif de ce tribomètre.

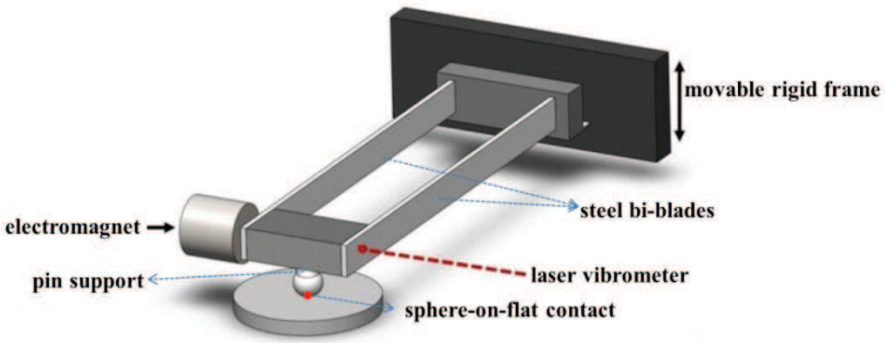

Figure 7. Le dispositif du nouveau tribomètre.

Ce tribomètre représente une configuration sphère-sur-plan (voir Figure 8). Le pion hémisphérique est relié à un support en aluminium monté sur un bilame en acier connecté à un plan rigide. Le bilame permet les oscillations du pion sphérique suivant la direction horizontale, dans un plan parallèle à l'échantillon à tester. Un électro-aimant est utilisé pour générer le déplacement initial du pion hémisphérique. Quand cet électro-aimant est désactivé, le pion oscille librement. La charge est appliquée à partir des déplacements micrométriques

du support. La mesure des réponses en déplacement et vitesse s'effectue à l'aide de la vélocimétrie laser, donc sans aucun contact.

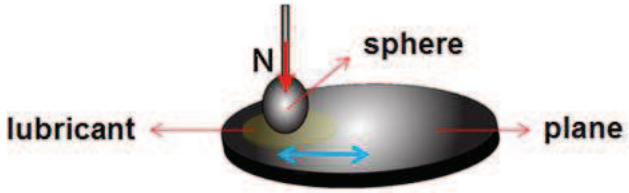

Figure 8. La configuration sphère-sur-plan du nouveau tribomètre.

De plus, nous pouvons mesurer la résistance électrique du contact grâce à ce tribomètre. Une tension continue, avec une limite de 2 mV, est appliquée sur le contact. Ainsi, le courant à travers l'interface est mesuré. Le courant est limité à 5 mA. La mesure de la résistance électrique varie de 1 Ω à 10^8 Ω. Par conséquent, les résultats de la résistance électrique sont présentés à l'échelle logarithmique.

0.2.3 Résultats expérimentaux

Nous avons effectué des expériences sur différents contacts acier-sur-acier avec ou sans revêtements DLC. Les combinaisons de contact sphère/plan sont comme la suivante : acier/acier, acier/acier revêtu par ta-C, acier/acier revêtu par a-C :H et acier revêtu par ta-C/acier revêtu par ta-C. Ces contacts ont été lubrifiés dans un premier temps avec du glycérol puis avec de l'acide oléique. Nous avons appliqué une charge normale de 0 à 0.60 N. Ces essais expérimentaux ont été réalisés à température ambiante.

Les contacts avec l'acide oléique montrent que la forme de l'enveloppe de réponse libre est linéaire. Nous pouvons expliquer cela par le fait que l'acide oléique est défini par un lubrifiant à viscosité faible. Ainsi, pour ces contacts, nous avons pu évaluer le frottement qui ne dépend pas de la vitesse, μ_0. Cependant, μ_1 est négligeable pour ces essais avec l'acide oléique. Les contacts avec une ou deux de ces surfaces revêtues donnent du frottement plus faible que celle en acier. Ces résultats sont en accord avec les résultats obtenus avec un tribomètre traditionnel. La combinaison ta-C/ta-C lubrifiée avec de l'acide oléique donne la valeur de μ_0 la plus basse (0,027) avec une erreur de ± 0,001(voir Figure 9).

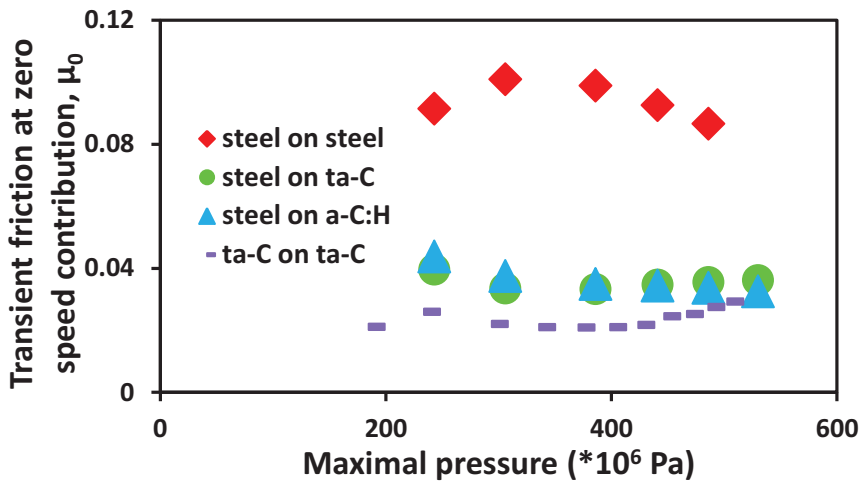

Figure 9. Frottement transitoire, μ_0, en fonction de la pression maximale correspondant aux contacts lubrifiés par l'acide oléique.

Pour les contacts lubrifiés par le très visqueux glycérol, les deux contributions de frottement, μ_0 et μ_1 sont évalués. Ceci indique que le régime de lubrification est décrit par l'élasto-hydrodynamique. Même avec ces essais, nous avons montré que le système ta-C/ta-C décrit sa meilleure performance dans la réduction de frottement à une vitesse nulle (voir Figure 10). Néanmoins, le système ta-C/ta-C donne le frottement visqueux, μ_1, le plus élevé (voir Figure 11).

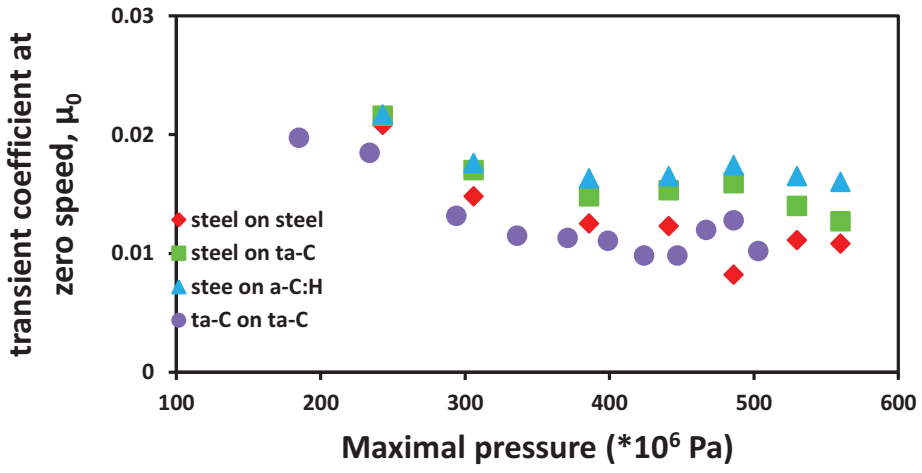

Figure 10. Frottement transitoire, μ_0, en fonction de la pression maximale correspondant aux contacts lubrifiés par le glycérol.

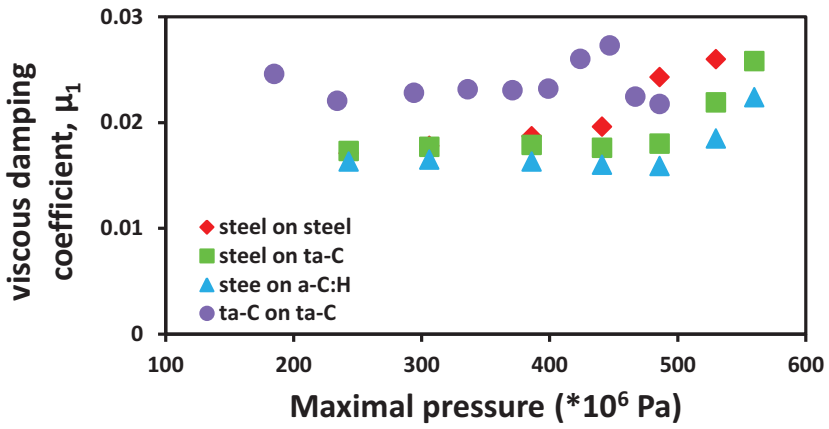

Figure 11. Frottement visqueux, μ_1, en fonction de la pression maximale correspondant aux contacts lubrifiés par le glycérol.

Afin d'étudier l'effet de la température sur les contacts acier/acier lubrifiés avec ou sans additifs sur le frottement, une série de six essais est effectuée sur le contact acier/acier. Différents lubrifiants avec ou sans additifs sont utilisés. Trois lubrifiants purs, le glycérol pur, l'huile de base 150 NS et le poly-alpha-oléfine PAO4, sont testés à différentes températures et charges normales appliquées. Puis, le lubrifiant PAO4 est testé avec trois différents additifs, l'acide oléique, l'acide linoléique et l'acide stéarique. La masse totale de chaque additif est 1% de la masse totale de la solution, PAO4+additif. Ces trois solutions, PAO4 avec des additifs, sont également testées à différentes températures et charges normales.

Quand la charge normale est appliquée sur le contact acier/acier lubrifié avec du glycérol pur, un amortissement visqueux dans le régime EHL est à l'origine de la plupart des pertes d'énergie jusqu'à une température d'environ 40°C, même si le frottement transitoire à vitesse nulle n'est pas négligeable. A des températures plus élevées, nous avons remarqué que le système fonctionne en régime limite (mis en évidence par la mesure de l'ECR). Le coefficient de frottement diminue avec la charge appliquée. Le coefficient du frottement transitoire, μ_0, diminue avec l'augmentation de la température jusqu'à une charge normale donnée où μ_0 diminue très légèrement (voir Tableau 1). Le glycérol apparaît comme un lubrifiant très efficace pour réduire la friction.

μ_0±0.001

T (°C)	at 0.05 N	at 0.10 N	at 0.20 N	at 0.30 N	at 0.40 N	at 0.50 N	at 0.60 N
22	0.035	0.024	0.016	0.015	0.015	0.016	0.016
37	0.049	0.034	0.024	0.022	0.020	0.019	0.018
75	0.061	0.046	0.037	0.036	0.032	0.029	0.025

Tableau 1. Le coefficient du frottement transitoire, μ_0, à différentes températures et charges normales correspondant au contact acier/acier lubrifié avec le glycérol pur.

Les deux lubrifiants, 150NS et PAO4, n'ont aucun effet sur le frottement visqueux de l'appareil. Les contacts acier/acier lubrifiés avec PAO4 ou 150NS sont dans les régimes mixtes et limites. Le fait que μ_0 diminue en fonction de la charge normale est expliqué par la théorie de contact hertzienne. Nous avons observé que le frottement est beaucoup plus élevé avec l'huile minérale qu'avec le glycérol, même si la viscosité n'est pas très différente à haute température.

Lorsque des additifs sont ajoutés dans le lubrifiant PAO4, le comportement d'amortissement du système est toujours réduit dans tous les conditions et donc la perte d'énergie est également réduite. La mesure de la résistance des contacts lubrifiés avec PA04+l'acide stéarique indique que le système est dans le régime mixte. Par contre, après l'ajoute des acides gras insaturés dans le lubrifiant PAO4, le système passe du régime mixte au régime limite. À basse pression ($243 * 10^6$ Pa), les acides gras insaturés donnent de meilleurs résultats que l'acide stéarique à 56, 65 et 79 ° C. Néanmoins, à plus basse température (42 ° C), l'acide stéarique est meilleur que l'acide oléique. En plus, nous avons observé que l'acide linoléique donne de meilleurs résultats à 42 ° C, alors que l'acide oléique est meilleur à 79 ° C. À des pressions supérieures à 300 MPa, tous les mélanges d'additifs ont un comportement très similaire.

0.2.4 Conclusion

Dans cette partie de la thèse, nous avons montré que le comportement de l'enveloppe de la réponse libre est important afin de déterminer les contributions de frottement. Nous avons également eu quelques informations sur l'épaisseur du film. De plus, nous avons déterminé le régime de lubrifiant en mesurant la résistance électrique de contact.

Le modèle de frottement utilisé dans cette étude était cohérent avec certains des tribosystèmes étudiés. Néanmoins, ce modèle ne peut pas être utile pour d'autres tribosystèmes. Ainsi, nous allons avoir dans la suite de l'étude une meilleure compréhension concernant les oscillations libres.

0.3 Loi de la décroissance de la réponse oscillant libre

0.3.1 Introduction

Le frottement est un aspect important pour les systèmes mécaniques. Toutefois, la modélisation de frottement reste un défi dans le domaine mécanique. Ko est ses collègues [27] ont proposé une loi de frottement polynomial en fonction de la vitesse de glissement afin de comprendre certains comportements dynamiques. En plus, il est très important d'analyser l'évolution des amplitudes d'un signal vibratoire. Feldman et Braun [28] ont montré que la forme d'évolutions de l'amplitude d'une réponse en déplacement est hyperbolique en utilisant la transformée de Hilbert.

En outre, des vibrations au niveau d'une interface de contact a été d'un grand intérêt dans la littérature en raison de son risque contre la fatigue et l'usure. Plusieurs études ont été effectuées sur la perte d'énergie du contact en utilisant des méthodes numériques et expérimentales afin de mieux comprendre le problème de vibration d'un contact.

Dans cette partie de l'étude, nous allons présenter un système masse-ressort d'un degré de liberté avec un modèle de frottement pseudo-polynomiale. Puis, on va étudier l'effet du modèle de frottement pseudo-polynomial sur le comportement des réponses oscillatoires. L'évolution de l'amplitude, nommée l'enveloppe, est déterminée en utilisant la transformée de Hilbert afin d'étudier et de mieux comprendre le comportement dynamique de ce système.

0.3.2 Description du modèle dynamique

Le système mécanique est décrit par un système masse-ressort d'un DDL ayant une masse, m, et un ressort de raideur, k (voir Figure 12).

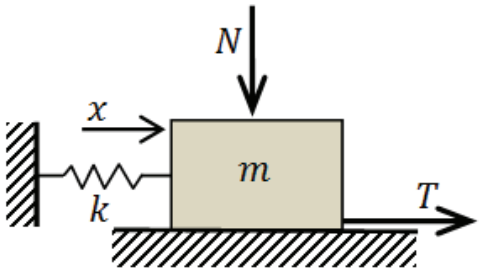

Figure 12. Le système masse-ressort à un DDL.

L'équation du mouvement de ce système peut être écrite comme suit :

$$m\frac{d^2x}{dt^2} + kx = -T(v) = -\mu_k(v)N \qquad (9)$$

où x est le déplacement de la masse, $v = \frac{dx}{dt}$ est la vitesse de glissement, $\frac{d^2x}{dt^2}$ est l'accélération et $\mu_k(v)$ est le coefficient du frottement cinématique. $\mu_k(v)$ est décrit par un modèle de pseudo-fiction polynôme. Sa forme générale est représentée comme suit :

$$\mu_k(v) = \sum_{j=0}^{n}[(p_{2j}v^{2j})sgn(v) + (p_{2j+1}v^{2j+1})] \qquad (10)$$

Considérant les paramètres suivants: $\Omega^2 = \frac{k}{m}, \tau = \Omega t, y = \frac{k}{N}x$ et $\mu_j = (\frac{N\Omega}{k})^j p_j$, l'équation du mouvement adimensionnée peut être présenté comme :

$$\ddot{y} + y = -f(\dot{y}) \qquad (11)$$

où

$$f(\dot{y}) = \sum_{n=0}^{+\infty} \mu_{2n}\dot{y}^{2n}\mathrm{sgn}(\dot{y}) + \sum_{n=0}^{+\infty} \mu_{2n+1}\dot{y}^{2n+1} \qquad (12)$$

0.3.3 Résultats

La solution de l'équation du mouvement non-linéaire peut être trouvée par la méthode de Runge-Kutta d'ordre 4 (RK4) [29]. Nous pouvons aussi présenter l'enveloppe de la réponse libre en utilisant des méthodes différentes. La définition de Mark et Crandall [30] peut représenter l'enveloppe comme suit:

$$A_{M\&C}(\tau) = \sqrt{y^2 + \dot{y}^2} \qquad (13)$$

Nous pouvons également utiliser la transformée de Hilbert afin de représenter l'enveloppe des réponses en déplacement et en vitesse respectivement comme dans les équations (14) et (15).

$$\boldsymbol{A_{H_y}(\tau) = \sqrt{y^2 + \hat{y}^2}} \qquad (14)$$

$$\boldsymbol{A_{H_{\dot{y}}}(\tau) = \sqrt{\dot{y}^2 + \hat{\dot{y}}^2}} \qquad (15)$$

où $\hat{y}$ et $\hat{\dot{y}}$ sont respectivement la transformée de Hilbert du déplacement et de la vitesse.

La Figure 13 présente l'enveloppe de la réponse correspondant à un système masse-ressort avec une loi de frottement quadratique en utilisant les deux méthodes numériques présentées ci-dessus.

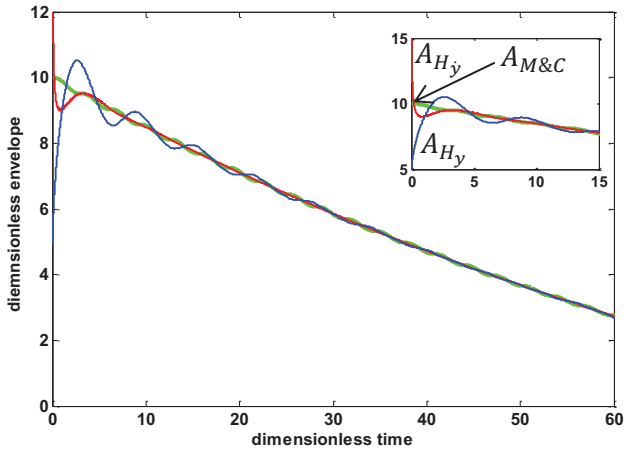

Figure 13. Les enveloppes $A_{M\&C}$, A_{H_y} and $A_{H_{\dot{y}}}$ en fonction de temps ayant le coefficient de frottement suivant $f(\dot{y}) = \mu_0 \mathrm{sgn}(\dot{y}) + \mu_1 \dot{y}$. $\mu_0 = 0.1$, $\mu_1 = 0.019$ et la conditions initiales : $Y_0 = 10$ et $\dot{y}_0 = 0$.

Nous pouvons observer de la figure ci-dessus quelques divergences au début de la réponse libre qui peuvent être liées au phénomène de Gibbs. Ce comportement est plus clair dans le cas d'un déplacement comparé au cas de la vitesse. Nous sommes également capables de présenter l'enveloppe analytiquement grâce à la méthode de la moyenne [31]. La dérivée de premier ordre de l'enveloppe, $\dot{A} = \frac{dA}{d\tau}$ nous permet d'étudier le comportement de la réponse dynamique. Cette dernière peut être dérivée comme :

$$F(A) = \frac{dA}{d\tau} = \dot{A} = \sum_{k=0}^{+\infty} a_n A^n \qquad (16)$$

avec

$$a_n = -\frac{\mu_n}{\pi} \int_0^{\pi} \sin^{n+1} \phi \, d\phi \qquad (17)$$

où

$$a_{2k} = -\frac{\mu_{2k}}{\pi} \frac{2^{2k+1} k!^2}{(2k+1)!} \qquad (18)$$

$$a_{2k+1} = -\frac{\mu_{2k+1}}{2^{2k+1}} \frac{(2k+2)!}{(k+1)!^2} \qquad (19)$$

avec $k \in \mathbb{N}$.

Nous pouvons déterminer la forme de l'enveloppe de la réponse libre en déterminant le signe de $F'(A)$ où $F'(A) = \frac{dF}{dA}$ (voir Tableau 2).

$F'(A)$	La forme de l'enveloppe
< 0	Convexe
$= 0$	Droite
> 0	concave

Tableau 2. La forme de l'enveloppe en fonction du signe de $F'(A)$.

Dans la suite, nous allons étudier numériquement les différents cas de la loi de frottement polynomiale. Le Tableau 3 résume les différents cas de la loi de frottement polynomiale. Voici quelques définitions des paramètres utilisés dans le tableau suivant :

$$\Delta^2 = {a_1}^2 - 4a_0a_2 \qquad (20)$$

et

$$A^* = -\frac{a_1}{2a_2} \qquad (21)$$

Loi de frottement	cas	Forme de l'enveloppe
Constant $f(\dot{y}) = \mu_0 \mathrm{sgn}(\dot{y})$	$\mu_0 > 0$	Droite $\forall A$
Visqueux $f(\dot{y}) = \mu_1 \dot{y}$	$\mu_1 > 0$	Convexe $\forall A$
Coulomb-visqueux $f(\dot{y}) = \mu_0 \mathrm{sgn}(\dot{y}) + \mu_1 \dot{y}$	$\mu_0 > 0$ et $\mu_1 > 0$	Convexe $\forall A$
	$\mu_0 > 0$ et $\mu_1 < 0$	Concave $\forall A$
Quadratique $f(\dot{y}) = (\mu_0 + \mu_2 \dot{y}^2)\mathrm{sgn}(\dot{y}) + \mu_1 \dot{y}$	$\Delta^2 < 0$: $\mu_0 > 0$, $\mu_1 > 0$ et $\mu_2 > 0$	Convexe $\forall A$
	$\Delta^2 < 0$: $\mu_0 > 0$, $\mu_1 < 0$ et $\mu_2 > 0$	Concave $\forall A \in [0, A^*]$ Convexe $\forall A \in]A^*, A_0]$
	$\Delta^2 = 0$: $\mu_0 > 0$, $\mu_1 < 0$ et $\mu_2 > 0$	Concave $\forall A$
	$\Delta^2 > 0$: $\mu_0 > 0$, $\mu_1 < 0$ et $\mu_2 < 0$	Concave $\forall A$
	$\Delta^2 > 0$: $\mu_0 > 0$, $\mu_1 > 0$ et $\mu_2 < 0$	Convexe $\forall A \in [0, A^*]$ Concave $\forall A \in]A^*, A_0]$
	$\Delta^2 > 0$: $\mu_0 > 0$, $\mu_1 < 0$ et $\mu_2 > 0$	Concave $\forall A$

Tableau 3. Résumé des différents cas de la loi de frottement polynomiale.

Enfin, nous allons présenter quelques essais expérimentaux. On a déterminé les différentes constantes de frottement grâce aux résultats expérimentaux de la réponse libre en déplacement et en vitesse. Puis, nous avons simulé le système en utilisant les coefficients calculés afin de préciser la loi de frottement du système. La figure ci-dessus (Figure 14) présente la réponse libre en déplacement simulée (en rouge) et expérimentale (en bleu) du contact acier/acier

lubrifié par l'acide oléique à 25 ° C avec une charge normale de 0,10 N. La loi de frottement constant est un modèle convenable pour ce système avec $\mu_0 = 0.1036$. La forme de l'enveloppe est droite pour toutes les valeurs de y.

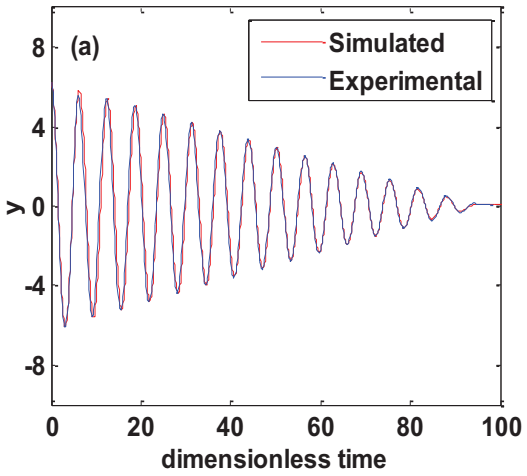

Figure 14. La réponse libre en déplacement simulée (rouge) et expérimentale (bleu) du contact acier/acier lubrifié par l'acide oléique à 25°C avec une charge normale de 0,10N.

La Figure 15 montre la réponse libre en déplacement simulée (en rouge) et expérimentale (en bleu) du contact acier/acier lubrifiée par le glycérol à 22 ° C avec une charge normale de 0,05 N. La loi de frottement Coulomb-visqueux est un modèle convenable pour ce système avec $\mu_0 = 0.034$ et $\mu_1 = 0.0304$. La forme de l'enveloppe est convexe pour toutes les valeurs de y.

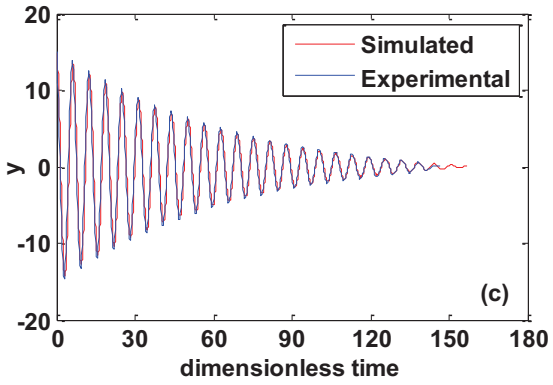

Figure 15. La réponse libre en déplacement simulée (rouge) et expérimentale (bleu) du contact acier/acier lubrifié par le glycérol à 22°C avec une charge normale de 0,05N.

La Figure 16 présente la réponse libre en déplacement simulée (en rouge) et expérimentale (en bleu) du contact acier/acier lubrifiée par l'huile de base 150NS à 42 ° C avec une charge normale de 0,10 N. La loi de frottement Coulomb-visqueux est un modèle convenable pour ce système avec $\mu_0 = 0.1694$ et $\mu_1 = -0.0076$. La forme de l'enveloppe est concave pour toutes les valeurs de y.

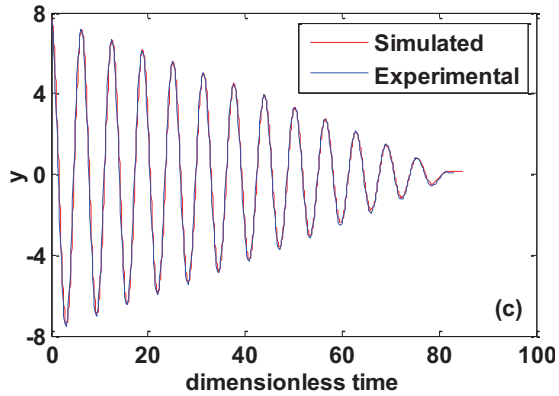

Figure 16. La réponse libre en déplacement simulée (rouge) et expérimentale (bleu) du contact acier/acier lubrifié par l'huile de base 150NS à 42°C avec une charge normale de 0,10N.

Dans la figure suivante (Figure 17), nous observons la réponse libre en déplacement simulée (en rouge) et expérimentale (en bleu) du contact acier/acier lubrifié par le glycérol à 61° C avec une charge normale de 0,05 N. La loi de frottement quadratique est le modèle convenable pour ce système avec $\mu_0 = 0.1107$, $\mu_1 = -0.0185$ et $\mu_2 = 0.0014$ La forme de l'enveloppe est concave pour tous $y \in [0,7.8]$ et convexe pour tous $y \in]7.8, 15.4]$.

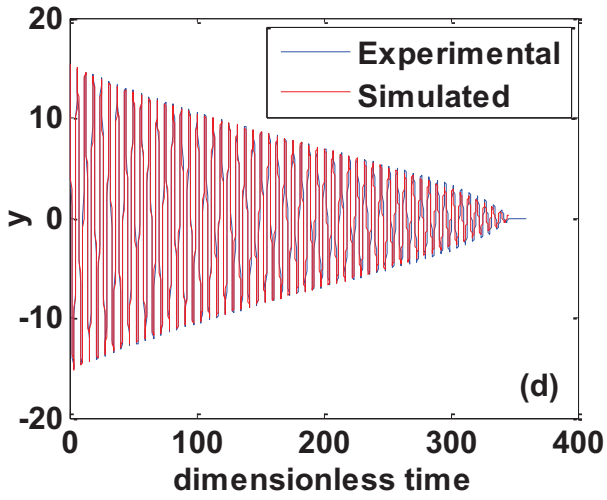

Figure 17. La réponse libre en déplacement simulée (rouge) et expérimentale (bleu) du contact acier/acier lubrifié par le glycérol à 61°C avec une charge normale de 0,05N.

0.3.4 Conclusion

Dans cette partie de la thèse, un système masse-ressort a été analysé avec une loi de frottement pseudo-polynomiale. Cette étude nous permet de comprendre le comportement des réponses libres et de déterminer la loi de frottement appropriée d'un système. En plus, nous avons montré que les résultats simulés et expérimentaux sont cohérents.

0.4 L'effet d'hystérésis de la force de frottement

0.4.1 Introduction

Le frottement est un phénomène naturel dans de nombreux systèmes mécaniques. Dans les cas où l'effet du frottement ne peut être ignoré, un modèle de frottement convenable est nécessaire afin d'analyser un système. Même si le concept de friction est facile à comprendre, il est difficile à modéliser et simuler. De nombreux modèles de frottement dépendent d'une variété de fonctions non linéaires telles que les discontinuités, l'hystérésis, la dynamique interne et d'autres contraintes. Dans ce contexte, nous sommes désireux de simuler un modèle qui nous permettrait de comprendre le comportement du frottement et de son effet sur le système mécanique.

Dans cette dernière partie de mes travaux, nous allons étudier le comportement de la force tangentielle expérimentale. Puis, nous allons présenter quelques résultats pour un système masse-ressort simulé avec la loi de frottement LuGre.

0.4.2 La mesure de la force tangentielle

Le tribomètre dynamique oscillant présenté dans la section 0.2 et dans [25, 26] nous permet de mesurer également la force tangentielle de frottement grâce à un capteur de force piézo-électrique. Quand une charge normale, N est appliquée sur le contact pion/plan, le pion sphérique oscille, où le plan est fixé. Cela permet au système de vibrer. Puis, le bilame vibre horizontalement. Ce dernier provoque un effort horizontal sur le transducteur piézo-électrique. Ainsi, la force tangentielle de frottement est mesurée. Les charges électriques sont recueillies par un amplificateur (Kistler 5015A), puis elles sont filtrées en utilisant un filtre passe-bas avec une fréquence de bande passante de 300 Hz. Enfin, les signaux analogiques sont converties numériquement en utilisant une résolution convertisseur analogique/ numérique (DAQ NI USB 6221) de 16 bits. La Figure 18 présente un schéma du dispositif expérimental utilisé pour mesurer de la force de frottement.

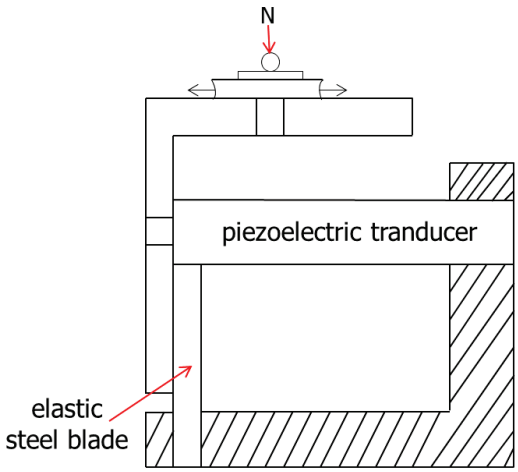

Figure 18. Un schéma de la mesure expérimentale de la force de frottement.

0.4.3 Résultats expérimentaux de la force tangentielle

Nous allons présenter la force tangentielle mesurée de différentes tribosystèmes. La Figure 19 présent la réponse de la vitesse et de la force tangentielle correspondant au contact acier/acier lubrifié par le glycérol pur à température ambiante avec une charge normale de 0.05 N.

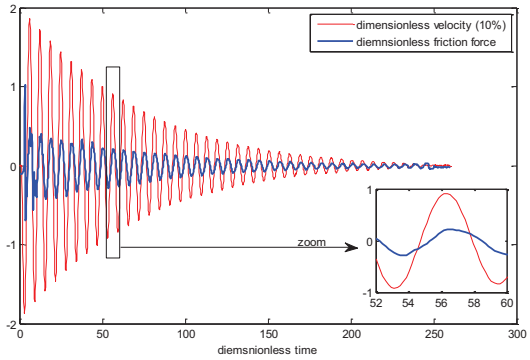

Figure 19. La réponse de la vitesse (en rouge) et de la force tangentielle (en bleu) du contact acier/acier lubrifié par glycérol pur à température ambiante avec une charge normale de 0,05 N.

Nous avons observé que l'enveloppe de la force tangentielle diminue avec le temps. Donc, on peut conclure que l'enveloppe correspondant à la force de frottement est décrite par une forme convexe. Nous avons aussi remarqué que la vitesse et la force de frottement ne passent pas par zéro exactement au même temps. Cela est dû au petit décalage dans le temps entre les deux réponses (environ 0,003 sec). De plus, lorsque le système s'arrête ($v = 0$), la force de frottement n'atteint pas directement zéro. Cela peut être expliqué par le fait que, à la fin de l'essai expérimental, le film lubrifiant peut provoquer du frottement, même si le système ne glisse plus. Ce dernier montre l'effet du frottement solide quand le système est au repos.

Pour le même tribosystème, nous traçons la force tangentielle en fonction de la vitesse (voir Figure 20).

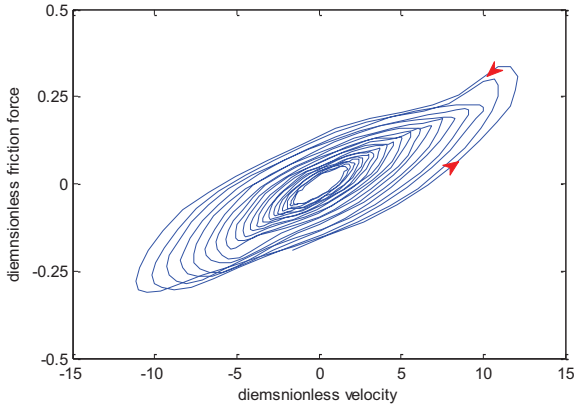

Figure 20. La force tangentielle en fonction de la vitesse correspondant au contact acier/acier lubrifié par le glycérol pur à température ambiante avec une charge normale de 0,05 N.

Le comportement de la force tangentielle en fonction de la vitesse est décrit par l'effet d'hystérésis. Nous avons aussi remarqué que la force du frottement augmente avec la vitesse relative. Cette dernière confirme ce qui a été observé par Hess et Soom en 1990 [9]. En plus, nous avons vu que le cycle d'hystérésis se rétrécit comme la vitesse relative diminue.

La Figure 21 présente les réponses de la vitesse et la force tangentielle du contact acier/acier lubrifié par l'huile de base 150NS à une température ambiante avec une charge normale de 0,10 N.

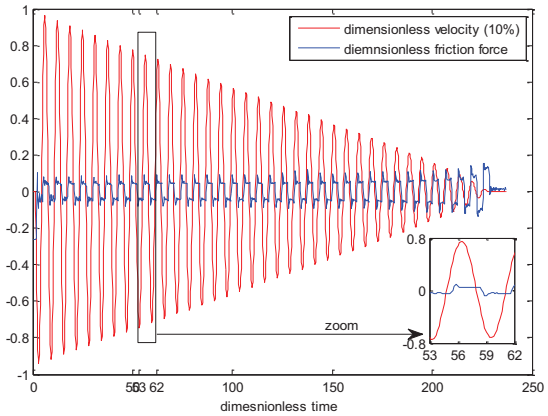

Figure 21. Le réponse de la vitesse (en rouge) et de la force tangentielle (en bleu) du contact acier/acier lubrifié par l'huile de base 150 NS à une température ambiante avec une charge normale de 0.10N.

La Figure 21 montre que la force tangentielle augmente avec le temps. Cette dernière correspond au cas où l'enveloppe de vitesse est décrite par une forme concave. Nous avons aussi remarqué que la vitesse et la force de frottement ne passent pas par zéro exactement au même temps ; cela étant dû au petit décalage dans le temps entre les deux réponses (environ 0,003 sec). Nous avons également observé que lorsque le système s'arrête ($v = 0$), la force de frottement atteint directement zéro. Cela peut être expliqué par la disparition du lubrifiant à la fin de l'essai expérimental. Nous avons observé aussi un peu de bruit dans la mesure de la force tangentielle. Cela peut être dû à des imperfections dans le système mécanique.

La Figure 22 présente la force tangentielle de frottement en fonction de la vitesse correspondant à ce tribosystème.

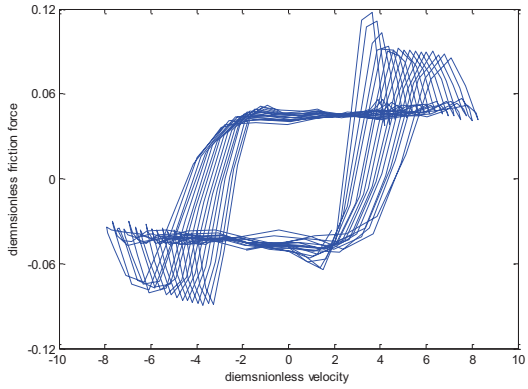

Figure 22. La force de frottement en fonction de la vitesse du contact acier/acier lubrifié par l'huile de base à une température ambiante avec une charge normale de 0,10N.

La Figure 22 montre que la force de frottement en fonction de la vitesse est décrite par un effet d'hystérésis. Nous avons conclu que, contrairement à l'exemple précédent, il n'y a pas de relation proportionnelle entre la force tangentielle et la vitesse.

0.4.4 La loi de frottement LuGre

Le système mécanique est décrit par un système masse-ressort d'un DDL ayant une masse, m, et un ressort de raideur, k (voir Figure 22).

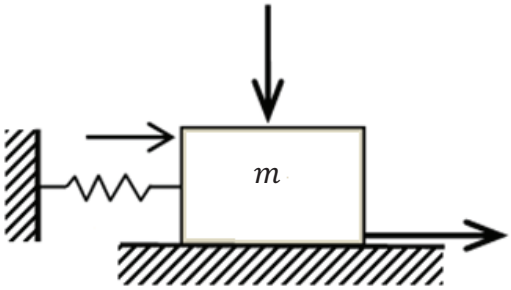

Figure 23. Le système masse-ressort oscillant d'un DDL.

L'équation du mouvement de ce système peut être écrite comme suit :

$$m\frac{d^2x}{dt^2} + kx = -F_T \qquad (22)$$

où

$$F_T = \sigma_0 z + \sigma_1 \frac{dz}{dt} + \sigma_2 v \qquad (22)$$

et

$$\frac{dz}{dt} = v - \frac{|v|}{g(v)} z \qquad (23)$$

La fonction $g(v)$ est toujours positive et dépende des propriétés du matériau, de la température et du lubrifiant. $g(v)$ peut-être écrit comme suit :

$$g(v) = F_c + (F_s + F_c)e^{-(v/v_s)^a} \qquad (24)$$

où F_c décrit le frottement Coulomb, F_s est définie par la force de frottement statique et v_s est la vitesse de Stribeck.

En considérant ces paramètres :

$$\tau = \Omega t,\ \Omega = \sqrt{\frac{k}{m}}, y_1 = \frac{k}{F_c}x, y_2 = \frac{\dot{x}}{v_s}, y_3 = \frac{\sigma_0}{F_c}z, \alpha = \frac{kv_s}{\Omega F_c}, \gamma = \frac{F_s - F_c}{F_c},\ \epsilon = \frac{k}{\sigma_0}, s_1 = \frac{\sigma_1 v_s}{F_c} \text{ et } s_2 = \frac{\sigma_2 v_s}{F_c} \qquad (25)$$

L'équation du mouvement globale adimensionnée peut être écrite sous la forme suivante :

$$y_2' = -\frac{1}{\alpha}\left[y_1 + y_3 + s_1\left(y_2 - \frac{|y_2|}{g(y_2)}y_3\right) + s_2 y_2\right] \qquad (26)$$

où

$$g(y_2) = 1 + \gamma e^{-|y_2|^a} \qquad (27)$$

et

$$y_3' = \frac{dy_3}{d\tau} = \frac{\alpha}{\epsilon}\left(y_2 - \frac{|y_2|}{g(y_2)}y_3\right) \qquad (28)$$

Nous avons simulé le système masse-ressort avec la loi de frottement LuGre en utilisant La fonction“odeset”sur MATLab. Le Tableau 4 présent les valeurs des paramètres utilisés.

Le système simulé est décrit par une masses m de $0.20\ kg$ et un ressort ayant une raideur de$225.591\ N.m^{-1}$. Les conditions initiales sont : $y_1(0) = 225.591$, $y_2(0) = 0$ et $y_3(0) = 0$.

Paramètres	Valeurs
σ_0	$1\ N.m^{-1}$
σ_1	$0.1\ N.sec.m^{-1}$
σ_2	$0.0004\ N.sec.m^{-1}$
F_c	$1\ N$
F_s	$1.5\ N$
v_s	$0.1\ m.sec^{-1}$
a	1

Tableau 4. Les paramètres du modèle de frottement LuGre.

La Figure 24 présente la réponse de la force tangentielle simulée.

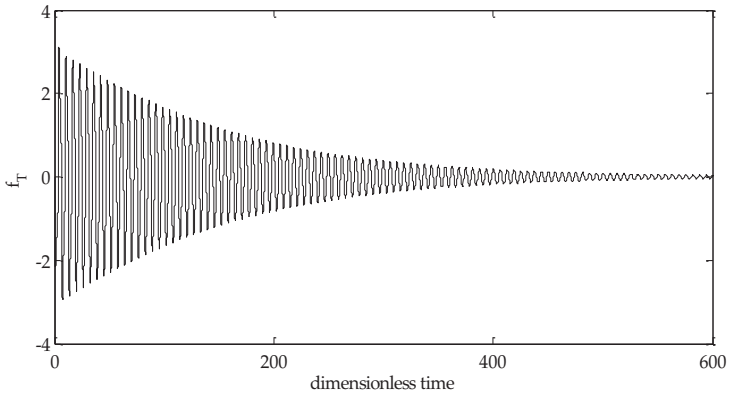

Figure 24. La réponse de la force tangentielle adimensionnée d'un système masse-ressort simulé avec une loi de frottement LuGre.

Nous avons observé dans la Figure 24 que la réponse de la force tangentielle est décrite par des oscillations libres avec une enveloppe convexe comme celui du déplacement et de la vitesse. Cette dernière observation est cohérente avec les résultats expérimentaux obtenus.

La Figure 25 montre l'effet hystérésis de la force tangentielle en fonction de la vitesse.

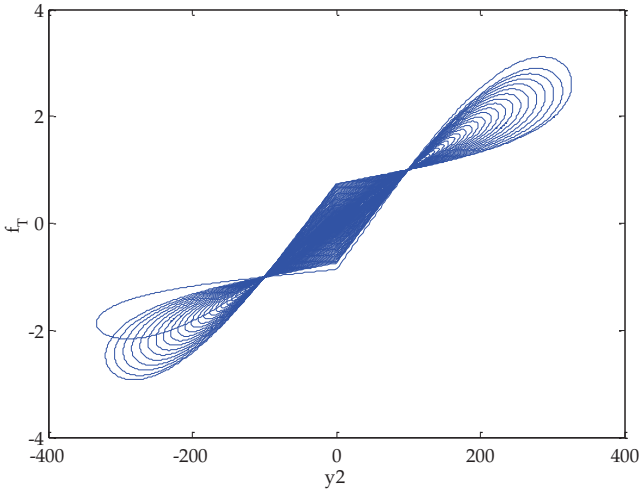

Figure 25. La force tangentielle en fonction de la vitesse dans la forme adimensionnée d'un système masse-ressort simulé avec une loi de frottement LuGre.

Nous avons trouvé que la force de frottement diminue avec la vitesse.

Le cycle d'hystérésis devient plus large quand la vitesse augmente. Cela ne peut pas être expliqué par les lois de frottement classiques, dans lesquelles le frottement est défini de façon unique pour chaque vitesse non-nulle.

Finalement, nous avons simulé le même système avec la loi de frottement polynomiale (Constant, visqueux, Coulomb-visqueux et quadratique) et nous avons observé que les réponses simulées avec la loi LuGre ne sont pas cohérentes avec celles simulées avec la loi polynomiale.

0.4.5 Conclusion

Dans cette dernière partie de la thèse, nous avons étudié l'effet d'hystérésis de la force tangentielle mesurée. Puis, nous avons simulé un système masse-ressort avec une loi de frottement LuGre qui montre l'effet d'hystérésis. Finalement, nous avons vu que la loi de frottement LuGre ne peut pas remplacer la loi de frottement polynomiale.

Conclusion générale et perspectives

Dans cette thèse, une nouvelle technique expérimentale a été utilisée. L'appareil mis à disposition nous a permis de mesurer le déplacement, la vitesse, la force tangentielle de frottement et la résistance de contact. Ensuite, le coefficient de frottement a été calculé à partir des réponses de déplacement et vitesse. Le dispositif expérimental est décrit par un système masse-ressort-amortisseur d'un degré de liberté. Les mesures ont été effectuées au contact d'un pion sphérique oscillant sur un plan fixe.

Nous avons testé différents contacts tribologiques. Pour ce groupe d'essais, nous avons utilisé la loi de frottement Coulomb-visqueux. Ainsi, les contributions de frottement transitoire à vitesse nulle μ_0 et visqueux μ_1 ont été évaluées de la réponse libre de déplacement et vitesse. De plus, la résistance électrique de contact nous a permis de déterminer le régime de lubrification de chaque tribosystème testé.

Tout d'abord, les différents contacts en acier/acier lubrifiés avec de l'acide oléique et du glycérol pur (lubrifiants "verts") ont été testés en utilisant cette technique expérimentale. Certaines surfaces ont été revêtus par des couches de carbone (ta-C ou a-C: H). Ces séries d'essais nous ont permis de comparer les deux lubrifiants différents (glycérol pur et acide oléique) et de bien comprendre également l'effet des revêtements des couches de carbone sur la surface en acier. Puis, nous avons effectué un test de contact acier/acier lubrifié avec trois lubrifiants différents (glycérol pur, huile de base 150NS et poly-alpha-oléfine PAO4). De plus, trois additifs différents (acide oléique, acide linoléique et acide stéarique) ont été mélangés avec le lubrifiant PAO4. Ces essais ont été réalisés à différentes températures. Ainsi le but de ces expériences est d'étudier d'une part l'effet de la température sur le contact acier/acier lubrifiés, d'autre part l'effet des différents additifs + PAO4 mais aussi de comparer les trois lubrifiants purs. Nous avons également observé les différentes formes de l'enveloppe de la réponse en déplacement et vitesse.

Afin de bien comprendre la décroissance des oscillations libres, nous avons appliqué une loi de frottement générale, définie par un modèle de frottement polynomial. Ainsi, un système masse-ressort d'un degré de liberté a été étudié et numériquement décrite par la loi de frottement pseudo-polynomiale. Nous avons utilisé la méthode numérique Runge-Kutta d'ordre 4 (RK4) afin des simuler les réponses libres oscillants. Ensuite, nous avons déterminé la forme de l'enveloppe correspondant aux réponses libres simulées grâce à la dérivation de deuxième ordre de l'équation analytique de l'amplitude. Nous avons montré quatre formes d'enveloppe numériquement différentes : droit, convexe, concave et une combinaison convexe-concave. Nous avons également calculé les constantes de frottement correspondant à la loi de frottement constante, visqueux, Coulomb-visqueux et quadratique. Puis, nous avons montré qu'une réponse libre expérimentale, décrite par une forme d'enveloppe droite, convexe ou concave, peut être modélisée par un modèle de frottement Coulomb-visqueux. Par contre, un système avec une réponse libre, ayant la forme de l'enveloppe convexe et concave, ne peut être modélisé par une loi de frottement non linéaire (i.e. la loi de frottement polynomial).

Ensuite, nous avons présenté la force tangentielle de frottement mesurée. La force de frottement en fonction de la vitesse est décrite par un effet d'hystérésis. De plus, nous avons montré différentes évolutions d'amplitude de la force tangentielle. Ainsi, quand la force tangentielle diminue avec le temps, l'enveloppe de la force est décrite par une forme convexe. Néanmoins, lorsque la force tangentielle de frottement augmente avec le temps, l'enveloppe de la force est décrite par une forme concave.

Finalement, nous avons simulé un système masse-ressort avec une loi de frottement LuGre qui montre l'effet d'hystérésis. Nous avons conclu que la loi de frottement LuGre ne peut pas remplacer la loi de frottement polynomiale.

Ces travaux doivent maintenant s'orienter sur la loi de frottement LuGre ou d'autres lois décrivant un phénomène d'hystérésis, puis appliquer ces types de frottement sur notre système expérimental. Cela pourrait être complémentaire à l'étude numérique et expérimentale effectuée dans cette thèse. En plus, nous pouvons aussi simuler une loi de frottement qui dépend non seulement de la vitesse, mais aussi de l'épaisseur du film de lubrifiant car nous avons observé que le régime de lubrification change d'un tribosystème à l'autre.

Les conditions, telles que la température, la vitesse de glissement, la pression et la configuration géométrique, présentées dans les résultats expérimentaux, sont limitées. Cependant, nous pourrions avoir des conditions optimales en améliorant le dispositif expérimental utilisé. Il serait également intéressant de réaliser un modèle numérique basé sur la dynamique moléculaire (MD) afin d'étudier les propriétés à l'interface pendant le mouvement oscillatoire.

Références

[1] Frene, J., Nicolas, D. and Godet, M., Lubrication Hydrodynamique: Paliers et Brutées, EYROLLES, 1990.

[2] Georges, J-M, Frottement, Usure et Lubrication : Introduction à la Tribologie et à ses applications, EYROLLES, 1999.

[3] Dowson, D., *History of Tribology,* Longman, London, 1979.

[4] Woydt, M. and Wasche, R., The History of the Stribeck curve and ball bearing steels: The role of Adolf Martens, Wear 268 (11-12), pp. 1542-1546, 2010.

[5] Andreaus, U. and Casini, P., Dynamics of friction oscillators excited by a moving base and/or driving force. Journal of Sound and Vibration 254 (4), pp. 685-699, 2001.

[6] Reynolds, O., On the theory of lubrication and its application to Mr. Beauchamp Tower's experiments of the viscosity of olive oil. Phil. Trans. Royal Soc.177, pp. 157-234, 1886.

[7] Ferri, A. A. and Anderson, J. R., Behavior of a single-degree-of freedom system with a generalized friction law. Journal of Sound and Vibration 140 (2), pp. 287-304, 1990.

[8] Reynolds, O. The Theory of Lubrication and its application to Mr. Beauchamp Tower's Experiments, including an Experimental Determination of the Viscosity of Olive Oil. Phil Trans Roy Soc Lon 177, 157-234 (1886).

[9] Hess, D. P. and Soom, A., Friction at a lubricated line contact operating at oscillating sliding velocities. Journal of Tribology 112 (1), pp.147- 152, 1990.

[10] Dahl, P., A solid friction model. Technical Report TOR-0158 (3107618)-1, The Aerospace Corporation, El Segundo, CA, 1968.

[11] de Vincente, J., Stokes, J.R. and Spikes, H.A., Soft lubrication of model hydrocolloids. Tribology International, 22, pp. 483-491, 2006.

[12] Canudas de Wit,C., Olsson, H., Member, K.J. and Lichinsky, P., A new model for control of systems with friction. Automatic Control 40 (3), pp. 419-425, 1995.

[13] Hoffman, N.P., Linear stability of steady sliding in point contacts with velocity dependent and LuGre type friction. Journal of Sound and Vibration 301 (3-5), pp. 1023-1034, 2007.

[14] Harnoy, A. and Friedland, B., Dynamic friction model of lubricated surfaces for precise motion control. In Preprint No. 93-TC-1D-2. Society of Tribologists and Lubrication Engineers.

[15] Tan X., Yan, X-T., Juster, N.P., Raghunathan, S. and Wang,J., Dynamic friction model and its application in flat rolling. Journal of Materials Processing Technology 207 (1-3), pp. 222-234, 2008.

[16] Martin, J-M. , Donnet, C. and Le Mogne, T., Superlubricity of molybdenum disulphide. Physical Review B 48(10), 1993.

[17] Erdemir, A. and Martin, J-M., *Superlubricity,*Elsevier, 2007.

[18] Kano M., Yashuda, Y, Mabucha, Y., Ye, J. and Konishi, S., Ultra-low friction of DLC lubricated with ester-containing oil-Part 1: pin-on-disc and SRV friction tests. Processes in Tribology 43, pp. 689-692, 2003.

[19] Kano M., Yashuda, Y., Okamoto, Y., Mabuchi, Y., Hamada, T., Ueno, T., Ye, J. Konishi, S., Takeshima, S., Martin, J. M., De Barros Bouchet, M. I. and Le Mogne, T., Ultralow friction of DLC in presence of glycerol mono-eleate. Tribology Letters 18 (2), pp. 245-251, 2005.

[20] Jolly-Potuz , Matta, C., De Barros Bouchet, M.I., Martin, J.M. and Sagawa, T., Superlow friction of ta-C lubricated by glycerol: An electron energy loss spectroscopy study. Journal of Applied Physics 102 (6), 2007.

[21] Kano M., Super low friction of DLC applied to engine cam follower lubricated with ester-containing oil. Tribology International 39 (12), pp. 1682-1685, 2006.

[22] Liang, J.W., A decrement for the simultaneous estimation of Coulomb and viscous friction. Journal of Sound and Vibration, 1996.

[23] Liang, J.W. and Feeny, B.F., Identifying Coulomb and viscous friction from free-vibration decrements. Nonlinear Dynamics 16 (4), pp. 337-347, 1998.

[24] Liang, J.W., Identifying Coulomb and viscous friction from free-vibration acceleration decrements. Journal of Sound and Vibration 282 (3-5), pp. 1208-1220, 2005.

[25] Rigaud, E., Perret-Liaudet, J., Belin, M., Joly-Pottuz, L. and Martin, J.M., An original dynamic tribotest to discriminate friction and viscous damping. Tribology International 431 (2), pp. 320-329, 2010.

[26] Belin, M., Kakizawa, M., Rigaud, E. and Martin, J.M., Dual characterization of boundary friction thanks to the harmonic tribometer: Identification of viscous and solid friction contributions. Journal of Physics: Conference Series, 258: 012008, 2010.

[27] Ko, P.L., Taponat, M.-C. and Pfaifer, R., Friction-induced vibration – with and without external disturbance. Tribology International 34, pp. 7-24, 2001.

[28] Fredman, M. and Braun, S., Identification of nonlinear system parameters via the instantaneous frequency: Application of the Hilbert transform and Wigner-Ville Techniques. Sem proceedings, pp.637-642, 1995.

[29] Butcher, J. C., The numerical analysis of ordinary differential equations: Runge-Kutta and general linear methods. Wiley-Interscience New York, NY. Pub. 1987.

[30] Langley, R. S., On various definition of the envelope of a random process. Journal of Sound and Vibration. 105(3), pp. 503-1512, 1986.

[31] Nayfeh, A.H. and Mook, D.T., Nonlinear Oscillations. Wiley-Interscience Pub. 1979.

INTRODUCTION

Introduction

Did you ever imagine what would life be without friction? Is it possible to spend a normal day without the existence of friction? Without friction, we would not be able to achieve or hinder many essential tasks in our daily life activities. For example, if friction doesn't exist between your shoes/feet and the floor, then you would stay in a certain place forever. The friction force is as well responsible for stopping your vehicle/bike once you step on the brakes. Moreover, heat is produced due to friction whenever you rub your hands together during winter period. Also, friction plays a role in other actions like brushing your teeth, rubbing two wooden sticks to produce fire, doing massage, etc. Indeed, a life without friction is certainly hard to imagine. Nevertheless, a life with controlled friction is one of the ultimate tasks for modern technology.

A vital portion of research has been contributed for the aim to control and optimize energy efficiency in many scientific and industrial communities. This is significant not only to preserve our limited energy resources but also to avoid our planet from hazardous emission and conserve the ultimate economic expenses for prosperous generations. These energy efficiencies are mostly due to the technological products that are operated using non-renewable energy sources such as transportation and robotic devices. Many of these devices generate mechanical energy via motion. Unfortunately, whenever there is motion, there is friction. In fact, friction losses between mechanical components account for the highest percentage of the total energy losses.

Lately, the research challenge has aimed not only to reduce and control friction, but also to observe the existence of near-zero-friction situations between two sliding solid surfaces. This is known as superlubricity. This latter phenomenon is defined by a regime of motion in which friction vanishes or nearly vanishes in which the friction coefficient becomes in the order of 10^{-3} to 10^{-4} and even lower.

In cases where the friction must be taken into consideration, a valid friction law is necessary in order to design the system. Since ancient years, man has aimed to reduce friction. In the antiquity (2000 years B.C.), Egyptians used lubricant in order to move stones on inclined planes. Friction is described by the force resisting the relative motion of two surfaces in contact. The friction coefficient is defined as the ratio of the friction force between two bodies with respect to the normal force. Although the concept of friction can be easily understood, it is difficult to be modeled and simulated. Many friction models are characterized by a variety of nonlinear features such as discontinuities, hysteresis and other constraints. Therefore, a friction model should be carefully chosen in a way that respects the properties of the system.

It is very essential, as well, to measure the different sources of energy dissipation for many mechanical systems. This latter is often due to the overall friction which may be characterized by velocity-dependent and velocity-independent friction contributions. The conventional tribometers are limited to determine the overall friction coefficient and as well to measure friction described by superlubricity. These classical tribometers are not able to measure the different contributions of friction in one experiment. Thus, an experimental technique that

enables us to determine the different friction contribution is of interest for many mechanical systems.

This present research deals with a promising technique, innovated in our laboratory, able to measure low friction by sliding a spherical pin on a flat plane. In such technique, the system is undergoes free responses which are characterized by the damped oscillatory motion. This apparatus measures the displacement and velocity responses thanks to a laser vibrometer. The friction coefficients are then evaluated from its corresponding decaying displacement and velocity responses. The principal objective of this work is to investigate this technique for a better knowledge. Indeed, there are many criteria that interfere in the study of this technique. The tribological properties of the contact are very important for these measurements. Moreover, the friction model plays an essential role in evaluating the friction. Also, it depends on the tribosystem. Numerical simulations are performed in order to model the system with an appropriate friction law and then compare the simulated responses with the experimental results.

This thesis begins with the state of art (Chapter 1). The state of art reviews the history of friction. Then, this chapter allows us to study the various friction laws found in literature in both steady and variable states. Finally, chapter 1 ends up by a general glimpse on friction in its low scale, i.e. superlubricity and its significance in everyday applications. This vast review permits us to interpret the experimental and numerical results presented in the following chapters.

In chapter 2, the experimental technique is described. Then, the experimental results are presented in two different parts. In the first bunch of experiments, different contacts lubricated with oleic acid or glycerol are tested using the technique. This part aims to study the effect of diamond-like-carbon coatings on steel/steel surfaces. Then, in the second part, the experimental results of lubricated steel/steel contacts are shown. Three different lubricants with/without additives are used. The effect of temperature is studied as well in this part.

The dynamic system induced by a polynomial friction law is studied numerically in the third chapter (Chapter 3). The decaying law for the free oscillating responses is analyzed using different numerical methods. Finally, the numerical results are presented allowing us to specify the friction model and compare the numerical results with the experimental ones.

Chapter 4 will revisit some experimental tests in order to study the measured tangential friction force. Then, a single degree-of-freedom oscillating system induced by a LuGre friction model is studied numerically.

Finally, the general conclusion section of this thesis recapitulates the main points of our research, briefly summarize the numerical and experimental results presented in the different chapters and finally recommend some perspectives for future work.

1 STATE OF ART

1 State of Art

Chapter 1: State of Art

1.1 Introduction

The main objective of this research is to better understand a dynamic tribometer based on the analysis of the free oscillating response corresponding to a one degree-of-freedom friction system. In this context, we will introduce the subject by reviewing the literature.

Friction is defined as the resisting force which hinders the relative motion experienced when two surfaces in contact are sliding across each other. Thus, the friction between them converts kinetic energy into heat. This latter phenomenon can be illustrated by the fact of the presence of friction between two pieces of wood, while rubbing them, to start a fire for example. Human's life depends on the friction phenomenon. For example, babies cannot crawl without the existence of friction. It is also present as well in all mechanical systems such as bearings, valves, brakes, wheels, etc. Therefore, understanding friction and its behavior is of great interest for many researchers. Friction science is a principal branch in the field of tribology. Friction is directly related to a normal force with a coefficient, called the friction coefficient. The friction coefficient depends on the material of the surfaces and even on the lubricant separating them if any. Friction occurs at the physical interface between contacts. Therefore, it is very essential to have a friction model for many systems. It is also desirable to have a model that provides the comprehension of the physical mechanisms of friction as well as the prediction of the qualitative behavior of a mechanical system [1].

There are several types of friction. In our study, we will spot the light on both dry and lubricated friction. Dry friction is known as the friction produced between two solid surfaces in contact without lubricant. However, lubricated friction is a case where two solid surfaces are separated by a lubricant film. Dry friction between two bodies in contact may result in material wear, fatigue, elastic or plastic deformation and surface adhesion with the generated heat between them. Nevertheless, when a lubricant separates two bodies in contact, it can accommodate their velocities difference resulting in friction and wear reduction.

When it comes to the new technologies and the small tribological systems that generate low, ultra-low or negligible friction, tribology becomes involved in studying these systems and shifting to new technologies that are capable to measure friction at this measurement scale limit. Chapter 1 starts with a brief history of friction. Then, it presents different friction models. Finally, this chapter ends by a general glimpse of superlubricity and few examples on its applications.

1.2 Friction: Historical Review

There is no doubt that man has thought about friction and the means to reduce it since long time before the industrial and scientific evolution [2] and [3]. Actually the first mechanical systems were made from wood and stone. Some of them have been lubricated by animal fat. Those systems were found before the period of 4000 B.C.

The study of friction has been explored since ancient times; however, it was limited to the development in the industrial fields of mechanics such as the design of machines. This study was limited until recently few researchers were involved in this issue independently. Nevertheless, with the industrial revolution and the invention of heavy machines that introduced heavy loads, different couplings, contacts and relative motions, it became important to analyze friction seriously because its comprehension could lead not only to the improvement of the lifetime of the mechanical elements but also the reliability productivity of a whole industrial chain. The first recorded studies on friction are dated in the fifteenth century and belong to the scholar Leonardo da Vinci (1452-1519). He realized the vitality of friction study in any mechanical system. Da Vinci simply stated two laws of friction. The first law says that the friction force is directly proportional to the applied load. In the second law, he stated that the friction law is independent on the apparent contact area. Figure 1 shows his sketches of the experiment performed on dry surfaces used to prove that the friction force is independent on the contact surface. Moreover, he observed that various materials move in different ease in which he concluded that smoother materials have lower friction coefficient. He also studied other topics related to friction such as wear and its mechanisms, lubricated systems, gears, screw-jacks and rolling-element bearings. Among his investigations, Leonardo Da Vinci studied the relationship between friction and the music of heavens. He knew that music is produced by the bumping and rubbing of the heavenly spheres. His work shows an incredible progress to the existing technology during his period. Da Vinci's observations became two hundred years later before the well-known scholar of friction, Guillaume Amonton. Figure 1 presents a schematic of Leonardo Da Vinci's experiments.

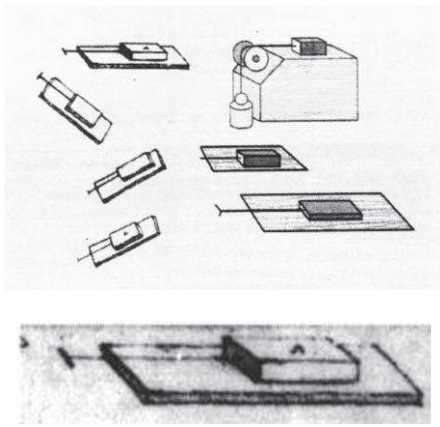

Figure 1. A schematic of Leonardo Da Vinci's experiments.

Guillaume Amonton was among the pioneers who put standards for the science of friction. He rediscovered the two basic laws previously found by Leonardo Da Vinci [4]. He also realized that friction is resulted from the surface roughness in which he believed that friction is used to lift one surface by the roughness, deformation or wear of the other surface. Amonton succeeded in his experiments on dry contacts using different materials in order to study the heat generation and solid adhesion as well as to analyze the effect of surface roughness on friction. In Figure 2, Amonton gives the basics of measuring friction in most of tribometers by using springs and measuring displacement according to the equation $F_{friction} = \mu N$.

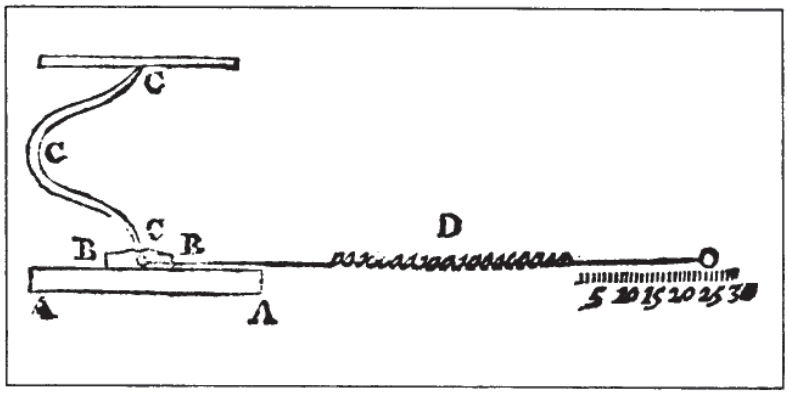

Figure 2. Basics of measuring friction in most tribometers by Amonton.

Nevertheless, the theoretical approach to the problem was introduced by Euler in 1750 in which he defined the concept of friction and its angle. These concepts of friction still exist nowadays in many engineering applications. The easiest set-up to understand static friction consists in a body placed on an inclined plane. This latter study was carried out by Leonardo da Vinci (1452-1519) (Figure 1) and Leonardo Euler (1707-1783). Euler also differentiated between static and dynamic friction and represented the surface roughness as a pyramid model. However, the first person to make a distinction between the static and dynamic friction was John Andreas Von Segner (1704-1777).

During the industrial revolution, Coulomb conducted several experiments in order to identify the parameters that influence the friction in sliding and rolling conditions. Among these parameters are the material properties, fluid lubrication, apparent contact area, loaded pressure and finally the relaxation time of the contacting surfaces prior to the experiment. His experiments were able to confirm Amonton laws and to show in addition that the friction coefficient does not vary with the sliding velocity. This was later attributed to him as a third law of friction: Strength due to friction is proportional to the compressive force. However, friction does not follow this law for large bodies. In fact, the Amontons-Coulomb laws of friction are applicable for many different material combinations and geometries.

Last but not least, in 1954 Bowdon and Tabor explained physically the preceding laws of friction. They proved that the true contact area is small relative to the apparent contact area.

They also showed that as the normal load increases, the more asperities are developed into the contact and this causes an increase in the contact area.

The first significant research on lubricated friction was carried out by Hirn in 1847 [5]. He studied experimentally the evolution of the friction coefficient under constant load and variable velocity in both dry and lubricated contacts. In lubricated contacts, he observed that the friction coefficient is unstable for low velocities. As the velocity increases, friction becomes stable and decreases until it reaches a minimum value. At a constant temperature, the friction increases proportionally to the velocity. These latter results are contradicted with Coulombs third law of friction. Thus, Hirn's results were rejected for publishing until 1854.

The behavior of friction has been extensively examined during the twentieth century. Lately, the interest in friction dynamics has increased. Thus, it is very essential to construct a specific friction model for a mechanical system. Some previous friction models will be reviewed in the section below.

1.3 Overview of Some Friction Models

It is crucial to obtain an appropriate friction model for several purposes. In few cases, it is preferable to have a friction model which provides some information for the physical behavior at the friction interface. Nevertheless, in other cases, it is sufficient to have a model that gives a global and qualitative behavior of a system characterized by friction. Thus, it is essential to bear in mind the purpose when studying a specific friction model.

This section presents an overview of some friction models studied previously. The aim of this part is not to review all the existing friction models but to show a glimpse of the huge spectrum of all the models. The friction models that will be presented are divided to two different categories: steady-state and variable-state friction laws.

In order to discuss friction corresponding to the existing models, it is known that the friction is represented by the friction coefficient denoted by μ. The friction force, F, can be written as follows:

$$F = \mu N \qquad (1)$$

N is the normal force exerted on the mass, m, represented in Figure 3. x and $\dot{x}$ are respectively the displacement and velocity of the system.

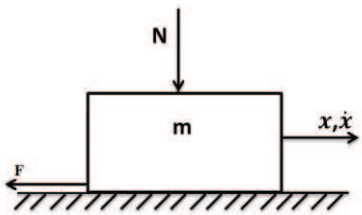

Figure 3. Mass system described by a normal force, $N$and a friction force F.

1.3.1 Steady-state friction laws

The steady-state friction laws have been used for centuries. This model consists of different components in order to roughly understand the behavior of friction, which agrees with simple experiments performed. The steady-state friction, described as a simple friction, can characterize dynamic systems having free oscillating responses. The friction coefficient of these models depends only and only on the relative instantaneous velocity and can be denoted as:

$$\mu = \mu(\dot{x}) \qquad (2)$$

1.3.1.1 Coulomb friction

In the 18th century, Coulomb worked again on the friction discovered by Da Vinci and then by Amonton in the late period of the 17th century. Coulomb friction depends on the motion of the system. His law states that friction opposes the motion and that the friction force is independent of the velocity and the contact area. The Coulomb friction coefficient is represented as follows:

$$\mu(\dot{x}) = \mu_c \mathrm{sgn}(\dot{x}) \qquad (3)$$

μ_c is the Coulomb friction constant and the function sgn preserves the asymmetry of the system. Figure 4 represents the Coulomb friction coefficient as a function of velocity. Thus, the friction coefficient value is within the range $-\mu_c$ and $+\mu_c$. Figure 4 shows that for a zero velocity, the Coulomb friction coefficient does not have a specific friction coefficient. Due to its simplicity, the Coulomb friction is used to model many mechanical systems [6].

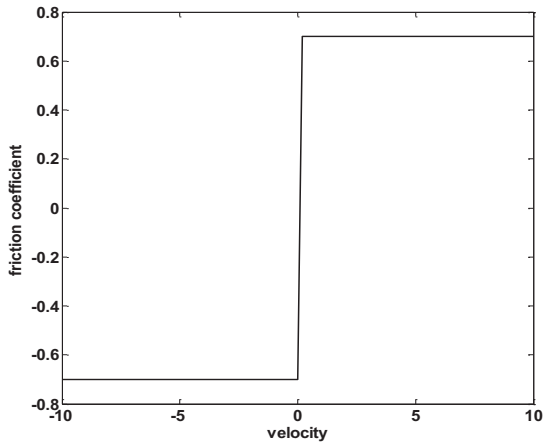

Figure 4. Coulomb friction coefficient as a function of the velocity with $\mu_c = 0.7$.

1.3.1.2 Viscous friction

In 1886, Reynolds has developed the theory of hydrodynamics in which he ended up in an equation for the friction force caused by the lubricant viscosity [7]. This latter law corresponds to a friction model, called the viscous friction [8]. The viscous friction coefficient is described as following:

$$\mu(\dot{x}) = \mu_v \dot{x} \qquad (4)$$

μ_v is the viscous friction constant. Figure 5 represents the viscous friction coefficient as a function of the velocity. The general equation of the viscous friction coefficient is denoted by the following general form:

$$\mu(\dot{x}) = \mu_v |\dot{x}|^{\delta_v} \mathrm{sgn}(\dot{x}) \qquad (5)$$

δ_v depends on the geometry of the application.

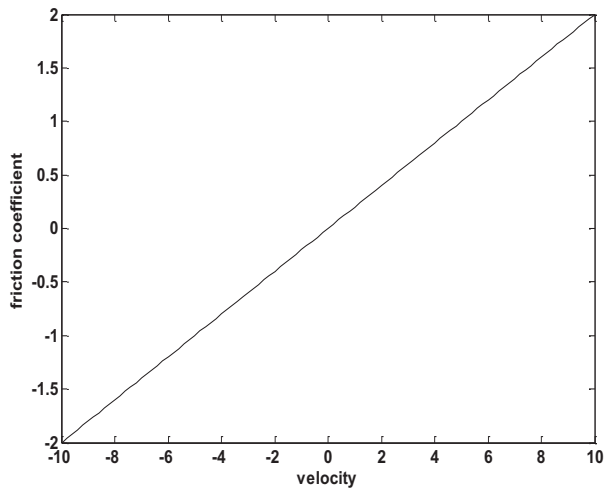

Figure 5. Viscous friction coefficient as a function of the velocity with $\mu_v = 0.2$.

The Coulomb and viscous friction can be combined to have the following friction coefficient:

$$\mu(\dot{x}) = \mu_c \mathrm{sgn}(\dot{x}) + \mu_v \dot{x} \qquad (6)$$

Figure 6 represents the relation between the friction coefficient and the velocity of a Coulomb-viscous friction model.

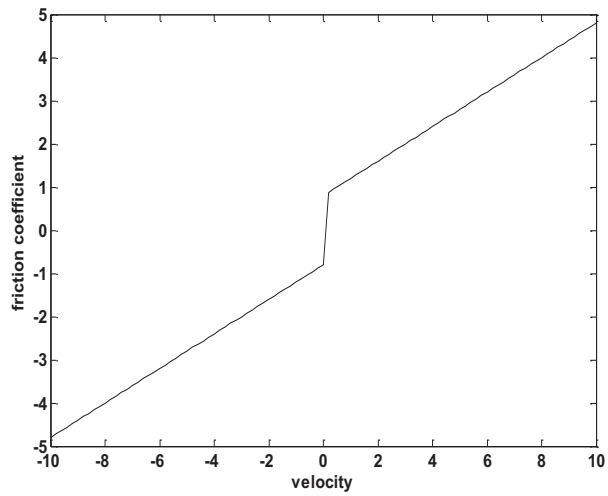

Figure 6. Coulomb- viscous friction coefficient as a function of the velocity with $\mu_c = 0.8$ and $\mu_v = 0.4$.

1.3.1.3 The classical Stribeck friction law

In real life, many tribological contacts are lubricated. Therefore, it is vital to simulate a friction model corresponding to these systems. The classical Stribeck friction law [9] can be representative for a system described by a lubricated contact due to its ability to show all the lubricant properties and friction at different states. Figure 7 demonstrate the Stribeck curve where the friction coefficient, μ, is presented as a function of the velocity U or the film thickness H. This law defines the friction by 3 different regimes [10].

In the hydrodynamic and elastohydrodynamic lubrication regimes (HL and EHL), the lubricant film fully separates the solid surface. The friction depends on both the viscosity and velocity. In this regime, the friction is also dependent on the rheological properties of the lubricant film. However, in the mixed lubrication regime which is the intermediate regime, more lubricant is entrained in the contact as the velocity decreases resulting in less asperities between the contact and hence a reduction in the friction coefficient. This latter friction regime lies between the hydrodynamic and boundary regimes. Finally, in the boundary lubrication regime the velocity occurs to be low where mostly no lubricant appears between the contacts. Thus, the load is fully supported by the contacting asperities or in other words by the lubricant film pressure.

Unfortunately, it is very difficult to have a theoretical model fully describing the Stribeck friction law from basic parameters. Thanks to Reynolds equation [11], it is possible to fit the friction coefficient during the elastohydrodynamic (EHL) regimeμ_{EHL}using a simple power law. It is represented as follows:

$$\mu_{EHL} = K(\eta\dot{x})^n \quad (7)$$

η is the lubricant viscosity, $\dot{x}$ is the velocity of the system, K is the EHL power-law coefficient and n is the EHL power-law index. The use of a power-law is explained by the linear relation of the friction coefficient with the velocity and the film thickness in a logarithmic scale during the EHL regime. The same law is applied for the boundary friction regime where the curve is approximately a straight line. Thus, the friction coefficient of this latter regime is written as:

$$\mu_{BL} = h(\eta\dot{x})^p \quad (8)$$

h and p are the power-law coefficient and index respectively. It is possible now to write an empirical equation for the entire Stribeck curve representing all the friction regimes. Thus, the total friction coefficient is represented in the following form:

$$\mu_{Total} = \mu_{EHL} + \frac{\mu_{BL}+\mu_{EHL}}{1+({}^{\eta\dot{x}}/_{B})^M} \quad (9)$$

B is the value of $\eta\dot{x}$ below which the boundary lubrication regime starts. M is the exponent of the mixed lubrication.

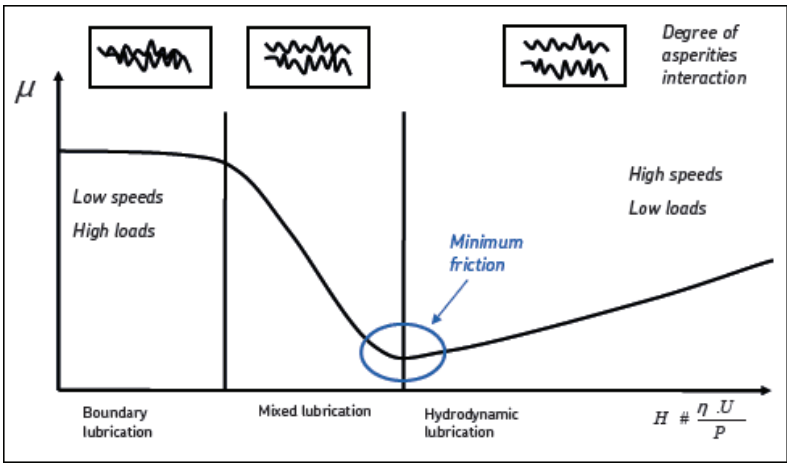

Figure 7. Stribeck friction illustrating the three friction regimes: full film (HDL and HL), mixed and boundary friction regimes [3].

1.3.1.4 The Modified friction law by Hess and Soom

In 1990, Soom and Hess [12] performed experiments on contacts operating under unsteady loading and sliding conditions. They recognized a friction-velocity relationship of line contacts under those conditions during the full and mixed lubrication regimes. After collecting the friction data resulted from the experiments [12] done at different operating conditions, they found that the friction data, continuously acquainted, is equivalent to the steady-state conditions. At the beginning, Hess and Soom plotted the friction as a function of the conventional Stribeck friction curve parameter, $\frac{\eta V}{W}$ (Figure 8). W is the normal load applied to the Hertzian line contact under pressure and V is the velocity.

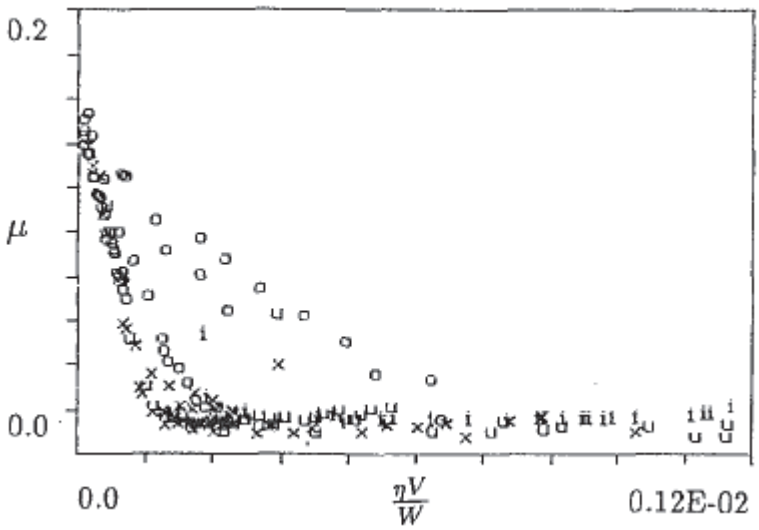

Figure 8. The conventional Stribeck curve presenting the friction data of Hess and Soom[12].

Later on, they used the approach suggested by Mckee and Mckee [13]. This approach is defined by presenting the friction coefficient as a function of the "modified Stribeck parameter" denoted by $\frac{\eta V}{\sqrt{(WE)^{0.5}}}$ (Figure 9). E is the Young's modulus. Actually, it is impossible to fully describe the friction coefficient, μ. However, Hess and Soom tried to obtain a satisfactory model for their experimental data. This model combined both the conventional and modified Stribeck friction laws. It is represented in the following equation.

$$\mu = \frac{\mu_b}{1+c_1(\frac{\eta V}{\sqrt{WE}})^2} + c_2\frac{\eta V L}{W} \text{ for } V > 0 \qquad (10)$$

μ_b is the friction coefficient at the boundary lubrication regime. The first term $\frac{\mu_b}{1+c_1(\frac{\eta V}{\sqrt{WE}})^2}$ is related to the modified Stribeck friction law and describes the mixed lubrication regime. However, the second term $c_2\frac{\eta V L}{W}$ with the contact length L represents the dimensionless form of the classical Stribeck parameter and determines the hydrodynamic regime. c_1 and c_2 are constants.

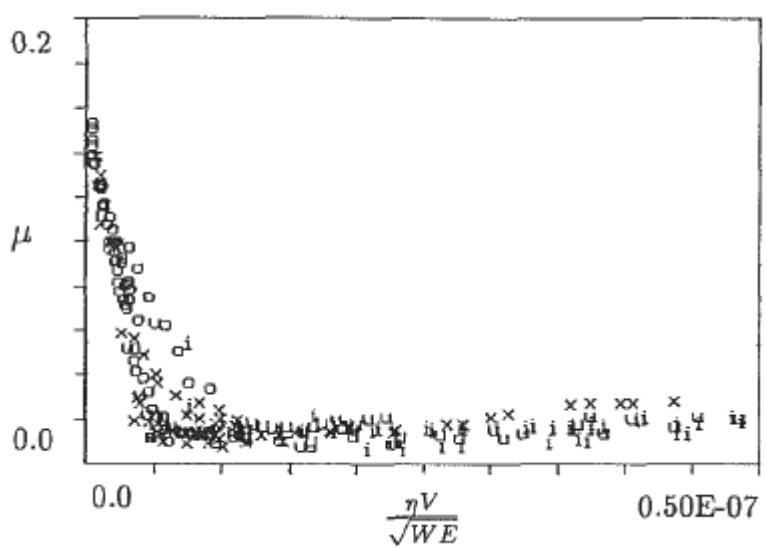

Figure 9. The modified Stribeck curve presenting the friction data of Hess and Soom[12].

1.3.2 Variable-state friction laws

Lately, variable-state friction laws have been of great interest for modeling many systems. With the raise of the complicated technological production, i.e. robotics firm, the modeling of variable-state friction has dominated. Thus, friction coefficient is written not only as a function of the global velocity of the system but also as a function of many parameters and mechanisms. In this action, some variable-state friction models are surveyed.

1.3.2.1 Dahl friction model

In 1968, Dahl introduced a friction model [14]. His aim was to simulate a friction model suitable for control systems. Later on, the model was discussed by Dahl and his colleague in [15] and [16]. The idea of this model was explored from several experiments performed on friction in servo systems with ball bearings. Dahl found that the friction in bearings functions similar to the phenomenon of solid friction. Moreover, he predicted that there are metal contacts between the surfaces. Thus, in order to obtain a simple model able to simulate friction in ball bearings, he used as a starting point the stress strain relation (Figure 10) in solid mechanics [17-18]. This relation explains the gradual increase of the friction force as the stress is subjected until rupture occurs. Thus, the total friction force depends on the strain caused by the external force. The model includes static friction if the strain characteristics correspond to ductile material which considers only friction due to contact between solids. However, the friction model corresponding to brittle material functions is properly related for both sliding and rolling friction between lubricated contacts.

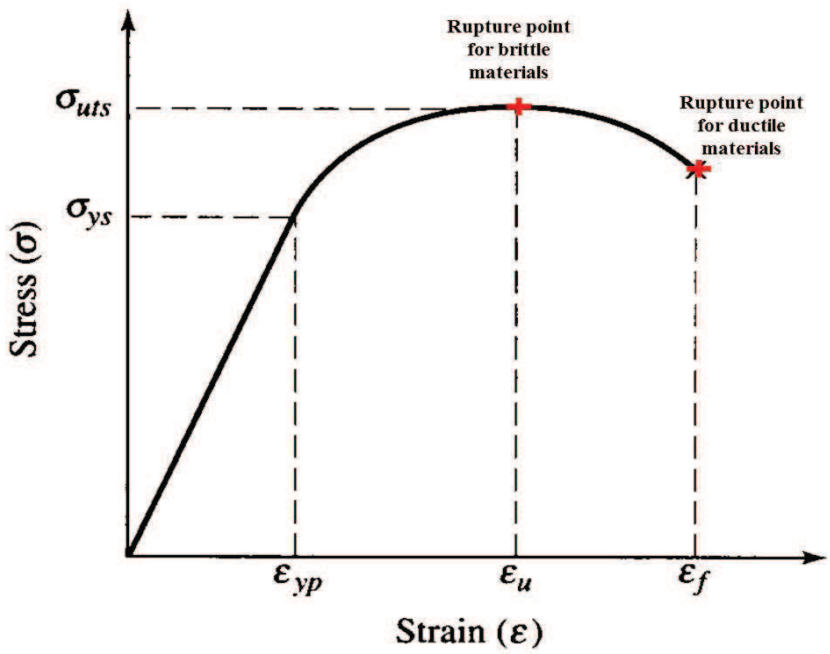

Figure 10. Stress-strain relation for both brittle and ductile materials.

Dahl [14] friction model is represented in the following form:

$$\frac{dF}{dx} = \sigma(1 - \frac{F}{F_c}\mathrm{sgn}(\dot{x}))^{\alpha} \qquad (11)$$

x is displacement, F is the frictional force and F_c is the Coulomb friction force. σ is defined by the stiffness coefficient and α by the parameter that determines the shape of the stress-strain curve. Usually, the value of α is used as 1. As α is greater, the stress-strain has a sharper bend. It is important to note that $|F|$ can never be greater than F_c such that $|F_0| < F_c$. The time domain force derivative $\dot{F}$ is obtained as follows:

$$\dot{F} = \frac{dF}{dt} = \frac{dF}{dx}\frac{dx}{dt} = \sigma\dot{x}(1 - \frac{F}{F_c}\mathrm{sgn}(\dot{x}))^{\alpha} \qquad (12)$$

Assuming $\alpha = 1$ and introducing $F = \sigma z$, the system is described in the following equation (13), (14) and (15).

$$z = \frac{F}{\sigma} \qquad (13)$$

$$\dot{z} = \dot{x} - \frac{\sigma|\dot{x}|}{F_c}z \qquad (14)$$

$$\dot{F} = \sigma\dot{x}(1 - \frac{\sigma z}{F_c}\mathrm{sgn}(\dot{x}))^{\alpha} \qquad (15)$$

The Dahl model permits to obtain a hysteresis operator [19]. This is shown in Figure 11 where the friction force is plotted as a function of the displacement.

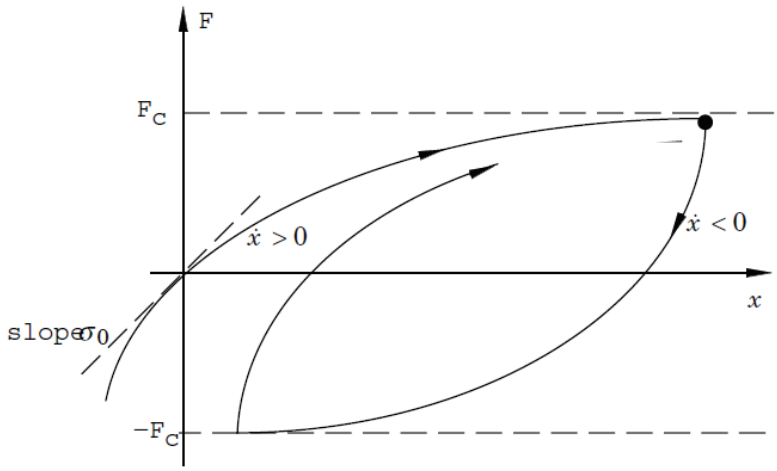

Figure 11. Friction force as a function of displacement corresponding to Dahl friction model [20].

1.3.2.2 LuGre friction model

Surfaces are irregular at the microscopic level and they form a contact at a certain number of asperities. When a tangential force is applied, the bristles deflect acting like a spring and end up in a friction force. Nevertheless if this force is large enough, some of the bristles deflect more leading to the slip phenomenon between each other. This causes new contacts to be formed. However, the process continues as long as the two surfaces continue to move. To demonstrate these surfaces, Canudas de Wit and his co-workers [21] developed a new model called the LuGre model. Figure 12 represents the friction interface between the contacts of two bristles.

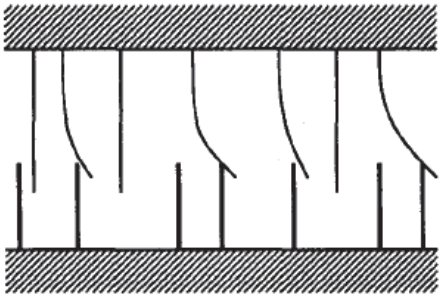

Figure 12. The friction interface between the contact of two bristles [22].

The LuGre friction model is based on an internal variable, known as the deflection of the bristles. This variable is denoted by z and modeled as follows:

$$\dot{z} = \dot{x} - \frac{|\dot{x}|}{g(\dot{x})} z \qquad (16)$$

Thus, $\dot{x}$ is defined as the relative velocity between the two surfaces. The function $g(\dot{x})$ is positive and depends on a variety of functions such as material properties, lubrication and temperature. Moreover, the function g describes the behavior of the Stribeck curve and can be written as:

$$g(\dot{x}) = F_c + (F_s + F_c)e^{-(\dot{x}/v_s)^2} \quad (17)$$

F_c is the Coulomb friction force, F_s is the Stiction force level and v_s is the Stribeck velocity. The total friction force of the LuGre model is presented as:

$$F = \sigma_0 z + \sigma_1 h(\dot{x})\dot{z} + \sigma_2 \dot{x} \qquad (18)$$

σ_0 is the stiffness which parameterizes the presliding displacement, σ_1 is the internal viscous frictional damping coefficient and $\sigma_2$is the viscous damping coefficient due to the relative velocity. $h(\dot{x})$ is an exponentially or fractionally decay function with respect to the velocity, satisfying $h(\dot{x}) < h(0) = 1$. The first two terms $\sigma_0 z + \sigma_1 h(\dot{x})\dot{z}$ represent the friction force generated from the bending of the bristles. However, the last term $\sigma_2 \dot{x}$ is added in order to account for the viscous friction. Moreover, the function $\sigma_0 z + \sigma_2 \dot{x}$ can be determined by measuring the steady-state friction force when the velocity is held constant.

This model better describes a relationship between the relative sliding velocity and the friction force [23]. Moreover, the friction force as a function of the sliding velocity is described by a hysteresis form (Figure 13).

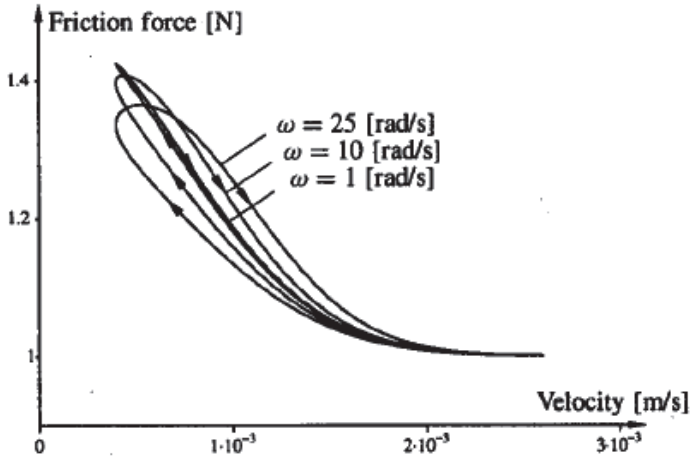

Figure 13. Hysteresis in friction force relationship with the sliding velocity [21].

1.3.2.3 Modified LuGre friction model

LuGre model has been widely used in friction modeling such as in [24] and [25]. However, there are some practical difficulties to apply this model for systems described by large range of motion speeds, for example the linear motor drive system studied by Lu and his colleagues [26]. Lu et al. proposed a modified LuGre friction model in order to improve the LuGre friction model. This modified model is equivalent to the LuGre model in the case of low speed for dynamic friction and in that of high speed for static friction. With the LuGre model, the friction force F is defined in section 1.3.2.2 (equation 18). However for high values of the velocities, it is sufficient to use the combined Coulomb and viscous friction presented in section 1.3.1.2 (equation 6). Its corresponding friction force can be written in the following form:

$$F = F_c \mathrm{sgn}(\dot{x}) + F_v \dot{x} \qquad (19)$$

It can be noted that F_c and F_v in (19) related respectively to $\sigma_0|z_{ss}|$ and σ_2 in (18). z_{ss} is the deflection of the bristles at steady state where $\frac{dz_{ss}}{dt} = 0$. However, it is very hard to estimate z when the speed shifts between low and high values. Therefore, Lu and his co-workers have developed a modified LuGre friction model. This proposed model is described by the following form:

$$F = \sigma_0 s(|\dot{x}|)z + \sigma_1 h(\dot{x})\dot{z} + F_c \mathrm{sgn}(\dot{x})[1 - s(|\dot{x}|)] + \sigma_2 \dot{x} \qquad (20)$$

$$\dot{z} = s(|\dot{x}|)(\dot{x} - \frac{|\dot{x}|}{g(\dot{x})} z) \qquad (21)$$

$$g(\dot{x}) = \alpha_0 + \alpha_1 e^{-(\dot{x}/v_s)^2} \qquad (22)$$

$s(|\dot{x}|)$ is defined by a non-increasing continuous function of $|\dot{x}|$ where $s(|\dot{x}|) = 0$ if $|\dot{x}| < l_2$, in which $l_2 > l_1 > 0$. l_2 and l_1 are the cutoff velocities chosen according to the characteristics of the system used. Unfortunately, experimental data doesn't exist in order to assume such a modified model.

The steady-state friction force of the modified LuGre model is written as following for any constant speed $\dot{x}$ and a negligible $\dot{z}$.

$$F = \{\sigma_0 s(|\dot{x}|)g(\dot{x}) + F_c[1 - s(|\dot{x}|)]\}\mathrm{sgn}(\dot{x}) + \sigma_2\dot{x} \quad (23)$$

From the above equation (23), one can recognize that F_c can be different than $\sigma_0\alpha_0$. Moreover, it is possible to replace $\sigma_2\dot{x}$ by $\sigma_{21}\dot{x}s(|\dot{x}|) + \sigma_{22}x[\dot{1} - s(|\dot{x}|)]$, which is capable to prove that the viscous term differs at high speed from that at low speed. Thus, this modified model permits us to fit the measured friction data over a large range of velocities.

1.3.2.4 Friction model of lubricated contacts

In most engineering applications, the contact interfaces are lubricated. Thus, friction models have been derived using hydrodynamics. Viscous friction model is an example; however, other models exist as well. In 1993, Haroy and Friedland [27] have suggested a friction model based on the hydrodynamics of a lubricated journal bearing. The friction is simplified by the following friction form:

$$F = K_1(\varepsilon - \varepsilon_{tr})^2\Delta + \frac{K_2}{\sqrt{1-\varepsilon^2}}\dot{x} \quad (24)$$

K_1 and K_2 are constants. ε is eccentricity of the bearing. Δ is an indicator function in which it is 1 for $\varepsilon > \varepsilon_{tr}$ and zero for all other cases. Thus, one can conclude that friction does not exist for small eccentricities due to the presence of asperities between the contacts. The eccentricity determines the pressure distribution found in the lubricant. Therefore, ε has a 4th order differential equation form. The first term $K_1(\varepsilon - \varepsilon_{tr})^2\Delta$ of the preceding equation (24) represents the shearing of the asperity contacts. However, the second term $\frac{K_2}{\sqrt{1-\varepsilon^2}}\dot{x}$ indicated the lubricant viscosity.

1.3.2.5 A numerical friction model of a real contact

The resistive forces, developed at the asperities of rough surfaces sliding against each other, represent the true contact of sliding surfaces in real life applications. In 2001, Karpenko and Akay [28] have presented a numerical model describing the friction of a contact, having rough surfaces. Figure 14 represents the schematic of a contact having rough surfaces.

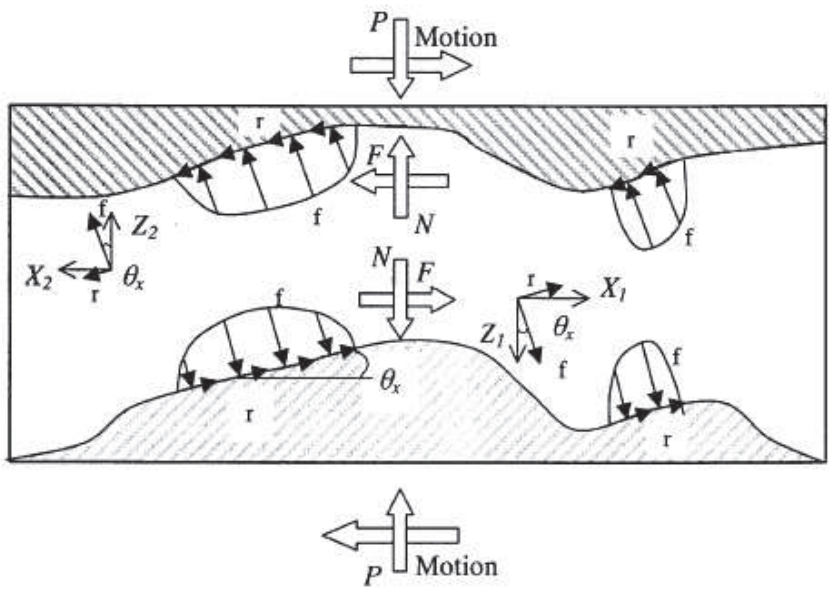

Figure 14. A schematic description of a contact with rough surfaces [28].

f is described by the spatial distribution of contact pressure, resulting from the deformation of the asperities. P is the normal component of the deformation and local friction forces corresponding to the asperities [29-30]. This latter is found as follows:

$$N = \iint_A (f \cos\theta_x - r \cos\theta_x) \cos\theta_y \, \mathrm{d}x\mathrm{d}y \qquad (25)$$

F is the corresponding sum of the projections of contact forces in the sliding direction. It is computed as the following:

$$F = \iint_A (f \cos\theta_x + r \cos\theta_x) \cos\theta_y \, \mathrm{d}x\mathrm{d}y \qquad (26)$$

Finally, the friction coefficient μ corresponding to rough surfaces is found to be as:

$$\mu = \frac{F}{P} \qquad (27)$$

1.3.2.6 Dynamic friction model of contact stresses

A dynamic friction model of contact stress can rarely be existed in literature. Thus, Tan and his group suggested a dynamic friction model that can successfully predict the contact stress distribution flat rolling [31]. This friction model combines both the viscosity and the stress distribution. Thus, the model is expressed in the following friction coefficient:

$$\mu = \frac{\eta}{P}\frac{d\dot{x}}{dz} \qquad (28)$$

η is the lubricant viscosity, P is the normal pressure, $\dot{x}$ is the velocity parallel to the friction stress and z is the coordinate having a normal direction to the velocity.

Tan et al. recognized that the local stress characterizes not only solid mechanics but also fluid mechanics. Thus, the friction stress τ is proportional to both the strain time rate $\frac{d\dot{x}}{dz}$ and the normal pressure P. Thus, the friction stress is written as follows:

$$\tau = \beta \frac{d\dot{x}}{dz} P \qquad (29)$$

β is the dynamic friction coefficient such that $\mu = \beta \frac{d\dot{x}}{dz}$. For a certain plasticity problems, β has to be determined experimentally, similarly to η and μ. In order to ensure their model, Tan and his colleagues have performed some experiments. They concluded that their model agrees with the experimental data of τ and P.

Finally, an overview of some existed friction models is studied. Thus, it is very crucial to properly choose the appropriate model corresponding to the system. However, the new technologies, i.e. micromotors, hard disks, etc. are characterized nowadays by low friction. The following part of this chapter will emphasize on the existence of low friction and even near-zero friction, known as the phenomenon of superlubricity. Moreover, some real life systems from literature will be reviewed later on.

1.4 Nonlinearities behavior in friction

It is one of the fundamental issues to study the frictional behavior of the dynamic responses corresponding to sliding surfaces in contact. Many scholars [32-34] have discussed the effect of the forces developed at the contact due to the relative motion. These forces affect the response amplitude, thus participating in increasing the energy dissipation in the mechanical system.

Some dynamic systems are described by nonlinearities behavior due to the non-linear friction forces. Moreover, some of them are based on oscillatory relative motion due to their vibrational components. These systems are characterized by a hysteresis cycle which presents the tangential friction force as a function of the relative displacement. The hysteresis cycle is described by two different regimes: microslip and gross-slip. Microslip corresponds to the part of the hysteresis cycle between stick-slip, where the sliding takes place only between the parts of the contact surfaces. In this part of the cycle, the tangential friction force depends on the relative displacement. However, the Gross-slip considers the sliding between all the points of the contact surfaces, where the tangential friction force is independent on the relative displacement.

In 2004, Filippi et al. [35] have used an experimental apparatus [36] that allows the measurement of hysteresis cycles during both Microslip and gross-slip regimes. Filippi and his colleagues discussed the friction behavior of contacts, described by damped vibrations of gas turbine blades. This latter was previously discussed in 1990 by Griffin [37]. This type of systems is known for their high contact pressure and low relative motion amplitude. Their corresponding measured hysteresis cycles show either microslip regime or a combination of both microslip and gross-slip regimes. Nevertheless, it was

clearly observed in these experimental results that the microslip regime is more significant than that of the gross-slip. This latter was shown as well by Menq et al. in 1986 [38-39]. It was also observed that the hysteresis cycle tends to converge with some dispersion. However, the dispersion seems to be very important in the presence of very small displacement.

1.5 Low scale of friction

Tribology has had an essential role to play in the development of energy technology at many different levels. One of the challenges in tribology is enabling many components to operate with low friction. However, one of the weak points in conventional tribometers is addressed by the limit of detecting very low values of friction coefficients. Thus, the aim of this part is to define the phenomenon of very low friction and the present of some tribosystems corresponding to this definition.

1.5.1 Superlubricity phenomenon

Some researchers were able to observe the existence of near-zero-friction between two sliding surfaces. This is known as the phenomenon of superlubricity [40]. Superlubricity is a regime of motion in which friction totally or nearly vanishes [41]. In this way, researchers were able to shift from a commensurate to an incommensurate state by the transition from a pure stick-slip where friction is high to smooth solid surfaces in contact where friction is negligible. This phenomenon occurs when two surfaces, having crystal lattices, are defined by an incommensurate contact. This means that the crystal arrangement is in a manner such that only a minority of the atoms on the surface comes in contact with the opposing surfaces generating very low friction. Thus, superlubricity is interesting because it takes place in dry environment rather than in wet environment associated with lubricants in the contact. A simple and important example of superlubricity is the vertebral joint with its amazing properties of low friction and resistance to squeezing. Another good example of superlubricity is an incommensurate egg package where its valleys and hills do not line up.

The terminology “Superlubricity” was first defined by Hirano [41] in order to describe the theoretical sliding regime in which friction or resistance to sliding completely disappears. In this regime, the physical and chemical interactions are extremely small or negligible. Thus, the surfaces can slide over each other without causing much friction. Historically, the earliest studies on superlubricity were performed in the mid of 1980s. However, the important progress happened during the 1990s. The first theoretical study was done by professors Sokoloff and Hirano. They proved the existence of such superlubricity states between weak and atomic interacting surfaces. Their research has provided significant and fundamental insight on the atomic scale origins of friction generally and superlubricity particularly.

Until now, it has been impossible to experimentally investigate friction described by the phenomenon of superlubricity under the conditions of real engineering applications. In 1997, Ando explains that if two solid surfaces are in contact under low normal load, the

adhesion force and viscous resistance of condensed liquid increases the friction force [42]. This causes the friction coefficient between the two surfaces to be reduced. So far, literature has found limited combinations for the materials producing ultra-low friction coefficients [43]. For many moving mechanical assemblies such as MEMs devices and journal bearings, superlubricity under dry sliding conditions is rarely achieved [44].

In this context, many researchers have been recently studying surfaces that are able to enrich the literature with a better comprehension of superlubricity. One of these many surfaces are those coated with diamond-like carbon (DLC) coatings, which will be discussed in the following sub-section.

1.5.2 The significance of Superlubricity and its Applications

Reducing friction is an essential issue in our daily life activities. It is beneficial not only to preserve our limited energy resources but also to avoid our planet from hazardous emission for the prosperous generation. Until now, it has been impossible to experimentally investigate friction described by the phenomenon of superlubricity under the conditions of real engineering applications. However, Ando [31] predicted that friction can be reduced between two surfaces if the normal load decreases. So far, literature has found limited combinations for the surfaces and lubricants producing very low friction coefficients [45].

1.5.2.1 Diamond-like carbon coatings

Over the last decades, the thin layers of carbon-based, known as diamond-like carbon (DLC) have been of great interest in the scientific and industrial communities thanks to their physical, mechanical, biomedical and tribological capabilities. These coatings are characterized for their very high mechanical hardness, up to 90 GPa. They have as well convenient and significant tribological properties; they provide very low friction and mostly no wear. The combination of all these exceptional properties in one material is very rare which allows the DLC coating to be considered as a solution for a wide range of applications and attract as well the attention of many researchers.

The DLC coatings exist in seven different forms of amorphous carbon materials that display some of the unique properties of diamond. They are usually applied as coatings to surfaces that benefit from their properties. These materials contain a mixture of carbon atoms having either sp^2 or sp^3 bonding configuration and of hydrogen atom as well. The reason in which there are different types is that even diamond can be found in two crystalline polytypes. The current one has its carbon atoms arranged in a cubic while the very rare one has a hexagonal lattice. By mixing these polytypes in various ways at the nanoscale level of the structure, DLC coatings become meanwhile amorphous, flexible and yet purely sp^3 bonded diamond. The DLC coatings are classified in two main groups, the hydrogenated and non-hydrogenated amorphous carbons. The hydrogenated amorphous carbons, known by the term a-C:H, is performed using the chemical vapor deposition (CVD) process. In this kind of coatings, the hydrogen content varied depending on the deposition process, the hydrocarbon gas sources and deposition parameters used. Thus, the content of hydrogen may reach up to 50%. However, the sp^3 bonding rate is

between 20 and 80%. This latter group of carbon is significant since it permits to have a high electrical resistance and thus, stabilizing the structure of diamond by fully maintaining the sp^3 bonding configuration [46]. There is also in this group the tetrahedral hydrogenated amorphous carbon, ta-C, that contains more than 70% of the sp^3 bonding configuration and very few hydrogen content. The second principal group of carbon coatings is the non-hydrogenated amorphous carbon. They are obtained using the physical vapor deposition (PVD) process. In these coatings, hydrogen atoms are generally considered as impurities. They are divided in two groups. The first one is a-C which has sp^2 bonding configuration. However, the other is the tetrahedral non-hydrogenated amorphous carbon, ta-C, which contains sp^3 bonding configuration. The ta-C is also called amorphous diamond since it has tetrahedral shape as diamond and characterizes by the same properties as that of diamond. The tetrahedral amorphous carbons are considered the hardest and strongest in this group. Figure 15 presents a diagram of the composition of different amorphous carbon films. This diagram is proposed by Jacob and Moller [47] then developed by Robertson [48-51].

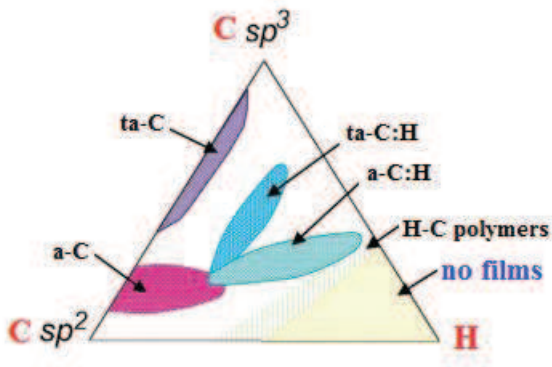

Figure 15. Phase diagram of the composition of amorphous carbons [51].

As mentioned previously, DLC coatings are often used to prevent wear due to its excellent tribological properties. They are very resistant to abrasive and adhesive wear making them suitable for applications that experience extreme contact pressure in both reciprocating and rolling movements. They are often used as well to prevent wear on razor blades and metal cutting tools. These coatings are used in bearings, cams, shafts and cam followers in the automobile industry. As an example, the DLC coatings reduce wear during the break-in period when drive train component starve for lubrication.

Nevertheless, DLC can be used on medical applications. The implantable human heart can be considered as the ultimate biomedical applications in which amorphous carbon materials are used on blood contacting surfaces of the device components. Moreover, at low voltages and temperatures, electrodes coated with DLC can emit enough electrons to be arranged into disposable micro-x-ray tubes as small as the radioactive seeds that are introduced into arteries or tumors in convention radiotherapy. In addition, the diamond-like carbon coated materials can be usable for artificial articulation thank to their biocompatibility and anti-wear specifications.

As the name implies, diamond-like carbon has some of the valuable properties of diamond. It can be applied as a coating on almost any material that is compatible with vacuum in which it is usually produced. Moreover, DLC coatings are applied more and more on many tribological applications in both dry and vacuum atmospheres. This goes behind the reason that they are made of carbon and they are environmentally friendly. Thus, these coatings were studied in the literature and they are still of great interest for present and future researchers.

In literature, low friction has been recognized between surfaces coated with diamond-like carbon (DLC). In 2003, Kano et al. [52] observed from the friction test that DLC lubricated with ester-containing oil produces super-low friction properties. Two years later, Kano et al. [53] carried out some experiments. They examined ultra-low friction from DLC coated surfaces having glycerol mono-oleate (GMO) as a lubricant. By comparing the 3 contacts: steel-on-steel, a-C:H-on-steel and ta-C-on-steel using different tribometers and lubricants, they found out that the lowest friction coefficient is 0.02 and belongs to ta-C-on-steel contact lubricated with poly-alpha-olefin oil (PAO) and GMO using the pin-on-disc tribometer. The latter different results are shown in figure 16.

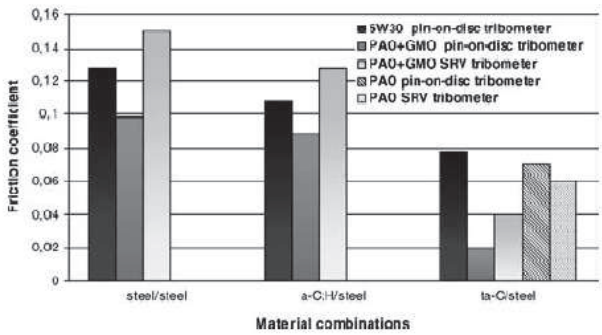

Figure 16. Comparison of three different contacts: steel/steel, a-C:H/steel and ta-C/steel lubricated with different lubricants using different tribometers [53].

In 2003, Yasuda et al. [54] performed experiments by sliding a steel (AISA 52100) pin on DLC (of 2 types: a-C:H and a-C) coated surface lubricated by engine oil 5W-30. The results have shown that a-C gives a low friction (0.07) compared to a-C:H (0.11). Neville et al. [55] has explained that the low friction observed in the case of a-C is due to its high surface energy compared to a-C:H. Thus, a tribofilm is formed at the a-C:H coated surface. In the case of a-C, the oil additive is easily adsorbed and passivated in the surface resulting in low friction. However, in the case of a-C:H, the dangling covalent bonds of the sp^2 bonded cluster are passivated by the hydrogen atoms. Then, the H-C combinations produce low surface energy due to the non-polar inert surface which causes poor wettability and little or no adsorption of oil additives in the surface.

In the early 2006, Kano and his group [56] performed an experiment by sliding three pins, made of bearing steel sliding on a rotating disc made of carburized steel (see figure 17). The rotating disc was coated by amorphous carbon in air. Two kinds of DLC were prepared for the test: a-C:H by CVD process and ta-C by PVD process. As a result, the

friction coefficient reduces from 0.8 to 0.1. However, the effect of the DLC coating on the engine oil was very limited [56]. They did not examine any tribofilms on the DLC-coated disc due to the inactive chemical properties of DLC. The ZDDP additive film formed causes the friction to increase. Nevertheless, the film derived from MoDTC affects a reduction in the film coefficient.

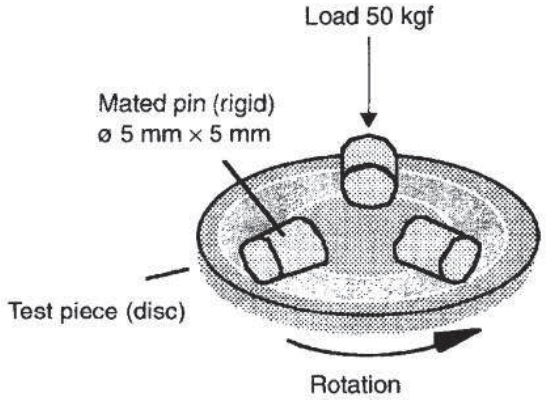

Figure 17. The three pins sliding on a rotating disc [56].

Moreover, Kano [56] et al. recognized that the friction force for the film derived from 5W-30 oil is greater than that from 5W-20 oil. The results are show in figure 18. One can understand that the increase in the friction coefficient of steel-on-steel contact can be due to the high shear strength of the film derived from ZDDP. However, one can understand that the reduction in the friction coefficient of steel-on-steel contact, lubricated by 5W-20 oil and MoDTC as an additive, can be due to the formation of MoS_2 solid lubricant derived from MoDTC.

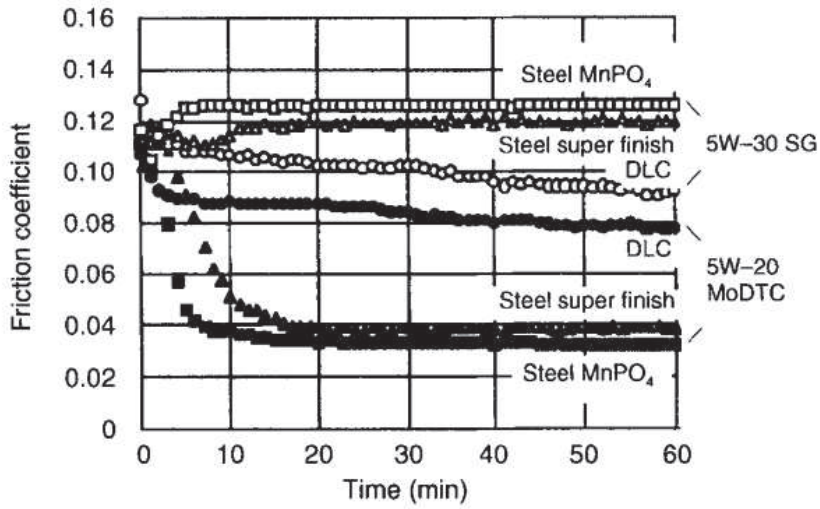

Figure 18. Friction coefficient as a function of time of two different oils (5W-20 and 5W-30) [56].

Finally, Kano and his colleagues [57] found that the friction coefficient decreases with the percentage of hydrogen found in the hydrogenated amorphous carbons [57]. They also studied the friction coefficient with different materials for the pin-on-disc as a function of

the rotational speed (see Figure 19). A super low friction coefficient of 0.006 is resulted with a speed of 0.1 m/s (100 rpm) for a steel pin-on-ta-C disc contact lubricated by PAO-ES 1 oil.

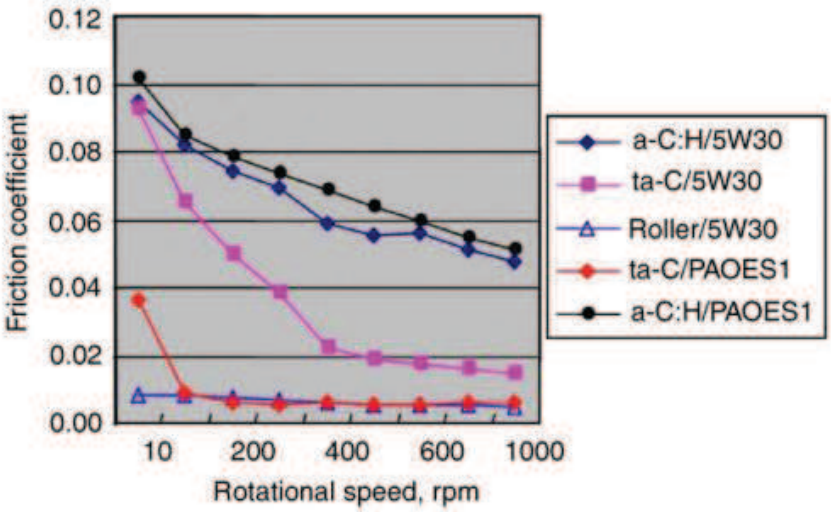

Figure 19. Friction coefficient as a function of the rotational speed of DLC coated contacts [57].

Other tribological results published recently [58] showed that the non-hydrogenated amorphous carbon (ta-C) coated materials provides ultra-low friction levels. These friction coefficients are able to reach superlubricity when some alcohols are used as lubricants. According to the friction measurements performed by the Cameron-Plint tribometer, characterized by a cylinder-on-plane configuration, friction coefficients were investigated by Jolly-Pottuz et al [58] for steel/steel, ta-C/ta-C and a-C:H/a-C:H contacts, each lubricated by pure glycerol. Results shows that ta-C/ta-C contact exhibits an ultra-low friction coefficient of about 0.025 compared to that of a-C:H/a-C:H (0.1) and steel/steel (0.15) contacts (see figure 20).

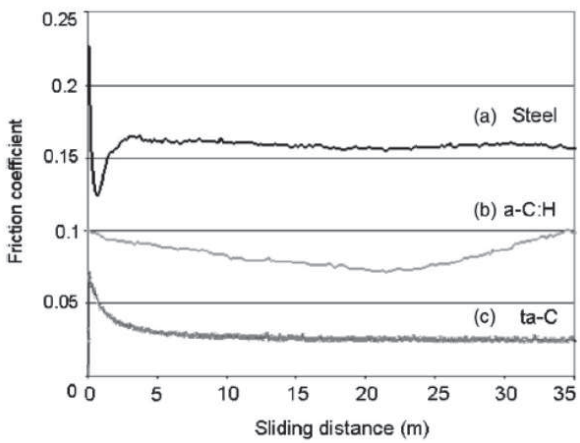

Figure 20. Friction coefficient of (a) steel/steel, (b) a-C:H/a-C:H and (c) ta-C/ta-C contacts lubricated by pure glycerol [58].

De Barros Bouchet and Kano [59] have studied the effect of various coatings on the valve train torque. These coatings are the phosphate, TiN, ta-C:H and ta-C coatings. Figure 21

presents the valve train friction torque as a function of the engine speed. The experiment was performed by testing the motor using the actual engine valve train. Results show that the tetrahedral non-hydrogenated DLC coating (ta-C) reduces the friction torque by 45% compared to that of the phosphate coating at an engine speed of 2000 rpm. Then, a durability test was conducted at an engine speed of 4000 rpm for about 300 hours. After the test, there wasn't any adhesive or abrasive wear on the cam/follower interfaces. Therefore, they decided to use ta-C coatings for valve lifters lubricated with newly formulated engine oil. Thus, a friction reduction of more than 45% is expected at an engine speed of 2000 rpm.

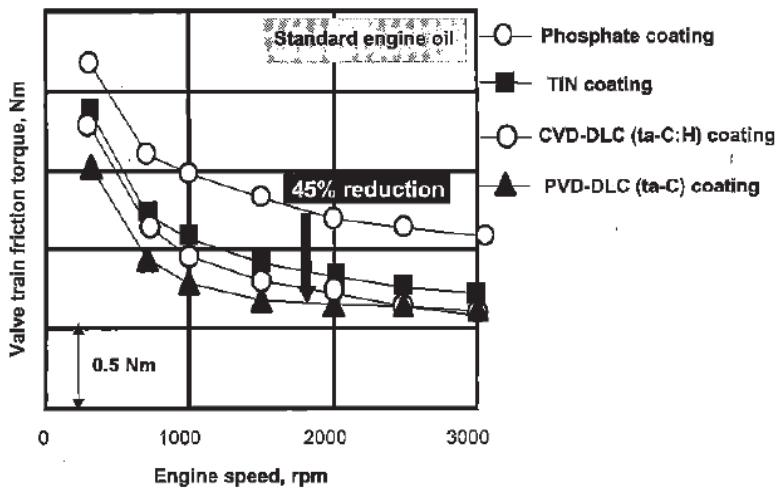

Figure 21. The effect of different coatings on the valve train friction as a function of the engine speed.

Andersson et al. [44] have studied the frictional behavior of ta-C films in different atmospheres (vacuum, oxygen, hydrogen and water vapor). Experimental results showed that the friction coefficient is lowered from 0.65 to 0.07 when passed from vacuum to water vapor. From Figure 22, it can be concluded that the best friction occurred for ta-C coated surfaces in the presence of water molecules in the test chamber.

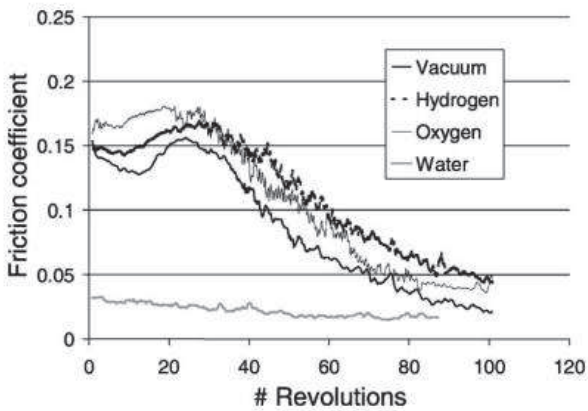

Figure 22. Friction coefficients of ta-C coated surfaces in different atmospheres [44].

In 2013, Kosarieh et al. [60] has performed a tribotest by sliding a cast iron (CI) pin on steel plate coated with 15 at % hydrogenated DLC (a-C:15H) in order to study the tribological performance when lubricated in a fully formulated oil and base oil. Results have shown that the additives containing oil can avoid the surface coated with a-C:15H from failure since these additives form a protective tribofilm on the surface. It is also concluded that base oil of group III has a better wear than that of PAO. Thus, friction reduction is not essential when using fully formulated oils since the phosphate is formed on the surface.

1.5.2.2 Other tribosystems and conditions

There also exist in the literature other coatings and materials that are able to attain super-low friction. For example, the use of molybdenum disulfide (MoS_2) and tungsten disulfide (WS_2) coatings without the presence of any amount of water results in a friction coefficient smaller than 0.01 [61]. These coatings are mostly used as applications in the field of aerospace specifically for rolling element bearings, sliding bearings and actuator gears [62].

In 1991 and 1996, Erdemir discussed the friction behavior of boric acid films [63-64]. They found that boric acid is an active super-low friction material thanks to the reaction of boric acid with ambient humidity. Thus, the use of boric acid as an ultra-low friction coating is therefore limited to humid conditions.

In 2002, Chen and his colleagues have shown that water lubrication of certain ceramics, such as silicon nitride (Si_3N_4) and silicon carbide (SiC), can lead to super low friction coefficients [65]. However one year earlier, Kato presented experimental results with oxide-based ceramics and he showed that these latter ceramics doesn't present any improvement in the friction coefficient under water lubricated conditions [66].

Later on, Ando performed many experiments in order to study the variation of a friction coefficient by using different materials for a pin-on-flat plane contact [67]. Nevertheless, he found that the variety of the material properties is the main reason behind the friction coefficient variation. Moreover, Ando concluded that the values of ultra-low friction coefficients can be obtained during low sliding speed in vacuum. Thus, he predicted that the friction coefficient decreases with very low sliding speed, even smaller than 0.1µm/sec. This shows that viscous resistance still prevails in the friction force.

It is known that superlubricity appears between two ideal surfaces. In 1989, Alsten and Granick [68] studied the phenomenon of ultra-low friction between mica surfaces in atmospheric air. They showed that when the normal load varies, thus varying the friction force, the friction coefficient remains equal to 0.0001.

However, several years ago, Amontons demonstrated that the friction coefficient is independent of the normal load for many combinations of materials [69]. Later on, Bowden and Tabor confirmed the latter fact [70-71]. Nevertheless, load-dependent friction behavior has often been reported for materials such as polymers, diamond, ceramics such as silicon carbide (SiC) and thin solid lubricating films on hardness substrates. It is

predicted that the friction coefficient decreases with increasing normal load. Thus, the Hertzian contact model is one of the models that has been used to explain the decrease in the friction coefficient with increasing contact pressure. Singer explained the usefulness of the Hertzian model for molybdenum sulfide (MoS_2)-coated bearing materials under elastic contact conditions. Singer et al. [72] show that the friction coefficient of MoS_2 coatings under elastic conditions depends on two different contributions. These contributions are described by the mechanical contact conditions accounted by the Hertzian pressure and the shear strength of the interface. An experiment was held by Singer and his colleagues in order to obtain the accurate low friction coefficients variation between the ball-on-plane contact coated with thin films of about 1 μm of MoS_2 at a speed of 2 cm/sec in dry air (humidity > 1%) at room temperature.

Moreover, some studies reported that the friction force is affected by the adhesion force [73]. This can be explained by the fact that the adhesion force caused by van der Waals force and/or surface tension of water has an influence not only on the real contact but also on the surrounding of this contact area. Therefore, the contact area includes the effective load which consists of the normal load and the adhesion force. As a result, the friction force is proportional to the sum of the normal load and adhesion force since both the friction force and the real contact area are dependent.

In 1996, Donnet et al. [74] proved that under the environment characterized by the absence of oxygen and/or water vapor, MoS_2 coatings result in an ultra-low friction. Thus, the atmosphere has a vital effect on the friction coefficient. In both ultra-high vacuum and dry nitrogen conditions, the friction coefficient reduces drastically after few cycles from 0.01 to 0.0001-0.0003. However in the case of high vacuum, the friction coefficient remains stable between 0.015 and 0.018 over hundred cycles. Whereas in air, the average friction coefficient ranges between 0.15 and 0.20 which was also observed by Moser and Lèvy [75].

1.6 Conclusion

This bibliographical chapter assists in the understanding of previous friction models in both steady and variable states. Later, the phenomenon of superlubricity and its application gives us a hope and a promising perspective for the research field.

Following this bibliographical study, we will describe in the following chapter the dynamic oscillating setup. This latter apparatus will be used for many tribosystems, allowing us to present the first series of our results.

References

[1] Thesis of Henrik Olsson, Control Systems with Friction. Lund, 1996.

[2] Frene, J., Nicolas, D. and Godet, M., Lubrication Hydrodynamique: Paliers et Butées, EYROLLES, 1990.

[3] Georges, J-M, Frottement, Usure et Lubrication : Introduction à la Tribologie et à ses applications, EYROLLES, 1999.

[4] Dowson, D., *History of Tribology,* Longman, London, 1979.

[5] Woydt, M. and Wasche, R., The History of the Stribeck curve and ball bearing steels: The role of Adolf Martens, Wear 268 (11-12), pp. 1542-1546, 2010.

[6] Andreaus, U. and Casini, P., Dynamics of friction oscillators excited by a moving base and/or driving force. Journal of Sound and Vibration 254 (4), pp. 685-699, 2001.

[7] Reynolds, O., On the theory of lubrication and its application to Mr. Beauchamp Tower's experiments of the viscosity of olive oil. Phil. Trans. Royal Soc.177, pp. 157-234, 1886.

[8] Ferri, A. A. and Anderson, J. R., Behavior of a single-degree-of freedom system with ageneralized friction law. Journal of Sound and Vibration 140 (2), pp. 287-304, 1990.

[9] Jacobson, B., The Stribeck memorial lecture. International Tribology 36, pp. 781-789, 2003.

[10] Bongaerts, J.H.H., Fourtouni and Spikes, J.R., Soft tribology: Lubrication in a complaint PDMS-PDMS contact. Tribology International, 40, pp. 1531-1542, 2007.

[11] de Vincente, J., Stokes, J.R. and Spikes, H.A., Soft lubrication of model hydrocolloids. Tribology International, 22, pp. 483-491, 2006.

[12] Hess, D. P. and Soom, A., Frictiona at a lubricated line contact operating at oscillating sliding velocities. Journal of Tribology 112 (1), pp.147- 152, 1990.

[13] Mckee, S.A. and Mckee, T.R., Journal bearing friction in the regions of thin-film lubrication. SEA Journal 31, pp.371-377, 1932.

[14] Dahl, P., A solid friction model. Technical Report TOR-0158 (3107618)-1, The Aerospace Corporation, El Segundo, CA, 1968.

[15] Dahl, P., Solid friction damping of spacecraft oscillations. AIAA Paper No. 75-1104 presented at the AIAA Guidance and Control Conference, Boston Mass, 1975.

[16] Philip, R. and Dahl, P., Solid friction damping of mechanical vibrations. AIAA Journal 14(12), pp. 1675-82, 1976.

[17] Ramberg, W. and Osgood, W.R., Description of stress-strain curve by three parameters. Tech. Note 902, National Advisory Committee for Aeronautics, Washington, 1943.

[18] Sargin, M., Stress-strain relationship for concrete and the analysis of the structural concrete sections. SM Study 4, Solid Mechanics Devision, University of Waterloo, Canada, 1971.

[19] Bliman, P. A., Mathematical study of the Dahl's friction model. European Journal of Mechanics, A/ Solids 11(6), pp. 835-848, 1992.

[20] Olsson, H., Astrom, K.J., Canudas de Wit,C., Gafvert, M. and Lischinsky, Friction models and friction compensation. Journal of Control 4, pp. 176-195,1998.

[21] Canudas de Wit,C., Olsson, H., Member, K.J. and Lichinsky, P., A new model for control of systems with friction. Automatic Control 40 (3), pp. 419-425, 1995.

[22] Nitche, R. and Gaul, L., Smart friction driven systems. Smart. Mater. Struct. 14, pp. 231-236, 2005.

[23] Hoffman, N.P., Linaer stability of steady sliding in point contacts with velocity dependent and LuGre type friction. Journal of Sound and Vibration 301 (3-5), pp. 1023-1034, 2007.

[24] Yanada, H. and Sekikawa, Y., Modeling of dynamic behaviors of friction. Mechatronics 18 (7), pp. 330-339, 2008.

[25] Khayati, K., Bigras, P. and Dessaint, L-A, LuGre model-based friction compensation and positioning control for pneumatic actuators using multi-objective output-feedback control via LMI optimization. Mechatronics 19 (4), pp. 535-547, 2009.

[26] Lu, L., Yao, B., Wang, Q. and Chen, Z., Adaptive robust control of linear motors with dynamic friction compensation using modified LuGre model 45 (12), pp. 2890-2896, 2009.

[27] Harnoy, A. and Friedland, B., Dynamic friction model of lubricated surfaces for precise motion control. In Preprint No. 93-TC-1D-2. Society of Tribologists and Lubrication Engineers.

[28] Karpenko, Y. A. and Akay, A., A numerical model of friction between rough surfaces. Tribology International 34, pp. 531-545, 2001.

[29] Bengisu, M.T. and Akay, A., Relation of dry-friction to surface roughness. ASME J Trib 119, pp. 18-25, 1997.

[30] Bengisu, M.T. and Akay, A., Stick-slip oscillations: dynamics of friction and surface roughness. J Acoust Soc Am 105 (1), pp. 194-205, 1999.

[31] Tan X., Yan, X-T., Juster, N.P., Raghunathan, S. and Wang,J., Dynamic friction model and its application in flat rolling. Journal of Materials Processing Technology 207 (1-3), pp. 222-234, 2008.

[32] Den Hartog, J. P., Forced Vibrations with Combined Coulomb and Viscous Friction. Transactions of ASME, APM-53-9, pp. 107-115, 1931.

[33] Griffin, J. H., Friction Damping of Resonant Stresses in Gas Turbine Engine Airfoils. Journal of Engineering for Power 102, 1980.

[34] Plunkett, R., Friction Damping. Damping Applications for Vibration Control, ASME AMD, ed. Torvik 38, pp. 65-74, 1980.

[35] Filippi, S., Citelli, M. and Akay, A., Measurement of transient friction hysteresis. Transient Processes in Tribology, G. Dalmaz et al.,(ed.), pp. 495-506, 2004.

[36] Filippi, S., Gola, M. M. and Akay, A., A New Design to Measure Contact Hysteresis. Proceedings of ASME-ESDA 2002, Eng. Sys. Design Analysis, Istanbul, Turkey, ESDA2002/APM-127.

[37] Griffin, J. H., A Review of Friction Damping of Turbine Blade Vibration. International Journal of Turbo and Jet-Engines 7, pp. 297-307, 1990.

[38] Menq, C. H., Bielak, J. and Griffin, J. H., The influence of microslip on vibratory response, Part I: a new microslip model. Journal of Sound and Vibration 107 (2), pp. 279-293, 1986.

[39] Menq, C. H., Griffin, J. H. and Bielak, J., The influence of microslip on vibratory response, Part II: a comparison with experimental results. Journal of Sound and Vibration 107(2), pp. 295-307, 1986.

[40] Martin, J-M. , Donnet, C. and Le Mogne, T., Superlubricity of molybdenum disulphide. Physical Review B 48(10), 1993.

[41] Erdemir, A. and Martin, J-M., *Superlubricity,*Elsevier, 2007.

[42] Ando, Y., Decreasing friction coefficient under extremely low load, in: D. Dowson, et al. (Ed.), Elastohydrodynamis 96: Fundamental and Application in Lubrication and Traction, Elsevier, Amsterdam, 1997.

[43] Enke, K., Dimigen, H. and Hubsh, H., Frictional properties of diamond-like carbon layers. Applied Physics Letters 36(4), pp. 291-292, 1980.

[44] Andersson, J., Erck, R.A. and Erdemir,A., Friction of diamond-like carbonfilms in different atmospheres. Wear 254 (11), pp. 1070-1075, 2003.

[45] Enke, K., Dimigen, H. and Hubsh, H, Frictional properties of diamond-like carbon. Applied Physics Letters 36 (4), pp. 291-292, 1980.

[46] Donnet, C. and Grill, A., Friction control of diamond-like carbon coatings. Surface and Coatings Technology 94-95, pp. 456-462, 1992.

[47] Jacob, W. and Moller, W., On the structure of thin hydrocarbon films. Applied Physics Letters 63 (13), pp. 1771-1773, 1993.

[48] Robertson, J., Deposition mechanism of diamond-like carbon, in amorphous carbon: state of art. Proceeding of 1st International Specialist Meeting on Amorphous Carbon, 1997, Silva, S. R. P., Robertson, J., Milne, W. I. and Amaratunga, GA. J., World Scientific Publicating.

[49] Robertson, J., Deposition and properties of diamond-like carbons. Material Research Society Symposium Proceeding 555 (12), 1999.

[50] Robertson, J., Electronic and atomic structure of diamond-like carbon. Semiconductor Science and Technology 18 (S 12), 2003.

[51] Casiraghi, C., Robertson, J. and Ferrari, A.C., Diamond-like carbon for data and beer storage. Materials Today 10 (1-2), pp. 44-53, 2007.

[52] Kano M., Yashuda, Y, Mabucha, Y., Ye, J. and Konishi, S., Ultra-low friction of DLC lubricated with ester-containing oil-Part 1: pin-on-disc and SRV friction tests. Processes in Tribology 43, pp. 689-692, 2003.

[53] Kano M., Yashuda, Y., Okamoto, Y., Mabuchi, Y., Hamada, T., Ueno, T., Ye, J. Konishi, S., Takeshima, S., Martin, J. M., De Barros Bouchet, M. I. and Le Mogne, T., Ultralow friction of DLC in presence of glycerol mono-eleate. Tribology Letters 18 (2), pp. 245-251, 2005.

[54] Yasude, Y., Kano, M., Mabuchi, Y. and Abou, S., Diamond-like carbon coatings for low-friction valve filter. SAE paper 2003-01-1101, 2003.

[55] Neville, A., Morina, A., Haque, T. and Voong, M., Compatibility between tribological surfaces and lubricant additives-How friction and wear reduction can be controlled by surface/lube synergies. Tribology International 40, pp. 1680-1695, 2007.

[56] Kano M., Yashuda, Y, Mabucha, Y., Ye, J. P., The effect of ZDDP and MoDTC additives in engine oil on the friction properties of DLC-coated and steel cam followers. Lubrication Science 17 (1), pp. 95-103, 2004.

[57] Kano M., Super low friction of DLC applied to engine cam follower lubricated with ester-containing oil. Tribology International 39 (12), pp. 1682-1685, 2006.

[58] Jolly-Potuz , Matta, C., De Barros Bouchet, M.I., Martin, J.M. and Sagawa, T., Superlow friction of ta-C lubricated by glycerol: An electron energy loss spectroscopy study. Journal of Applied Physics 102 (6), 2007.

[59] De Barros Bouchet, M.I. and Kano, M (2007). *Superlubricity*. Erdemir, A. and Martin, J.M. (Ed.). pp. 471-491. Elsevier B.V.

[60] Kosarieh, S. Morina, A., Lainé, E., Flemming, J. and Neville, A., Tribological performance and tribochemical process in a DLC/steel system when lubricated in a fully formulated oil and base oil. Surface & Coatings Technology 217, pp. 1-12, 2013.

[61] Directorate, M., Patterson, W. and Base, A., F. Pulsed-laser deposition of tungsten disulphide films on aluminum metal-matrix composite substrates. Scanning 11, pp. 1282-1284, 1992.

[62] Fleischauer, P. D., Tribology in the space environment, new directions in tribology. Proceedings of the 1st World Tribology Congress, ImechE Publishers, pp. 217-227, 2007.

[63] Erdemir, A., Bindal, C., Zuiker, C. and Savrun, E., Tribology of naturally occurring boric acid films on boron carbide; Surface and Coatings Technology 86-87 (2), pp. 507-510, 1996.

[64] Erdemir, A., Erck, R. A. and Robles, J., Relation of Hertzian contact pressure to friction behavior of self-lubricating boric acid films. Surface and Coatings Technology 49 (1-3), pp. 435-438, 1991.

[65] Chen, M., Kato, K. and Adachi, K., The comparisons of sliding speed and normal load effect on friction coefficients of self-mated Si_3N_4 and SiC under water lubrication, Tribology International 35 (3), pp. 129-135, 2002.

[66] Kato, K., Water lubrication of ceramics. Proceedings of the 2nd World Tribology Congress, Austrian Tribology Society, pp. 51-58, 2001.

[67] Ando, Y., Lowering friction coefficient under low loads by minimizing effects of adhesion force and viscous resistance. Wear 254 (10), pp. 965-973, 2003.

[68] Alsten, J. V. and Granick, S., Friction measured with surface force apparatus. Tribology Transactions 32 (2), pp. 246-250, 1989.

[69] Amontons, G., Mémoire de l'Académie Royale des Science, Amesterdam, pp. 257-282, 1706.

[70] Bowden, F. P. and Tabor, D., *The friction and lubrication of solids, part I*, Clarendon, Oxford, p. 98, 1950.

[71] Bowden, F. P. and Tabor, D., *The friction and lubrication of solids, part II*, Clarendon, Oxford, chapter MXIV, 1964.

[72] Singer, I.L., Bolster, R. N., Wegand, J., Fayeulle, S. and Stupp, B. C., Hertzian stress contribution to low friction behavior. Applied Physics Letters 57 (10), pp. 995-007, 1990.

[73] Ando, I. and Ino, J., Friction and pull-off forces on submicron-size asperities. Wear 216 (1-2), pp. 115-122, 1998.

[74] Donnet, C., Martin, J. M., Le Mogne, T. and Belin, M., Super-low friction of MoS_2 coatings in various environments 29 (2). Tribology International 29, pp. 123-128, 1996.

[75] Moser, J. and Lèvy, F., MoS2−x lubricating films: structure and wear mechanisms investigated by cross-sectional transmission electron microscopy. Thin Solid Films 228 (1-2), pp. 257-260, 1993.

2 A NOVEL EXPERIMENTAL TECHNIQUE

2 A Novel Experimental Technique

Chapter 2: A Novel Experimental Technique

2.1 Introduction

It is essential to reduce energy consumption, especially in the transportation field. Controlling energy loss by reducing friction can partially attain this issue. However, the tribological systems presenting low friction coefficients are considered as a challenge for many researchers in the area of tribology. Actually, the classical tribometers measure the friction coefficient directly in which this coefficient is simply defined as the ratio of the total friction force (usually tangential force) to the normal load applied on the contact. Nevertheless in real life applications, neither the total friction force nor the normal load is measured directly. They are usually determined from the tangential and normal force measured through a transducer in contact with the assembly parts of the system. However, it is very difficult to obtain a precise and accurate measurement for the friction corresponding to an interface described by low shear strength [1 and 2].

Furthermore, most of the mechanical systems are described by nonlinear behavior [3]. Thus, with the development of nonlinear systems, material with higher damping has been used for reducing the vibration and noise of the systems. The friction is the major cause of nonlinearities in a system. However, the main source of energy dissipation corresponds to friction and viscous damping that is related to the viscosity of the lubricant. One of the drawbacks of the classical tribometers is that an overall value of the friction coefficient is measured, in steady-state sliding conditions. The conventional tribometer does not allow characterizing friction by velocity-dependent and velocity-independent coefficients after a single experiment.

In order to overcome these drawbacks, an experimental apparatus for measuring friction has been developed corresponding to a sphere-on-flat friction machine [4]. This novel apparatus is described by its performance in measuring low friction coefficients since the signal excitation duration becomes larger as the dissipation forces are increased. Consequently, the lower the friction is, the more the friction can be evaluated with accuracy and precision. During the experimental sliding test, both the displacement and velocity free responses of the spherical pin are measured simultaneously using a laser velocimeter. This permits the determination of both the kinetic and potential energies in addition to the energy decay curve of the corresponding dynamic system.

Based on these measurements, it is possible to distinguish the different contributions of friction, i.e. the velocity-dependent and velocity-independent contributions.

In this chapter, we will start by presenting the new technique used in this chapter. A description of its parts, tribological configuration and mechanical system will be demonstrated. Then, we will show the importance of this apparatus by explaining the

measurements that can be attained using this technique. Next, some results are presented for different tribosystems including diamond-like-carbon (DLC) coatings, some lubricants and additives at different parameters such as different normal loads, temperatures, contact pressures, natural frequencies, etc. Finally, we will end up with a conclusion summarizing our experimental results and proposing some ideas regarding the friction used which will be spread in the following chapter.

2.2 The novel technique

Based on the theoretical background reported in the above section, a new technique, called the "dynamic oscillating tribometer" has been developed in our laboratory by Rigaud et al. [4] in order to characterize the friction coefficient into different contributions. The experimental setup is also known as the "relaxation" and harmonic tribometer [5-6].

2.2.1 Description of the original tribometer

This apparatus corresponds to a sphere-on-plane contact tribometer with a reciprocation movement. Figure 1 shows a schematic representation of the new tribometer with some of its major parts. The apparatus consists of a pair of elastic blades. They are made of steel having a dimension of 76*10*0.1 mm. The dimension of the steel blades are selected in a way to couple this mode and the first mode corresponding to the vertical vibrations and governed by the Hertzian contact law [7-8]. These steel blades allow the spherical pin to oscillate horizontally. Initially, the head is set out of the equilibrium position, allowing a deviation parallel to the sliding direction. An electromagnet is used to fix the initial horizontal position parallel to the motion allowing its amplitude to vary up to a limit of $1.0*10^{-3}$ m. As the head is released, the elastic energy accumulated in the elastic bi-blades is released as well. This produces the oscillations of the system.

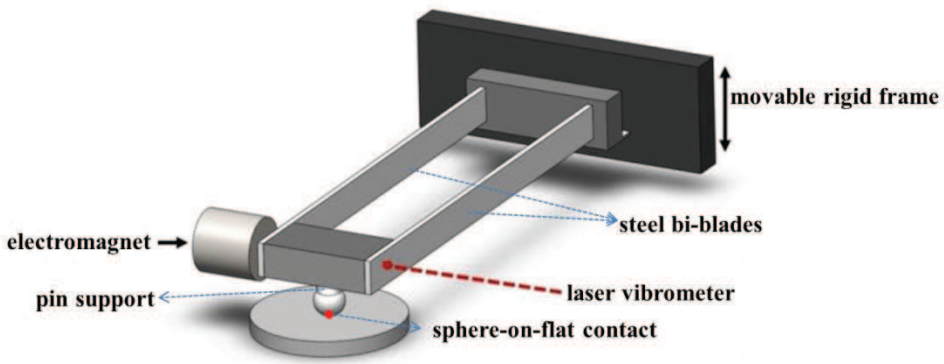

Figure 1. A schematic representation of the novel technique.

Moreover in [5], they presented experiments with the new apparatus by considering no contact between the spherical pin and the flat plane in order to identify the damping and dynamic characteristics of the instrument itself. They found that there are different reasons

behind the apparatus dissipation: inner damping derived from the used materials, damping caused by the micro-sliding between the assembly mechanical parts, damping caused by air (or liquid) displacement, the acoustic radiation of the sliding surfaces' vibrations and that transmitted to the flat plane. For these reasons, under mixed and boundary lubrication, friction coefficients below 10^{-3} are unlikely to occur in such practical cases. Coefficients below 10^{-3} are only observed in hydrodynamic and aerodynamics lubrication regimes (i.e. thrust bearings).

The materials used for the machine and its connecting mechanical parts are carefully chosen in a way to minimize the damping of the apparatus. More precisely, the damping corresponding to the apparatus was investigated by measuring the free oscillating response of the system without any contact. This later is appeared to be equivalent to viscous damping with a damping coefficient close to 0.0011.

2.2.1.1 The mechanical dynamic system

The tribometer is characterized by a mass-spring-damper mechanical system (see Figure 2). Initially, this system is modeled by a pseudo-linear kinematic friction coefficient, μ_K. The equation of motion is written by:

$$m\ddot{x} + c\dot{x} + kx = -\mu_K(\dot{x}) \quad (1)$$

with

$$\mu_K(\dot{x}) = \mu_0 sign(\dot{x}) + \mu_1\dot{x} \quad (2)$$

x is the displacement of the system, $\dot{x}$ is the sliding velocity and $\ddot{x}$ is the corresponding acceleration. m is the mass of the system, thus the mass of the spherical pin, c is the damping coefficient, k is the spring stiffness and N is the normal load applied on the spherical pin. μ_0 and μ_1 are two different contributions of friction. μ_0 can be defined as a velocity-independent friction coefficient. Then, μ_0 does not depend on the sliding velocity and it differs from the static and dynamic friction coefficients at constant speed. On the other hand, the damping friction coefficient, μ_1 can be considered as a velocity-dependent friction contribution. Based on the previous concept, this tribometer allows the evaluation of the two introduced friction coefficients, μ_0 and μ_1, thanks to the free dynamic oscillating responses measured.

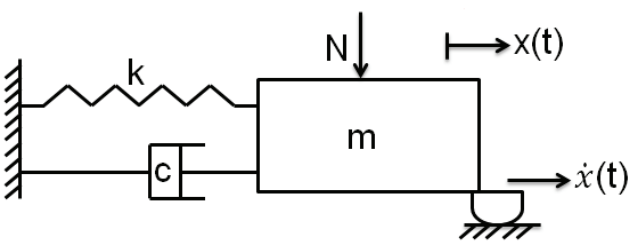

Figure 2. Mass-spring-damper mechanical oscillating system.

Recently, Liang and Feeny [9-10-11] presented an exact method that permits the estimation of both Coulomb and viscous damping friction coefficients. These parameters are identified

from the successive peaks of either the displacement or acceleration vibrational responses. However, Jacobsen and Ayre [12] have identified the analytical solution of the free dynamic responses along with its corresponding Coulomb and viscous friction since 1958. He also presented an approximate method to determine both parameters. Moreover, earlier in 1924, Lorenz [13] was the first who observed that the successive amplitude in vibrational response of a system decreases with a constant slope. Thus, one can extract Coulomb friction coefficient (see equation 1) from the constant decrement of the free oscillations described by a constant damping behavior. Later on in 1945, Rayleigh [14] was able to determine the viscous friction coefficient (see equation 2) from the logarithmic decrement method proposed by Helmhotz [15]. The method explains that the difference in the logarithms of the vibrational responses successive is approximately constant.

$$\mu_{Coulomb} = \frac{1}{4\eta}(y_p - y_{p+2n}) \qquad (3)$$

$$\mu_{viscous} = \frac{1}{4\pi\eta} ln(\frac{y_p}{y_{p+2n}}) \qquad (4)$$

y_p and y_{p+2n} are two points corresponding to the displacement free response.

Thus, μ_0 and $\mu_1$can be determined from the analysis of the mechanical energy decay, deduced from both the displacement and velocity-time responses. The values of μ_0 and $\mu_1$are optimized using the least-square method [16].

2.2.1.2 Applying a normal load

A rotational knob permits to apply a micrometric vertical position in which a normal load, N is applied on the contact. The normal load is accommodated through an elastic deformation of the steel blade corresponding to a cantilever beam. The apparatus has been calibrated using a precise balance instead of the plane. Thus, a linear relationship is occurred corresponding to the measured force as a function of the vertical displacement described by a constant slope of 1 $N.mm^{-1}$. The vertical displacement ranges between 0 and 2 mm corresponding to an applied normal load varying between 0 to 0.64 N. The applied normal load remains constant during the oscillatory test since the spherical pin motion is very small and also parallel to the flat plane.

2.2.1.3 Temperature variation

It is also essential to measure friction at variable temperatures up to 100 °C. Thus, a thermocouple resistance is connected to the flat plane in order to heat the contact. The apparatus has been calibrated using the thermocouple. Thus, the voltage is increased using a DC power supply that leads to an increase in the temperature. Therefore, we are able to have a relationship for the temperature as a function of the voltage (see Figure 3).

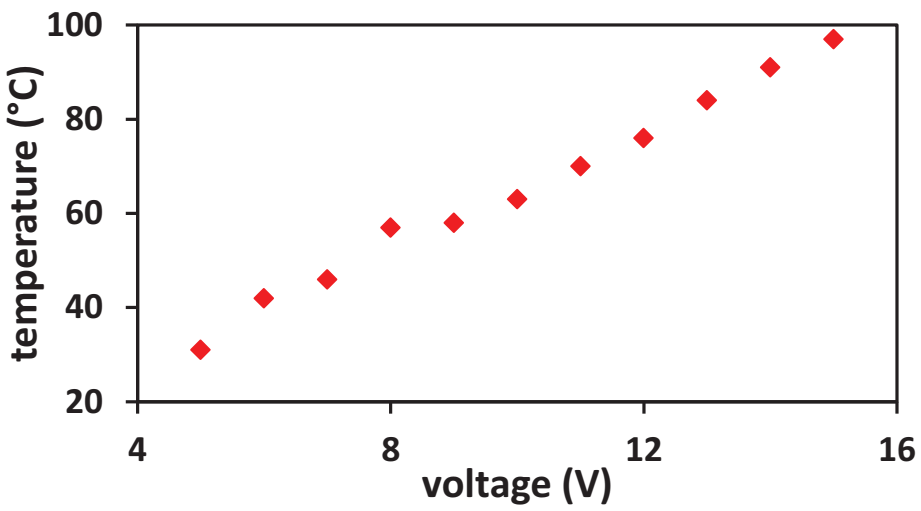

Figure 3. Temperature (°C) as a function of the voltage (V) resulted from the calibration process.

2.2.1.4 Experimental measurements

The displacement and velocity time responses are determined using a laser vibrometer based on Doppler principle, measuring back-scattered laser light at the vibrating spherical pin. Thus, the mechanical energy decay of the system can be directly determined.

Moreover, the electrical contact resistance (ECR) between the two counterparts is measured. A DC voltage is applied on the two contacting surfaces resulting current passing through the interface is measured. Both the current and voltage are limited to low values, in order to limit the electrical power that could be dissipated in the contact. These limited values are respectively $5*10^{-3}$ A and $2*10^{-3}$ V. The dynamic of ECR measurement is quite large ranging from 1 Ω to 10^{8} Ω. Consequently; the electric contact resistance results are plotted in logarithmic scale as a function of the time. Obviously, the measurement of the ECR is restricted to contacts in which the two rubbing materials are conductive.

Eventually, the evaluation of the friction coefficients, μ_0 and μ_1, can be derived. The measurement of friction in this novel technique is based on the oscillating behavior of the mass-spring damper system.

The repeatability of the oscillating experiments can be checked by running each experiment n-times for the same contact conditions.

2.3 Applying lubricated diamond-like-carbon coatings in no-wear conditions using the novel technique

This section focuses on studying the effect of two kinds of DLC (tetrahedral hydrogen-free, ta-C and hydrogenated a-C:H) coatings on steel surfaces lubricated with either oleic acid or glycerol using the new technique explained in section 2.2. Diamond-like carbon coatings are becoming potential candidates for automotive engine parts thanks to their physical and tribological properties [17]. They are considered unique because of their excellent friction and

wear resistance properties [18]. Thus, these tribological systems are known in the literature described by an extremely low friction coefficient, approaching 10^{-2}. They are also used in engine components in order to improve the fuel economy. On the other hand, both glycerol and oleic acid are considered as biodiesel lubricants. They are characterized as important renewable fuel for transportation sector [19]. Glycerol is an ester that is usually used as a friction-reducing additive in engine oils. Previously, the effect of glycerol is studied on ta-C coatings using an analytical ultra-high vacuum (UHV) tribometer. Results show that ultra-low friction is obtained [20]. Moreover, oleic acid which is a fatty acid, is increasingly applied as raw material in various industrial areas? It is described by its great advantage for excellent biodegradability and renewability [21]. Therefore, the following study permits us to measure with a great accuracy and without any force transducer the two different contributions of friction, μ_0 and μ_1 of steel/steel, steel/DLC and DLC/DLC contacts. Moreover, the results will be compared with those applied using a conventional reciprocating cylinder-on-plane tribometer working on constant speed.

2.3.1 Tribological parameters

The spherical pin-on-flat contact is conducted in different tests. Four sets of experiments are performed. The first one is described by a steel spherical pin sliding on a steel flat disc. The second contact is a steel spherical pin sliding on a circular steel flat disc coated with hydrogen-free diamond-like carbon (DLC), ta-C, then on a circular steel flat disc coated with hydrogenated diamond-like carbon (DLC), a-C:H. The last set is described by a contact of a steel spherical pin on a circular steel flat disc, both surfaces coated with ta-C. Table 1 shows the different sets of the contact.

sphere	flat plane
Steel	steel
Steel	steel coated with DLC (ta-C)
Steel	steel coated with DLC (a-C:H)
steel coated with DLC (ta-C)	steel coated with DLC (ta-C)

Table 1. Different sets of the contact.

Each of the four contacts is applied twice with two pure lubricants, oleic acid and glycerol. All the samples have approximately the same roughness, which is about 5 nm Ra. Figure 4 presents optical images of the three DLC-coated samples.

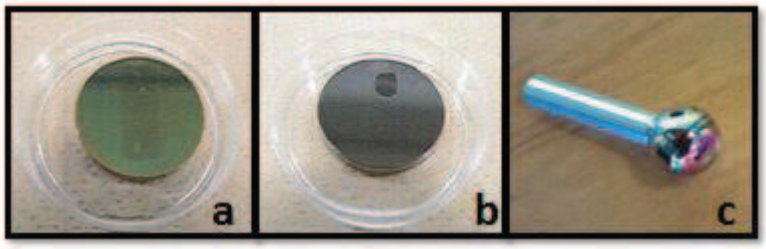

Figure 4. (a) Circular flat steel discs coated with ta-C. (b) Circular flat steel plane coated with a-C:H. (c) Spherical steel pin coated with ta-C.

The steel spherical pins have a diameter of $6.0*10^{-3}$ m and are made of hardened bearing steel (AISI 52100). The steel flat disc has dimensions of $9.0*10^{-3}$ m length, $7.0*10^{-3}$ m width and $2.5*10^{-3}$ m in thickness. However, the ta-C coated steel spherical pins are of $9.0*10^{-3}$ m-diameter and both the ta-C and a-C:H coated steel planes measure $33.0*10^{-3}$ m in diameter and $2.5*10^{-3}$ m in thickness.

The steel spherical pins and the steel flat discs are prepared by a polishing process using metallographic silicon carbide papers in three consecutive steps of P400, P1200 then P2400, in order to obtain a mirror-polished surface. The procedure is terminated by polishing the sample with a monocrystalline $1.0*10^{-6}$ m diamond suspension for few minutes.

As for the samples coated with diamond-like carbon (ta-C and a-C:H), they were prepared by Kano et al., where ultra-low friction has been reported [22]. The polished carburized steel disc and the hardened steel pin are coated by ta-C of $0.5*10^{-6}$ m thickness. The ta-C coatings were deposited by a PVD technique, Filtered Arc ion plating. This special deposition method enables to avoid droplets of carbon on the surface and then the final roughness is the same as the substrate. They did not contain any hydrogen [23]. The hydrogen-containing DLC (a-C:H) coating is applied to the polished carburized steel disc with $1.0*10^{-6}$ m thickness by a plasma-assisted chemical vapor deposition (CVD) process from hydrocarbon gas. It contains about 20 at.% of hydrogen [24]. This hydrogen content is evaluated by SIMS analysis and compared with a hydrogen content well-known standard sample. The surface roughness of these two kinds of coatings is in the range $5*10^{-9}$ m range [22].

2.3.2 Operating conditions with the dynamic oscillating tribometer

The oleic acid $CH_3(CH_2)_7CH=(CH_2)_7COOH$, used as a lubricant, is defined by a dynamic viscosity of 0.028 Pa.s at room temperature. The other lubricant used, glycerol $C_3H_8O_3$, is much more viscous than that of oleic acid and has a viscosity of 0.610 Pa.s at room temperature. This permits the lubrication regime in the experiments to be varied. These lubricants have a quite low piezo-viscosity coefficient (between 5 and 10 GPa^{-1}, depending on the temperature).

The experimental test starts without applying a normal load and without adding lubricant in the contact. Then, a lubricant, oleic acid or glycerol, is added in the contact with an applied normal load, ranging from 0.05 to 0.60 N. The corresponding Hertzian pressure varies from $243*10^6$ to $560*10^6$ Pa. The liquid stays in the contact by capillary forces only.

The experiment takes place at room temperature. The tests last about 20 seconds for those without a normal load, and 3 seconds or less for those with a normal load applied. Each experiment consists of four repetitions with the same conditions in order to check the repeatability of the oscillating time responses. The initial displacement is fixed to $667*10^{-6}$ m. The initial velocity is 0 m/s when the oscillator is released.

2.3.3 Reciprocating traditional tribometer

In parallel, a traditional friction test was performed previously by using a 5 mm long steel cylindrical pin (diameter 9 mm) on the two samples coated with DLC (ta-C and a-C:H) lubricated with oleic acid using the classical reciprocating tribometer (Figure 5).

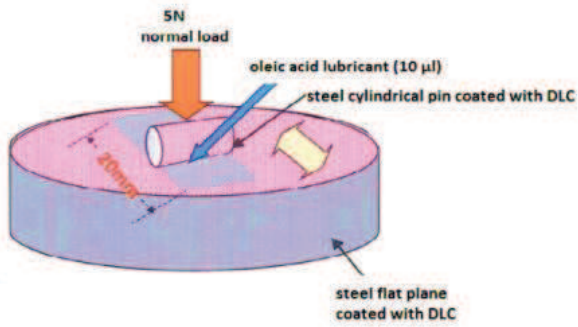

Figure 5. A schematic of the steel cylindrical pin on the circular flat steel plane both coated with DLC coatings. The contact is lubricated with oleic acid.

The friction test had a duration of about 1800 seconds. The temperature was fixed at 296 K with a maximal speed of $55*10^{-3}$ m/sec and a maximum pressure of 200 MPa was applied. In another study, Kano [24] was able to approach "superlubricity" by sliding three hardened steel cylindrical pins on a hydrogenated-free diamond-like carbon (DLC) flat plane (ta-C) lubricated with a poly-alfa-olefin (PAO) oil containing GMO. The test motion is described as reciprocating as shown from the wettability of the plane sample after the test is performed on the reciprocating tribometer (see Figure 6).

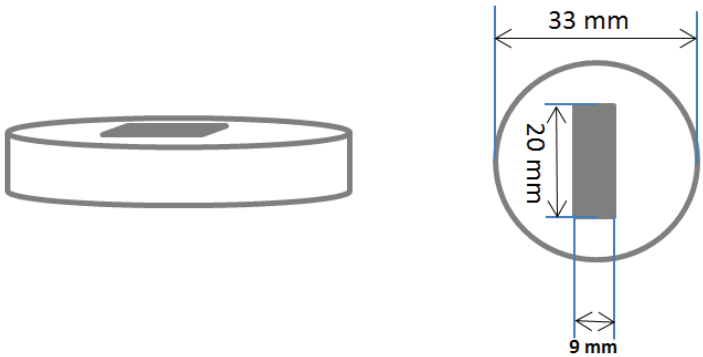

Figure 6. Geometric representation of the DLC (ta-C/a-C:H) coated planes after test. The wettability of the plane (in gray) describes that the reciprocating test motion.

2.3.4 Results

2.3.4.1 Intrinsic internal damping of the apparatus

The first step in this experimental technique is to characterize the internal damping of the instrument itself, without any contact or lubricant meniscus. This procedure has a major importance in determining the limit of sensitivity of the future experiments. The system is described by a free damped oscillation, with the same initial elastic energy in the elastic setup. The initial out-of-equilibrium position is set to $667*10^{-6}$ m. After releasing the elastic bi-blade, the system is found to relax during more than 300 oscillations. Identification of the experimental response is then processed. The viscous-type contribution value is found to be $\mu_1 = 0.0011 \pm 0.0002$. The transient coefficient at zero speed is found to be negligible (μ_0 less than 10^{-5}). These values do not depend on the nature of the upper and lower surfaces. As expected, the intrinsic damping of such an elastic 1D oscillator is purely viscous, in the millimeter range value. We will observe that for all the experiments run on loaded contact, dry or lubricated, the velocity-dependent contribution as identified by the technique is always larger than that of the instrument itself.

2.3.4.2 Results of contacts lubricated with oleic acid

In this subsection, we will present and discuss the results of different contacts lubricated by oleic acid.

2.3.4.2 a) steel/steel contacts

We carried out 4 sets of experiments using the steel/steel contact as a reference for the other contacts lubricated with oleic acid. Different normal loads were applied varying from 0.05 N to 0.40 N, corresponding to a maximum contact pressure of $243*10^6$ to $486*10^6$ Pa, respectively. In the contrary to the traditional tribometers, it is important to notice that pressure contact is conserved during the tests on the new tribometer because practically no wear in the Hertzian contact is visible by optical microscopy. At the beginning of the experiment, 50µl of oleic acid is injected in the interface. For each normal load, the test is repeated four times in order to ensure the experimental accuracy. Figure 7 presents the velocity free responses at each normal load applied. Unlike the system without contact characterized by a purely viscous damping, the steel-on-steel contact exhibits a transient friction contribution at zero speed, μ_0. The viscous damping coefficient, μ_1, for this set of experiments is found negligible compared to μ_0.

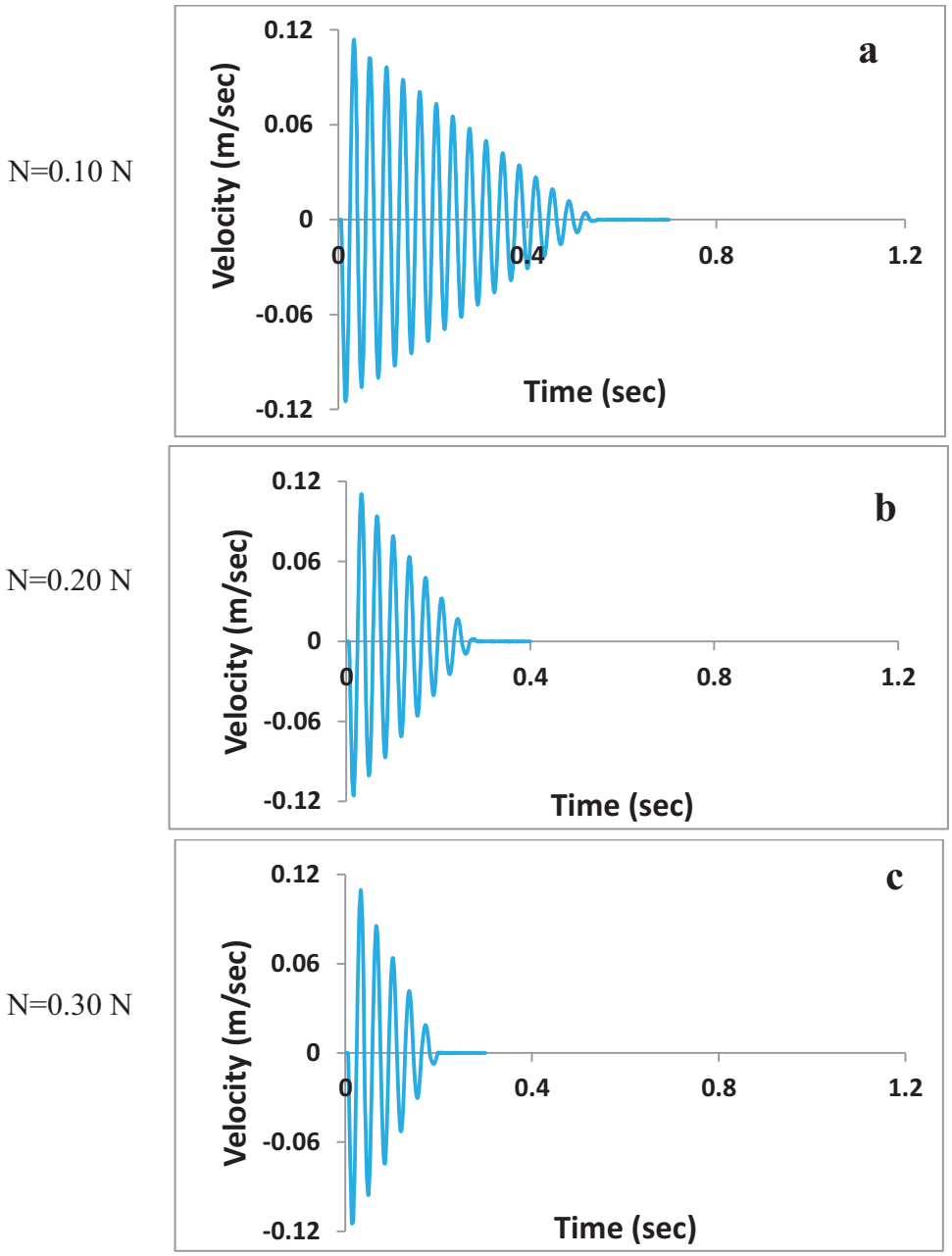

Figure 7. Velocity free responses for steel/steel contacts lubricated with oleic acid at (a) N=0.10 N, (b) N=0.20 N and (c) N=0.30 N.

Figure 8 presents the electrical contact resistance (ECR) in logarithmic scale at the steel on steel contact. For oleic acid, there is always a solid contact during sliding, even at maximum velocity. The logarithmic value of the ECR is fluctuating during the oscillating test (Figure 8) showing that full film lubrication cannot be achieved. After stopping, the final value of ERC is about 3 log(Ω). This unexpected high value is explained by the presence of some insulating products in the actual interface or in other parts of the electronic circuit. Thus, we can conclude that the system runs in the severe mixed lubrication regime with a friction that is independent on the velocity. As the pressure applied increases, the friction contribution, μ_0, increases slightly.

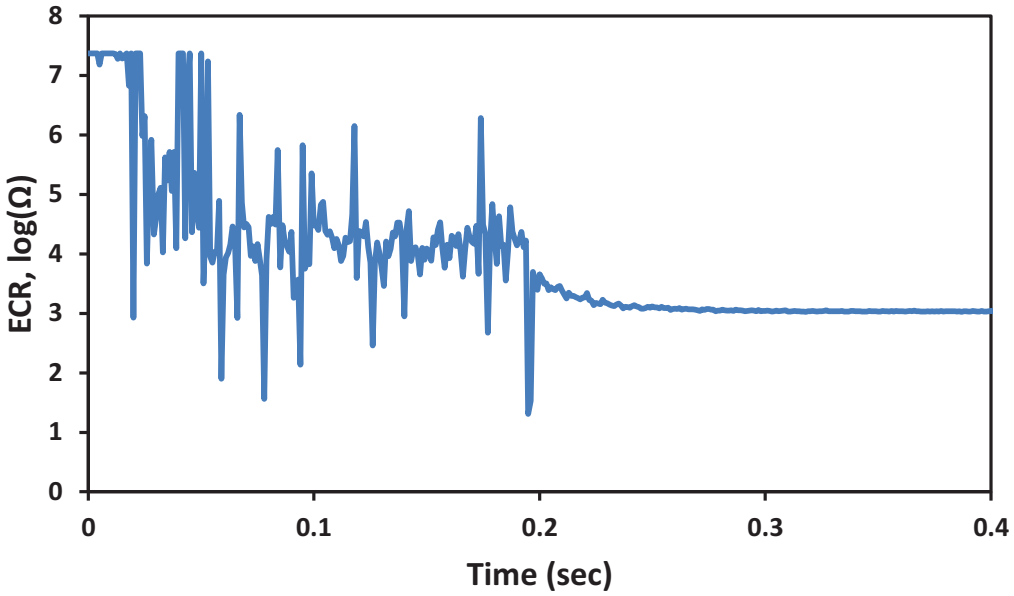

Figure 8. Electrical contact resistance for steel/ steel contact lubricated with oleic acid, N=0.20 N.

The film thickness of oleic acid at the interface between steel-on-steel contact is calculated using the Harmock's theory. At room temperature, the viscosity η of oleic acid is taken to be 27.64 mPa.sec and its corresponding piezo-viscosity coefficient α is 7 GPa^{-1}. At the maximum velocity (≅0.11 m/sec), the film thickness of oleic acid is found to be 9.10 nm.

2.3.4.2 b) steel/ta-C contacts

We carried out 6 sets of experiments using the steel/ta-C coated contact lubricated with oleic acid. Different normal loads were applied, varying from 0.05 N to 0.50 N, corresponding to contact pressure of $243*10^6$ to $530*10^6$ Pa respectively. At the beginning of the experiment, some droplets of oleic acid are added in the contact. For each normal load, the test is repeated four times in order to ensure the experimental accuracy. Figure 9 presents the velocity free responses at each normal load applied. In this case of contact, unfortunately, we are not able to measure the ECR because DLC coated surfaces are not electrically conductive.

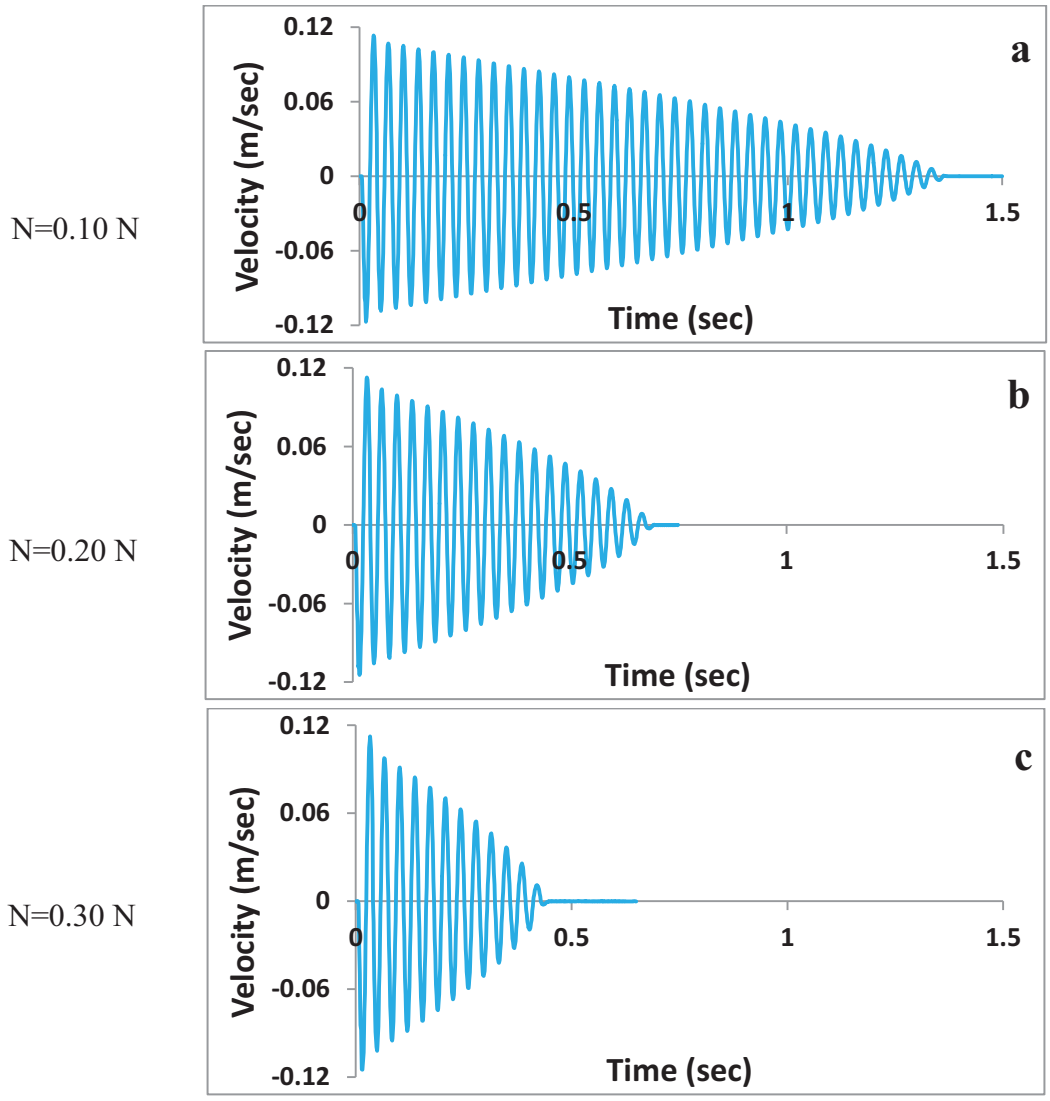

Figure 9. Velocity free responses for steel/ta-C coated contacts lubricated with oleic acid at (a) N=0.10 N, (b) N=0.20 N and (c) N=0.30 N.

The free responses in Figure 9 shows that steel/ta-C coated contacts are much less damped compared to that of steel-on-steel contacts, although the roughness of surface is the same. Similar to steel/steel contact, the steel/ta-C coated contact exhibits a transient friction coefficient, μ_0 and a negligible viscous damping coefficient, μ_1. However, μ_0 decreases significantly when the lower surface is coated with ta-C. For example at 0.10 N, steel/ta-C coated contact has a solid damping contribution μ_0 =0.033 compared to steel-on-steel contact which has a μ_0 =0.101. This shows that DLC coatings play an essential role in decreasing the zero speed friction contribution even if only the lower surface is coated with ta-C.

2.3.4.2 c) steel/a-C:H contacts

Six sets of experiments are performed on the steel/a-C:H coated contact lubricated with oleic acids. Different normal loads are applied varying from 0.05 N to 0.50 N, corresponding to contact pressure of $243*10^6$ to $530*10^6$ Pa, respectively. At the beginning of the experiment, some droplets of oleic acid are added between the two surfaces. For each normal load, the test

is repeated four times in order to ensure the experimental accuracy. Figure 10 presents the velocity free responses at three different normal loads applied.

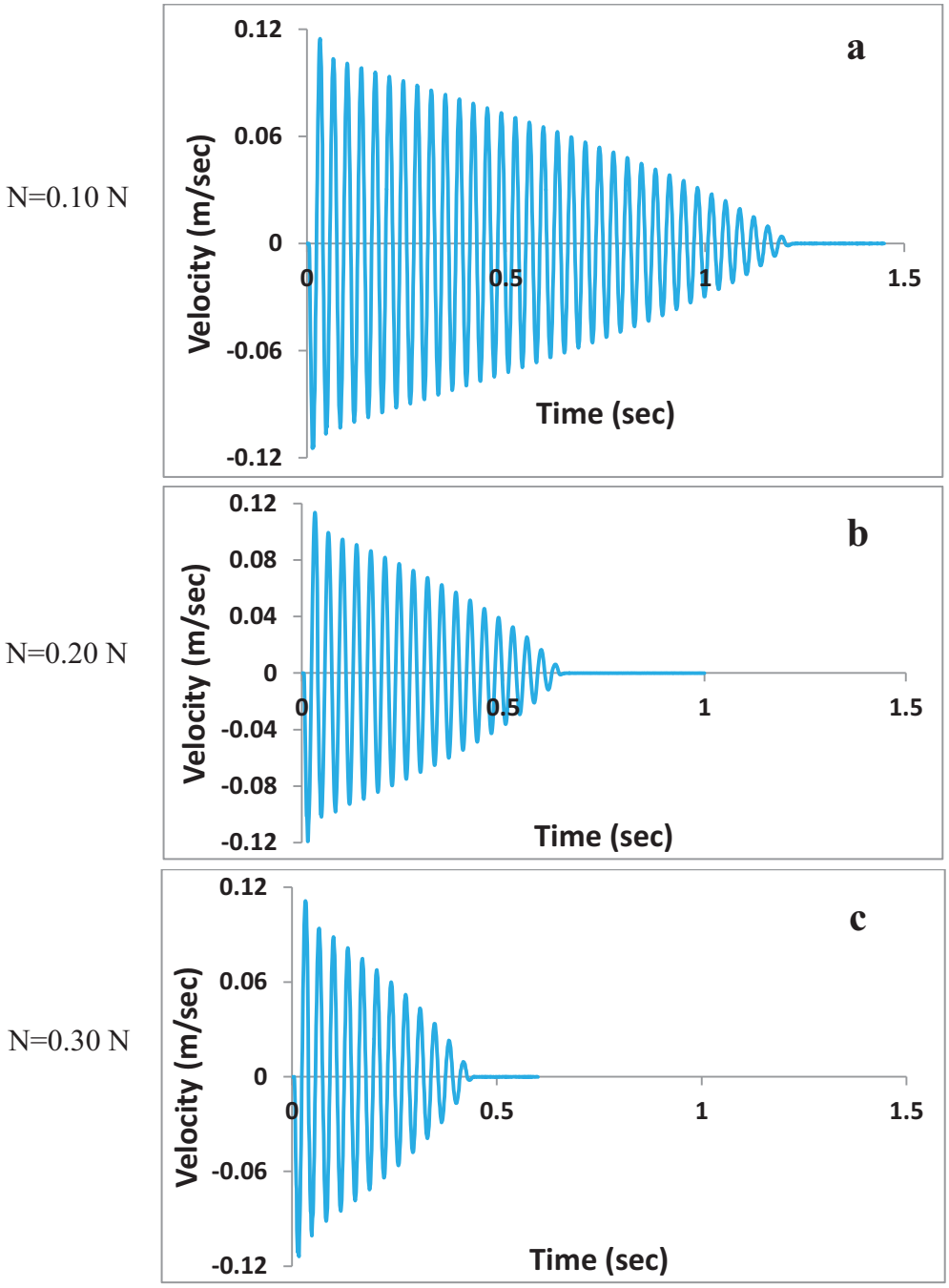

Figure 10. Velocity free responses for steel-on-a-C:H coated contacts lubricated with oleic acid at (a) N=0.10 N, (b) N=0.20 N and (c) N=0.30 N.

Figures 10 (a) and (b) show that the free responses of steel on a-C:H coated contacts are slightly more damped compared to that of steel/ta-C coated contacts. Similar to steel-on-steel contact, the steel/a-C:H coated contact exhibits a transient friction coefficient, μ_0 and a negligible viscous damping coefficient, μ_1. However, μ_0 decreases when the lower surface is coated with a-C:H. Hydrogenated (a-C:H) and hydrogen-free (ta-C) diamond-like carbon coatings have approximately the same effect on μ_0. Table 2 compares the values of μ_0 for

steel/steel and steel/DLC coated contacts lubricated with oleic acid. The results of μ_0 for the three other repeated tests give very close values. Thus, the error of μ_0 for the repeated tests is ±0.001 as shown in Table 2.

Oleic acid lubricated contacts	N=0.10 N (±0.001)	N=0.20 N (±0.001)	N=0.30 N (±0.001)
Steel/steel	0.101	0.099	0.093
Steel/ta-C coated	0.033	0.033	0.035
Steel/a-C:H coated	0.037	0.035	0.034

Table 2. Transient friction coefficient, μ_0, for contacts lubricated with oleic acid.

2.3.4.2 d) ta-C/ta-C contacts

We carried out 11 sets of experiments using the ta-C/ ta-C coated contact lubricated with oleic acid. Different normal loads are applied varying from 0.05 N to 1.0 N, corresponding to contact pressure of $185*10^6$ to $503*10^6$ Pa, respectively. At the beginning of the experiment, 50µl of oleic acid is injected between the interface. For each normal load, the test is repeated four times in order to ensure the experimental accuracy. Figure 11 presents the velocity free responses for two different normal loads applied.

N=0.40 N

N=0.90 N

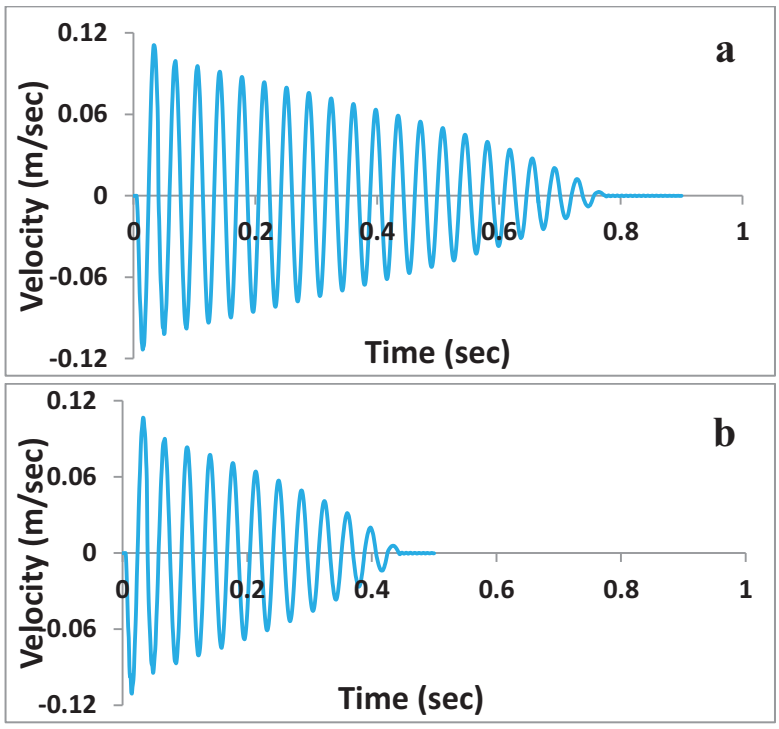

Figure 11. Velocity free responses for steel/ a-C:H coated contacts lubricated with oleic acid at (a) N=0.40 N and (b) N=0.90 N.

Figure 11 (a) shows that the free responses of ta-C/ ta-C coated contacts are more damped compared to that of steel-on-steel, steel/DLC (ta-C and a-C:H) coated contacts. Similar to steel/steel and steel/DLC contacts, the ta-C/ta-C coated contact exhibits a transient friction

coefficient, μ_0 and a negligible viscous damping friction contribution, μ_1. Table 3 presents μ_0 corresponding to the four different contacts at $486*10^6$ Pa. Both hydrogen-free (ta-C) and a-C:H coated contacts have lower μ_0 than steel/steel oleic acid lubricated contacts. For steel/a-C:H contact, μ_0 gave practically the same value for the four repeated tests.

Oleic acid lubricated contacts	μ_0	Error
Steel/steel	0.086	±0.001
Steel/ta-C coated	0.035	±0.001
Steel/a-C:H coated	0.034	±0.001
ta-C/ ta-C coated	0.027	±0.001

Table 3. Transient friction, μ_0, for contacts lubricated with oleic acid at $486*10^6$ Pa.

Figure 12 presents the transient friction coefficient, μ_0 as a function of contact pressure in all cases at room temperature. For oleic acid lubricated contacts, there is no clear effect of the velocity on the friction. Thus, we can say that these systems are mainly lubricated under the boundary regime or the severe thin film EHL on the Stribeck curve.

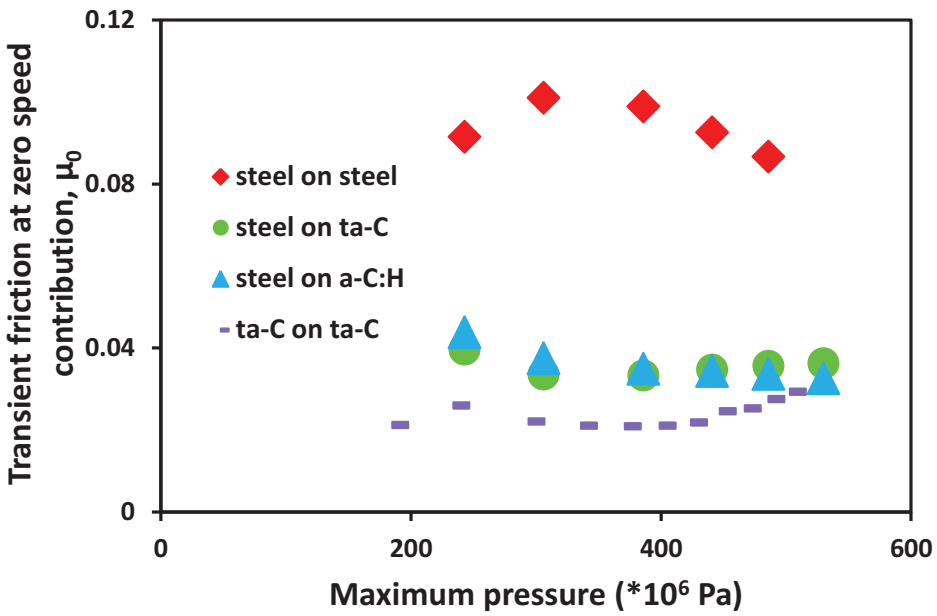

Figure 12. Transient friction contribution, μ0, as a function of the maximal pressure for steel/steel, steel/ta-C, steel/a-C :H and ta-C/ta-C contacts.

The above results (Figure 12) are coherent with Kano's results with tests at constant speed (Figure 13) performed previously on the 3 contacts, steel/steel ta-C/ta-C and a-C:H/a-C:H coated contacts lubricated with oleic acid using the reciprocating tribometer having a cylinder-on-disc configuration (Figure 5). It is also interesting to see that for sliding speeds below 50 mm/s, Kano's results show no speed significant dependence of friction, in agreement with our data. Results with this new technique show that the ta-C/ta-C coated contact gives the lowest friction. However, the friction values are not exactly

comparable with Kano's results since the conditions, parameters and geometry configurations of both the reciprocating tribometer and the dynamic oscillating tribometer are not the same. Moreover, our conditions are not steady-state.

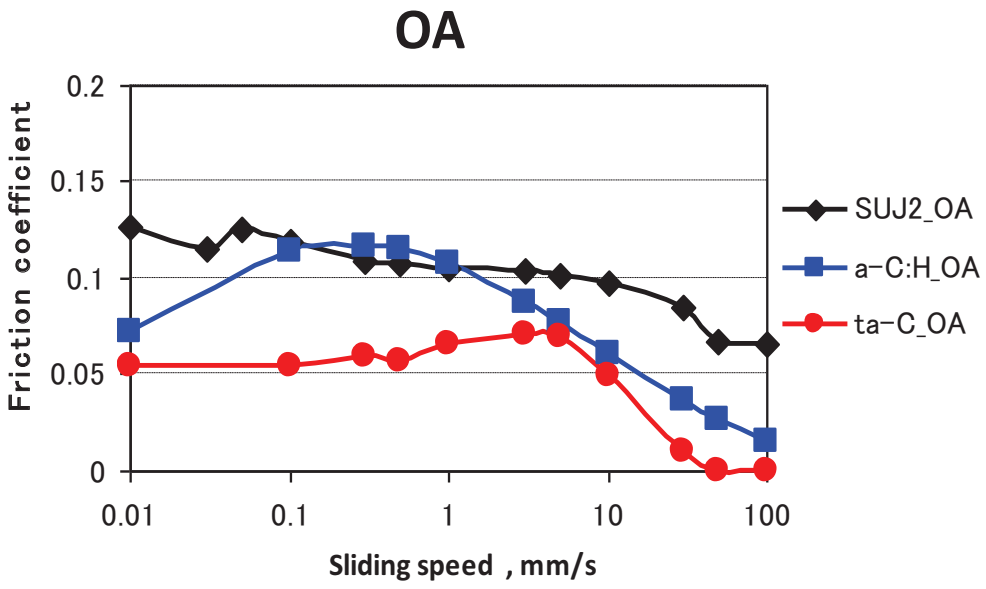

Figure 13. Friction coefficient as a function of the sliding speed of 3 tribosystems (black: steel/steel, blue: a-C:H/a-C:H and red: ta-C/ta-C) lubricated by oleic acid performed by Kano.

2.3.4.3 Results of steel/steel, steel/ta-C, steel/a-C:H and ta-C/ta-C contacts lubricated with glycerol

In this subsection, the results of different contacts lubricated with glycerol will be studied and explained.

2.3.4.3 a) Free responses

The same sets of experiments are repeated with the same normal loads, but in the presence of pure glycerol as a lubricant. Because it is much more viscous, glycerol lubricated contacts exhibit the existence of both the transient friction at zero-speed and viscous damping friction coefficient, μ_0 and μ_1 respectively. This may be explained by the fact that glycerol is 20 times more viscous than oleic acid at ambient temperature. Figure 14 represents the velocity free responses for the 4 different contacts at $486*10^6$ Pa.

Steel/steel contact

N= 0.40 N

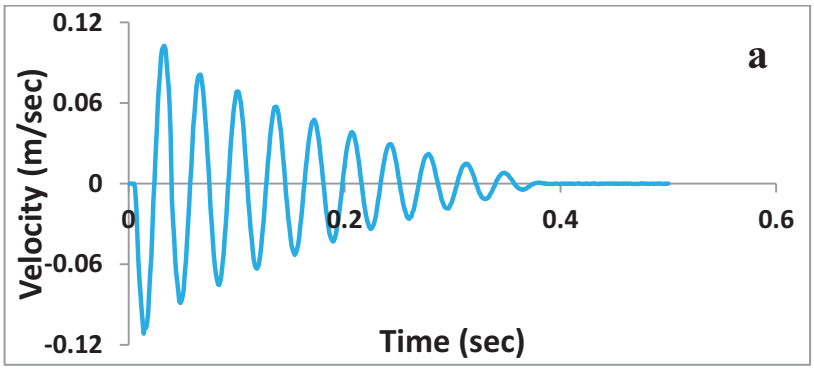

Steel/ta-C coated contact

N= 0.40 N

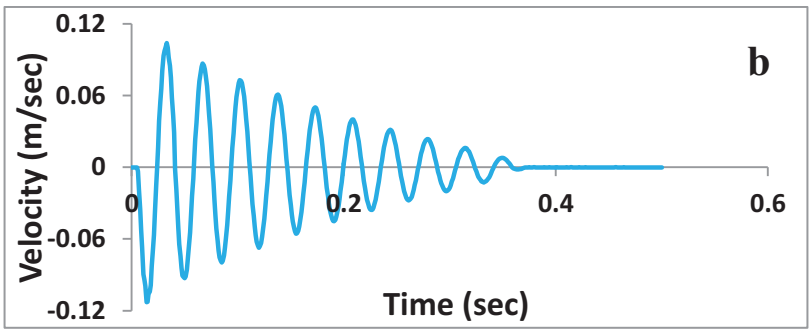

Steel/a-C:H coated contact

N= 0.40 N

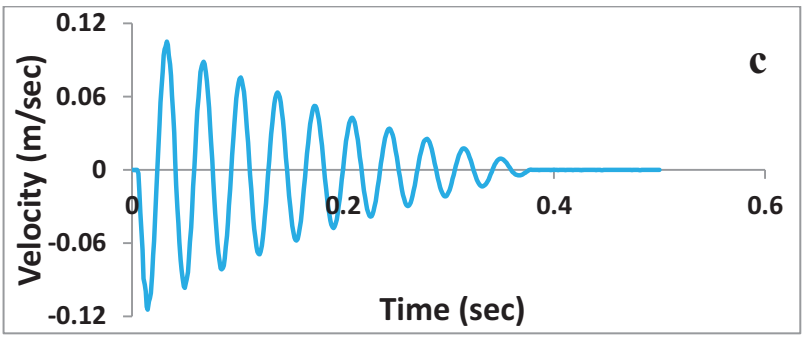

ta-C/ ta-C coated contact

N= 0.90 N

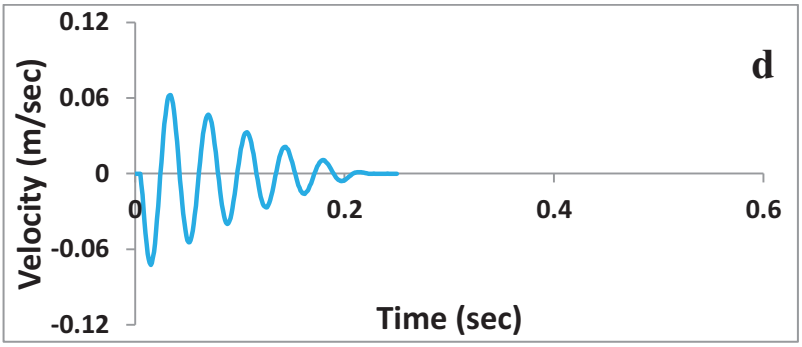

Figure 14. Velocity free responses of glycerol lubricated steel/steel, steel/ta-C, steel/a-C:H and ta-C/ta-C contacts at 486*106 Pa.

The envelope of the velocity free responses shown above (see Figure 14) is exponential. This latter explains the existence of both transient friction at zero speed and viscous damping parameters, μ_0 and μ_1, respectively. Figure 15 presents the ECR evolution of the steel on steel contact in logarithmic scale. For glycerol, the friction mostly occurs at a complete lubricant film thickness, even when the sliding direction changes or in other words even when the velocity is negligible. Indeed, the logarithmic value of ECR during sliding stays constant having an approximate value of 7.2 log(Ω). Unlike the oleic acid lubricated contact, we can

observe that glycerol lubricant is fully present during the whole sliding test, even at zero speed at changing of direction. Thus, we can conclude that the system is running under quasi-elastohydrodynamic lubrication EHL regime. After stopping, the final value of ERC is about 4 log(Ω). This unexpected high value is explained by the presence of some insulating products in the actual interface.

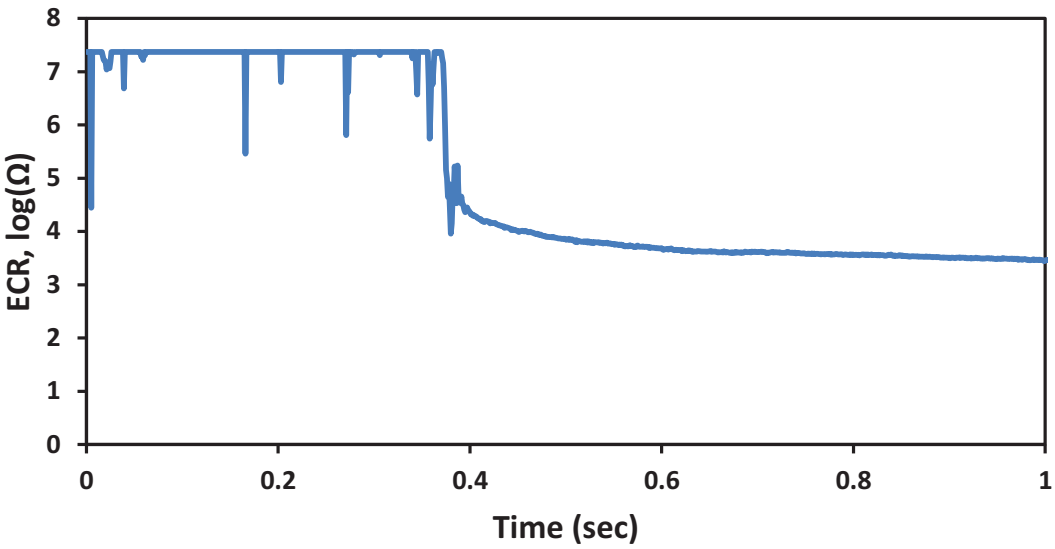

Figure 15. Electric contact resistance (ECR) for steel/steel contact lubricated with glycerol, N=0.40 N.

The film thickness of glycerol at the interface between steel-on-steel contact is calculated using the Dowson's theory. The viscosity η of glycerol at 25°C is 934 mPa.sec [25] and its piezo-viscosity coefficient α is 5GPa^{-1}. At the maximum velocity (≅0.11 m/sec), the film thickness of glycerol is found to be 80.5 nm.

2.3.4.3 b) Transient friction at zero-speed and viscous damping friction

By sliding the diamond-like-carbon friction pair (ta-C/ ta-C) in the presence of pure glycerol as a lubricant, the velocity-independent friction contribution, μ_0, decreases compared to that of steel-on-steel contact (see Figure 16). However, μ_1 for ta-C/ ta-C coated contacts is greater than that of steel/steel contact (see Figure 17). These results are in agreement with the results in [26, 27].

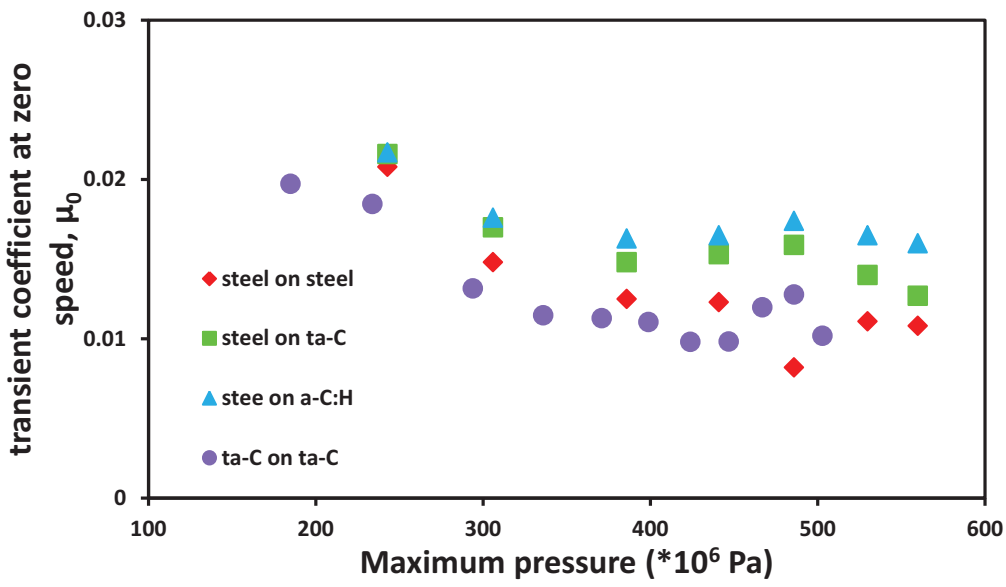

Figure 16. Transient friction at zero speed contribution, μ_0 , as a function of the maximum pressure.

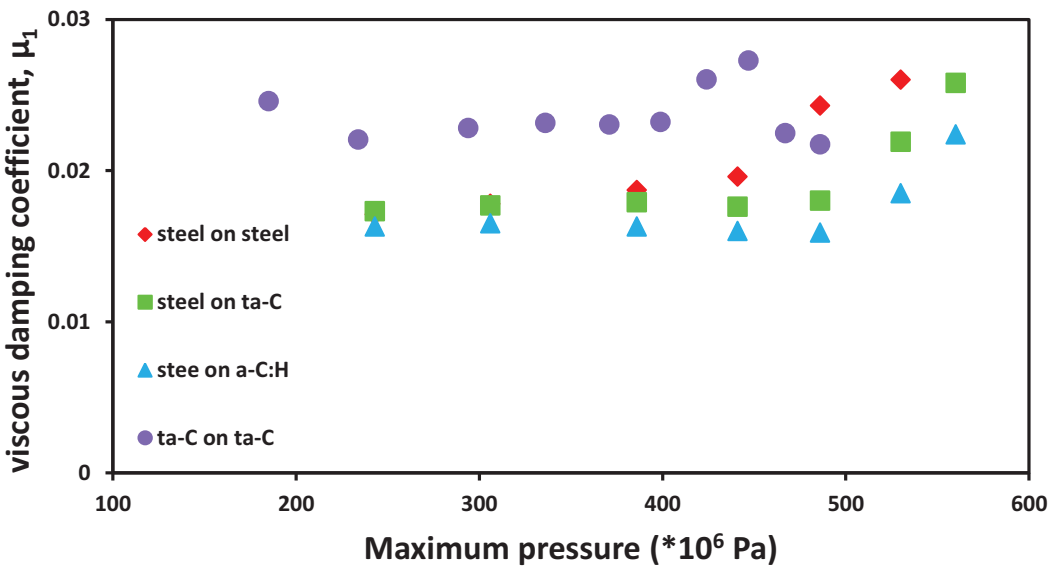

Figure 17. Viscous damping friction contribution, μ_1 , as a function of the maximum pressure.

For lubricated contacts by glycerol, there is a clear viscous effect on the friction. However, the friction increases with the velocity according to the friction model used. Moreover, as the two surfaces are sliding, a film of glycerol always exists in the contact. Thus, we can say that the system is in the EHL regime of the Stribeck curve and that the chemistry of the surface does not play a significant role.

2.4 The effect of temperature on lubricated steel/steel contacts with or without additives on friction using the novel apparatus

This section summarizes a set of experiments performed on steel/steel contact using the oscillating dynamic tribometer. Different base oils were tested in the contact at different temperatures and normal loads. In addition, the effect of some additives was studied as well since additive is considered one of the solutions to control friction. In literature mixtures of unsaturated fatty acids such as oleic, linoleic and stearic acids are usually utilized as friction modifiers in fuels i.e. conventional diesel fuel and also lubricating oils [28, 29]. It is shown a great interest of these latter lubricants due to their occurrence in blends of biodiesel with ultra-low sulfur petroleum-based fuel [30].

2.4.1 Tribological parameters

A set of six experiments is carried out on the steel/steel pin-on-flat configuration of the novel apparatus presented in section 2.2. Different lubricants with and without additives are studied. Three pure lubricants, pure glycerol, base oil 150 NS and poly-alpha-olefin PAO4, are tested at different temperatures and normal loads applied. Moreover, the PAO4 lubricant is tested using three different additives, oleic acid, linoleic acid and stearic acid. The total mass of PAO4 solution with each additive contains 1% additive of the solution total mass. These three solutions, PAO4 with additives, are also tested as well at different temperatures and normal loads.

The steel spherical pins have a diameter of $6.0*10^{-3}$ m. They are made of hardened bearing steel (AISI 52100). However, the flat planes are described by a rectangular geometry of $9.0*10^{-3}$ m length, $7.0*10^{-3}$ m width and a thickness of $2.5*10^{-3}$ m. A 50 µL of the different lubricants is added in the contact during the experimental test. All the surfaces have a roughness of 5 nm R_a.

2.4.2 Operating conditions

The pure glycerol $C_3H_8O_3$, used as a lubricant, is characterized by a dynamic viscosity of $14.80*10^{-3}$ Pa.sec at 100°C and a very low piezo-viscosity coefficient of 5 GPa^{-1} at 25°C. However, the other two pure lubricants used, poly-alpha-olefin PAO4 and base oil 150NS, are described by a very low dynamic viscosity compared to that of pure glycerol, but a much higher piezo-viscosity coefficient, about 3 times of that of pure glycerol. The pure poly-alpha-olefin PAO4 has a dynamic viscosity of $3.90*10^{-3}$ Pa.sec at 100°C, while the pure base oil 150NS has a lower dynamic viscosity of $3.36*10^{-3}$ Pa.sec at 100°C (see Table 4). Three different fatty acids are used as additives with PAO4. These fatty acids are the oleic acid $CH_3(CH_2)_7CH=(CH_2)_7COOH$ or C18:1 cis-9, linoleic acid ($C_{18}H_{32}O_2$ or C18:2 n-6) and stearic acid $C_{18}H_{36}O_2$; This variation in the lubricants and additives permits us to study friction at different lubrication regimes in the Stribeck curve.

Pure lubricants	Viscosity at 100°C (Pa.sec)
Glycerol	$14.80*10^{-3}$
PAO4	$3.90*10^{-3}$
150NS base oil	$3.36*10^{-3}$

Table 4. The viscosity of three different pure lubricants at 100°C.

The experimental test starts by studying the internal damping of the apparatus, as before. This is performed by testing the open contact in air, without adding any lubricant and without applying a normal load. Afterwards, a small quantity of lubricant is added (about 50 µl). The normal load N, ranges from 0 to 0.70 N for pure glycerol lubricated contact corresponding to a calculated Hertzian pressure ranging from 0 to $585*10^6$ Pa. However for the other lubricated contacts, the normal load is varied from 0 to 0.20 N corresponding to calculated Hertzian contact pressures varying from 0 to$386*10^6$.

The experiment takes place at a temperature varying from room temperature (of about 23°C) up to about 80°C. The tests last about 40 seconds for those without a negligible applied normal load and 4 seconds or less for those with an applied normal load. Each experiment is repeated four times with the same conditions in order to check the repeatability of the oscillating time responses. The initial displacement and velocity are set to be $667*10^{-3}$ m and 0 m/sec respectively, as the oscillator is released.

After adding the lubricant in the interface, we waited for about 15 minutes before applying the lowest temperature since the kinetic adsorption of molecules on the steel surface is unknown. This latter time corresponds to the duration where the lubricant is adsorbed by the contact and the applied normal load is stabilized. For the same lubricated and loaded contacts, the temperature is increased. At each temperature, the experimental test is performed 4 times. The free responses of the system corresponding to these 4 repetitions do not vary at a specific normal load even at the lowest load. Therefore, one can conclude that the kinetic adsorption is very fast and stabilized during all our experimental tests.

2.4.3 Results

This section aims to observe the effect of temperature on different tribosystems studied. Moreover, we will compare three different pure lubricants. Finally, the importance of some additives on PAO4 will be tested.

2.4.3.1 Contacts lubricated with three different pure lubricants

A steel/steel contact was tested with three different pure lubricants: pure glycerol, poly-alpha-olefin PAO4 and 150 NS base oil separately at different temperatures and normal load. For the pure glycerol lubricated contact, the test is performed at a temperature varying between the ambient temperature (22°C) and 75°C and at a normal load, N from 0.05 to 0.70 N. The

total duration of the experiments is 50 minutes. Then, another steel/steel contact is tested lubricated with PAO4 at ambient temperature (25°C) up to 79°C and with an applied load varying from 0.05N to 0.20 N. These experiments are performed in about 30 minutes. Later, a new steel/steel friction pair is lubricated with 150NS base oil is tested at ambient temperature (25°C) up till 78°C and at a normal load ranging between 0.05N and 0.20N which take a total duration of about 30 minutes. Each of the three lubricated tribosystems is tested without applying any normal load at ambient temperature in order to determine the effect of the different pure lubricants on the system.

2.4.3.1 a) Pure glycerol lubricated contact

The first step in these experimental tests is to identify the effect of pure glycerol effect without any contact on the steel/steel tribosystems at ambient temperature (22°C). A droplet of 50 µl pure glycerol was added in the contact. The initial-out-of-equilibrium position is set to be $667*10^{-6}$ m. After releasing the elastic bi-blade, the system oscillates for more than 100 oscillations. Thus, the experimental displacement and velocity-time responses are identified. The viscous damping friction contribution is found to be μ_1 0.0086 ± 0.0002. However, the transient friction coefficient at zero speed μ_0 cannot be evaluated at this stage since there doesn't exist any contact between the sphere and the plane. In section 3.1, we had already determined the viscous damping contribution μ_1 of the apparatus itself (0.0011 ± 0.0002). Thus, one can say that the pure glycerol contributes to the system with a viscous damping friction μ_1 of 0.0075. We will observe that the velocity-dependent friction contribution is larger than that of the machine (>0.0011); otherwise, it is negligible.

Then, after about 15 minutes, we carried out 8 sets of experiments using the same pure glycerol lubricated steel/steel contact with applied normal loads varying from 0.05 to 0.70 N, corresponding to a maximum contact pressure of $243*10^6$ to $585*10^6$ Pa, respectively. Each set is tested at a specific temperature from 22°C to 75°C. Figure 18 (a-c) shows the velocity-time responses of glycerol lubricated steel/steel contact corresponding to an applied normal load of 0.20 N at three different temperatures: (a) 22°C, (b) 51°C and (c) 75°C. At 22°C, the system has a transient contribution at zero speed μ_0 of 0.016 and a viscous damping contribution μ_1 of 0.0159. However, in Figures 18(b) and 18(c) transient friction contribution at zero speed μ_0 has a value of 0.028 at 51°C and 0.037 at 75°C respectively. Moreover, their corresponding viscous damping friction contributions μ_1 are negligible. The ability to evaluate both μ_0 and μ_1 corresponding to 22°C (Figure 18a) can be explained by the exponential form of the velocity response envelope different from that in Figures 18(b) and 18(c).

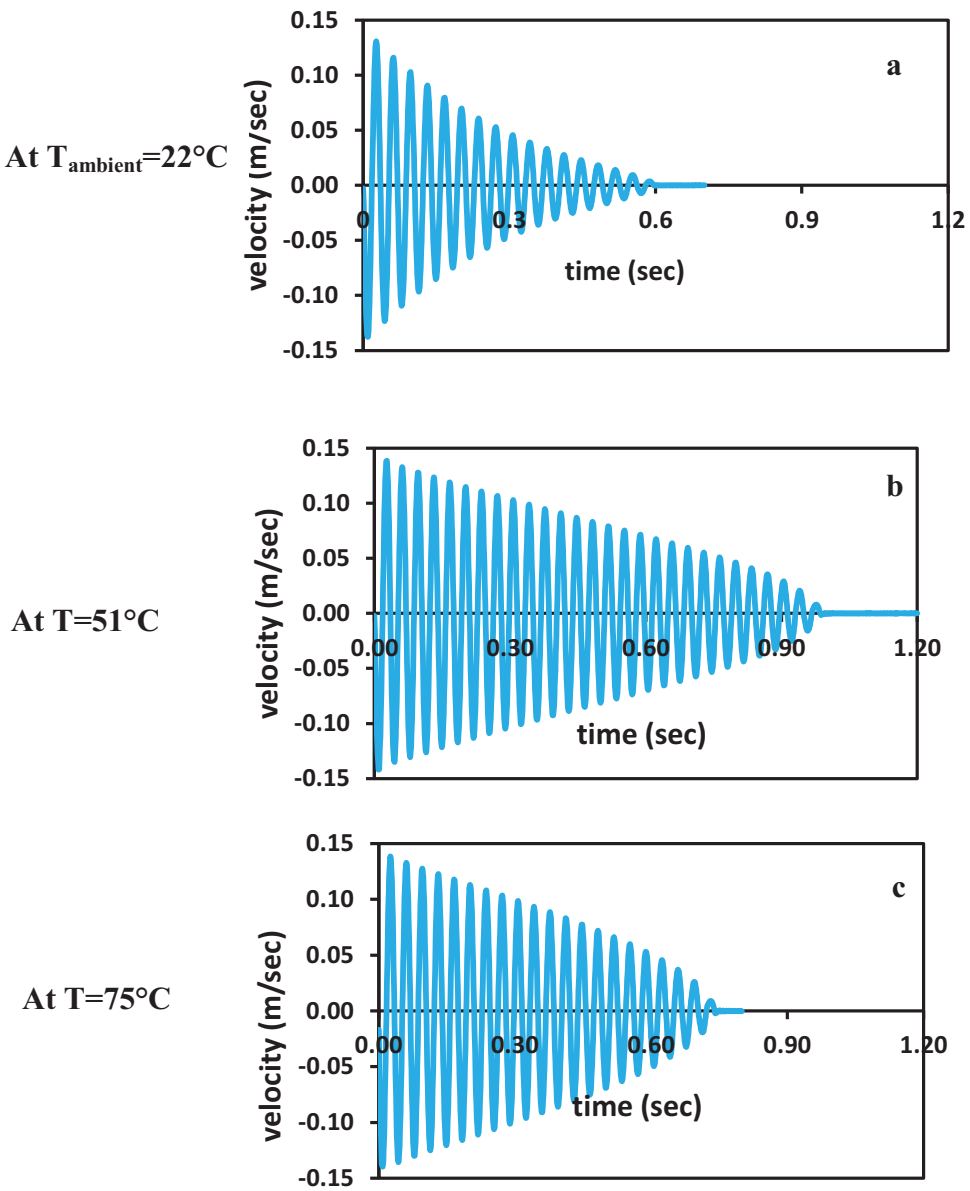

Figure 18. Velocity-time responses corresponding to pure glycerol lubricated steel/steel contact having a normal load of 0.20 N at (a) 22°C, (b) 51°C and (c) 75°C.

As the contact is applied, the number of oscillations increases with the temperature. Thus, the damping decreases with higher temperature. This latter is related to the fact that the viscosity of pure glycerol decreases as the temperature increases. However, at a certain temperature, the damping started to increase. Therefore, it is significant to notice that there is a limited temperature for the system studied depending on the normal load. Figure 19 presents the oscillation number of the time-response as a function of the temperature for the different normal load applied. Moreover, we can conclude from Figure 19 that as the normal load, N increases the number of oscillations decreases, thus damping increases.

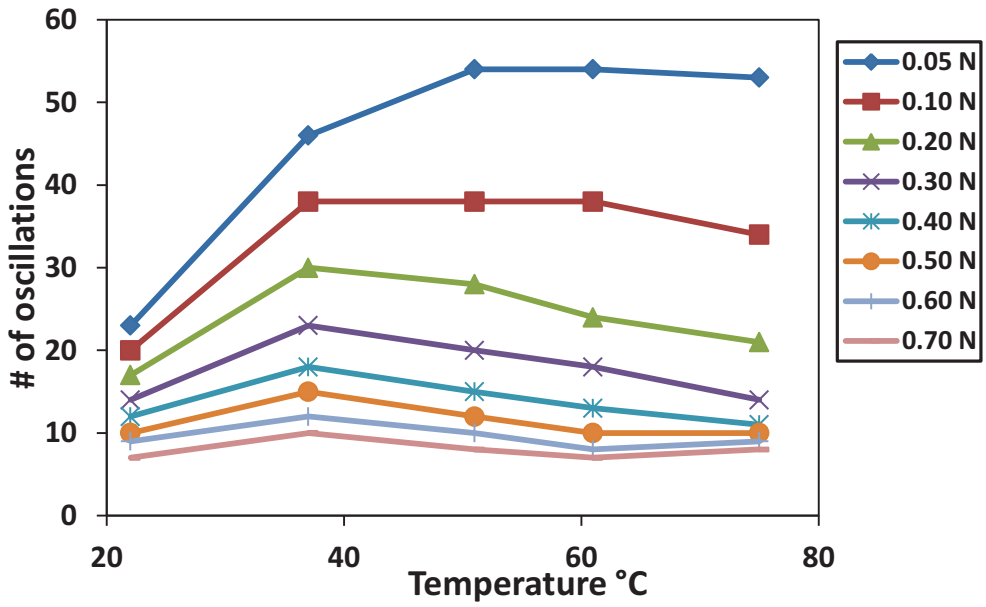

Figure 19. Number of oscillations as a function of the temperature for different normal loads applied.

In this system, the transient friction value at zero speed increases with temperature. Table 5 presents the transient friction value at zero speed μ_0 corresponding to the pure glycerol lubricated steel/steel contact at different temperatures T and normal loads N. The velocity-independent friction value μ_0 is in centimeter scale. The error of μ_0 is ±0.001. The velocity-dependent friction value μ_1 is negligible for most of the loaded contact starting from a temperature of about 37°C. The damping viscous friction contribution μ_1 is in millimeter scale and has an error of ±0.0002.

μ_0±0.001

T (°C)	at 0.05 N	at 0.10 N	at 0.20 N	at 0.30 N	at 0.40 N	at 0.50 N	at 0.60 N
22	0.035	0.024	0.016	0.015	0.015	0.016	0.016
37	0.049	0.034	0.024	0.022	0.020	0.019	0.018
75	0.061	0.046	0.037	0.036	0.032	0.029	0.025

Table 5. The transient friction contribution values μ_0 at different applied normal loads and temperatures.

Figure 20 (a-b) presents the electrical contact resistance (ECR) evolution in logarithmic scale of the pure glycerol lubricated steel/steel contact having a normal load of 0.10 N at two different temperatures (a) 22°C and (b) 75°C. At 22°C, the friction mostly occurs at a complete lubricant film, even when the sliding direction changes or in other words, even when the velocity passes through zero. We can recognize that the ECR stays more or less

constant during the oscillatory test having a value of about 7.4 log(Ω). However at a high temperature 75°C, significant fluctuations are produced from the resistance measurements. Thus, it shows that the full film cannot be attained during the test at 75°C. Therefore, one can conclude that the system runs under very thin EHL lubrication regime; however at high temperature, it is at a severe mixed lubrication regime. This may be due to the absorption of pure glycerol at the interface while the temperature is increased gradually from 22 to 75°C. Moreover, after the experiments is terminated, the final values of ECR at 22 and 75°C are 3.4 and 0.6 log(Ω) respectively. This unexpected values (≢0) is assumed to be related to the presence of some insulating products in the actual interface. Finally, it is essential to note that during the experiment at a constant temperature with variable normal loads, the lubrication regime does not change.

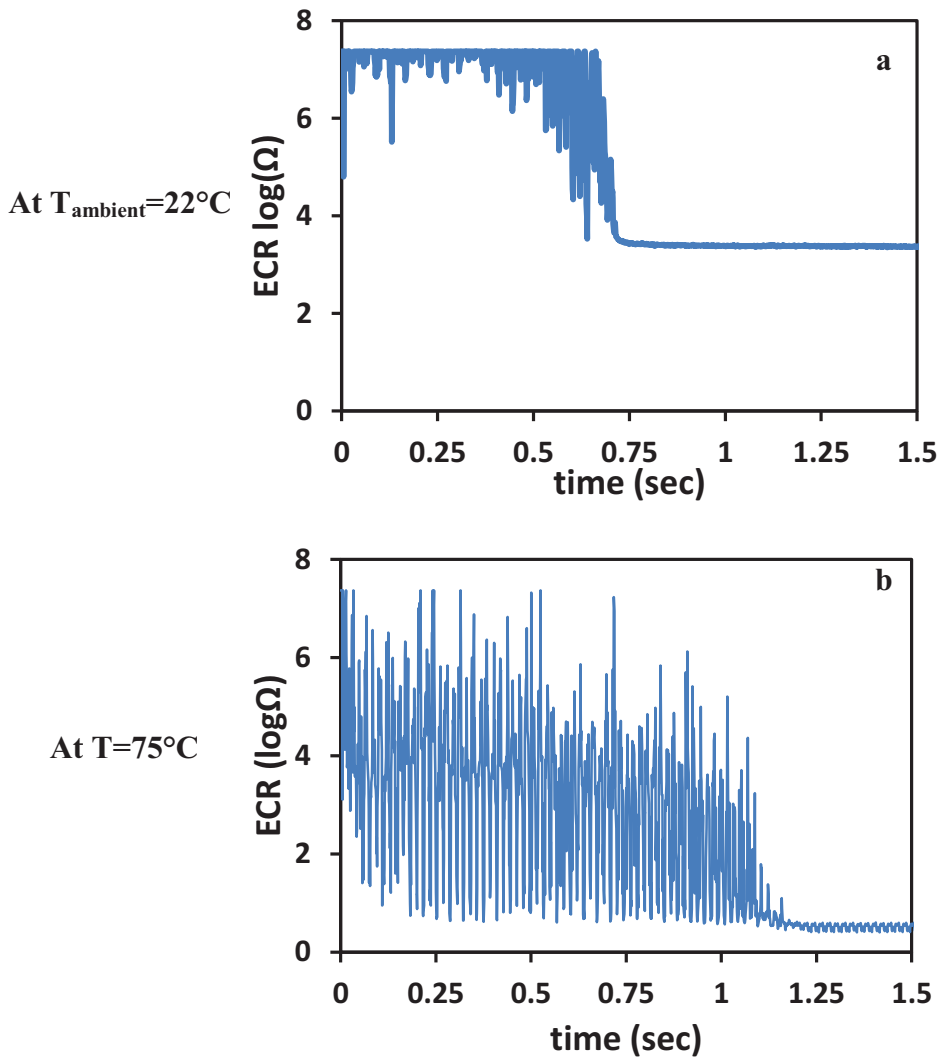

Figure 20. Electrical contact resistance (ECR) as a function of time in logarithmic scale corresponding to a pure glycerol lubricated steel/steel contact having a normal load of 0.10 N at a temperature of (a) 22°C and (b) 55°C.

From these results, we can explain the energy dissipation mechanism of glycerol in our experiments as follows:

- Below a temperature of about 40 °C, the viscosity of glycerol in the contact is high. Moreover, most of the energy loss is due to viscous damping of glycerol in the bulk of the lubricant film, as shown by the measured values of μ_1. However, the existence of quite high values of μ_0 is surprising because no metallic contact occurs as shown by the ECR values along the test. This effect could be attributed to pressure-viscosity effect and the lubricant inside the contact at zero speed is mostly solid-like. Nevertheless, this has a little impact on the number of oscillations during the test.
- At a temperature above 40 °C, μ_1 is negligible and friction is not dependent on the sliding speed. This is more related to boundary conditions. The fact that friction coefficient decreases as a function of the normal load is predicted from the Hertzian theory (adhesive and load-controlled hard contact from Singer [31] and Israelachvili [32]) where the friction coefficient varies as a function of the inverse power of the load (see equation (5)).

$$\mu = \frac{\tau}{P} = \tau_0 . p . (\frac{3R}{4E})^{2/3} . W^{1/3} + \alpha \qquad (5)$$

- However, in a paradoxical way, the tangential force (responsible of the decrease of the number of oscillations and therefore of energy loss per second) increases with the load applied. The slight increase of $\mu_0$with temperature at a given load is in good correlation with the evolution of the number of oscillations which slightly decreases with the load.

2.4.3.2 b) Base oil 150NS lubricated contact

We started this experiment by showing the effect of base oil 150NS as a lubricant. This latter is performed by adding 50µl of base oil 150NS between the steel/steel tribosystem without any normal load at ambient temperature (25°C). The initial displacement is set to be $667*10^{-6}$ m. The experimental test takes 40 sec after releasing the elastic bi-blades. The system runs for more than 100 oscillations. Finally, the viscous damping contribution $\mu_1$is determined to be as 0.0013±0.0002. Knowing that μ_1 of the apparatus itself is 0.0011±0.0002, one can conclude that there is no effect of the 150NS lubricant on the tribosystem. The transient friction value at zero speed $\mu_0$is not quantified for this experiment since there is no contact between the spherical pin and the flat plate. This can be explained by the low viscosity of the mineral base oil compared with that of glycerol.

Then, 4 sets of experiments using this latter 150NS lubricated steel/steel tribosystem are carried out by applying 4 different normal loads varying from 0.05 to 0.20N. We were not able to investigate higher loads because the number of oscillations is too small to be properly analyzed with our model. Each set of the experiments is tested at a temperature starting from 25 to 79°C. Figure 21 presents the number of oscillations as a function of the temperature for different normal loads. When the contact is applied, the number of oscillations decreases with the normal load. Unlike glycerol lubricated steel/steel contacts, the number of oscillations decreases with the temperature (see Figure 21). However, at a specific temperature, the

oscillations number starts to increase. Therefore, we can conclude that damping decreases at higher temperature (starting from 67°C in this tribosystem).

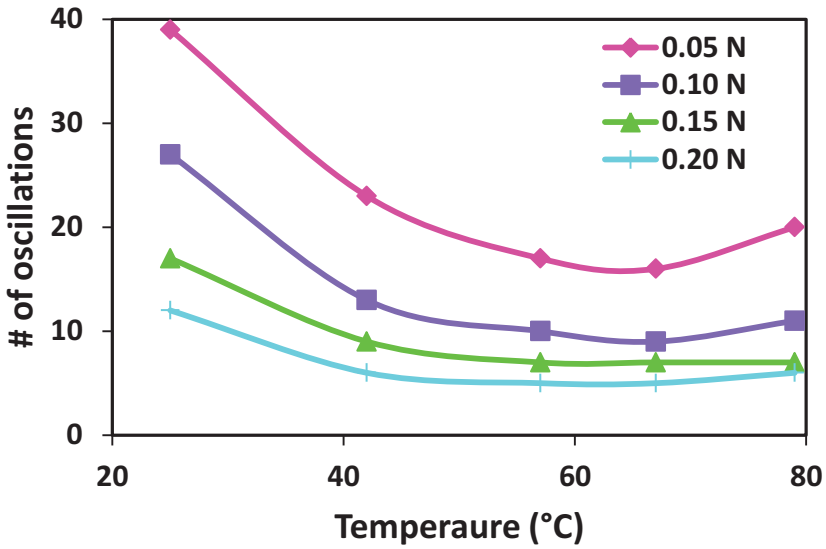

Figure 21. Number of oscillations as a function of the temperature of 150NS lubricated steel/steel pin-on-flat contact for different applied normal loads.

For all loaded 150NS steel/steel contacts at any temperature, the viscous damping friction contribution μ_1 is considered negligible since μ_1 is determined to be smaller than that of the machine (>0.0011). The values of the transient friction μ_0 are shown in Table 6. The error of μ_0 is ±0.001. At 25°C, the velocity-independent friction μ_0 is in decimeter scale; however, at other temperatures (42-79°C) it is in centimeter scale. The transient friction increases with temperature. Nevertheless, at 79°C μ_0 starts to decrease.

Transient friction contribution at zero speed μ_0 (±0.001)

T(°C)	at 0.05 N	at 0.10 N	at 0.15 N	at 0.20 N
25	0.092	0.063	0.065	0.072
42	0.161	0.142	0.141	0.142
57	0.211	0.177	0.169	0.169
67	0.223	0.190	0.182	0.174
79	0.179	0.164	0.163	0.153

Table 6. The transient friction contribution μ_0 with different normal loads and at different temperatures T for 150NS lubricated steel/steel contacts.

The electrical contact resistance (ECR) measured during the experimental test shows that the system runs under the mixed lubrication regime with any normal load and at any temperature. Figure 22 presents the ECR of steel/steel contact lubricated with 150NS with 0.10 N and at 25°C. The final value of the electrical resistance contact after the experiment is about 3 log(Ω). This unexpected value (≠ 0) is assumed to be due to the presence of some insulating products in the interface.

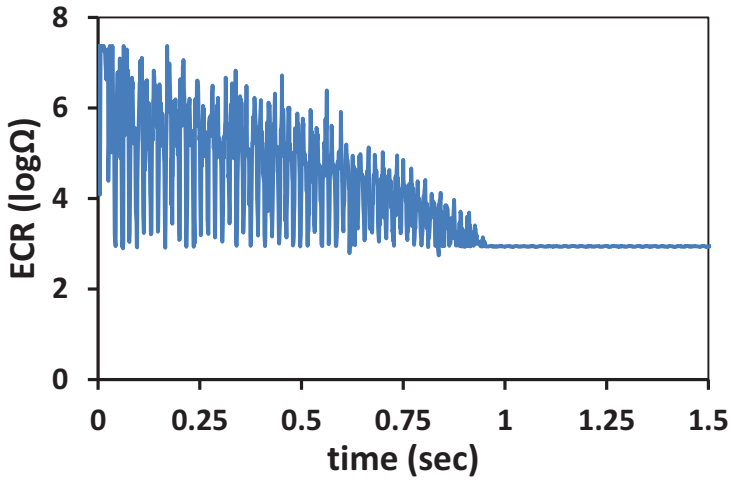

Figure 22. Electrical contact resistance (ECR) as a function of time in logarithmic scale corresponding to base oil 150 NS lubricated steel/steel contact having a normal load of 0.10 N at a temperature of 25°C.

From these results, the energy dissipation mechanism of mineral base oil in our experiments can be explained as follows. At any temperature, the tribometer is operating in the boundary lubrication regime (especially at low sliding speeds) and in very thin EHL during the rest of the time (see ECR values in Figure 23). There is few contribution of viscous damping in the energy loss during the whole experiment. The fact that μ_0 decreases as a function of the load applied is also explained by the Hertzian contact theory, as in the previous case. It is interesting to observe that the friction is much higher with the mineral oil than that with glycerol, even if the viscosity is not significantly different at high temperature. This is well explained by the lower pressure-viscosity coefficient of glycerol [33].

At the highest temperature (79 °C), although the boundary regime operates certainly all the time during the experimental test (see Figure 23), energy loss and μ_0 decrease (N increases) compared with lower temperatures. This may be explained by some tribochemical reactions at the contact during very severe conditions and the formation of a low shear strength tribofilm. Another possible explanation is a thermal/oxidative degradation of the base oil at this temperature, generating possible polar compounds reducing friction.

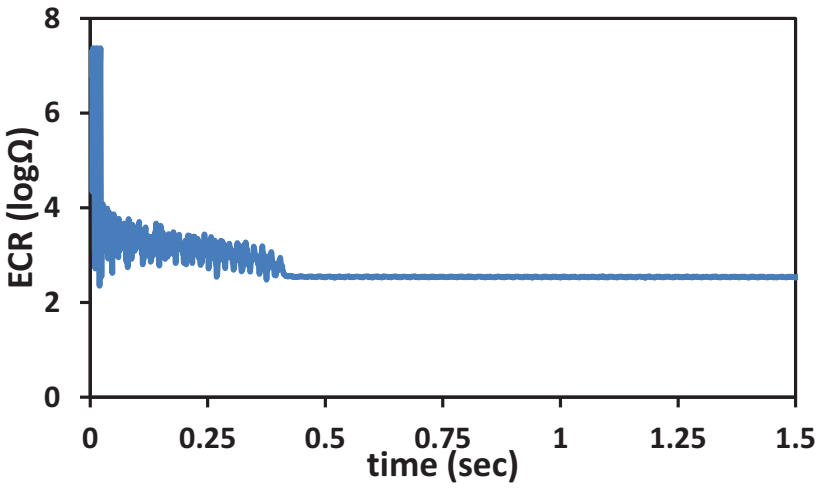

Figure 23. Electrical contact resistance (ECR) as a function of time in logarithmic scale corresponding to base oil 150 NS lubricated steel/steel contact having a normal load of 0.10 N at a temperature of 79°C.

2.4.3.2 c) Poly-alpha-olefin PAO4 lubricated contact

At the beginning, 50 µl of PAO4 is added at the interface of the steel/steel tribosystem without any normal load. It corresponding μ_0 is found to be negligible since there does not exist any contact at the interface. Moreover, the PAO4 lubricant does not have any effect on the μ_1 of the system. Thus, both 150NS and PAO4 lubricants have the same effect on the system. Similarly to 150NS lubricated contacts, the number of oscillations corresponding to PAO4 lubricated contacts decreases with the temperature until a specific temperature, where the number of oscillations starts to increase. Thus, damping increases from 25 to 67°C, then it starts to decrease at 67°C. Figure 24 shows the damping behavior by presenting the number of oscillations as a function of the temperature for different applied normal loads.

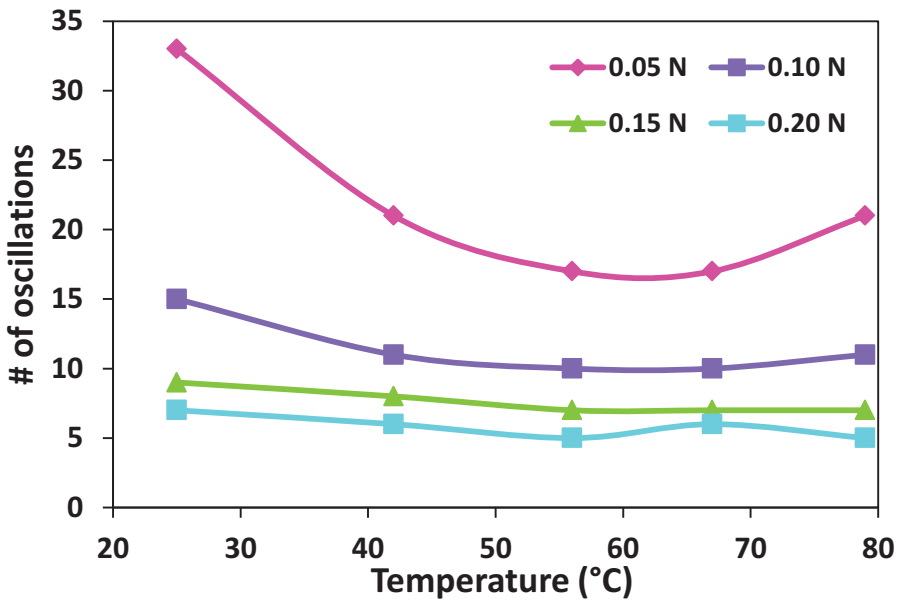

Figure 24. Number of oscillations as a function of temperature for different normal loads corresponding to steel/steel contact lubricated with PAO4.

The velocity-dependent values μ_1 for loaded 150NS lubricated contacts are not quantified since they are smaller than that of the system (<0.0011). The results of μ_1 corresponding to 150NS lubricant are similar to that of PAO4. The transient friction contribution μ_0 increases when the temperature varies from 25 to 56°C. However, at 56°C μ_0 starts to increase. The velocity-independent values μ_0 have an error of ±0.001. Table 7 presents the values of μ_0 corresponding to this current tribosystem.

Transient friction contribution at zero μ_0 (±0.001)

T(°C)	at 0.05 N	at 0.10 N	at 0.15 N	at 0.20 N
25	**0.111**	**0.127**	**0.134**	**0.138**
42	**0.167**	**0.163**	**0.156**	**0.155**
56	**0.211**	**0.181**	**0.169**	**0.159**
67	**0.201**	**0.176**	**0.164**	**0.157**
79	**0.173**	**0.165**	**0.161**	**0.158**

Table 7. The transient friction contribution μ_0 with different normal loads and at different temperatures *T* for PAO4 lubricated steel/steel contacts.

Figure 25 represents the ECR measurements in logarithmic scale as a function of the experimental time for 0.10 N at ambient temperature of 25°C. The logarithmic values of ECR are fluctuating during the oscillating test. After stopping, the final value of ECR is about 3.4 log(Ω). This unexpected high value is assumed to be related to the presence of some insulating products in the actual interface. This latter may be resulted from the short time of the experiment. Then, we can conclude that the steel/steel contact lubricated with PAO4 runs at a severe mixed lubrication regime at any condition. Thus, both PA04 and 150NS have the same ECR behavior.

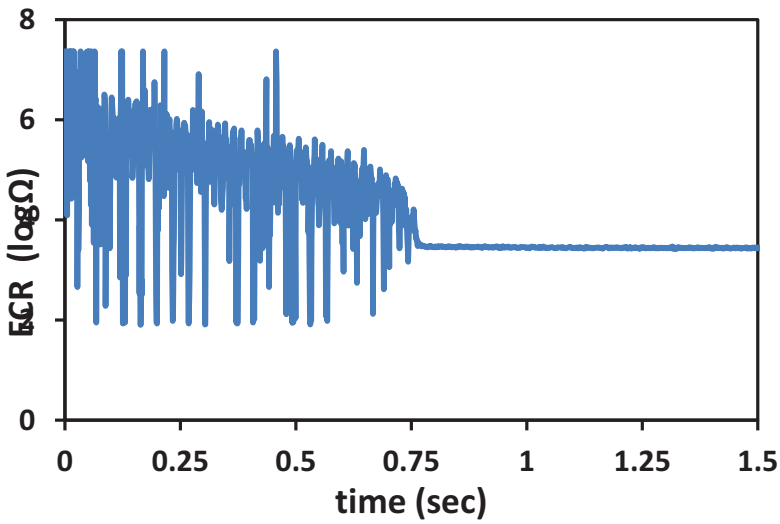

Figure 25. Electrical contact resistance (ECR) as a function of time in logarithmic scale corresponding to poly-alpha-olefin PAO4 lubricated steel/steel contact having a normal load of 0.10 N at a temperature of 25°C.

2.4.3.3 d) Comparison between the three pure lubricants

In this subsection, glycerol, 150NS and PAO4 lubricated steel/steel contacts are compared. Figure 26 presents the number of oscillations as a function of temperature for a normal load of 0.20 N. This figure shows that glycerol lubricated steel/steel tribosystems are less damping compared to that lubricated with PAO4 and 150NS since glycerol lubricated contact has the highest number of oscillations compared to the other two systems. Both PAO4 and 150NS lubricated systems are described by a similar damping behavior; however, at ambient temperature (25°C), the system lubricated with PA04 is more damped than that with 150NS.

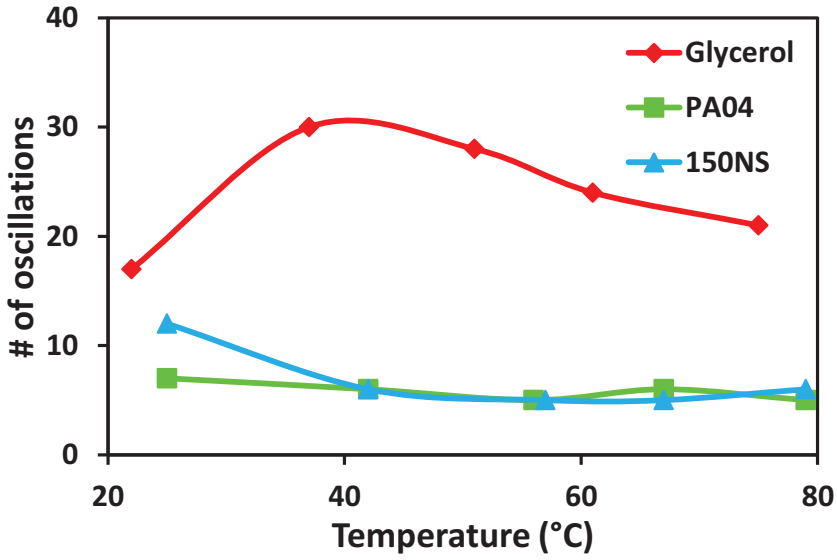

Figure 26. Number of oscillations as a function of temperature of three different lubricated steel/steel contacts loaded with 0.20 N.

When a lubricant is added in the contact, only glycerol shows an increase in the viscous damping contribution μ_1 from that of the system (0.0011±0.0002) unlike that of 150NS and PAO4. The velocity-dependent friction values μ_1 for loaded contacts are only evaluated for glycerol lubricated contacts at ambient temperature.

Figure 27 presents the transient friction values μ_0 for the 3 lubricated contacts loaded with 0.05 N as a function of different temperatures. It shows that glycerol lubricated contacts is described by the lowest μ_0 compared to that of PAO4 and 150NS lubricants.

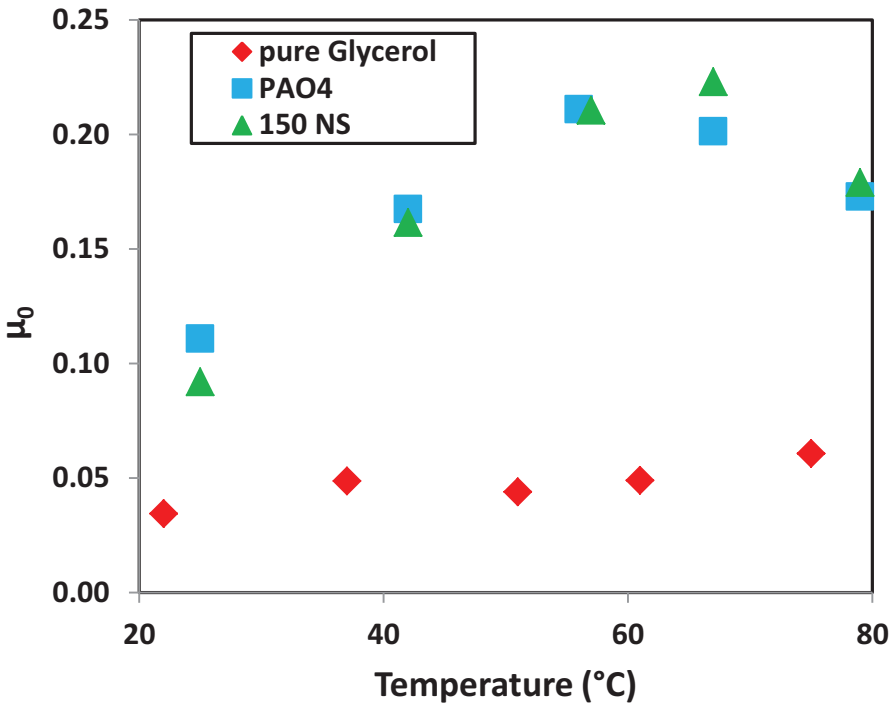

Figure 27. The transient friction contribution μ_0 as a function of the temperatures for 0.05 N loaded steel/steel contact lubricated with three different lubricants: glycerol, PAO4 and 150NS.

2.4.3.2 The effect of different additives on PAO4 lubricated contacts

In the following, the effect of 3 different additives on PAO4 lubricant will be investigated. Three different tests were performed by adding each additive with an amount of 1% of the total weight of solution including the PAO4 and the additive: oleic acid, linoleic acid or stearic acid.

2.4.3.2 a) Damping behavior

Figure 28 presents the number of oscillations as a function of various contact pressures corresponding to four steel/steel contacts lubricated with PAO4, PAO4+1% oleic acid, PAO4 +1% linoleic acid and PAO4 +1% stearic acid at a temperature of 65°C. This shows that the oscillations number of pure PAO4 lubricated contacts have the lowest number of oscillations compared to those lubricated with PA0O4+ 1% additive. Therefore, one can conclude that the presence of the additive in the PAO reduces energy loss for any contact pressure up to $386*10^6$ Pa corresponding to a normal load of 0.2 N. Above this value, the effect of the

additives disappears. Now we have to study the origin of the increase of oscillations due to fatty acids.

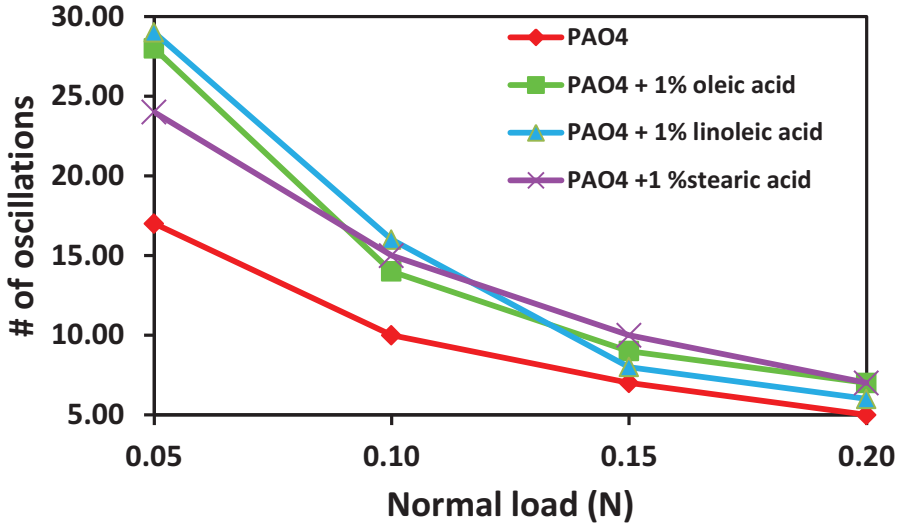

Figure 28. Number of oscillations as a function of different normal loads at 65°C for steel/steel contacts lubricated with pure PAO4, PAO4 +1% oleic acid, PAO4 +1% linoleic acid and PAO4 +1% stearic acid.

Table 8 presents all the data concerning the number of oscillations at different maximal pressures up to 350 MPa and temperatures of contacts lubricated with pure PAO4 and PAO4+1% additives. At all the temperatures studied, pure PAO4 lubricated contacts have the lowest oscillations number and thus the lowest ability to reduce energy loss. Comparing the three different additives, PAO4+1% linoleic acid lubricant, having the lowest contact pressure ($243*10^6$ Pa), is defined by the highest number of oscillations thus by the lowest damping behavior at 42, 56 and 65°C. However, at the highest temperature (79°C), PAO4+1% oleic acid lubricated contact corresponds to the lowest damping behavior at a P_{max} of $243*10^6$MPa. We can also observe that stearic acid with P_{max} of $243*10^6$ Pa does not have any effect on PAO4 at a temperature of 79°C since the number of oscillations remains 21 when 1% of stearic acid is added. At higher contact pressure, the oscillations numbers are very close for contacts lubricated with PAO4+1% of the 3 different additives and it is not possible to differentiate the additive performance. This is indeed a limitation in our tribometer to study higher pressures and this is given by the bi-blade elasticity.

		# of oscillations			
	$P_{max}(10^6$ Pa)	PAO4	PA04+1% oleic acid	PA04+1% linoleic acid	PA04+1% stearic acid
at 42°C	243	21	27	33	30
	306	11	15	15	16
	350	8	10	10	10
	386	6	7	7	8
at 56°C	243	17	28	29	24
	306	10	14	16	15
	350	7	9	8	10
	386	5	7	6	7
at 79°C	243	21	31	27	21
	306	11	15	14	14
	350	7	10	9	10
	386	5	7	6	7

Table 8. Number of oscillations at different maximal pressure and temperature of PAO4 and PAO4+1%additives lubricated contacts.

2.4.3.2 b) Transient friction at zero speed and viscous damping friction contributions

Comparing the pure PAO4 lubricated steel/steel contact with those lubricated with PA04 with 1% of additive, one can easily observe that the presence of additives in the pure PAO4 lubricant leads to a decrease in the transient friction value at zero speed μ_0. Figure 29 presents the transient friction values as a function of different temperatures for 4 steel/steel contacts each lubricated with pure PAO4, PAO4+1% oleic acid, PAO4+1%linoleic acid and PAO4+1% stearic acid and having a normal load of 0.05N. This figure shows that the velocity-independent friction contribution μ_0 contacts lubricated with PAO4+1% linoleic acid is the smallest compared to those lubricated with PAO4+1% oleic acid and PAO4+1% stearic acid. However, μ_0 corresponding to PAO4+1% oleic acid is lower than that of PAO4+1% stearic acid. Moreover, it is difficult to understand the relation between μ_0 and the contact pressure for PAO4+1% additive lubricated contacts.

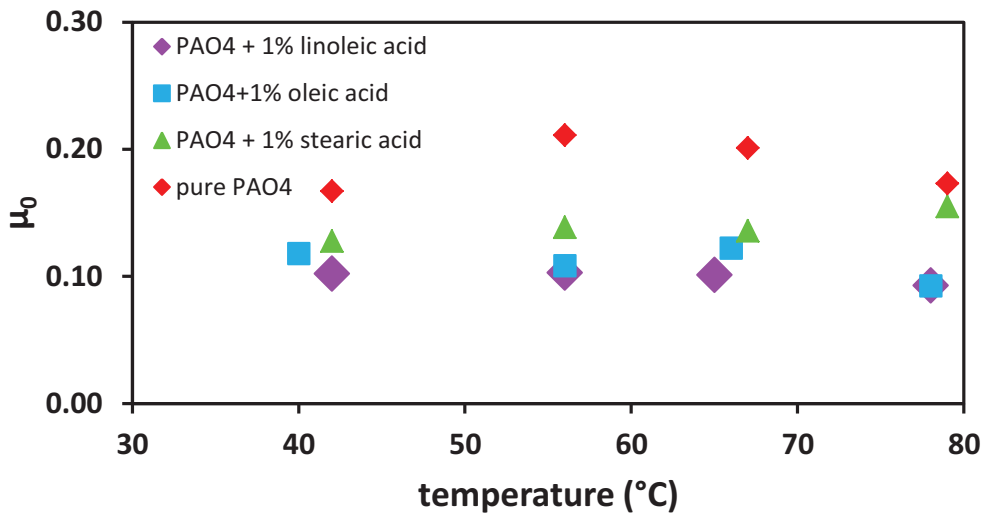

Figure 29. The transient friction at zero speed μ_0 as a function of temperature corresponding to steel/steel contacts having a normal load of 0.05 N and lubricated with pure PAO4, PAO4 +1% oleic acid, PAO4 +1% linoleic acid and PAO4 +1% stearic acid.

Neither the pure PAO4 nor PAO4 with 1% of additives affects the viscous damping friction contribution μ_1 when added in the steel/steel contact since their corresponding μ_1 does not differ from that of the apparatus (0.0011±0.0002). For loaded steel/steel contacts lubricated with PAO4+ 1% of additives, the velocity-dependent friction μ_1 is evaluated in most of the conditions. However, μ_1 is not quantified for all loaded steel/steel contacts lubricated with pure PAO4. Figure 30 presents μ_1 as a function of the temperature corresponding to steel/steel contacts having a normal load of 0.05N and lubricated with PAO4 + 1% of 3 different additives. Comparing the 3 additives, PAO4 with 1% of stearic acid gives the lowest viscous damping friction contribution.

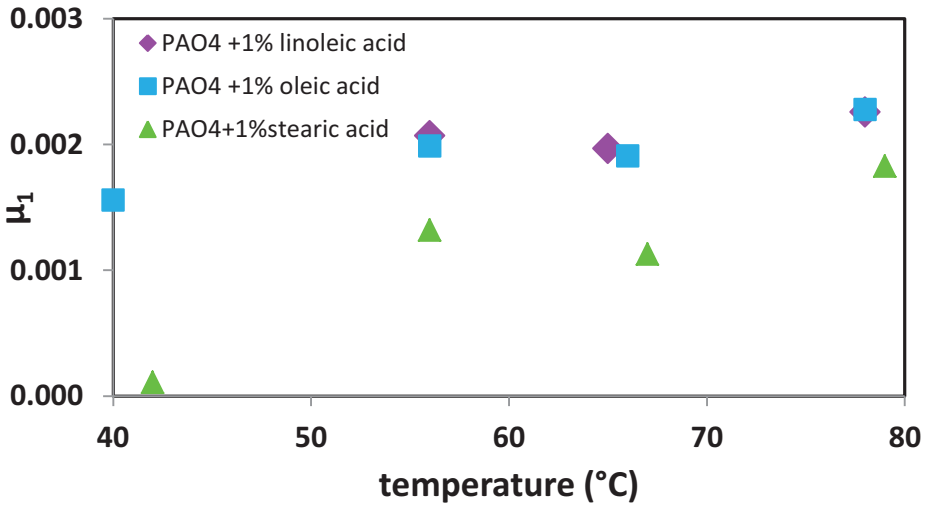

Figure 30. The viscous damping friction μ_1 as a function of temperature corresponding to steel/steel contacts having a normal load of 0.05 N and lubricated with PAO4 +1% oleic acid, PAO4 +1% linoleic acid and PAO4 +1% stearic acid.

Table 9 presents the values of μ_1 corresponding to PAO4+1% stearic acid lubricated contact having a normal load of 0.05 N. AT 42°C, the viscous damping friction is considered negligible since it is lower than that of the apparatus (<0.0011).

Temperature (°C)	Viscous damping friction μ_1 (±0.0002)
42	-
56	0.0013
67	0.0011

Table 9. The viscous damping friction μ_1 at different temperatures corresponding to steel/steel contacts having a normal load of 0.05 N and lubricated with PAO4 +1% stearic acid.

2.4.3.2 c) The electrical contact resistance

Figure 31 presents the measurements of electrical contact resistance (ECR) in logarithmic scale as a function of the experimental time for steel/steel contacts loaded with 0.10 N and

lubricated with (a) PAO4+ 1% of oleic acid at 23.3°C, (b) PAO4 +1% of linoleic acid at 24.4°C and (c) PAO4 + 1% of stearic acid at 42.0°C. Both tribosystems lubricated with PAO4+1% oleic acid and linoleic acid run at the very beginning of the experimental tests in the mixed lubrication regime then in the boundary regime. However, the logarithmic scale of the ECR measurement corresponding to the steel/steel contact lubricated with PAO4+ 1% of stearic acid is fluctuating during the oscillating test. Thus, this latter tribosystem runs at severe mixed lubrication regime. This can explain the reason behind the lowest viscous damping friction corresponding to contact lubricated with PAO4+ 1% of stearic acid. After the experiment is terminated, the final value of ECR id not zero in the 3 tribosystems (Figure 32 a, b and c). The final value is about 1.5 log(Ω) for PAO4+ 1% linoleic acid lubricated contacts; however it is about 3.0 log(Ω) for PAO4+ 1% oleic acid and PAO4+ 1% stearic acid lubricated contacts.

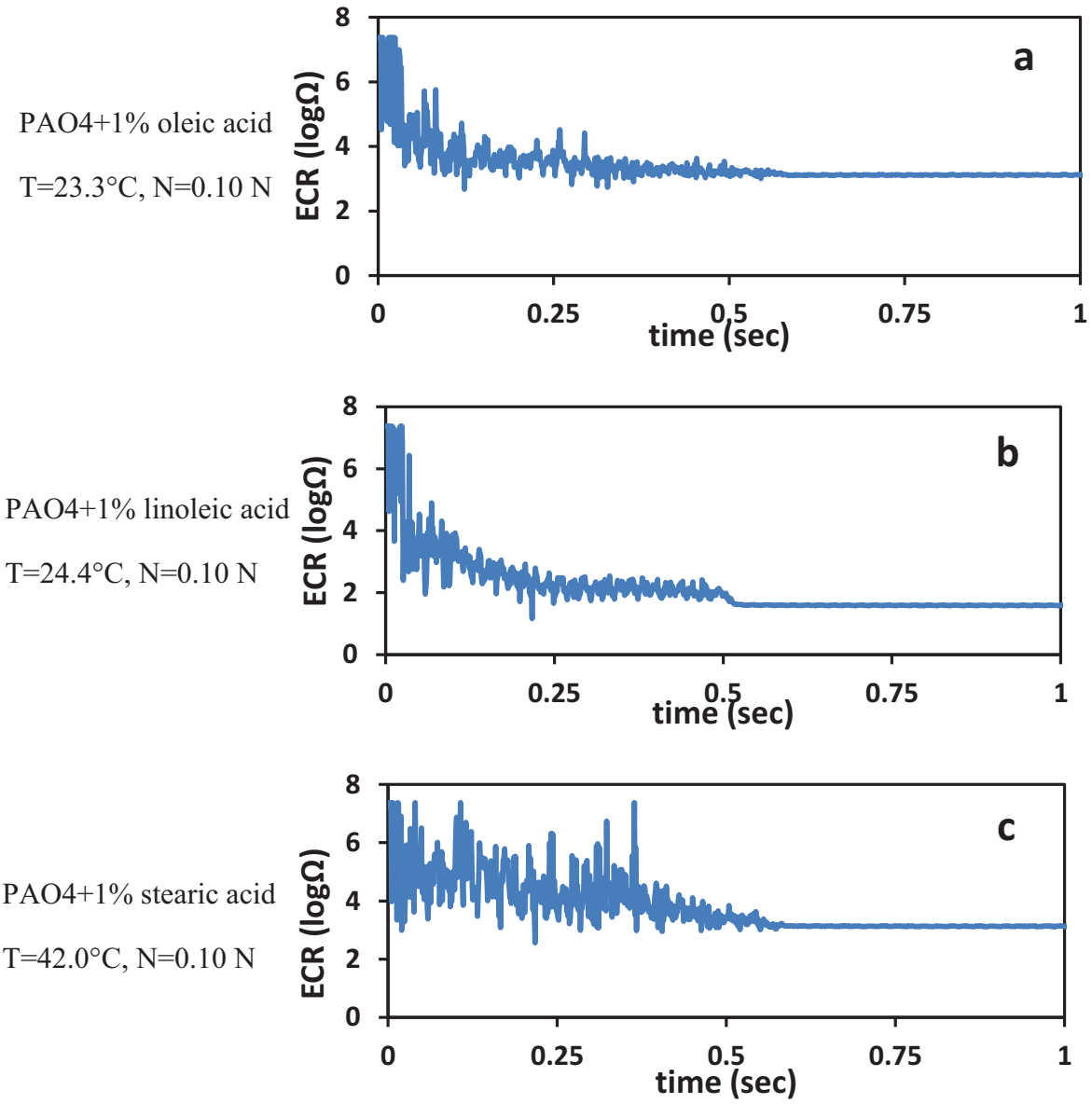

Figure 31. The electrical contact resistance in logarithmic scale as a function of the time for steel/steel contacts loaded with 0.10 N and lubricated with (a)PAO4 + 1% oleic acid at 23.3°C, (b)PAO4 + 1% linoleic acid at 24.4°C and (c)PAO4 + 1% stearic acid at 42.0°C.

2.5 Conclusions

Using the novel technique, which permits us to evaluate both the velocity-independent friction contribution μ_0 and the viscous damping friction contribution μ_1 derived from the free oscillating responses of the system, Chapter 2 presents the experimental results in two different studies. The first concentrated on the effect of DLC coatings on the lubricated steel-on-steel contacts. However, the second series of the experiments aims to study the effect of temperature on lubricated steel/steel contacts with or without friction modifiers.

In addition, we show that the envelope of the decreasing damping response plays an essential role in determining the friction contribution type. We are also able by measuring the electrical contact resistance (ECR) to extract some information on the film thickness and determine the lubricant regime of the system.

The following results are determined:

1. The dynamic tribometer showed an unrivaled accuracy.
2. As for the number of oscillations, the data is not consistent if there are less than 5 oscillations. Overall, this study focuses on a paradox of the Hertzian theory that is observed very easily in our method: the value of the friction coefficient does not always reflect the energy loss in the test (characterized by the number of oscillations).

3. For low viscosity oleic acid as a green lubricant, the linear envelope shows only the occurrence of transient friction contribution, defined by μ_0. Compared to steel/steel contact, the coating of one (or two) surfaces causes friction to decrease, in agreement with data obtained with a traditional tribometer. The ta-C/ta-C combination lubricated with oleic acid gives the lowest transient friction at zero speed value, μ_0 of 0.027 with an error of ±0.001.
4. For very viscous glycerol lubricated contacts, both transient friction μ_0 and contribution the velocity-dependent μ_1 are detected. This indicates that the lubrication regime belongs at least partially to elastohydrodynamic lubrication (EHL). Again we show that ta-C/ta-C system has the best performance in reducing friction near zero speed.
5. The electrical contact resistance measurements show that the steel-on-steel contact, lubricated with oleic acid, run in the severe mixed lubrication regime. However, those lubricated with glycerol runs at the elastohydrodynamic lubrication regime.
6. As the normal load is applied on lubricated steel/steel contact, damping decreases for glycerol lubricated systems with temperature until a certain temperature. However for 150NS and PAO4 lubricated contacts, damping increases with temperature until a certain temperature limit is reached.
7. For high viscous glycerol lubricated contacts, the transient friction μ_0 is smaller than that of those lubricated with PAO4 and 150NS.
8. It is shown that both 150NS and PAO4 do not have any effect on the damping viscous friction of the apparatus.

9. The viscous damping friction value μ_1 corresponding to PAO4 and 150NS lubricated and loaded steel/steel contacts is considered as negligible at any temperature since its corresponding value is less than that of the apparatus.
10. When additives are used in PAO4 lubricant, the damping behavior of the system is reduced.
11. Three different additives are tested with PAO4, oleic acid, linoleic acid and stearic acid. Results show that linoleic acid has the lowest μ_0; however, stearic acid has the lowest μ_1.

The friction model used in this chapter is coherent with some of the tribosystems studied. Nevertheless, this model may not be useful for some other tribosystems. Therefore a better understanding of the decreasing damping free oscillations will be presented in the following chapter. This will be performed by using a more general friction model defined by a polynomial friction law in the next chapter.

References

[1] Schmitz, T., Action, J., Ziegert, J. and Sawyer, G., The difficulty of measuring low friction: uncertainty analysis for friction coefficient measurements. Journal of Tribology 127 (4), pp. 673-680, 2005.

[2] Burris, D. and Sawyer, G., Adressing practical challenges of low friction coefficient measurements. Tribology Letters 35 (1), pp. 17-23, 2009.

[3] Wu, Z., Liu, H., Liu, L. and Yuan, D., Identification of nonlinear viscous damping and Coulomb friction from the free response data. Journal of Sound and Vibration 304 (1-2), pp. 407-414, 2007.

[4] Rigaud, E., Perret-Liaudet, J., Belin, M., Joly-Pottuz, L. and Martin, J.M., An original dynamic tribotest to discriminate friction and viscous damping. Tribology Internation 431 (2), pp. 320-329, 2010.

[5] Belin, M. and Kakizawa, M., Rigaud, E. and Martin, J.M., Dual characterization of boundary friction thanks to the harmonic tribometer: Identification of viscous and solid friction contributions. Journal of Physics: Conference Series, 258: 012008, 2010.

[6] Belin, M., Towards low- and super-low friction characterization thanks to the relaxation tribometer. Invited seminar at Iwate University (Japan), 2012.

[7] Rigaud, E. and Perret-Liaudet, J., Experiments and numerical results on nonlinear vibration of an impacting Hertzian contact. Part I: harmonic excitation. Journal of Sound and Vibrations 265 (2), pp. 289-307, 2003.

[8] El Kilali, T., Perret-Liaudet, J. and Mazuyer, D., Experimental analysis of a high pressure lubricated contact under dynamic normal excitation force. Transient processes in Tribology, Lyon: Elsevier, p. 409-18, 2004.

[9] Liang, J.W., A decrement for the simultaneous estimation of Coulomb and viscous friction. Journal of Sound and Vibration, 1996.

[10] Liang, J.W. and Feeny, B.F., Identifying Coulomb and viscous friction from free-vibration decrements. Nonlinear Dynamics 16 (4), pp. 337-347, 1998.

[11] Liang, J.W., Identifying Coulomb and viscous friction from free-vibration acceleration decrements. Journal of Sound and Vibration 282 (3-5), pp. 1208-1220, 2005.

[12] Jacobsen L. and Ayre, R., *Engineering Vibrations: with application to structures and machinery*, McGraw Hill, New York, 1958.

[13] Lorenz, H., *Lehrbuch der Technischen Physik. Erster Band: Techniste Mechanik Starrer Gebilde*, Verlag von Julius Springer, Berlin, 1924.

[14] Rayleigh, L., *The Theory of Sound*, Vol. 1, Dover Publications, New York, 1877 (re-issued 1945, pp. 46-51).

[15] Helmholtz, H.L.F., *On the sensations of tone as physiological basis for the theory of music*, Dover, New York, p. 406, 1954.

[16] Marquardt, D.W., An algorithm for least-squares estimation of nonlinear parameters. Journal of the society for Industrial and Applied Mathematics 11(2), pp. 431-441, 1963.

[17] Erdemir, A. and Donnet, C., Tribology od diamond-like carbon films: recent progress and future prospects. Journal of Physics D: Applied Physics 2006: R113-27.

[18] Vengudusamy, B., Green, J. H., Lamb, G. D. and Spikes, H. A., Influence of hydrogen and tungsten on the tribological properties of DLC/DLC contacts with ZDDP. Wear 289-299, pp. 109-119, 2013.

[19] Lertlukkanasuk, N. et al., Reactive distillation for synthesis of glycerol carbonate via glycerolysis of urea. Chemical Engineering and Processing. In Press, 2013.

[20] Matta, C., De Barros Bouchet, M. I., Le Mogne, T., Vachet, B., Martin, J.M. and Sagawa, T., Tribochemistry of tetrahedral hydrogen free amorphous carbon coatings in the presence of OH-containing lubricants. Lubrication Science 26, pp. 137-149, 2008.

[21] Kleinova, A., Fodran, P., Brncalovà, L. and Cvengros, J., Substituted esters of stearic acid as potential lubricants. Biomass & Bioenergy 32, pp. 366-371, 2008.

[22] Kano, M., Yasuda, Y., Okamoto, Y., Mabuchi, Y., Hamada, T., Ueno, T., Ye, J., Konoshi, S., Takeshima, S., Martin, J. M., De Barros Bouchet, M. I., and Le Mogne, T., Ultralow friction of DLC in presence of glycerol mono-oleate (GMO). Tribology Letters 18(2), pp. 245-251, 2005.

[23] Yasuda, Y., Kano, M., Mabuchi, Y., and Abou, S. Research on Diamond-Like Carbon Coatings for Low-Friction Valve Lifters. SAE Technical Paper 2003; doi:10.4271/2003-01-1101.

[24] Kano, M., Super low friction of DLC applied to engine cam follower lubricated with ester-containing oil. Tribology International 39(12), pp. 1682-1685, 2006.

[25] Lide, D.R., *Handbook of chemistry and physics.*CRC Press 8th edition, 2004-2005.

[26] De Barros Bouchet, M.I., Matta, C., Le Mogne, T., Martin, J.M. Zhang, Goddard III, W., Kano, M., Mabuchi, Y. and Ye, J., Superlubricity mechanism of diamond-like carbon with glycerol: Coupling of experimental and simulation studies. Journal of Physics: Conference series 89, 012003, 2007.

[27] Matta, C., Martin, J.M., Yoshida, K., Kano, M., De Barros Bouchet, M.I., Majdoub, F. and Belin M., Lubrication of DLC by environmentally friendly lubricants. Oral Presentation at ASME/STLE 2011 International Joint Tribology Conference (IJTC 2011), Los Angeles, California, USA.

[28] Lundmen, S.M., Persson, K., Mueller, G., Kronberg, B., Clarke, J., Chtaib, M. and Claesson, P.M., Unsaturated fatty acids in alkane solution: adsorption to steel surfaces. Langmuir 23, pp. 10598-10602, 2007.

[29] Lundmen, S.M., Ruths, M., Danerlöv, K. and Persson, K., Effects of unsaturation on film structure and friction of fatty acids in a model base oil. Journal of Colloid and Interface Science 326 (2), pp. 530-536, 2008.

[30] Knothe, G. and Steidley, K. R., Lubricity of components of biodiesel and petrodiesel: The origin of biodiesel lubricity. Energy fuels 19 (3), pp. 1192-1200, 2005.

[31] Singer, I. L., Bolster, R. N., Wegand, J., Fayeulle, S. and Stupp, B.C., Hertzian stress contribution to low friction behavior of thin MoS_2 coatings. Applied Physics Letters 57 (10), pp. 995-997, 1990.

[32] Israelachvili, J. N., Perez, E. and Tandon, R. K., On the adhesion force between deformable solids. Journal of Colloid and Interface Science 78, p. 260, 1980.

[33] Habchi, W., Matta, C., Joly-Pottuz, L., De Barros, M. I., Martin, J. M. and Vergne, P., Full film, boundary lubrication and tribochemistry in steel circular contacts lubricated wih glycerol. Tribology Letters 42, pp. 351-358, 2011.

3 DECAYING LAW FOR THE FREE OSCILLATING RESPONSE

3 Decaying law for the free oscillating response

Nomenclature

m = mass of the studied dynamic system

k = stiffness of the linear spring

T = friction force

N = Normal load applied to the contact interface

x = displacement of the system

$v = \frac{dx}{dt}$ = sliding velocity of the system

$\frac{d^2x}{dt^2}$ = acceleration of the system

$\mu_k(v)$ = kinematic friction coefficient having a polynomial power series form

p_{2j} , p_{2j+1} = constants of the kinematic friction coefficient, $\mu_k(v)$

μ_s = static friction coefficient

Ω = undamped circular natural frequency

τ = dimensionless time of the system

y = dimensionless displacement of the system

$\dot{y} = \frac{dy}{d\tau}$ = dimensionless velocity of the system

$\ddot{y} = \frac{d^2y}{d\tau^2}$ = dimensionless acceleration of the system

$f(\dot{y})$= dimensionless friction force having a polynomial power series form

μ_{2j} , μ_{2j+1} = constants of the dimensionless friction force $f(\dot{y})$

ϵ= total energy of the system

$A(\tau)$= envelope of the system

$F(A) = \frac{dA}{d\tau}$ = First order derivative of the envelope having a polynomial power series form

a_n = constants of $F(A)$

$F'(A)$ = First order derivative of $F(A)$

$\ddot{A} = = \frac{d^2A}{d\tau^2}$ Second order derivative of the envelope, $A(\tau)$

Chapter 3: Decaying law for the free oscillating response of a sliding SDOF system

3.1 Introduction

Friction is an essential aspect for different mechanical systems. Thus, many researchers have been involved in various friction models. For example, in the case of Coulomb friction, it is modeled as a constant value independent of the sliding velocity. In other cases, viscous friction is introduced to model a linear relationship with its sliding velocity. Sometimes, Stribeck effect has also been introduced [1]. In fact, friction modeling remains a challenge in mechanical systems. In order to analyze the dynamic behavior, one of the solutions is to introduce a polynomial expansion of the friction coefficient as a function of the sliding velocity [2]. Moreover, it is essential to find out the amplitude evolution of a vibrational signal. Feldman and Braun [3] use the Hilbert transform for the vibration analysis. By considering a displacement-time response of a nonlinear differential equation with dry friction, they get a hyperbolic form for the amplitude as a function of time using the Hilbert transform. Thus, this method is effective in order to evaluate some particular properties for nonlinear vibrational systems.

Moreover, vibratory motion at contact interfaces has been of great interest to several investigators due to its risk against fatigue and wear, i.e. the railroad wheel-rail contact interface. Previous studies on the contact loss were carried out using numerical and experimental methods in order to investigate contact vibration problems. In 1972, Nayak [4] has proposed a single degree-of-freedom dynamic system in order to study the contact interface. Thus, he was able to obtain the time response analytically using the single term harmonic balance method. In 1991, Hess and Soom [5] have analyzed the reduction of the average friction coefficient induced by the dynamic oscillating responses using the multiple methods. Later on, Perret-Liaudet and Rigaud [6, 7] used the shooting method in conjunction with parametric continuation technique in order to solve an impacting Hertzian contact. They perform an explicit numerical time integration scheme, specifically the central difference method in order to solve the equation of motion.

In chapter 2, the measured displacement and velocity free responses corresponding to the experimental tests of some tribological systems show a variety of amplitude evolution forms. These forms can be explained depending on the friction model of the system. This later will be discussed in the present chapter.

In this context, we will demonstrate a single degree-of-freedom (SDOF) mass-spring system having a pseudo-polynomial friction model. We will solve the differential equation of motion using the Runge-Kutta time scheme numerical integration in order to obtain the displacement and velocity-time responses. We will study the effect of the pseudo-polynomial friction model on the behavior of the free oscillatory responses by varying the constants carried in the

friction coefficient. The amplitude evolution, known as the envelope, is determined using the Hilbert Transform. In order to better understand the friction model, the first and second derivative of the amplitude is analyzed.

3.2 The dynamic model

3.2.1 Description of the system and its friction model

The studied dynamic system consists of a SDOF mass-spring system (see Figure 1), having a mass m and a linear spring of stiffness k. The mass can slide freely on a fixed massive plane. A constant normal load N is applied to the contact interface resulting in a friction force T opposite to the motion. This friction force is related to the normal force through the friction coefficient μ which is a function of the sliding velocity v having both the same sign, i.e. $T = \mu_k(v)N$.

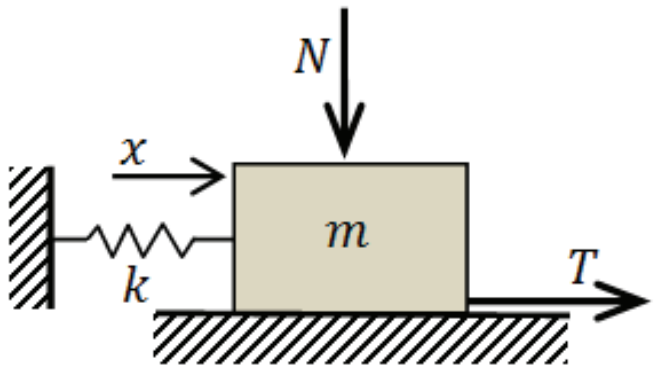

Figure 1. The studied SDOF mass-spring mechanical system.

The out of static equilibrium equation of motion which governs the free oscillating response of the studied dynamic system is written as follows:

$$m\frac{d^2x}{dt^2} + kx = -T(v) = -\mu_k(v)N \qquad (1)$$

where x is the displacement of the system, $v = \frac{dx}{dt}$ is the sliding velocity of the system, $\frac{d^2x}{dt^2}$ is the acceleration corresponding to the system and $\mu_k(v)$ is the kinematic friction coefficient. $\mu_k(v)$ is described by a pseudo-polynomial friction model. It is introduced as a power series of the sliding velocity v, including the sign function. Its general form is represented as follows:

$$\mu_k(v) = (p_0 + p_2v^2 + \cdots)\mathrm{sgn}(v) + (p_1v + p_3v^3 + \cdots) \qquad (3)$$

i.e.

$$\mu_k(v) = \sum_{j=0}^{n}[(p_{2j}v^{2j})\mathrm{sgn}(v) + (p_{2j+1}v^{2j+1})] \qquad (4)$$

The sign function preserves the asymmetry of the friction coefficient. Thus sign function $\mathrm{sgn}(v)$ preserves the odd property of $T(v)$. Actually, we must have $T(-v) = -T(v)$. Furthermore, coefficients μ_m must be in such a way that $T(|v|) > 0$ to ensure the dissipative behavior of the friction force. Notice that the polynomial power series is not obtained from a Taylor expansion of the kinematic coefficient around zero.

3.2.2 Equilibrium state

Conditions for the equilibrium can be easily found as follows:

$$\boldsymbol{\frac{d^2x}{dt^2} = 0, \frac{dx}{dt} = 0, |x_s| < +\frac{\mu_s}{k}} \qquad (5)$$

$\boldsymbol{\mu_s}$ is the static friction coefficient of the system.

3.2.3 Dimensionless equation of motion

Equation (1) is conveniently rewritten in a dimensionless form by performing the necessary replacements using the Vaschy-Buckingham theorem. We use the following rescaling:

$$\Omega^2 = \frac{k}{m}, \tau = \Omega t, y = \frac{k}{N}x \qquad (6)$$

where Ω is the undamped circular natural frequency, τ is the dimensionless time and y is the dimensionless displacement. For the dimensionless velocity $\dot{y}$ and acceleration $\ddot{y}$, we have

$$\dot{y} = \frac{dy}{d\tau} = \frac{k}{N\Omega}\frac{dx}{dt}, \ \ddot{y} = \frac{d^2y}{d\tau^2} = \frac{k}{N\Omega^2}\frac{d^2x}{dt^2} \qquad (7)$$

The dot represents the derivative with respect to the dimensionless time τ. Thus, the dimensionless equation of motion is derived to be:

$$\ddot{y} + y = -f(\dot{y}) \qquad (8)$$

where $f(\dot{y})$ is the friction coefficient as a function of the dimensionless velocity $\dot{y}$, that is

$$f(\dot{y}) = \mu\left(\frac{N\Omega}{k}\dot{y}\right) \qquad (9)$$

Thus, the constants of the friction coefficient $f(\dot{y})$ can be written as the above:

$$\mu_j = (\frac{N\Omega}{k})^j p_j \qquad (10)$$

i.e. for the first 4 terms:

$$\mu_0 = p_0, \mu_1 = \frac{N\Omega}{k}p_1, \mu_2 = (\frac{N\Omega}{k})^2 p_2 \text{ and } \mu_3 = (\frac{N\Omega}{k})^3 p_3 \qquad (11)$$

Without loss of generality, the friction coefficient $f(\dot{y})$ can be defined to have a general pseudo-polynomial expansion as a function of the dimensionless velocity $\dot{y}$ such that

$$f(\dot{y}) = (\mu_0 + \mu_2\dot{y}^2 + \cdots)\mathrm{sgn}(\dot{y}) + (\mu_1\dot{y} + \mu_3\dot{y}^3 + \cdots) \quad (12)$$

i.e.

$$f(\dot{y}) = \sum_{n=0}^{+\infty}\mu_{2n}\dot{y}^{2n}\mathrm{sgn}(\dot{y}) + \sum_{n=0}^{+\infty}\mu_{2n+1}\dot{y}^{2n+1} \quad (13)$$

The sign function $\mathrm{sgn}(\dot{y})$ preserves the odd property of $f(\dot{y})$. Actually, we must have $f(-\dot{y}) = -f(\dot{y})$. Furthermore, coefficients μ_m must be in such a way that $f(|\dot{y}|) > 0$ to ensure the dissipative behavior of the friction force. As $f(\dot{y})$ is not differentiable in the neighborhood of zero, notice that the pseudo-polynomial form equation (13) cannot be obtained simply from a Taylor series expansion around $\dot{y} = 0$. Figure 2 shows an example of a friction model characterized a cubic polynomial friction model. This figure presents the dimensionless friction force as a function of the dimensionless velocity having the following form: $f(\dot{y}) = (1 - 0.2\dot{y}^2)\mathrm{sign}(\dot{y}) + \frac{1}{3}(0.4\dot{y} + 0.1\dot{y}^3)$.

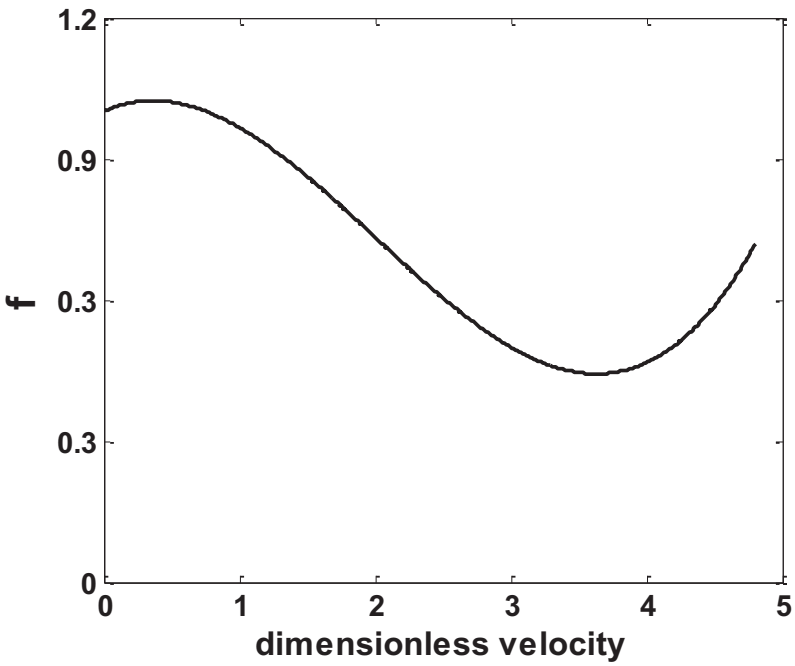

Figure 2. Dimensionless friction force as a function of the dimensionless velocity corresponding to cubic polynomial kinematic friction model having the following form: $f(\dot{y}) = \mu_3\dot{y}^3 + \mu_2\dot{y}^2 sgn(\dot{y}) + \mu_1\dot{y} + \mu_0$ where $\mu_3 = 0.1/3$, $\mu_2 = -0.2$, $\mu_1 = 0.4/3$ and $\mu_0 = 1$.

In dimensionless form, the state of equilibrium becomes as the following:

$$\ddot{y} = 0, \dot{y} = 0, |y| < \mu_k \qquad (14)$$

3.3 The dynamic free responses and its envelope

The sliding SDOF system undergoing dynamic free responses is analyzed in this section. Without loss of generality, we consider the free motion to the initial conditions $y(0) = Y_0$ and $\dot{y}(0) = 0$, assuming that Y_0 is large enough in order to produce motion. Actually, we need to break the equilibrium subjected to the static friction force. Furthermore, this study is focused on the underdamped cases in a way that motion is oscillatory with decreasing amplitude. In this context, the principal aim of this study is to analyze the decreasing envelope $A(\tau)$ of the response as a function of the introduced friction law. Indeed, it is related to the decay of energy resulting from the dissipative nature of friction.

3.3.1 Numerical methods

The nonlinear differential equation of motion, equations (4) and (7), can be numerically integrated using classic computational integration time methods, such as for example the common fourth-order Runge-Kutta (see Appendix A) or RK4 method [8]. Following the RK4 method, the envelope can be found from the approximate solution of Equation (4). Various definitions for the envelope of oscillating responses have been introduced. Among these definitions, we will introduce at the beginning the definition of Mark and Crandall [9]. The advantage of this envelope, $A_{M\&C}(\tau)$, is that it is directly related to the total energy $\mathcal{E}$ of the system. Indeed, we have

$$A_{M\&C}(\tau) = \sqrt{y^2 + \dot{y}^2} = \sqrt{2\mathcal{E}} \qquad (15)$$

This latter also corresponds to the instantaneous radius of the dynamic response described in the phase plane from the particular equilibrium state ($y_e = \dot{y}_e = 0$). Figure 3 shows an example of trajectory in the phase plane, whereas the corresponding time histories of displacement and velocity are given in Figure 4.

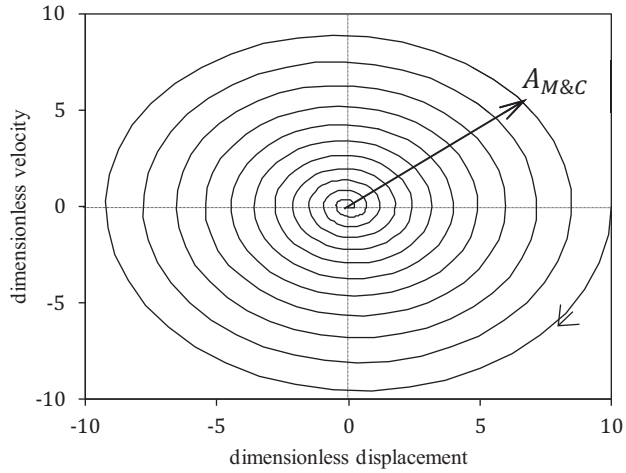

Figure 3. Trajectory and envelope radius $A_{M\&C}$ on the phase plane $(y, \dot{y})$ with friction coefficient $f(\dot{y}) = \mu_0 \mathrm{sgn}(\dot{y}) + \mu_1 \dot{y}$. $\mu_0 = 0.1$, $\mu_1 = 0.019$ and initial conditions $Y_0 = 10$.

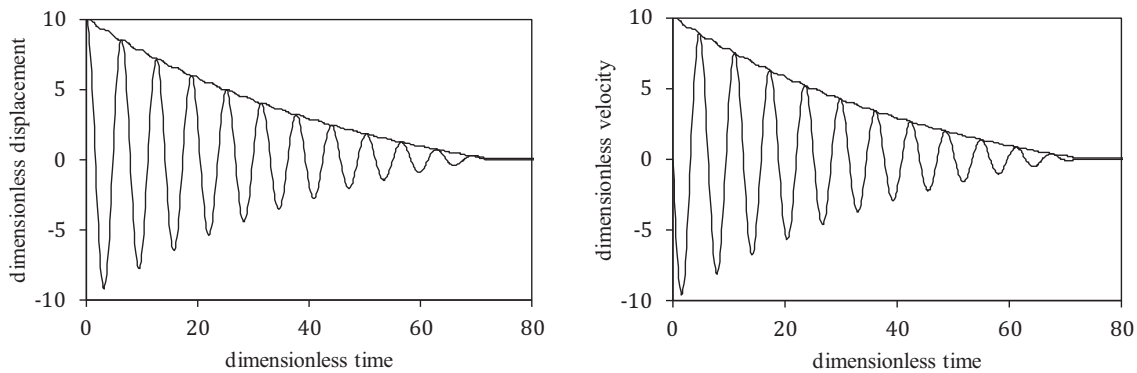

Figure 4. Displacement, velocity and envelope $A_{M\&C}$ time responses with friction coefficient $f(\dot{y}) = \mu_0 \mathrm{sgn}(\dot{y}) + \mu_1 \dot{y}$. $\mu_0 = 0.1$, $\mu_1 = 0.019$ and initial conditions $Y_0 = 10$.

An alternate description of the envelope of the oscillating response can be performed using the Hilbert transform (see appendix B) [10]. Thus, we consider the Hilbert transform $\hat{y}(\tau)$ of the displacement response $y(\tau)$ as follows

$$\hat{y}(\tau) = \mathcal{H}\{y\} = h * y = \frac{1}{\pi} \mathrm{p.v.} \int_{-\infty}^{+\infty} \frac{y(s)}{\tau - s} ds \quad (16)$$

where $*$ denotes the convolution product and

$$h(\tau) = \frac{1}{\pi\tau} \qquad (17)$$

Then, the envelope is given by

$$A_{H_y}(\tau) = \sqrt{y^2 + \hat{y}^2} \qquad (18)$$

As the same procedure can be applied on the dimensionless velocity response $\dot{y}(\tau)$, one can defined another envelope A_{H2} by

$$A_{H_{\dot{y}}}(\tau) = \sqrt{\dot{y}^2 + \hat{\dot{y}}^2} \qquad (19)$$

Figure 5 shows the same example as depicted in Figures 3 and 4 in order to compare the various definitions of the envelope.

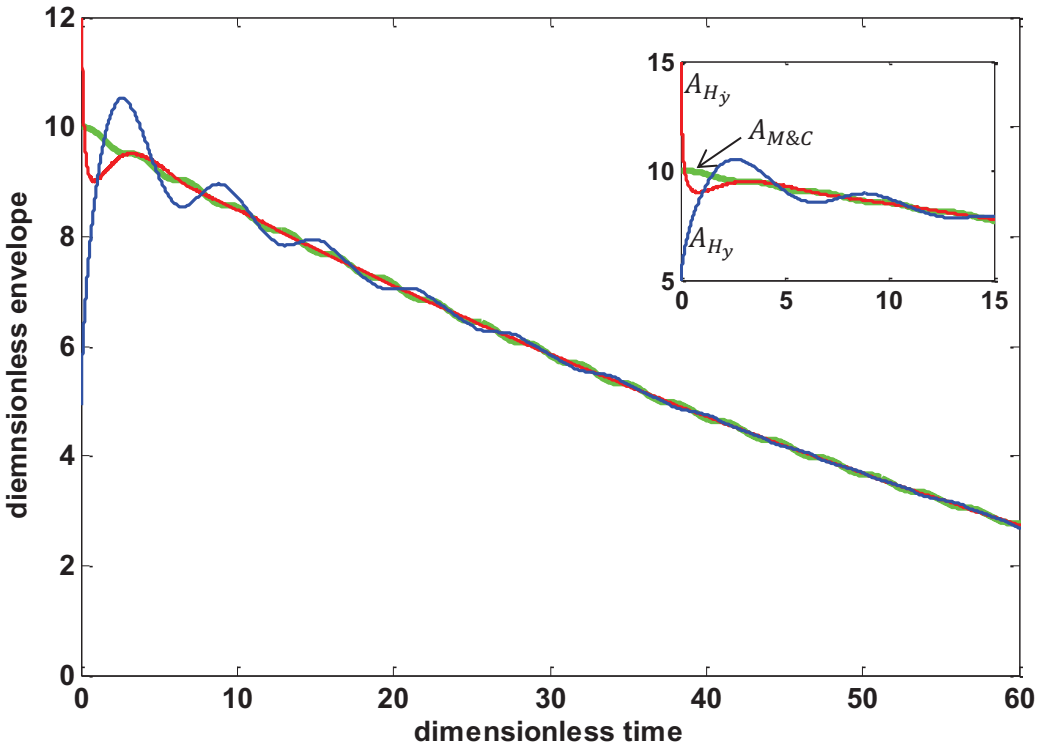

Figure 5. Envelopes $A_{M\&C}$, A_{H_y} and $A_{H_{\dot{y}}}$ time responses with friction coefficient $f(\dot{y}) = \mu_0 \mathrm{sgn}(\dot{y}) + \mu_1 \dot{y}$. $\mu_0 = 0.1$, $\mu_1 = 0.019$ and initial conditions $Y_0 = 10$.

We can notice from the above figure (Figure 5) discrepancies at the beginning of the free response that are related to the Gibbs phenomenon. This behavior is more highlighted in the case of the displacement than that of the velocity.

3.3.2 The averaging method

In order to better understand the behavior of the dynamic response, the decaying envelope can be also obtained analytically from the method of averaging [11]. Following this method, a slow time-variation of the amplitude and the phase of the response compared to the period of the oscillating part of the system is assumed. Thus, the displacement and velocity responses have the following approximate dimensionless form:

$$y(\tau) = A(\tau)\cos\big(\tau + \varphi(\tau)\big) = A\cos(\phi) \qquad (20)$$

and

$$\dot{y}(\tau) = -A(\tau)\sin\big(\tau + \varphi(\tau)\big) = -\,A\sin(\phi) \qquad (21)$$

where amplitude $A(\tau)$ and phase $\varphi(\tau)$ vary slowly in time without affecting the oscillatory behaviour of the solution. By averaging out the variations in ϕ over one period 2π, the slow variations of A and φ are determined as follows:

$$\dot{A}(\tau) = \frac{1}{2\pi}\int_0^{2\pi} \sin\phi\, f(-Asin\phi)d\phi \qquad (22)$$

and

$$\dot{\varphi}(\tau) = \frac{1}{2\pi A}\int_0^{2\pi} \cos\phi\, f(-Asin\phi)d\phi \qquad (23)$$

After the integration process and taking into account the pseudo-polynomial expansion equation (12), equation (22) becomes $\dot{\varphi}(\tau) = 0$ and the first order derivative of the envelope is obtained as follows

$$\frac{dA}{d\tau} = \dot{A} = F(A) = -\sum_{n=0}^{+\infty}\{[\frac{\mu_n}{\pi}\int_0^{\pi} \sin^{n+1}\phi\, d\phi]A^n\} \qquad (24)$$

with $n \in \mathbb{N}$

In general, $F(A)$ is written as the following

$$F(A) = \frac{dA}{d\tau} = \dot{A} = \sum_{k=0}^{+\infty} a_n A^n \qquad (25)$$

with

$$a_n = -\frac{\mu_n}{\pi}\int_0^{\pi} \sin^{n+1}\phi\, d\phi \qquad (26)$$

After the calculation process (see Appendix C), we obtain the following:

$$a_{2k} = -\frac{2}{\pi}\mu_{2k}\prod_{j=1}^{j=k}\frac{2j}{2j+1} \qquad (27)$$

$$a_{2k+1} = -\mu_{2k+1}\prod_{j=1}^{j=k+1}\frac{2j-1}{2j} \qquad (28)$$

with $k \in \mathbb{N}$

The three first constants are

$$a_0 = -\frac{2}{\pi}\mu_0,\ a_1 = -\frac{1}{2}\mu_1,\ a_2 = -\frac{4}{3\pi}\mu_2 \qquad (29)$$

The decaying law of A can be analytically obtained by directly integrating equation (25) as follows:

$$\tau - \tau_0 = \int_{A_0}^{A} \frac{da}{F(a)} \tag{30}$$

However, for complicated integrations, numerical scheme such as the RK4 method can be used.

3.3.3 Behavior of the decreasing oscillations

General behavior of the envelope governed by equation (24) is directly determined from the sign of the function $F(A)$. Indeed, the envelope strictly decays if and only if $F(A) < 0$. Moreover, the knowledge of its fixed points A^* such that $F(A^*) = 0$ is essential for the analysis. As shown in equation (29), we can notice that the sign of a_0 is opposite to that of μ_0 which is positive for valid friction model. Thus, $F(A) < 0$ for $A \gtrsim 0$ which ensures valid decay of the envelope near zero. Therefore, the validity is defined from $A = 0$ to $A = A^*$ in which A^* is the fixed point where $F(A^*) = 0$. However, if the fixed point does not exist then, the validity is defined for all A from 0 to $+\infty$. More generally, the decaying envelope is always valid when $f(\dot{y})$ remains positive for all explored amplitudes.

In addition, we are able to get some information regarding the form of the envelope from the sign of the second time derivative of A, $\frac{d^2A}{d\tau^2}$. This latter is equal to $\ddot{A} = \frac{dF}{d\tau} = \frac{dF}{dA}\dot{A} = F(A)\frac{dF}{dA}$.

Knowing that $F(A) < 0$, the form of the envelope depends only on the sign of $\frac{dF}{dA} = F'(A)$. Table 1 summarizes the different possible forms of the envelope which can be convex, straight or concave. Moreover, mixed form is observed when the sign of $F'(A)$ changes with A.

$F'(A)$	envelope form
< 0	Convex
$= 0$	Straight
> 0	concave

Table 1. Envelope forms versus sign of $F'(A)$.

3.4 Numerical results

In the following, we will study the different cases of the friction models corresponding to the dimensionless displacement and velocity-time response, $y(\tau)$ and $\dot{y}(\tau)$ respectively. These latter responses are determined numerically using the Runge-Kutta method of order 4 (RK 4). We will present as well the decaying envelope of the oscillating responses using the definition of Mark and Crandall (Equation 15), Hilbert Transform (Equations 18 and 19) and the averaging method (Equation 24).

3.4.1 Constant friction coefficient

We consider in the first example a constant friction i.e. independent of the sliding velocity. In the case, the dimensionless friction force is represented by $f(\dot{y}) = \mu_0 \mathrm{sgn}(\dot{y})$. Thus, the decaying envelope for this case can be obtained analytically by integrating the following:

$$\tau - \tau_0 = \int_{A_0}^{A} \frac{dA}{a_0} \qquad (31)$$

where

$$a_0 = -\frac{2}{\pi}\mu_0 \qquad (32)$$

At the initial conditions $\tau_0 = 0$ and $A_0 = Y_0$, the decaying envelope analytical solution is determined as

$$A(\tau) = -\frac{2\mu_0}{\pi}\tau + Y_0 \quad (33)$$

This latter decaying envelope is valid for $\tau \leq \frac{\pi Y_0}{2\mu_0}$. Moreover, the decaying envelop form corresponding to this friction model is described by a straight line since $\mathrm{F}'(\mathrm{A}) = 0$.

Figure 6 (a) presents the dimensionless displacement, $\mathbf{y}$ response as a function of dimensionless time, $\boldsymbol{\tau}$ corresponding to a mechanical system described by a constant friction coefficient where the friction force is $\mathbf{f}(\dot{\mathbf{y}}) = \mathbf{0.2\ sgn}(\dot{\mathbf{y}})$. The initial conditions are taken as $\boldsymbol{y}(\mathbf{0}) = \boldsymbol{Y_0} = \mathbf{10}$ and $\dot{\boldsymbol{y}}(\mathbf{0}) = \mathbf{0}$. This latter friction model is valid when $\boldsymbol{\tau} \leq \mathbf{78}$. Figure 6 (b) shows the dimensionless amplitude of the latter system represented using four different method: averaging method (in black), definition of Mark and Crandall (in green), Hilbert transform of the displacement (in blue) and Hilbert transform of the velocity (in red).

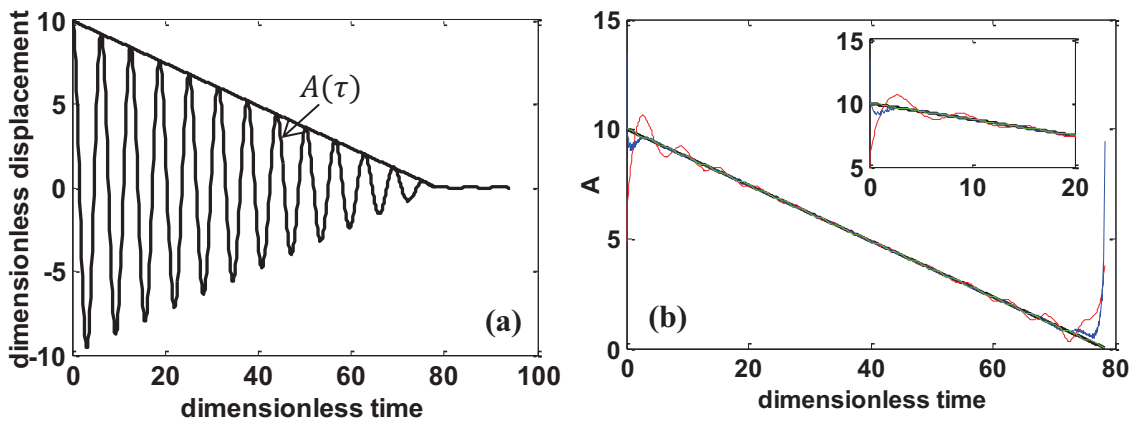

Figure 6. (a) Dimensionless displacement-time response $y(\tau)$ with its decaying amplitude $A(\tau)$ corresponding to a mechanical system having an equation of motion $\ddot{y} + y = -f(\dot{y}) = -\mu_0 sgn(\dot{y})$ where $\mu_0 = 0.2$ and initial conditions $y(0) = 10$ and $\dot{y}(0) = 0$. (b)Dimensionless amplitude as a function of the dimensionless time for the same system as 6(a) in four different methods: averaging method (black), definition of Mark and Crandall (green), Hilbert transform of the displacement (blue) and Hilbert transform of the velocity (red).

3.4.2 Viscous friction coefficient

As for the second example, we consider a viscous friction coefficient where $f(\dot{y}) = \mu_1 \dot{y}$. This friction has a linear relationship with the sliding velocity. Its corresponding constant μ_1 is positive in order to ensure the damping properties of the system. The decaying envelope for the viscous friction model can be obtained analytically by integrating the following:

$$a_1(\tau - \tau_0) = \int_{A_0}^{A} \frac{dA}{A} \quad (34)$$

where

$$a_1 = -\frac{1}{2}\mu_1 \quad (35)$$

The analytical solution of the decaying envelope describing this model can be obtained analytically having $\tau_0 = 0$ and $A_0 = Y_0$ as initial conditions.

$$A(\tau) = Y_0 e^{-\frac{\mu_1}{2}\tau} \text{ for all } \tau > 0 \qquad (36)$$

This latter decaying envelope describes the exponential decay law and it is always valid since $A(\tau) \geq 0$. Moreover, the envelope form corresponding to this friction model is convex since $\mathrm{F}'(\mathrm{A}) = \mathrm{a}_1 = -\frac{1}{2}\mu_1 < 0$.

The following figure 7 (a) presents the dimensionless displacement, y response as a function of dimensionless time, τ corresponding to a mechanical system described by a constant friction coefficient where the friction force is $\mathrm{f}(\dot{\mathrm{y}}) = 0.1\,\dot{\mathrm{y}}$. The initial conditions are described by $y(0) = Y_0 = 10$ and $\dot{y}(0) = 0$. Thus, the system is valid for all $\tau > 0$. Figure 7 (b) shows the dimensionless amplitude of the latter system represented using four different method: averaging method (in black), definition of Mark and Crandall (in green), Hilbert transform of the displacement (in blue) and Hilbert transform of the velocity (in red). The decaying envelope is characterized by a convex form since $F'(A) > 0$ for all $A > 0$

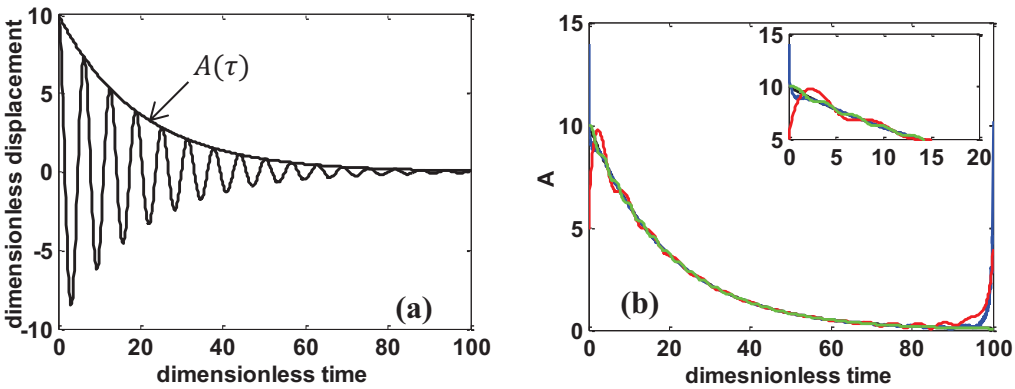

Figure 7. (a) Dimensionless displacement-time response $y(\tau)$ with its decaying amplitude $A(\tau)$ corresponding to a mechanical system having an equation of motion $\ddot{y} + y = -f(\dot{y}) = -\mu_1\dot{y}$ where $\mu_1 = 0.1$ and initial conditions $y(0) = 10$ and $\dot{y}(0) = 0$. (b)Dimensionless amplitude as a function of the dimensionless time in four different methods: averaging method (black), definition of Mark and Crandall (green), Hilbert transform of the displacement (blue) and Hilbert transform of the velocity (red).

3.4.3 Coulomb and linear viscous friction coefficient

We assume now that the function coefficient is a one variable affined as a function of the sliding velocity. The dimensionless friction force is written as $f(\dot{y}) = \mu_0 sign(\dot{y}) + \mu_1\dot{y}$ where μ_0 is positive. When $\mu_1 > 0$, the friction model is always valid. However, when $\mu_1 < 0$, the friction model is valid for all $y < -\frac{\mu_0}{\mu_1}$. The analytical equation of the decaying envelope is found to be

$$\tau - \tau_0 = \int_{A_0}^{A} \frac{dA}{a_1 A + a_0} \qquad (37)$$

where $a_0 = -\frac{2}{\pi}\mu_0$ and $a_1 = -\frac{1}{2}\mu_1$.

The initial conditions are defined by $\tau_0 = 0$ and $A_0 = Y_0$. Thus, the analytical equation of the decaying envelope is determined to be as follows:

$$A(\tau) = \left(Y_0 + \frac{4\mu_0}{\pi\mu_1}\right) e^{-\frac{\mu_1}{2}\tau} - \frac{4\mu_0}{\pi\mu_1} \qquad (38)$$

This friction model is valid when $\tau < \frac{2}{\mu_1}\ln(1 + \frac{\pi\mu_1 Y_0}{4\mu_0})$. Moreover, when $\mu_1 > 0$, the envelope form is described by a convex form since $F'(A) = -\frac{\mu_1}{2} < 0$. However when $\mu_1 < 0$, the envelope form is concave form since $F'(A) = -\frac{\mu_1}{2} > 0$.

In the following example (Figure 8), we consider a coulomb and linear viscous friction model with $\mu_1 > 0$. The mechanical system is described by the following equation of motion: $\ddot{y} + y = -(\mu_0 sgn(\dot{y}) + \mu_1\dot{y})$ where $\mu_0 = 0.08$ and $\mu_1 = 0.04$. The initial conditions are defined by $y(0) = y_0 = 10$ and $\dot{y}(0) = 0$. Figure 8 (a) presents the dimensionless

displacement-time response $y(\tau)$ along with its amplitude traced using its analytical equation. This latter friction model is valid for $\tau < 80$. Figure 8 (b) presents the decaying envelope of the response corresponding to this latter system using four different methods: averaging method (in black), definition of Mark and Crandall (in green), Hilbert transform of the displacement (in blue) and Hilbert transform of the velocity (in red). The decaying envelope is characterized by a convex form since $F'(A) < 0$ for all $A > 0$. Figure 8 (c) presents the dimensionless friction force f as a function of the dimensionless velocity $\dot{y}$. This shows that the friction model is valid for all values of A.

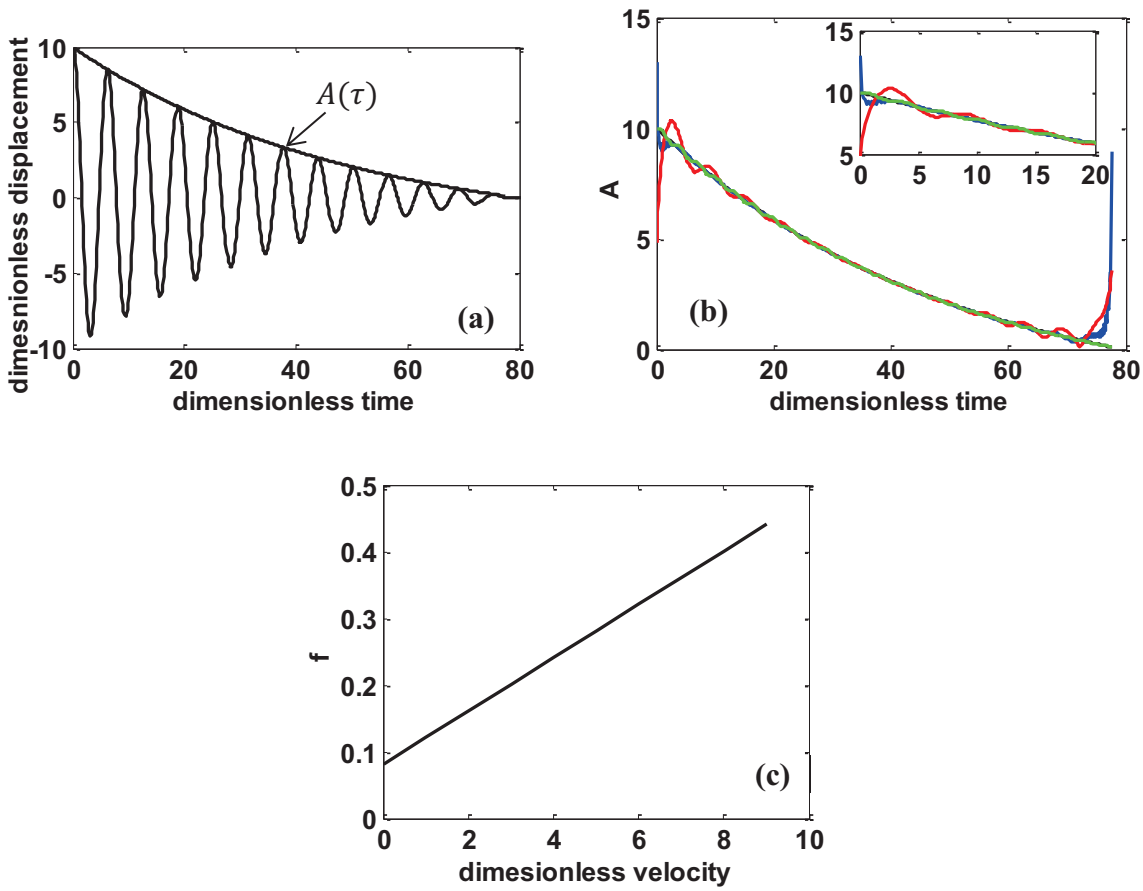

Figure 8. (a) Dimensionless displacement-time response $y(\tau)$ with its decaying amplitude $A(\tau)$ corresponding to a mechanical system having an equation of motion $\ddot{y} + y = -f(\dot{y}) = -(\mu_0 sgn(\dot{y}) + \mu_1 \dot{y})$ where $\mu_0 = 0.08$ and $\mu_1 = 0.04$ and initial conditions $y(0) = 10$ and $\dot{y}(0) = 0$. (b)Dimensionless amplitude as a function of the dimensionless time in four different methods: averaging method (black), definition of Mark and Crandall (green), Hilbert transform of the displacement (blue) and Hilbert transform of the velocity (red). (c) Dimensionless friction force as a function of the dimensionless velocity, $f(\dot{y}) = 0.08 + 0.04\dot{y}$ for all $\dot{y} \geq 0$.

Figure 9 presents an example on mechanical system having a coulomb and linear viscous friction model with $\mu_1 < 0$. The equation of motion is described by: $\ddot{y} + y = -(\mu_0 sgn(\dot{y}) + \mu_1 \dot{y})$ where $\mu_0 = 0.4$ and $\mu_1 = -0.04$. This latter friction model is valid for $\tau < 77$. The

initial conditions are defined by $y(0) = y_0 = 10$ and $\dot{y}(0) = 0$. The dimensionless displacement-time response $y(\tau)$ and its amplitude found analytically are presented in Figure 9 (a). Figure9 (b) shows the decaying envelope of the response corresponding to this latter system using four different methods: averaging method (in black), definition of Mark and Crandall (in green), Hilbert transform of the displacement (in blue) and Hilbert transform of the velocity (in red). The decaying envelope is characterized by a concave form since $F'(A) > 0$ for all $A > 0$. Figure 9 (c) and (d) present respectively the dimensionless friction force f as a function of the dimensionless velocity $\dot{y}$ and the function F as a function of the amplitude A. This shows that the friction model is valid for $y < 10$.

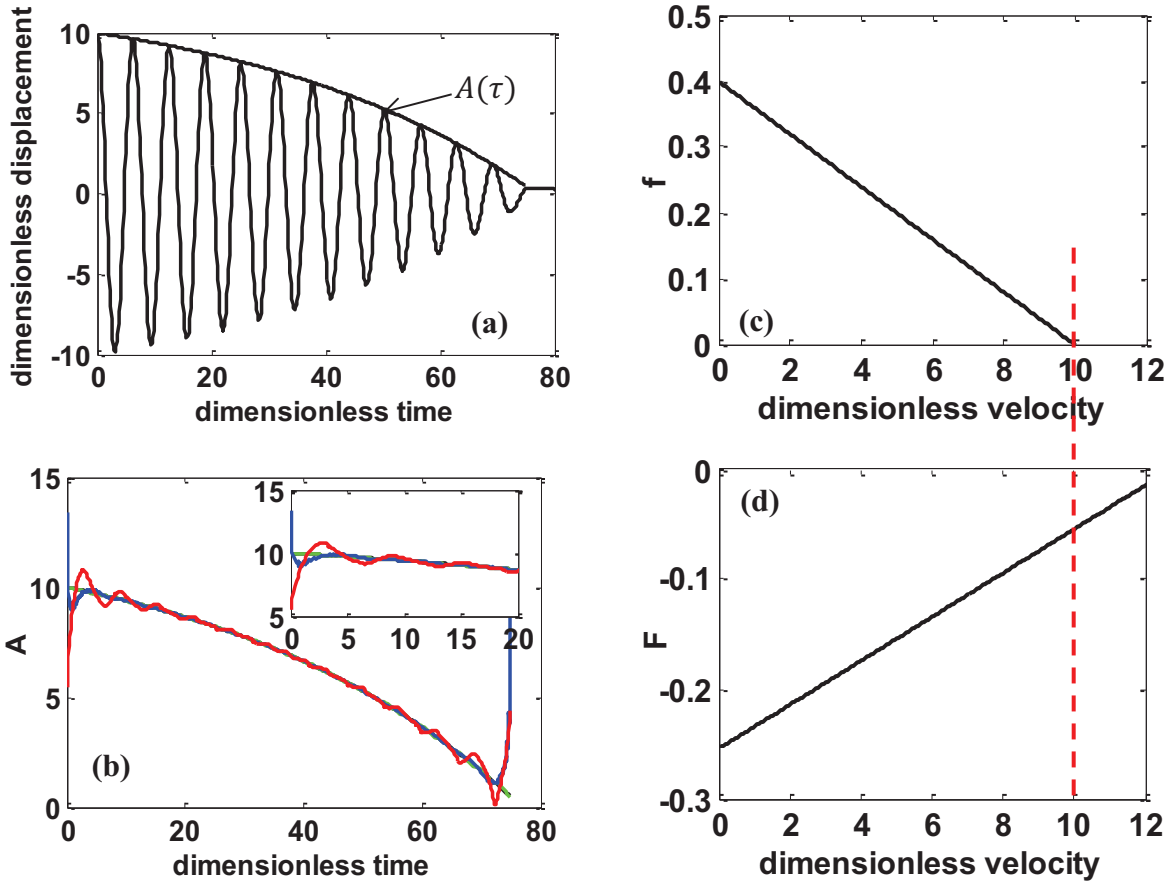

Figure 9. (a) Dimensionless displacement-time response $y(\tau)$ with its decaying amplitude $A(\tau)$ corresponding to a mechanical system having an equation of motion $\ddot{y} + y = -f(\dot{y}) = -(\mu_0 sgn(\dot{y}) + \mu_1 \dot{y})$ where $\mu_0 = 0.4$ and $\mu_1 = -0.04$ and initial conditions $y(0) = 10$ and $\dot{y}(0) = 0$. (b)Dimensionless amplitude as a function of the dimensionless time in four different methods: averaging method (black), definition of Mark and Crandall (green), Hilbert transform of the displacement (blue) and Hilbert transform of the velocity (red). (c) Dimensionless friction force as a function of the dimensionless velocity, $f(\dot{y}) = 0.4 - 0.04\dot{y}$ for all $\dot{y} \geq 0$. (d) F as a function of A.

3.4.4 Quadratic friction coefficient

For the 4th friction model, we consider a quadratic friction coefficient written as follows:

$$f(\dot{y}) = (\mu_0 + \mu_2 \dot{y}^2) sign(\dot{y}) + \mu_1 \dot{y} \qquad (39)$$

Using the averaging method, the first order derivative of the envelope is represented in the following quadratic form:

$$F(A) = \frac{dA}{d\tau} = a_2 A^2 + a_1 A + a_0 \qquad (40)$$

a_2, a_1 and a_0 are written as a function of μ_2, μ_1 and μ_0 respectively as shown in equations (27) and (28).

$$a_2 = -\frac{4}{3\pi}\mu_2,\ a_1 = -\frac{1}{2}\mu_1 \text{ and } a_0 = -\frac{2}{\pi}\mu_0 \quad (41)$$

The decaying envelope for the quadratic friction model is determined analytically by performing the following integration process (see Appendix D):

$$\tau - \tau_0 = \int_{A_0}^{A} \frac{dA}{a_2 A^2 + a_1 A + a_0} \qquad (42)$$

The initial conditions are defined by $\tau_0 = 0$ and $A_0 = Y_0$. We can obtain three different analytical solutions of the decaying envelopes. This latter depends on the sign of Δ^2 which is defined as follows:

$$\Delta^2 = {a_1}^2 - 4a_0 a_2 \qquad (43)$$

Thus, the three analytical solution of the decaying envelope, $A(\tau)$ are determined in the below 3 cases.

<u>Case 1</u>: $\Delta^2 < 0$

The analytical solution of the decaying envelope, $A(\tau)$ for $\Delta^2 < 0$ is determined to be as follows:

$$A(\tau) = \frac{|\Delta|}{2a_2} tan\left[\frac{|\Delta|}{2}\tau + \varphi\right] - \frac{a_1}{2a_2} \qquad (44)$$

with $\varphi = tan^{-1}\left(\frac{(2a_2 A_0 + a_1}{\sqrt{4a_0 a_2 - {a_1}^2}}\right)$

In this case, a_2 is always negative, thus $\mu_2 > 0$. Also, there does not exist any point of equilibrium. Thus, the envelope form of the time response having a quadratic friction model depends on the sign of a_1, thus μ_1, which have opposite signs.

If $\mu_1 > 0$, then $F'(A)$ is negative. Therefore, one can conclude that the decaying envelope corresponding to this latter case is described as a convex. However, when $\mu_1 < 0$, the decaying envelope has two different forms: convex and concave. The decaying envelope has a concave form for $A \in [0, A^*]$ where $F'(A) > 0$ for this range. Nevertheless, when $A \in$

$]A^*, A_0]$, the decaying envelope is described by a convex form since $F'(A) < 0$ for this range. Note that A^* is the solution of $F'(A)$ where $F'(A^*) = 0$.

Figure 10 presents an example of an oscillating system described by a quadratic friction model having $\Delta^2 < 0$ and $\mu_1 > 0$. The dimensionless friction force is defined as: $f(\dot{y}) = 0.005\dot{y}^2 sgn(\dot{y}) + 0.04\dot{y} + 0.1$. The corresponding initial conditions are defined as $Y_0 = A_0 = 10$ and $\dot{y}(0) = 0$. The dimensionless displacement-time response $y(\tau)$ is shown in figure 10 (a) with its analytical decaying envelope. Figure 10 (b) shows the decaying envelope of the response corresponding to this latter system using four different methods: averaging method (in black), definition of Mark and Crandall (in green), Hilbert transform of the displacement (in blue) and Hilbert transform of the velocity (in red). The dimensionless friction force f as a function of the dimensionless velocity $\dot{y}$ (Figure 10 (c)) shows that this latter friction model is valid for all $\dot{y}$. F'as a function of the amplitude A is presented in Figure 10 (d). We can conclude that the decaying envelope has a convex form since $F'(A) < 0$ for all $A > 0$.

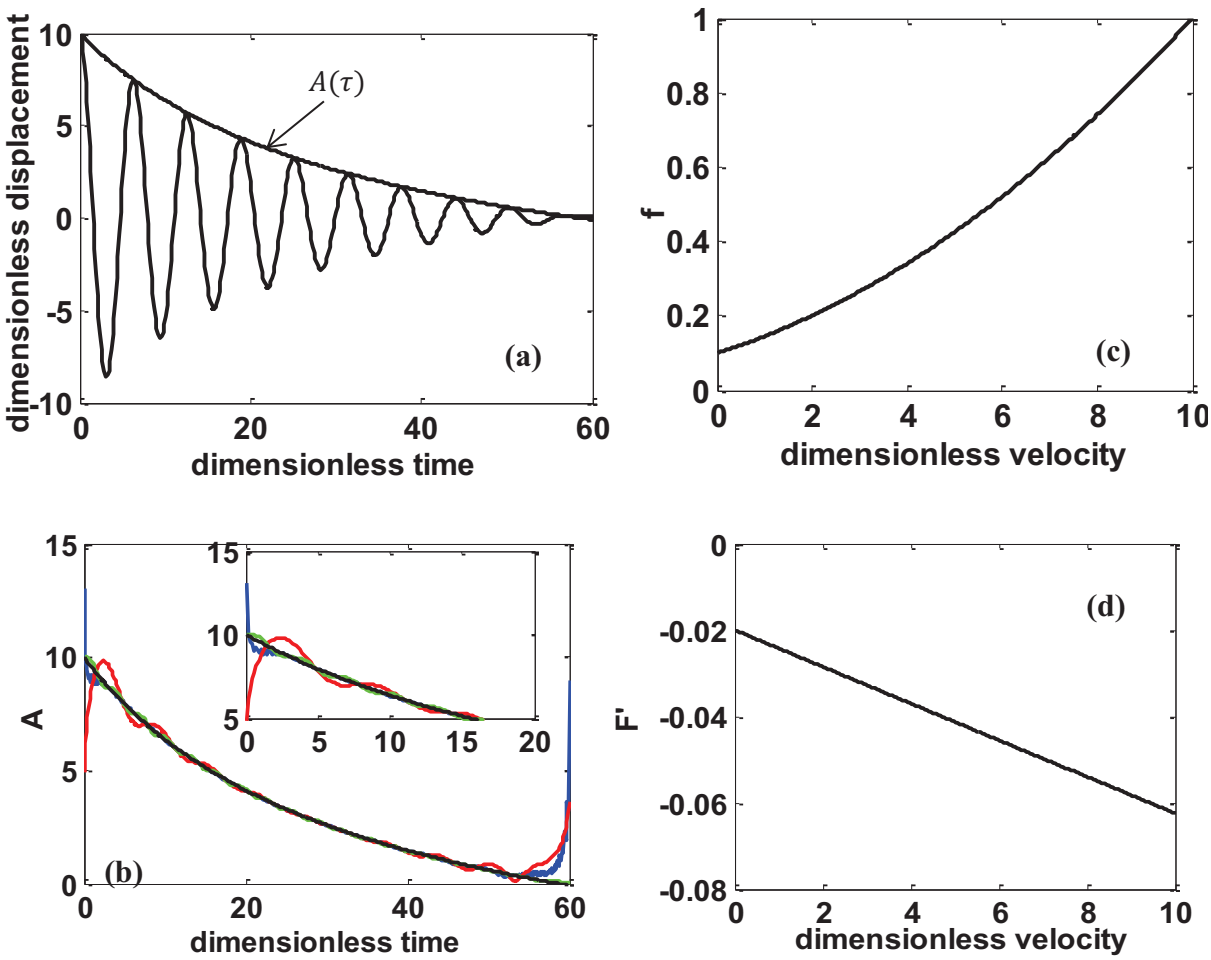

Figure 10. (a) Dimensionless displacement-time response $y(\tau)$ with its decaying amplitude $A(\tau)$ corresponding to a mechanical system having an equation of motion $\ddot{y} + y = -f(\dot{y}) = -(\mu_0 sgn(\dot{y}) + \mu_1\dot{y} + \mu_2\dot{y}^2 sgn(\dot{y}))$ where $\mu_0 = 0.1$, $\mu_1 = 0.04$, $\mu_2 = 0.005$ and initial conditions $y(0) = 10$ and $\dot{y}(0) = 0$. (b) Dimensionless amplitude as a function of the dimensionless time using four different methods: averaging method (black), definition of Mark and Crandall (green), Hilbert transform of the displacement (blue) and Hilbert transform of the velocity (red). (c) Dimensionless friction force as a function of the dimensionless velocity, $f(\dot{y})$ for all $\dot{y} \geq 0$. (c) F' as a function of A.

The example below presents an oscillating system described by a quadratic friction model having $\Delta^2 < 0$ and $\mu_1 < 0$. The dimensionless friction force is defined as: $f(\dot{y}) = 0.03\dot{y}^2 sgn(\dot{y}) - 0.25\dot{y} + 0.6$. The corresponding initial conditions are defined as $Y_0 = A_0 = 10$ and $\dot{y}(0) = 0$. Its dimensionless displacement-time response $y(\tau)$ is shown in figure 11 (a) with its analytical decaying envelope. The decaying envelope is described by both convex and concave forms. Figure 11 (b) shows the decaying envelope of the response corresponding to this latter system using four different methods: averaging method (in black), definition of Mark and Crandall (in green), Hilbert transform of the displacement (in blue) and Hilbert transform of the velocity (in red). Figure 11 (c) presents the dimensionless friction force f as a function of the dimensionless velocity $\dot{y}$. It shows that this latter friction model is valid for all $\dot{y}$. F'as a function of the amplitude A is shown in Figure 11 (d). We can conclude that the decaying envelope has a convex form when $y \in]4.9,10]$ since $F'(A) < 0$ for $A \in]4.9,10]$. However, the decaying envelop is described by a concave form when $y \in [0,14.7]$ since $F'(A) < 0$ for $A \in [0,4.9]$. The value 4.9 corresponds to A^* where $A^* = -\frac{a_1}{2a_2}$ (see Figure 11(d).

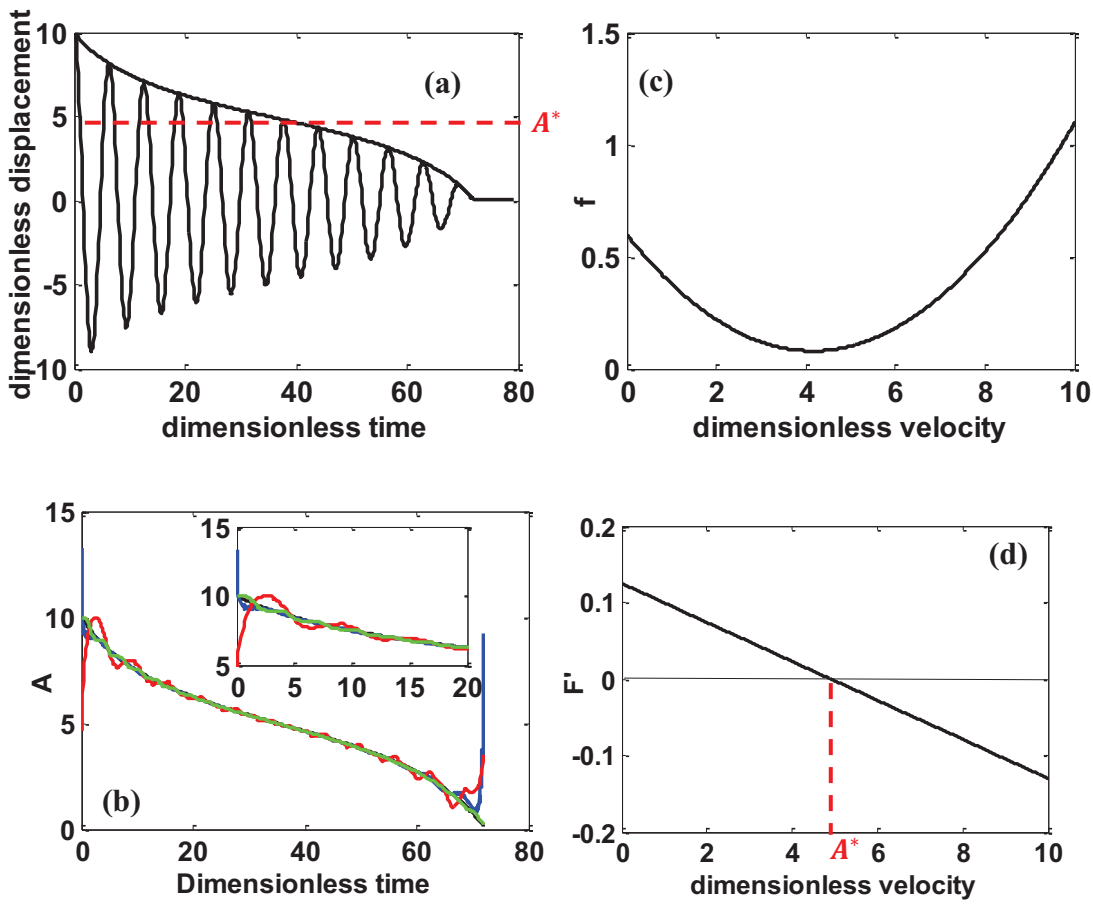

Figure 11. (a) Dimensionless displacement-time response $y(\tau)$ with its decaying amplitude $A(\tau)$ corresponding to a mechanical system having an equation of motion $\ddot{y} + y = -f(\dot{y}) = -(\mu_0 sgn(\dot{y}) + \mu_1\dot{y} + \mu_2\dot{y}^2 sgn(\dot{y}))$ where $\mu_0 = 0.6, \mu_1 = -0.25$, $\mu_2 = 0.03$ and initial conditions $y(0) = 10$ and $\dot{y}(0) = 0$. (b) Dimensionless amplitude as a function of the dimensionless time using four different methods: averaging method (black), definition of Mark and Crandall (green), Hilbert transform of the displacement (blue) and Hilbert transform of the velocity (red). (c) Dimensionless friction force as a function of the dimensionless velocity, $f(\dot{y})$ for all $\dot{y} \geq 0$. (d) F' as a function of A.

<u>Case 2</u>: $\Delta^2 = 0$

$$A(\tau) = \frac{A_0 + \frac{a_1}{2a_2}}{1 - a_2(A_0 + \frac{a_1}{2a_2})\tau} - \frac{a_1}{2a_2} \qquad (45)$$

In this case, a_2 is always negative, thus $\mu_2 > 0$ and a_1 is always positive, thus $\mu_1 < 0$. There exists only one point of equilibrium which is the solution of $F(A)$. For $\Delta^2 = 0$, the initial amplitude $A(0) = A_0$ is smaller than A^* where $A^* = -\frac{a_1}{2a_2}$. In other words, $A < -\frac{a_1}{2a_2}$. Then, we can conclude that $F'(A) = 2a_2A + a_1 > 0$ since $a_2 < 0$. Finally, one can say that the decaying envelope of the time response has a concave form.

Figure 12 presents an example of a dynamic system having a quadratic friction model with $\Delta^2 = 0$. The dimensionless friction force is described by $f(\dot{y}) = \mu_2\dot{y}^2 sgn(\dot{y}) + \mu_1\dot{y} + \mu_0 sgn(\dot{y})$ where $\mu_2 = 0.004$, $\mu_1 = -0.125$ and $\mu_0 = 0.904$. The initial conditions are defined as follows: $Y_0 = A_0 = 10$ and $\dot{y}(0) = 0$. Figure 12 (a) presents the dimensionless displacement y as a function along with its analytical representation of the decaying envelope $A(\tau)$. The decaying envelope of the response corresponding to this latter system, using four different methods: averaging method (in black), definition of Mark and Crandall (in green), Hilbert transform of the displacement (in blue) and Hilbert transform of the velocity (in red), is presented in Figure 12 (b). In Figure 12 (c), the dimensionless friction force as a function of the dimensionless velocity, $f(\dot{y})$ shows that the friction model of this system is valid for all $A \in [0,11.3]$. Figure 12 (d) presents $F'(A)$. $F'(A)$ is positive for all $A \in [0,18.8]$. Thus, the decaying envelope corresponding to this response is described by a concave form for all $A \in [0, A_0]$.

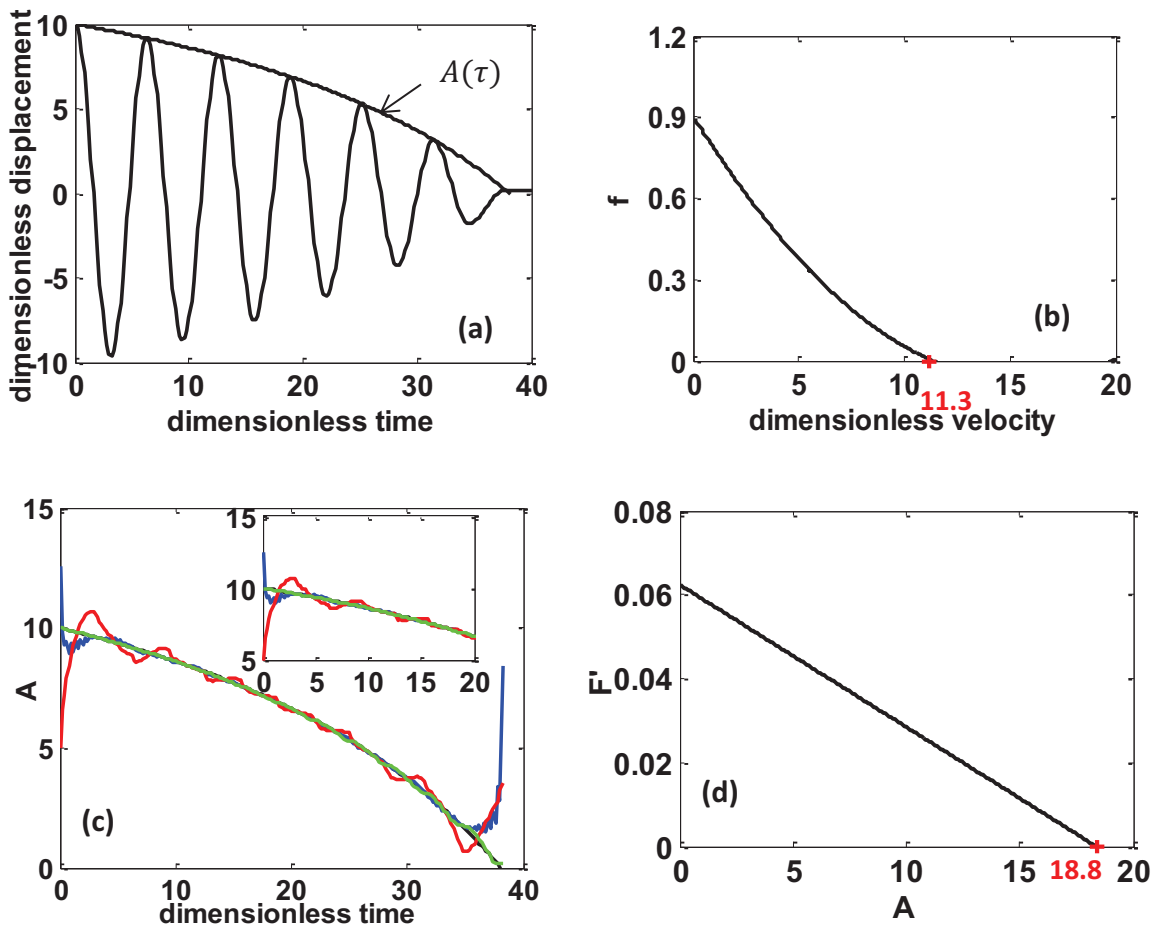

Figure 12. (a) Dimensionless displacement-time response $y(\tau)$ with its decaying amplitude $A(\tau)$ corresponding to a mechanical system having an equation of motion $\ddot{y} + y = -f(\dot{y}) = -(\mu_0 sgn(\dot{y}) + \mu_1\dot{y} + \mu_2\dot{y}^2 sgn(\dot{y}))$ where $\mu_0 = 0.904$, $\mu_1 = -0.125$, $\mu_2 = 0.004$ and initial conditions $y(0) = 10$ and $\dot{y}(0) = 0$. (b) Dimensionless amplitude as a function of the dimensionless time using four different methods: averaging method (black), definition of Mark and Crandall (green), Hilbert transform of the displacement (blue) and Hilbert transform of the velocity (red). (c) Dimensionless friction force as a function of the dimensionless velocity, $f(\dot{y})$ for all $\dot{y} \geq 0$. (d) F' as a function of A.

<u>Case 3</u>: $\Delta^2 > 0$

For $\Delta^2 > 0$, the response depends also on the solutions of $F(A)$. These latter are denoted by A_1 and A_2 where $A_1 = \frac{-a_1-\Delta}{2a_2}$ and $A_2 = \frac{-a_1+\Delta}{2a_2}$.

Case 3 (a): $A_1 < 0$ and $A_2 > 0$ where $|A_1| > |A_2|$.

In this case, both a_2 and a_1 are positive. Thus, both μ_2 and $\mu_1$are negative. Also, one can conclude that the decaying envelope has a concave form for all $A \in [0, A_0]$. The amplitude $A(\tau)$ in this case is defined as: $A_1 < 0 < A < A_2$ and the initial amplitude A_0 is chosen in a way where $A_1 < 0 < A_0 < A_2$. The analytical solution of the amplitude $A(\tau)$ corresponding to this case is derived as follows:

$$A(\tau) = \frac{A_2 + A_1 \frac{A_2 - A_0}{A_0 - A_1} e^{a_2(A_2 - A_1)\tau}}{\frac{A_2 - A_0}{A_0 - A_1} e^{a_2(A_2 - A_1)\tau} + 1} \qquad (46)$$

In the following figure, we present a dynamic system having a quadratic friction model corresponding to this latter case where $\mu_0 = 0.6$, $\mu_1 = -0.02$ and $\mu_2 = -0.003$. The initial conditions are defined as follows: $Y_0 = A_0 = 10$ and $\dot{y}(0) = 0$. Figure 13 (a), the dimensionless displacement-time response $y(\tau)$ shows that the decaying envelope has a concave envelope for all $A \in [0,10]$. Figure 13 (b) presents the dimensionless amplitude-response using 4 different methods. The dimensionless friction force as a function of the dimensionless velocity, $f(\dot{y})$ and $F'(A)$ are presented in Figures 13 (c) and (d). This shows that the system is valid and $F'(A) > 0$ for all $A \in [0,10]$. Thus, the decaying envelope has a concave form.

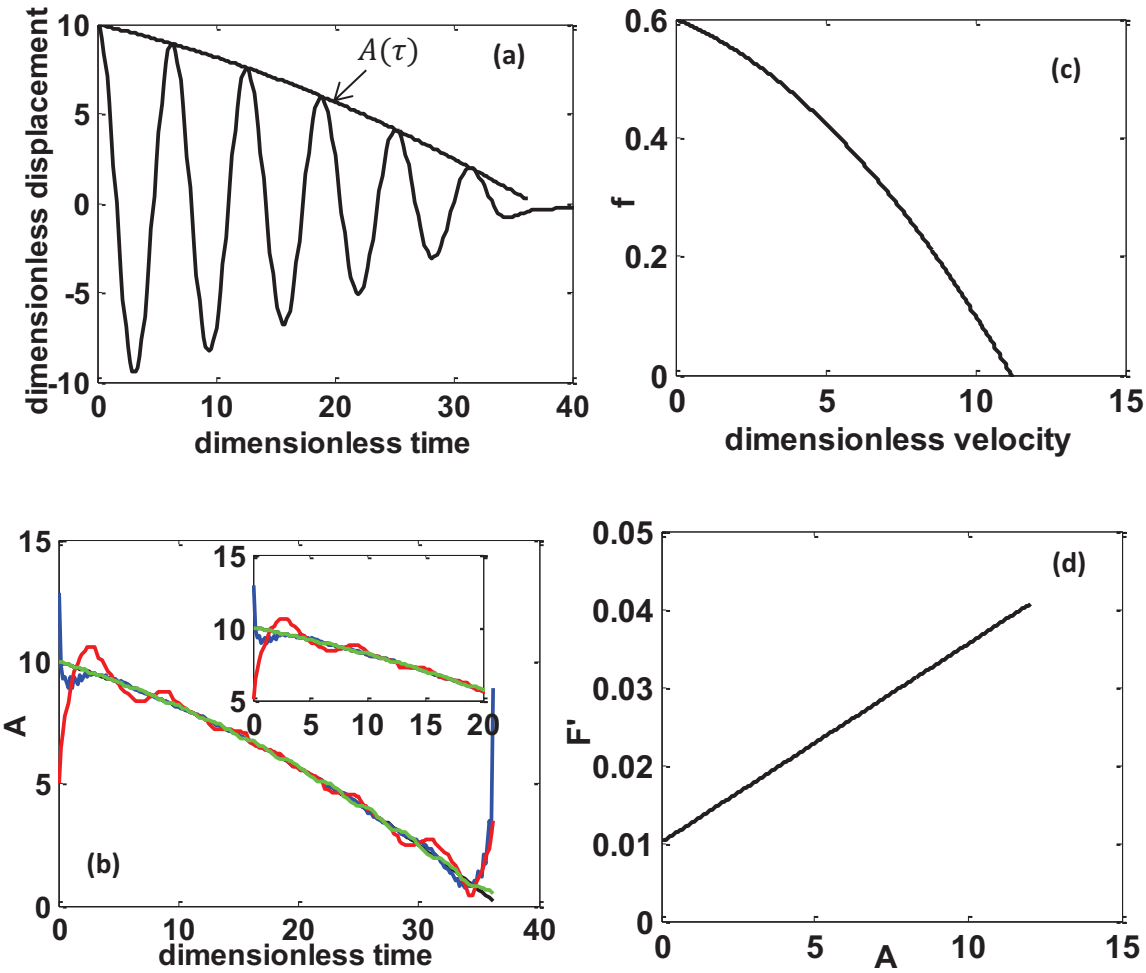

Figure 13. (a) Dimensionless displacement-time response $y(\tau)$ with its decaying amplitude $A(\tau)$ corresponding to a mechanical system having an equation of motion $\ddot{y} + y = -f(\dot{y}) = -(\mu_0 sgn(\dot{y}) + \mu_1\dot{y} + \mu_2\dot{y}^2 sgn(\dot{y}))$ where $\mu_0 = 0.6$, $\mu_1 = -0.02$, $\mu_2 = -0.003$ and initial conditions $y(0) = 10$ and $\dot{y}(0) = 0$. (b) Dimensionless amplitude as a function of the dimensionless time using four different methods: averaging method (black), definition of Mark and Crandall (green), Hilbert transform of the displacement (blue) and Hilbert transform of the velocity (red). (c) Dimensionless friction force as a function of the dimensionless velocity, $f(\dot{y})$ for all $\dot{y} \geq 0$. (d) F' as a function of A.

Case 3(b): $A_1 < 0$ and $A_2 > 0$ where $|A_1| < |A_2|$.

In this latter case, both a_2 is positive, thus $\mu_2 < 0$. However, a_1 is negative and $\mu_1 > 0$. The amplitude $A(\tau)$ in this case is defined as: $A_1 < A < A_2$ and the initial amplitude A_0 is chosen in a way where $A_1 < A_0 < A_2$. The decaying envelope has a convex form when $A \in [0, A^*]$ and a concave form when $A \in]A^*, A_0]$ where $A^* = -\frac{a_1}{2a_2}$. The analytical solution of the amplitude $A(\tau)$ corresponding to this case is derived as follows:

$$A(\tau) = \frac{A_2 + A_1 \frac{A_2 - A_0}{A_0 - A_1} e^{a_2 (A_2 - A_1)\tau}}{\frac{A_2 - A_0}{A_0 - A_1} e^{a_2 (A_2 - A_1)\tau} + 1} \qquad (47)$$

In the following figure, we present a dynamic system having a quadratic friction model corresponding to this latter case where $\mu_0 = 0.12$, $\mu_1 = 0.003$ and $\mu_2 = -0.004$. The initial conditions are defined as follows: $Y_0 = A_0 = 10$ and $\dot{y}(0) = 0$. The dimensionless displacement-time response $y(\tau)$ and its decaying envelope are presented in Figure 14 (a). Figure 14 (b) presents the decaying envelopes using 4 different methods. The dimensionless friction force as a function of the dimensionless velocity, $f(\dot{y})$ and $F'(A)$ are presented in Figures 14(c) and (d). Figure 14 (c) shows that the system is valid for all $A \in [0, A_0]$ since $f(\dot{y}) > 0$ for all $A \in [0, 10]$. We examine that the decaying envelope has a convex form when $A \in [0,4.42[$ and a concave form when $A \in [4.42,10]$ and since $F'(A) < 0$ for all $A \in [0,4.42[$ and $F'(A) > 0$ for all $A \in [4.42,10]$ (see Figure 14 (d)).

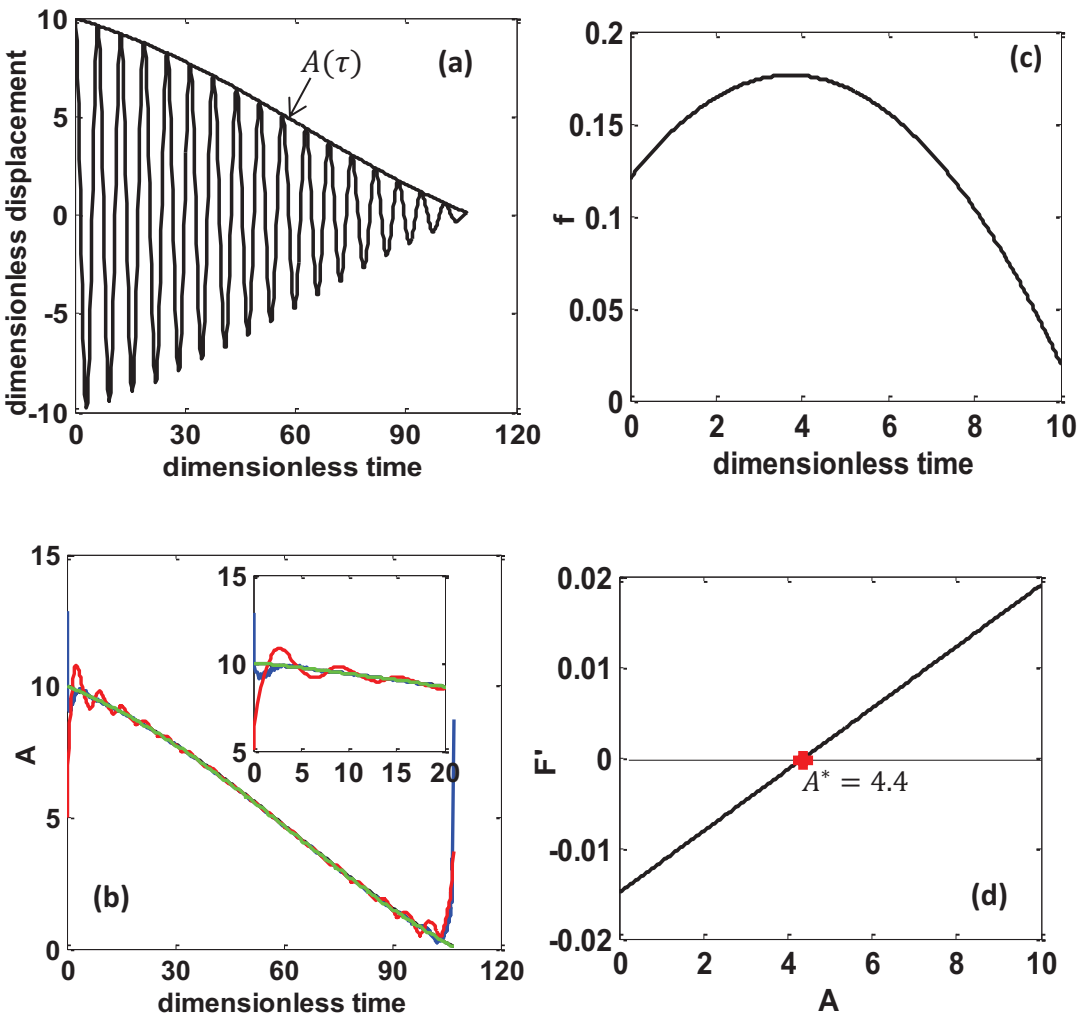

Figure 14. (a) Dimensionless displacement-time response $y(\tau)$ with its decaying amplitude $A(\tau)$ corresponding to a mechanical system having an equation of motion $\ddot{y} + y = -f(\dot{y}) = -(\mu_0 sgn(\dot{y}) + \mu_1\dot{y} + \mu_2\dot{y}^2 sgn(\dot{y}))$ where $\mu_0 = 0.12$, $\mu_1 = 0.03$, $\mu_2 = -0.004$ and initial conditions $y(0) = 10$and $\dot{y}(0) = 0$. (b) Dimensionless amplitude as a function of the dimensionless time using four different methods: averaging method (black), definition of Mark and Crandall (green), Hilbert transform of the displacement (blue) and Hilbert transform of the velocity (red). (c) Dimensionless friction force as a function of the dimensionless velocity, $f(\dot{y})$ for all $\dot{y} \geq 0$. (c) F' as a function of A.

Case 3(c): $A_1 > 0$ and $A_2 > 0$.

This case defines respectively the amplitude at any time $A(\tau)$ and the initial amplitude A_0 as follows: $A < A_2 < A_1$ and $A_0 < A_2 < A_1$. The constants a_1 and a_2 are respectively positive and negative thus, $\mu_1 < 0$ and $\mu_2 > 0$. The function $F'(A)$ is positive for all $A \in [0, A_0]$. Therefore, one can conclude that the decaying envelope of the response corresponding to this case is described by a concave form. The analytical solution of the amplitude $A(\tau)$ corresponding to this case is derived as follows:

$$A(\tau) = \frac{A_1 \frac{A_2 - A_0}{A_0 - A_1} e^{a_2(A_2 - A_1)\tau} - A_2}{\frac{A_2 - A_0}{A_0 - A_1} e^{a_2(A_2 - A_1)\tau} - 1} \qquad (48)$$

In the following figure, we present a dynamic system having a quadratic friction model corresponding to this latter case where $\mu_0 = 0.4$, $\mu_1 = -0.05$ and $\mu_2 = 0.0012$. The initial conditions are defined as follows: $Y_0 = A_0 = 10$ and $\dot{y}(0) = 0$. The dimensionless displacement-time response $y(\tau)$ and its decaying envelope are presented in Figure 15 (a). Figure 15 (b) presents the decaying envelope using 4 different methods. The dimensionless friction force as a function of the dimensionless velocity, $f(\dot{y})$ and $F'(A)$ are respectively presented in Figures 15 (c) and (d). Figure 15 (c) shows that the system is valid for all $A \in [0, A_0]$ since $f(\dot{y}) > 0$ for all $A \in [0, 10]$. The function $F'(A)$ is positive for all $A \in [0, 10]$. Therefore, we can conclude that the response has a concave decaying envelope for all $A \in [0, 10]$.

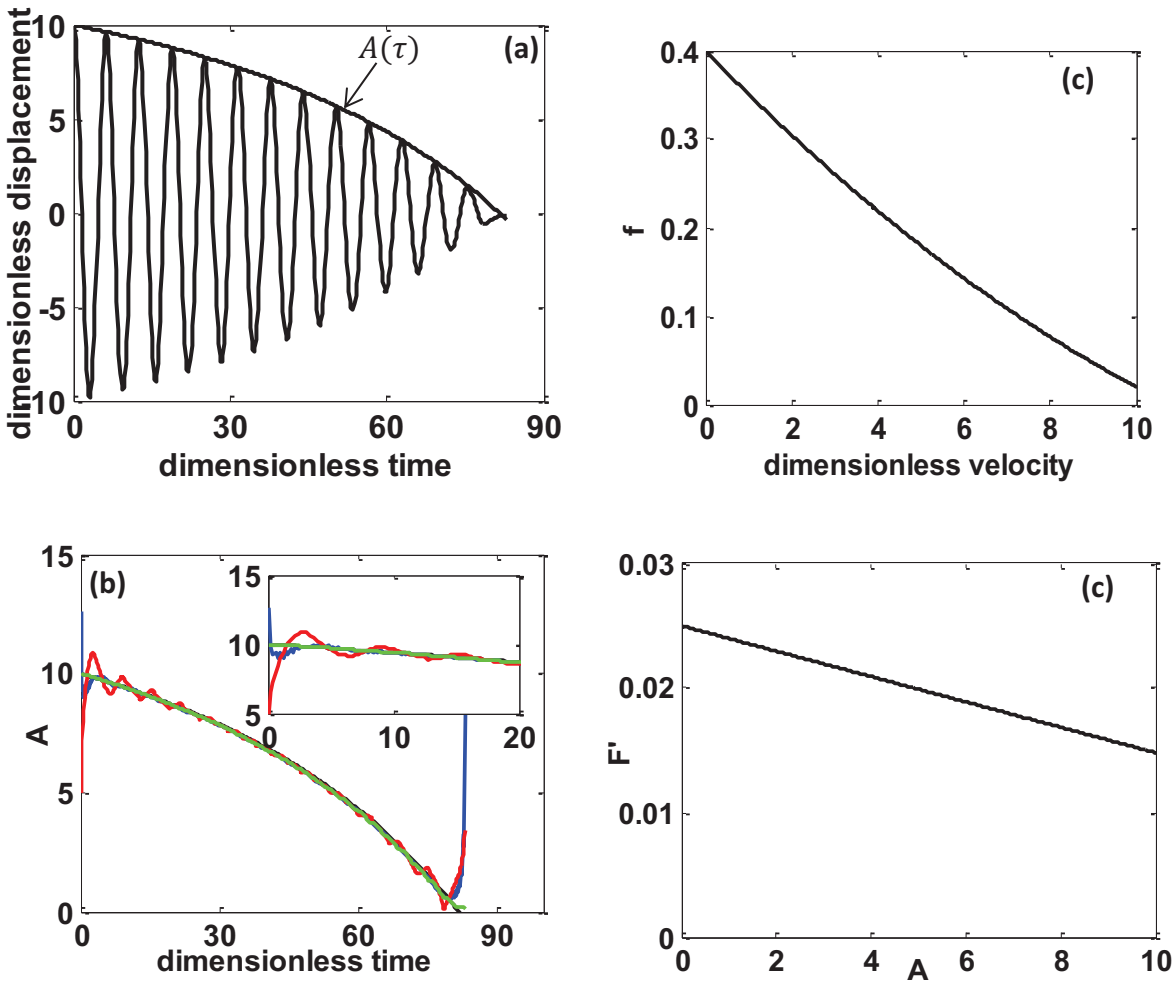

Figure 15. (a) Dimensionless displacement-time response $y(\tau)$ with its decaying amplitude $A(\tau)$ corresponding to a mechanical system having an equation of motion $\ddot{y} + y = -f(\dot{y}) = -(\mu_0 sgn(\dot{y}) + \mu_1\dot{y} + \mu_2\dot{y}^2 sgn(\dot{y}))$ where $\mu_0 = 0.4$, $\mu_1 = -0.05$, $\mu_2 = 0.0012$ and initial conditions $y(0) = 10$ and $\dot{y}(0) = 0$. (b) Dimensionless amplitude as a function of the dimensionless time using four different methods: averaging method (black), definition of Mark and Crandall (green), Hilbert transform of the displacement (blue) and Hilbert transform of the velocity (red). (c) Dimensionless friction force as a function of the dimensionless velocity, $f(\dot{y})$ for all $\dot{y} \geq 0$. (d) F' as a function of A.

3.5 Specifying the friction law

In order to specify the actual friction law from the free dynamic response, it is necessary to introduce an appropriate numerical procedure able to evaluate the constants μ_j. On the other hand, it is interesting to determine the relevance of introducing sophisticated models, i.e. quadratic friction law versus Coulomb-viscous friction law.

For this latter, we have simulated dynamic responses in which the friction law is defined. Then, we have examined different algorithms devoted to determining the constants μ_j corresponding to the friction models. We found that the Levenberg-Marquardt Algorithm (LMA), also known as the damped least-square (DLS) method [13 and 14] is sufficiently preferment. This method is based on optimizing the second order differential equation of a function. This procedure is applied using a MATLAB® function known as $lsqnonlin$. The theoretical amplitude is calculated using the Runge-Kutta method of the 4th order (RK4). However, the experimental amplitude is determined from the experimental displacement and velocity responses using the definition of Crandall and Mark.

At the beginning, the free responses are simulated using a known friction law. Then, using the Levenberg-Marquardt Algorithm, the friction constants μ_{2n} and μ_{2n+1} corresponding to constant, viscous, Coulomb- viscous and quadratic friction laws are computed. The computed friction coefficients are compared to that simulated in order to be able to specify the friction law of the system.

Table 2 presents the first set of friction constants used for simulating the response and the calculated friction constants from the simulated responses.

Friction model	Constant	Viscous	Coulomb and viscous		Quadratic		
Simulated cases	μ_0	μ_1	μ_0	μ_1	μ_0	μ_1	μ_2
$\mu_0 = 0.2$	**0.1998**	0.0414	**0.2004**	**-0.0001**	0.1994	0.0004	-0.0001
$\mu_1 = 0.1$	0.2352	**0.0998**	**0.004**	**0.0997**	-0.0003	0.1009	-0.0002
$\mu_0 = 0.08$ $\mu_1 = 0.04$	0.2343	0.0607	**0.0805**	**0.0398**	0.0795	0.0406	-0.0001
$\mu_0 = 0.4$ $\mu_1 = -0.04$	0.1666	0.0295	**0.4003**	**-0.0401**	0.3997	-0.0398	0

Table 2. . Calculated friction constants of different friction laws from simulated responses.

Figure 16 (a) presents a simulated dimensionless time-response for a system described by a Coulomb friction law having $\mu_0 = 0.2$. The oscillatory system is described by a straight envelope. The different friction coefficients presented in Figure 16 (b) show that the friction model may be constant, Coulomb-viscous or quadratic; however, it cannot be viscous. This can be also seen from the constants computed in Table 2.

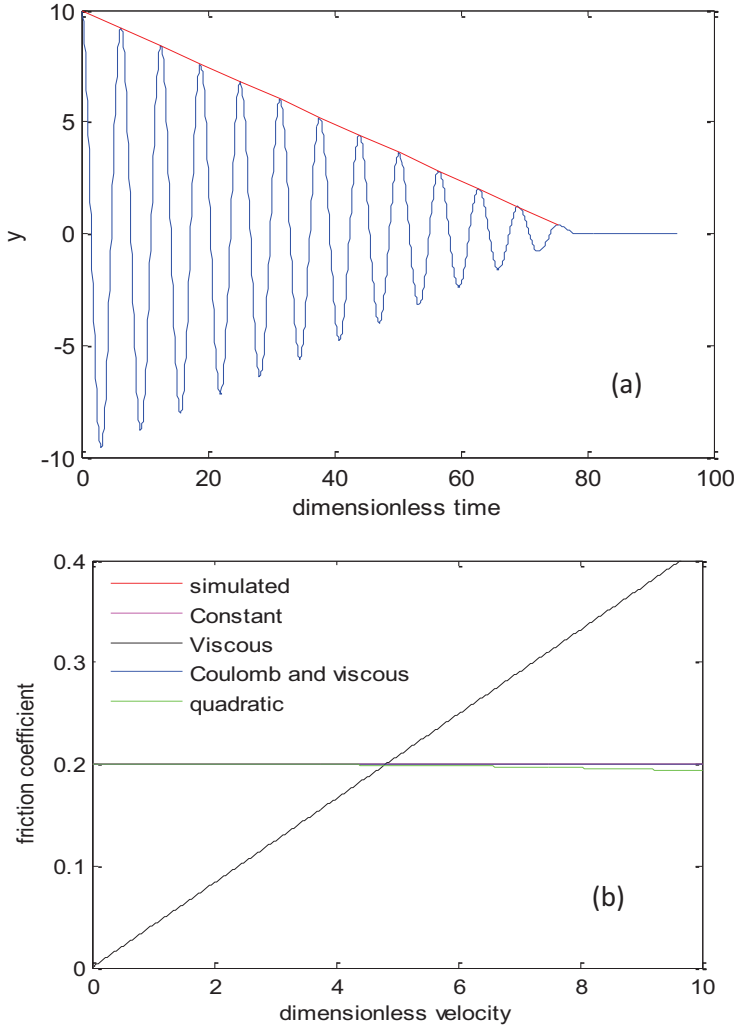

Figure 16. (a) Simulated dimensionless displacement response for a system having a Coulomb friction law where $\mu_0 = 0.2$. (b) Friction coefficient as a function of dimensionless velocity.

Figure 17 (a) presents a system having a viscous friction model $\mu(\dot{y}) = \mu_1\dot{y}$ with $\mu_1 = 0.1$ where the oscillatory system is described by a convex envelope. Figure 17(b) shows the behavior of different friction models, presented in Table 2, as a function of the dimensionless velocity. It is concluded that the viscous, Coulomb-viscous and quadratic friction models are coherent with the simulated model.

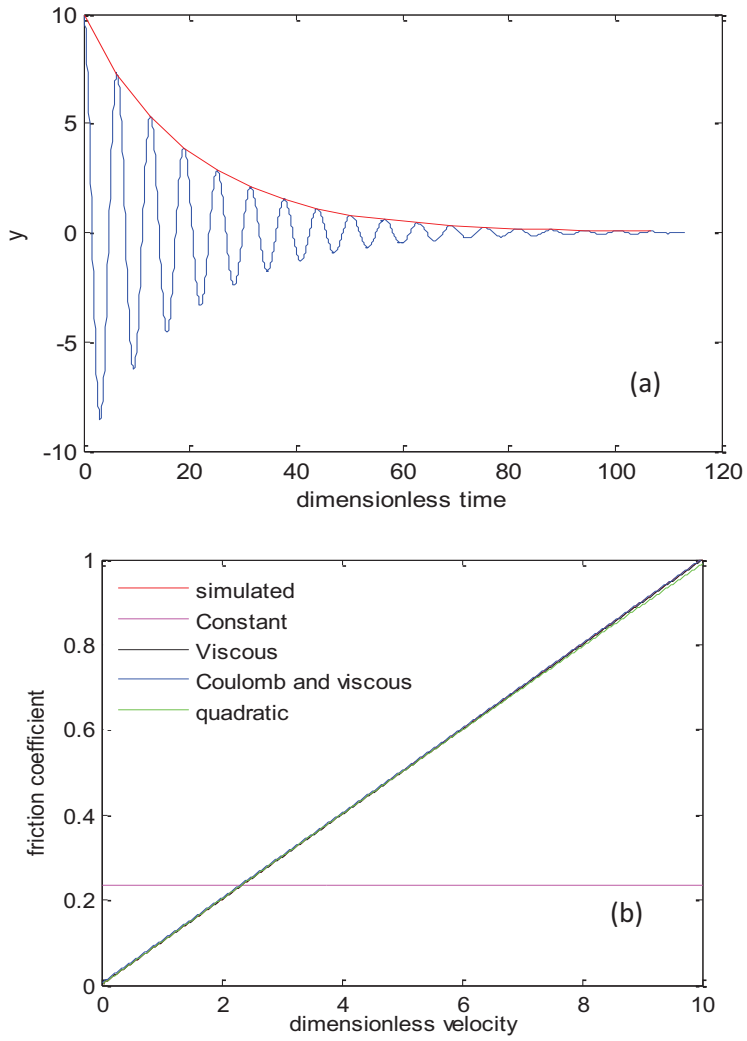

Figure 17. (a) Simulated dimensionless displacement response for a system having a viscous friction law where $\mu_1 = 0.1$. (b) Friction coefficient as a function of dimensionless velocity.

A system having a Coulomb-viscous friction model $\mu(\dot{y}) = \mu_0 + \mu_1\dot{y}$ with $\mu_0 = 0.08$ and $\mu_1 = 0.04$ is simulated (see Figure 18(a)). The oscillatory system is described by a convex envelope. Figure 18 (b) describes the friction coefficient of different friction laws as a function of the dimensionless velocity. It is clearly shown that both the Coulomb-viscous and quadratic friction model are coherent with the simulated one. The computed friction constants corresponding to the different friction models are presented in Table 2.

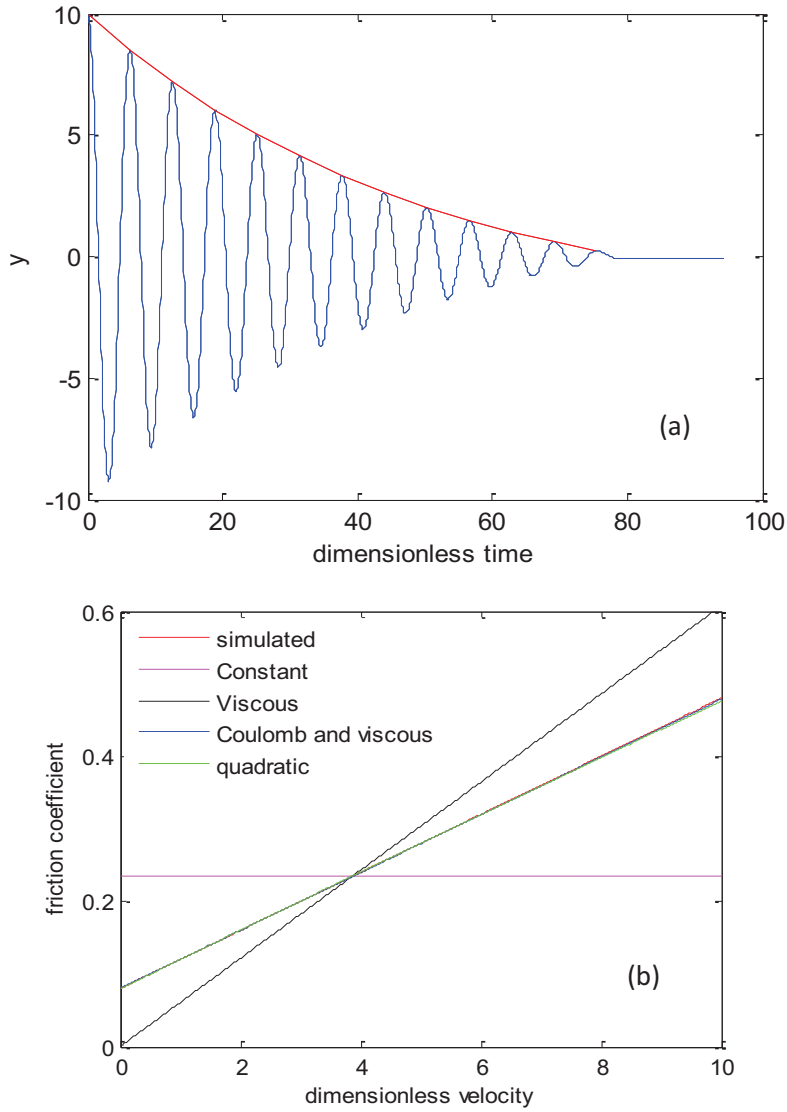

Figure 18. (a) Simulated dimensionless displacement response for a system having a Coulomb-viscous friction law where $\mu_0 = 0.08$ and $\mu_1 = 0.04$. (b) Friction coefficient as a function of dimensionless velocity.

Figure 19 (a) presents a simulated oscillatory system having a concave envelope. The friction law used is described by a Coulomb-viscous friction with $\mu(\dot{y}) = \mu_0 + \mu_1\dot{y}$ where $\mu_0 = 0.4$ and $\mu_1 = -0.04$. Figure 19 (b) shows the friction coefficient of different friction models as a function of the dimensionless velocity. One can conclude that both Coulomb-viscous and quadratic friction models are suitable for this simulated system.

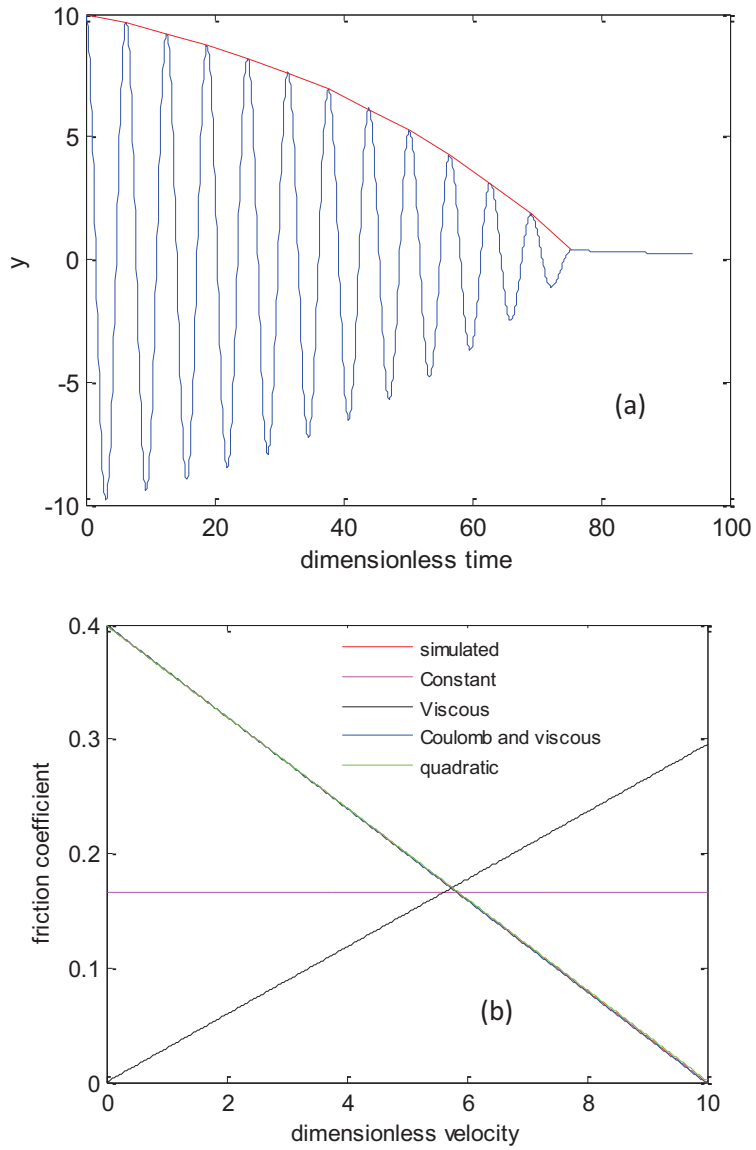

Figure 19. (a) Simulated dimensionless displacement response for a system having a Coulomb-viscous friction law where $\mu_0 = 0.4$ and $\mu_1 = -0.04$. (b) Friction coefficient as a function of dimensionless velocity.

In the first set of simulated responses, one can conclude that the Coulomb-viscous friction law can be used since it gives perfect results even for those simulated using the Constant friction law (Figure 16) and that simulated using the viscous friction model (Figure 17).

Table 3 presents the friction constants corresponding to the second set of free response simulated using the quadratic friction law. In this table, the constants corresponding to the constant, viscous, Coulomb-viscous and quadratic friction models are computed from the simulated free responses.

Friction model	Constant	Viscous	Coulomb and viscous		Quadratic		
Simulated cases	μ_0	μ_1	μ_0	μ_1	μ_0	μ_1	μ_2
$\mu_0 = 0.1$ $\mu_1 = 0.04$ $\mu_2 = 0.005$	0.3235	0.0935	***0.0613***	***0.0759***	**0.0991**	**0.0411**	**0.0048**
$\mu_0 = 0.904$ $\mu_1 = -0.125$ $\mu_2 = 0.004$	0.3461	0.0630	***0.8221***	***-0.0833***	**0.9045**	**-0.1245**	**0.0039**
$\mu_0 = 0.6$ $\mu_1 = -0.02$ $\mu_2 = -0.003$	0.3707	0.0667	***0.6776***	***-0.0537***	**0.5965**	**-0.0180**	**-0.0032**
$\mu_0 = 0.4$ $\mu_1 = -0.05$ $\mu_2 = 0.0012$	0.1498	0.0257	***0.3678***	***-0.0363***	**0.3995**	**-0.0497**	**0.0012**

Table 3. Calculated friction constants of different friction laws from free responses simulated using the quadratic friction law.

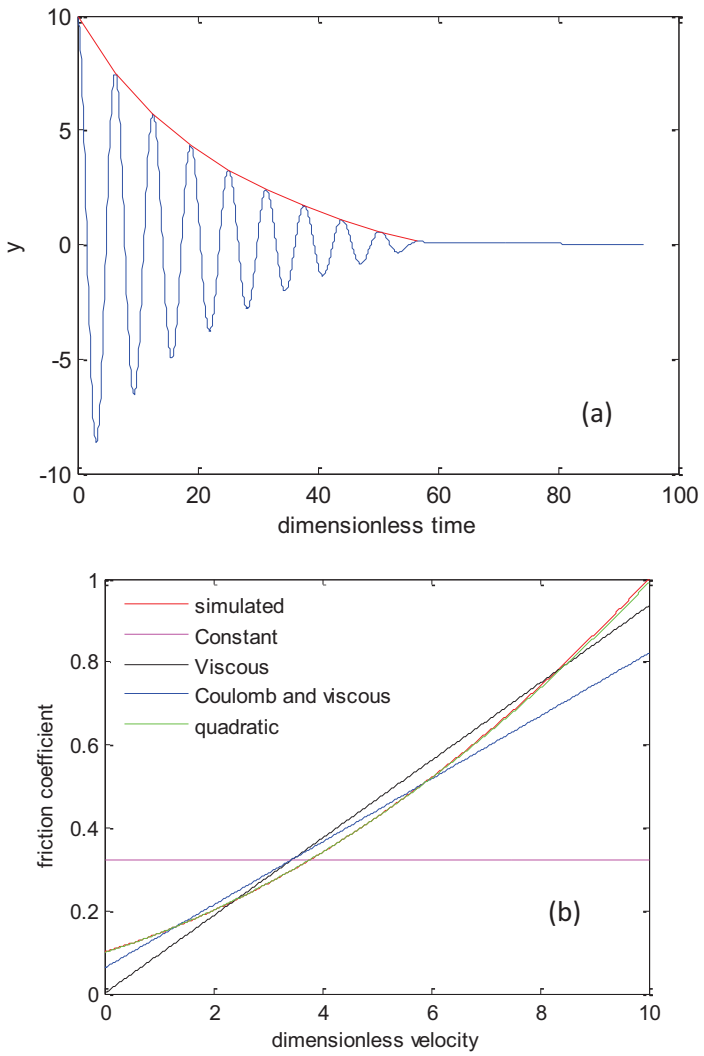

Figure 20. (a) Simulated dimensionless displacement response for a system having a quadratic friction law where $\mu_0 = 0.1$, $\mu_1 = 0.04$ and $\mu_2 = 0.005$. (b) Friction coefficient as a function of dimensionless velocity.

The above figure (Figure 20) presents the results corresponding to an oscillatory system is simulated with a quadratic friction model having a friction coefficient of $\mu(\dot{y}) = \mu_0 + \mu_1\dot{y} + \mu_2\dot{y}^2$ with $\mu_0 = 0.1$, $\mu_1 = 0.04$ and $\mu_2 = 0.005$. The time-response corresponding to this latter system is presented in Figure 20 (a) and it is described by a convex envelope. Figure 20 (b) shows the friction coefficient as a function of the dimensionless velocity for different friction laws. The quadratic friction model is the best suitable law for this simulated system. Moreover, both viscous and Coulomb-viscous friction laws are close to the simulated quadratic friction law.

A system is simulated using a quadratic friction model having a coefficient of $\mu(\dot{y}) = \mu_0 + \mu_1\dot{y} + \mu_2\dot{y}^2$ where $\mu_0 = 0.904$, $\mu_1 = -0.125$ and $\mu_2 = 0.004$ (see Figure 21 (a)). The friction constants corresponding to different friction laws are computed (Table 3). Figure 21 (b) presents the friction coefficient as a function of the dimensionless velocity. The quadratic friction model best suits the simulated system. However, both the viscous and Coulomb-viscous friction can approximately model the simulated system.

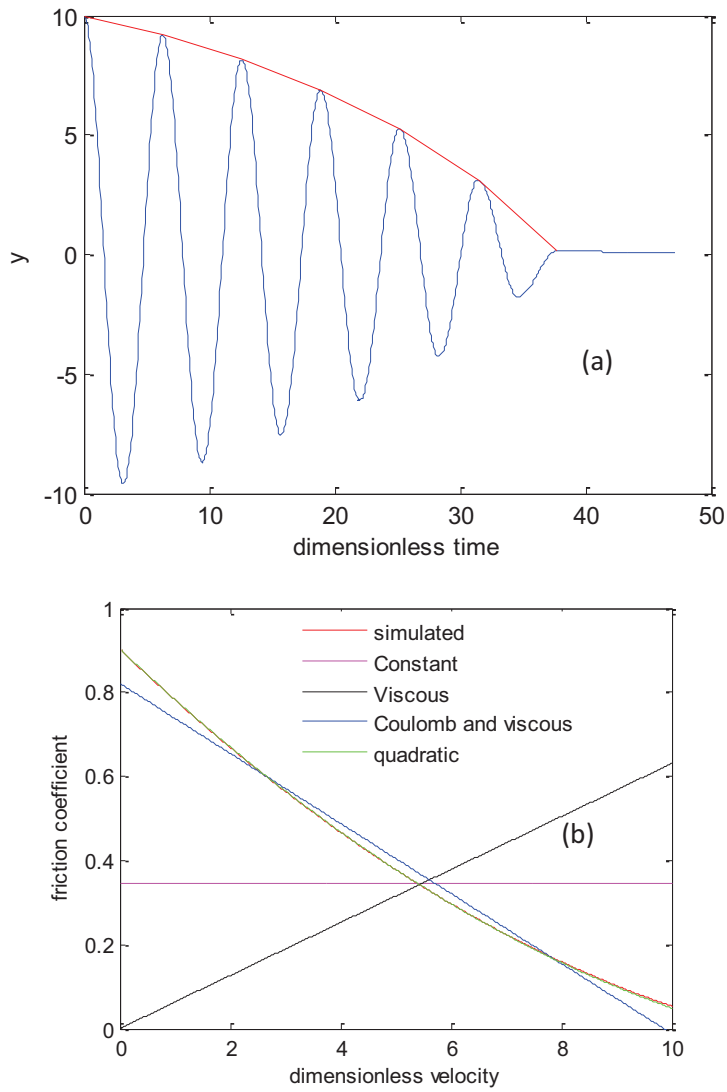

Figure 21. (a) Simulated dimensionless displacement response for a system having a quadratic friction law where $\mu_0 = 0.904$, $\mu_1 = -0.125$ and $\mu_2 = 0.004$. (b) Friction coefficient as a function of dimensionless velocity.

Figure 22 (a) presents the dimensionless displacement response corresponding to a simulated system defined by quadratic friction model having $\mu_0 = 0.6$, $\mu_1 = -0.02$ and $\mu_2 = -0.003$. The friction coefficient as a function of the dimensionless velocity is presented in Figure 22 (b) for different friction laws. Similarly to the system simulated in Figure 21, the quadratic friction is the most suitable to this latter system. However, both viscous and Coulomb-viscous friction can model approximately this simulated system.

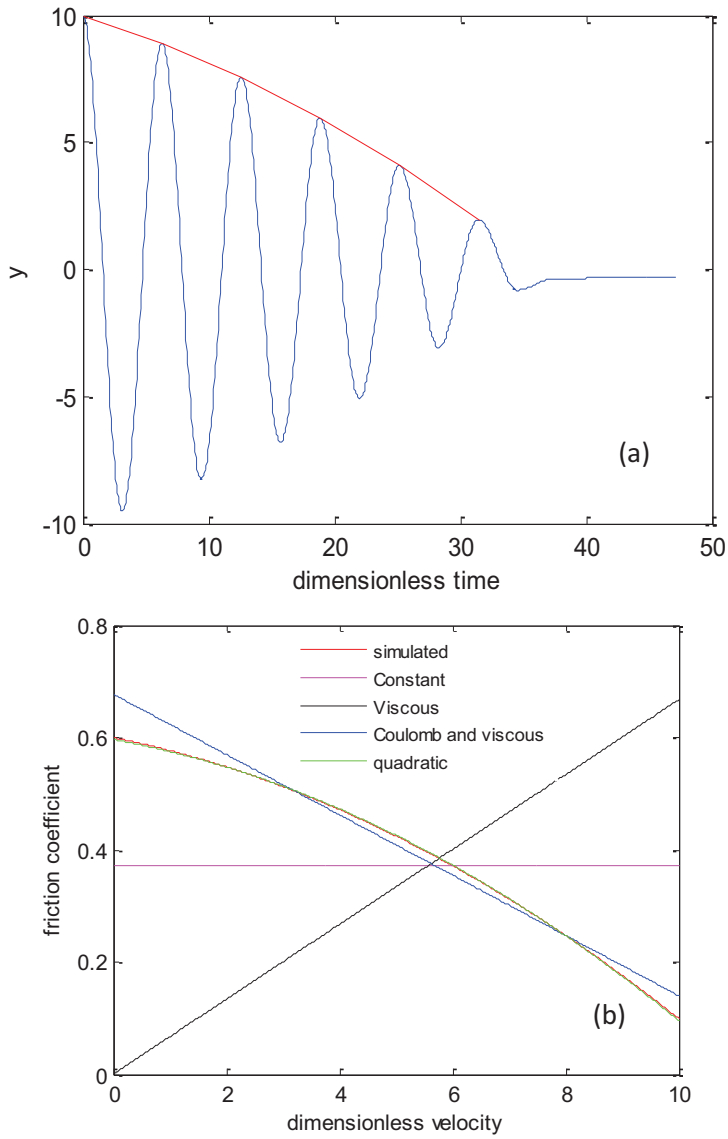

Figure 22. (a) Simulated dimensionless displacement response for a system having a quadratic friction law where $\mu_0 = 0.6$, $\mu_1 = -0.02$ and $\mu_2 = -0.003$. (b) Friction coefficient as a function of dimensionless velocity.

Figure 23 (a) demonstrates the dimensionless displacement response corresponding to a simulated system described by a quadratic friction model having $\mu_0 = 0.4$, $\mu_1 = -0.05$ and $\mu_2 = 0.0012$. The friction coefficient as a function of the dimensionless velocity is

presented in Figure 23 (b) for different friction laws. The most suitable to this latter system is the quadratic friction. However, both viscous and Coulomb-viscous friction models are very close to the friction law describing the latter simulated system.

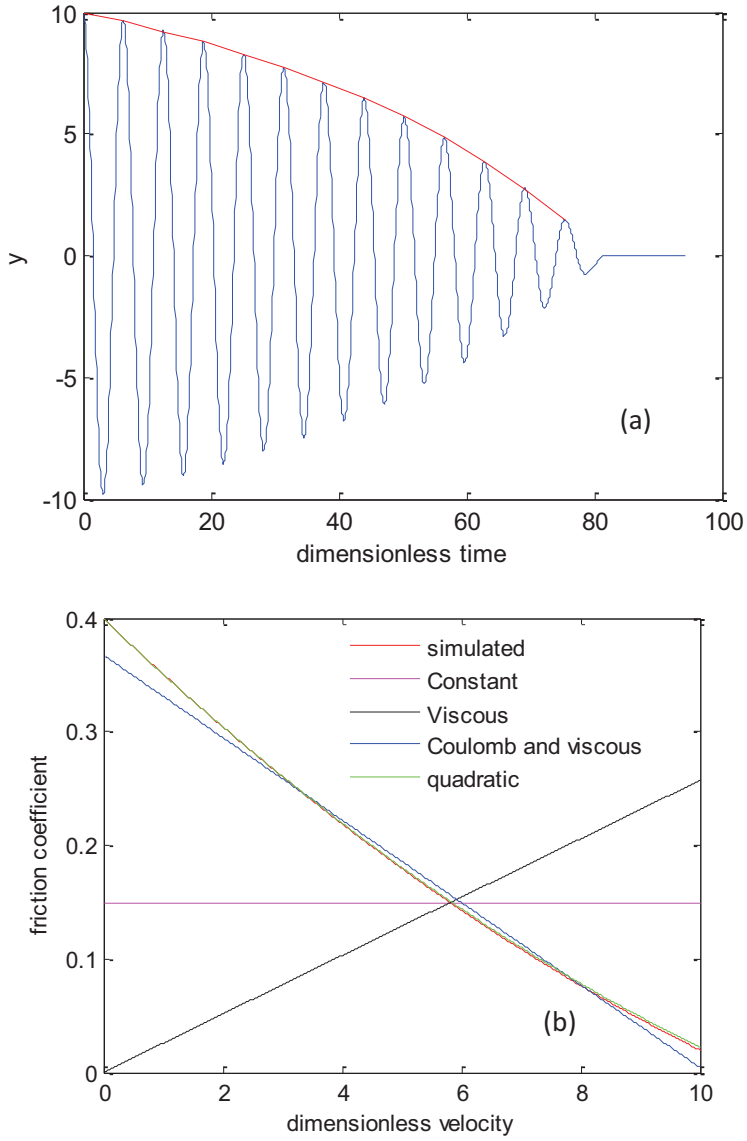

Figure 23. (a) Simulated dimensionless displacement response for a system having a quadratic friction law where $\mu_0 = 0.4$, $\mu_1 = -0.05$ and $\mu_2 = 0.0012$. (b) Friction coefficient as a function of dimensionless velocity.

For the above 4 free responses simulated using the quadratic friction law, we can conclude that the Coulomb-viscous friction law is the most appropriate to be used.

Table 4 shows the friction constants corresponding to the third set of free response simulated using the quadratic friction law. In this table, the constants corresponding to the constant, viscous, Coulomb-viscous and quadratic friction models are computed from the simulated free responses.

Friction model	Constant	Viscous	Coulomb and viscous		Quadratic		
Simulated cases	μ_0	μ_1	μ_0	μ_1	μ_0	μ_1	μ_2
$\mu_0 = 0.6$ $\mu_1 = -0.25$ $\mu_2 = 0.03$	0.2058	0.0438	0.0484	0.0333	**0.6006**	**-0.25**	**0.03**
$\mu_0 = 0.12$ $\mu_1 = 0.03$ $\mu_2 = -0.004$	0.1424	0.0286	0.2184	-0.0140	**0.1195**	**0.0303**	**-0.004**

Table 4. Calculated friction constants of different friction laws from free responses simulated using the quadratic friction law.

Figure 24 (a) presents an oscillatory system having both concave and convex envelopes. This latter system is described by a quadratic friction coefficient $\mu(\dot{y}) = \mu_0 + \mu_1\dot{y} + \mu_2\dot{y}^2$ where $\mu_0 = 0.6$, $\mu_1 = -0.25$ and $\mu_2 = 0.03$. The friction coefficient of different friction laws is shown in Figure 24 (b) as a function of the dimensionless velocity. Among these friction laws, the suitable friction law for this simulated system is the quadratic friction model.

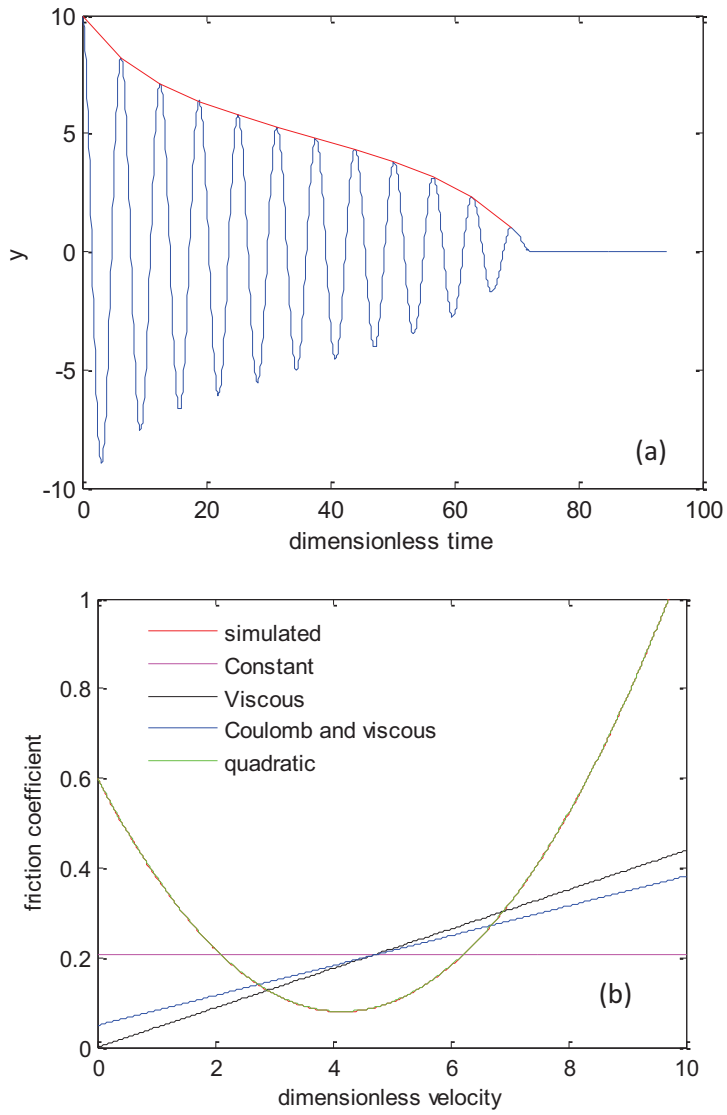

Figure 24. (a) Simulated dimensionless displacement response for a system having a quadratic friction law where $\mu_0 = 0.6$, $\mu_1 = -0.25$ and $\mu_2 = 0.03$. (b) Friction coefficient as a function of dimensionless velocity.

Figure 25 (a) demonstrates a simulated system defined by a quadratic friction law having the following friction constants: $\mu_0 = 0.12$, $\mu_1 = 0.03$ and $\mu_2 = -0.004$. The oscillatory dimensionless displacement response corresponding to this latter system is described by both convex and concave envelopes. The friction coefficient of different friction laws as a function of the dimensionless velocity is presented in figure 25 (b). The only appropriate friction law corresponding to this simulated system is described by a quadratic friction model.

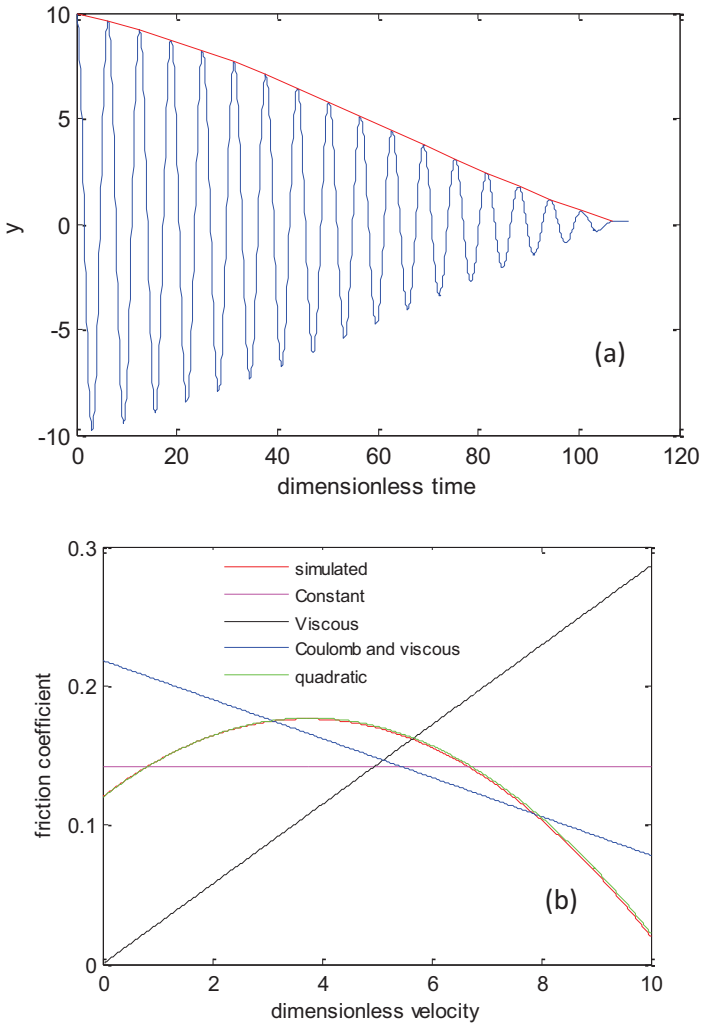

Figure 25. (a) Simulated dimensionless displacement response for a system having a quadratic friction law where $\mu_0 = 0.12$, $\mu_1 = 0.03$ and $\mu_2 = -0.004$. (b) Friction coefficient as a function of dimensionless velocity.

From the above simulated free responses, we concluded that the Coulomb-viscous friction law cannot be used to model the system.

Finally, we can conclude that the Coulomb-viscous friction law can be perfectly used in the case where the free responses are simulated using a constant, viscous or Coulomb-viscous friction model. Moreover, the Coulomb-viscous friction law can be quite good for free responses simulated by a quadratic friction law and uniquely described by either a convex or concave envelope from. However, for free responses simulated by a quadratic friction law

and described by both convex and concave envelope from, the Coulomb-viscous friction law cannot be used. In all the simulated free responses examples presented above, the quadratic friction law works perfectly. In this section, we were able to show that the Coulomb-viscous friction law cannot be used to all systems described by an oscillatory free responses as it was assumed previously for the dynamic oscillating tribometer.

3.6 Experimental Results

The measured oscillating responses using the original tribometer described in [12] and also presented in Chapter 2 show promising results. Indeed, they demonstrate the different forms of the time-responses' envelopes described in section 3.4.

The friction constants $\boldsymbol{\mu_{2n}}$ and $\boldsymbol{\mu_{2n+1}}$ are computed from the experimental displacement and velocity time-responses. The calculated constants $\boldsymbol{\mu_{2n}}$ and $\boldsymbol{\mu_{2n+1}}$ corresponds to four different friction laws: constant, viscous, coulomb-viscous and quadratic friction laws are presented in the below table (Table 5).

Friction model	Constant	Viscous	Coulomb- viscous		Quadratic		
Tribological system	μ_0	μ_1	μ_0	μ_1	μ_0	μ_1	μ_2
Steel/steel Oleic acid 0.10 N 25°C	**0.1036**	0.0348	**0.0967**	**0.0023**	**0.1003**	**-0.0012**	**0.0006**
Steel/steel Glycerol 0.05 N 22°C	0.2003	0.0366	**0.034**	**0.0304**	**0.0389**	**0.0276**	**0.0002**
Steel/steel 150NS 0.10 N 42°C	0.0632	0.0172	**0.0806**	**-0.0046**	**0.1014**	**-0.0202**	**0.0022**
Steel/steel Glycerol 0.05 N 61°C	0.0066	0.0090	0.0054	0.0017	**0.011**	**-0.0184**	**0.0138**

Table 5. Computed friction constants of some tribological systems depending on teh friction law used.

When steel-on-steel sphere-on-flat plane lubricated with oleic and loaded with a normal load of 0.10 N is tested at a temperature of 25°C. Figure 26 represents the experimental dimensionless displacement-time responses corresponding to this latter tribological system along with the envelope. Its envelope is seems to have a straight form.

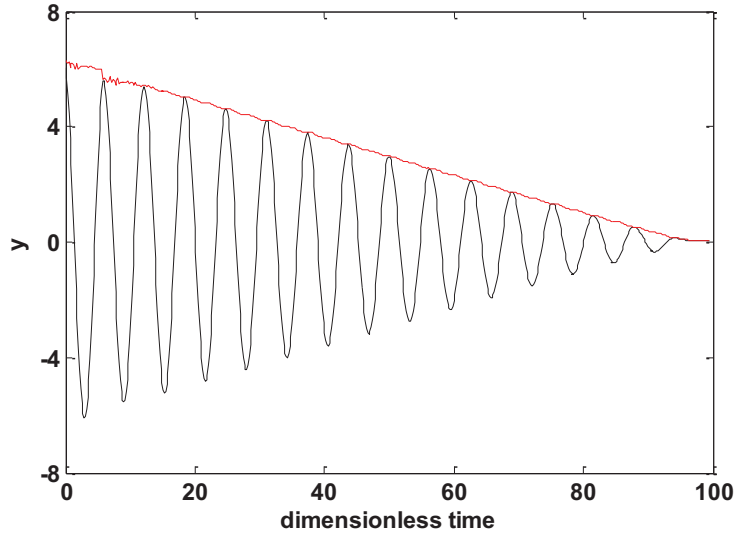

Figure 26. Dimensionless displacement-time response of steel-on-steel sphere-on-flat plane lubricated with oleic acid loaded with 0.10 N at 25°C.

Both the experimental and simulated amplitudes are compared (see Figure 27) corresponding to the steel/steel contact lubricated with oleic acid and having a normal load of 0.10 N at 25°C. Figures 27 (a) presents the amplitude of the system responses, experimentally using the definition of Crandall & Mark and numerically modeled using the constant, viscous, coulomb-viscous and quadratic friction laws. The experimental and numerical dimensionless displacement-time response is represented in Figure 27 (b). The numerical response is simulated using the quadratic friction model.

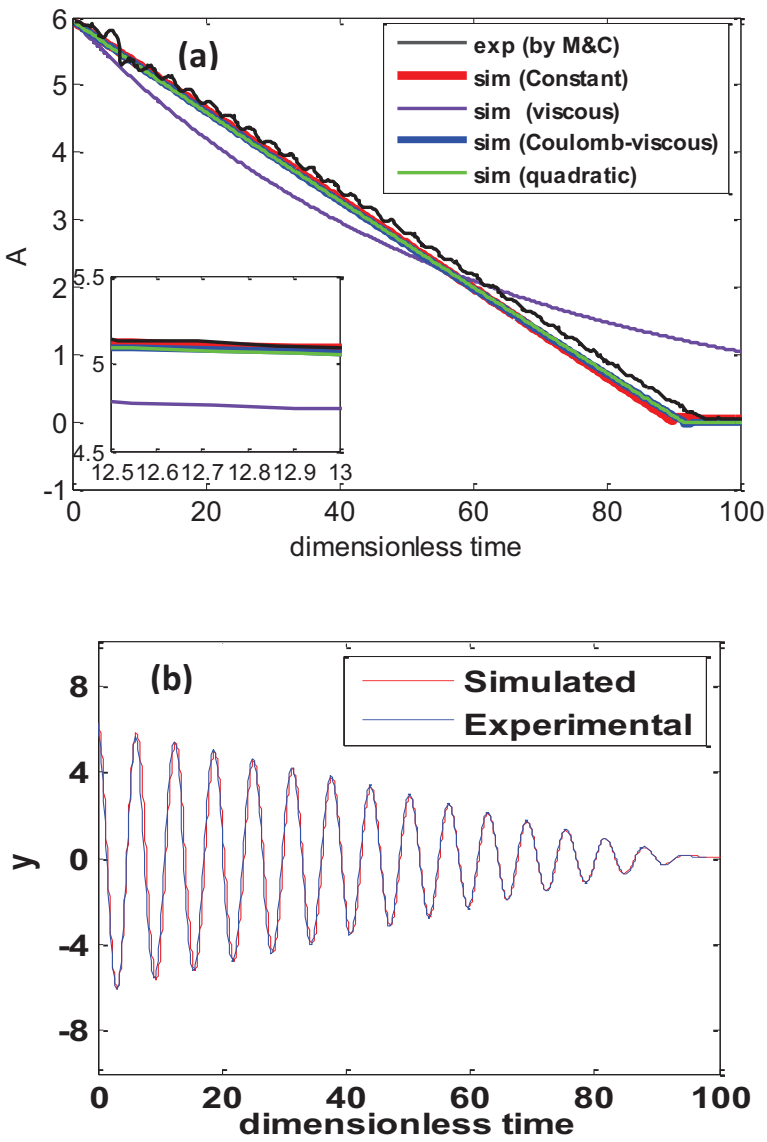

Figure 27. (a) Experimental v/s Simulated envelope with different friction models (b) Experimental v/s simulated dimensionless displacement time-responses.

It is concluded that the 3 friction laws, constant, Coulomb-viscous and quadratic friction laws, can be used to model this latter tribological system. However, the viscous friction law is not useful to model such a system.

When a steel sphere is oscillating on a fixed steel flat surface having glycerol as a lubricant and a normal load of 0.05N at 22°C, the measured free response is characterized by a convex envelop form. Figure 28 represents the dimensionless velocity-time responses and its envelop for this latter tribological system.

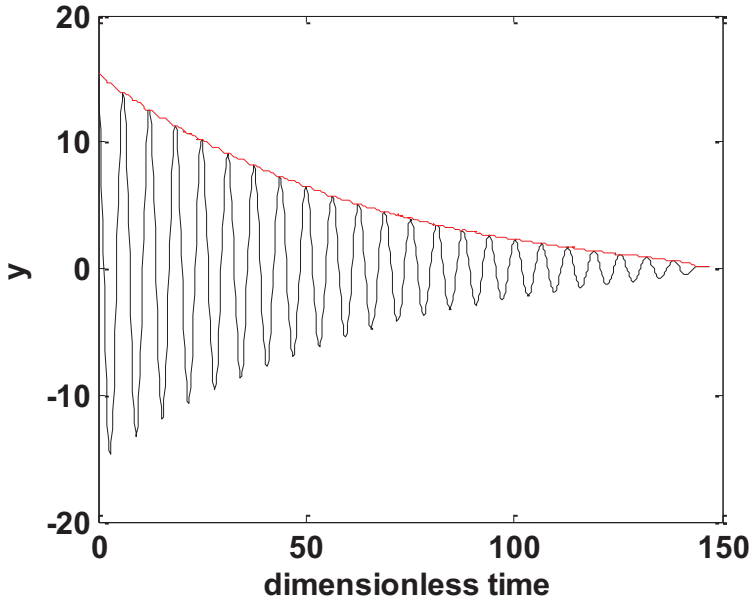

Figure 28. Dimensionless displacement-time response of steel-on-steel sphere-on-flat plane lubricated with glycerol loaded with 0.05 N at 22°C.

In Figure 29, both the experimental and simulated amplitudes are compared corresponding to the steel/steel contact lubricated with glycerol and having a normal load of 0.05 N at 22°C. Figures 29 (a) presents the amplitude of the system responses, experimentally using the definition of Crandall & Mark and numerically modeled using the constant, viscous, coulomb-viscous and quadratic friction laws. Figure 29 (b) shows a comparison between the experimental and simulated dimensionless displacement-time responses using the quadratic friction model. Figure 29 (b) shows the dimensionless-time response experimentally and numerically modeled by the quadratic friction law.

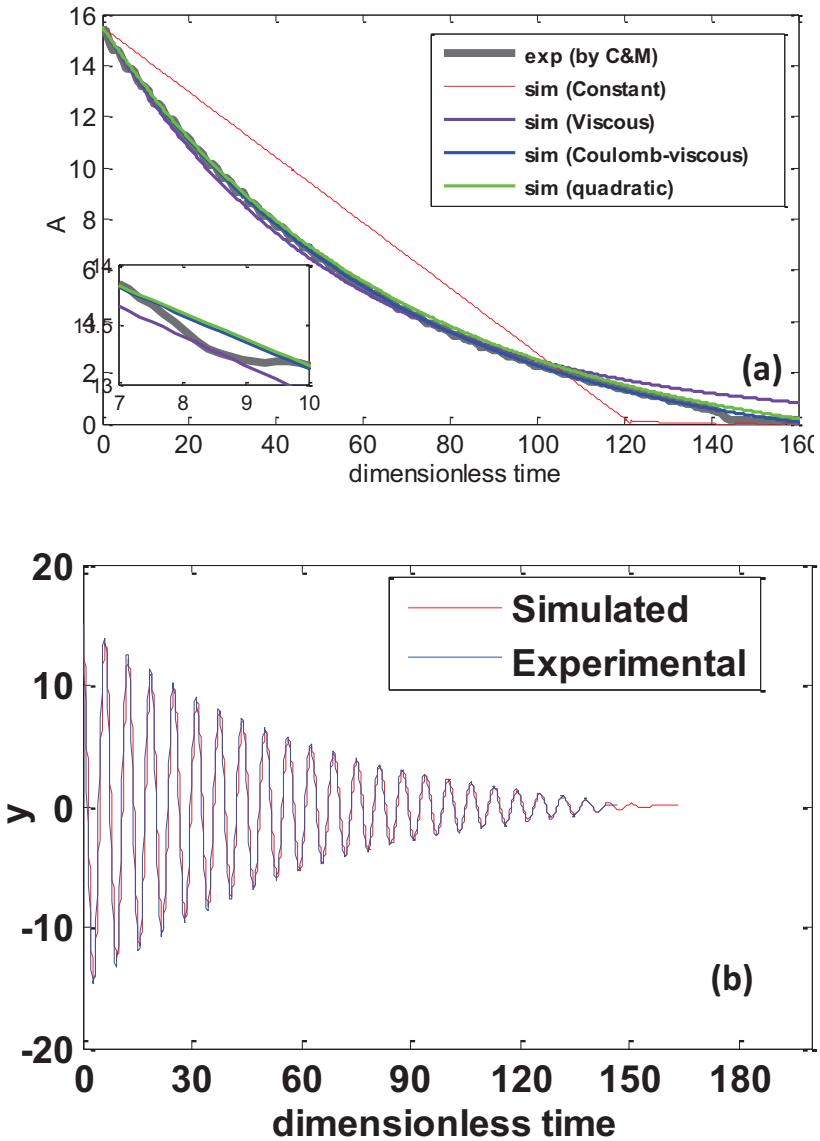

Figure 29. (a) Experimental v/s Simulated envelope with different friction models (b) Experimental v/s simulated dimensionless displacement time-responses.

Among these four friction laws, both coulomb-viscous and quadratic friction laws can numerically model the system. The function $F'(A)$ is negative; thus, the envelope is defined by a convex form.

Moreover, a concave form of the amplitude evolutions was shown in the experimental procedure. This latter is shown when a steel-on-steel surfaces having base oil 150NS as a lubricant and 0.10 N as a normal load at a temperature of 42°C(see Figure 30).

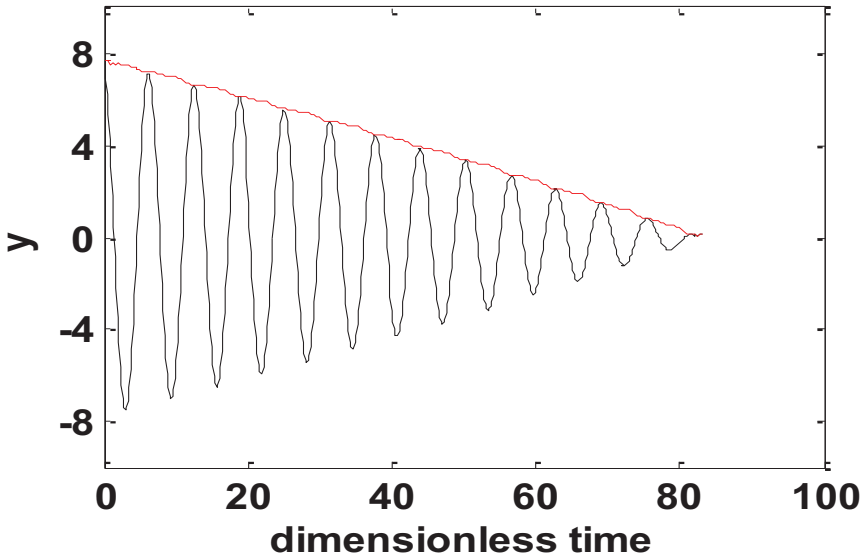

Figure 30. Dimensionless displacement-time response of steel-on-steel sphere-on-flat plane lubricated with pure base oil 150NS loaded with 0.10 N at 42°C.

A comparison between the experimental and numerical results are presented in the following figure. The numerical results are simulated using four friction laws: constant, viscous, Coulomb-viscous and quadratic friction models. Figure 31(a) presents a comparison between experimental and numerical amplitudes. Figure 31(b) represents the

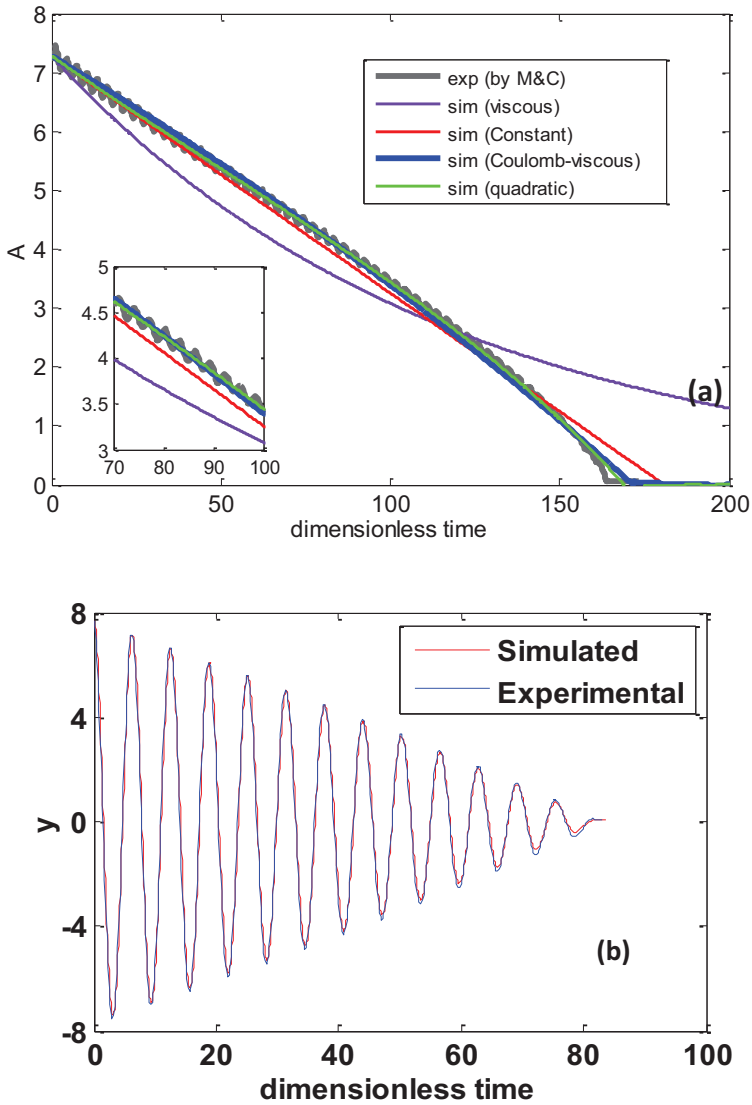

Figure 31. (a) Experimental v/s Simulated envelope with different friction models (b) Experimental v/s simulated dimensionless displacement time-responses.

Figure 31 shows that that both Coulomb-viscous and quadratic friction laws can be used to model the current system. The function $F'(A)$ is positive for all $A \in [0, A_0 = 7.7]$. This latter shows that the envelope of the response is described by a concave form.

From the experimental results, we are also able to examine an envelope form containing both concave and convex (see Figure 32). Figure 32 presents the dimensionless velocity-time response corresponding to steel on steel contact lubricated with pure glycerol and loaded with 0.05 N at 61°C. The response below starts with a convex envelope form then at a certain value of the amplitude the envelope continues with a concave form.

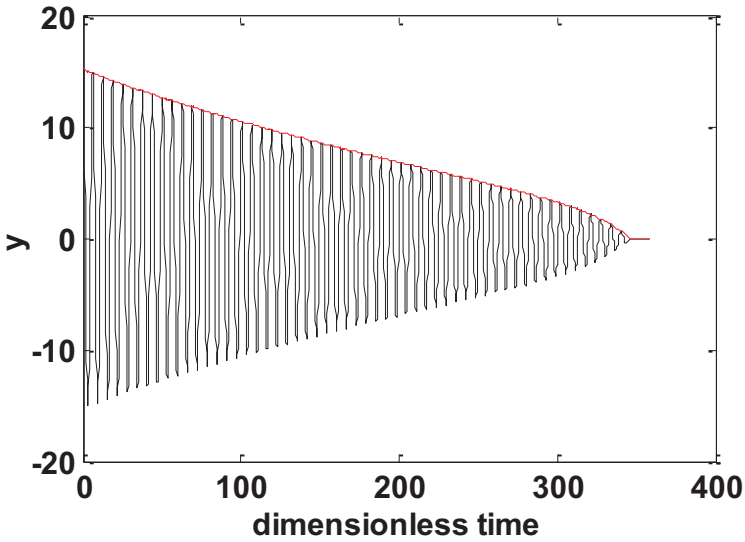

Figure 32. Dimensionless velocity-time response of steel-on-steel sphere-on-flat plane lubricated with pure glycerol loaded with 0.05 N at 61°C.

The oscillatory system is simulated using four different friction models. They are then compared with the experimental responses. The amplitudes of the response is shown in Figure 33 (a) having 4 different friction laws: Constant, viscous, Coulomb-viscous and quadratic. Figure 33 (b) presents the comparison between the experimental (in blue) and numerical (in red) responses simulated by a quadratic friction laws.

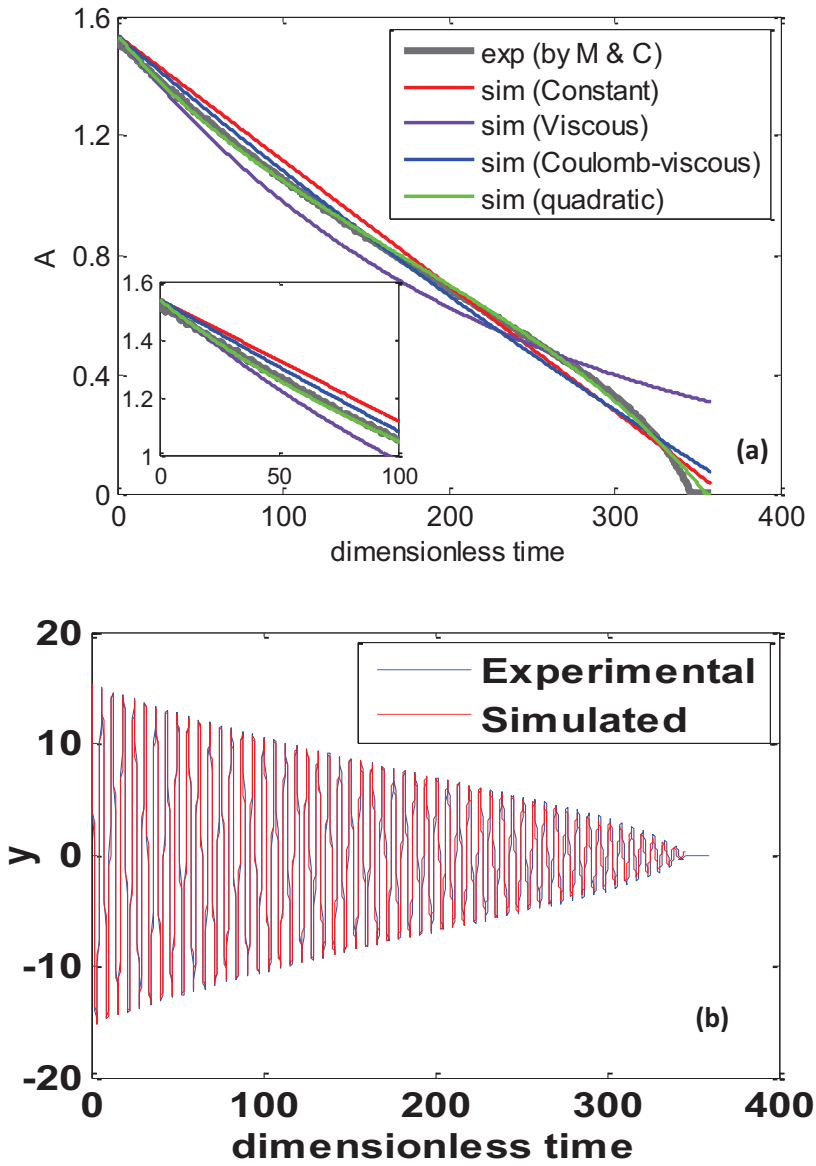

Figure 33. . (a) Experimental v/s Simulated envelope with different friction models (b) Experimental v/s simulated dimensionless displacement time-responses.

One can conclude that among those 4 friction laws, only the quadratic friction law can perfectly model this system. The quadratic friction model corresponds to the case where $\Delta^2 < 0$ and $\mu_1 < 0$. $F'(A)$ is positive for all $\in [0,7.8]$ and negative all $A \in [7.8, A_0 = 15.4]$. Therefore, the oscillatory response is described by a concave form for all $A \in [0,7.8]$ and by a convex all $A \in [7.8, A_0 = 15.4]$.

3.7 Discussion

It is very interesting to investigate the friction models at different amplitude of the oscillatory response. Indeed, if the chosen friction law is inadequate, then the coefficient of friction will vary with the amplitude.

In the following, we will concentrate on two cases, the Coulomb-viscous friction model, used in [15] and the quadratic friction law, proposed in this thesis.

In order to do that, the oscillatory response is divided over 5 time sequences, denoted by T_1 to T_5. For each temporal sequence, one can associate the starting amplitude, denoted by A_1 to A_5. Figure 34 presents the velocity-time response in dimensionless form, corresponding to the system steel/steel lubricated with glycerol at 22°C having a normal load of 0.05N. The 5 temporal sequences are represented in the above Figure 34.

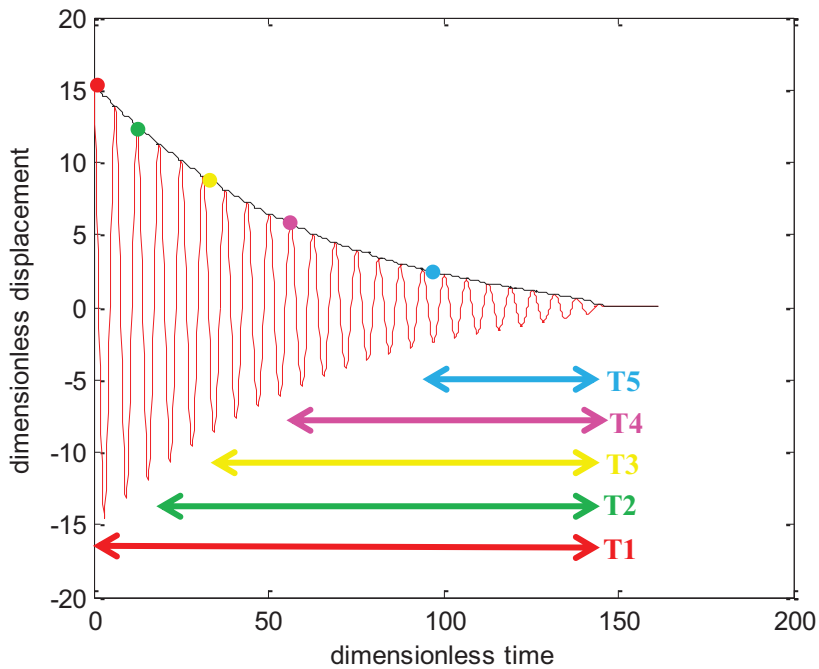

Figure 34. Dimensionless displacement-time response corresponding to steel/steel lubricated with glycerol at 22°C with a normal load of 0.05N.

The constants, corresponding to both Coulomb-viscous and quadratic friction models are evaluated and presented in Table 6.

Test	Coulomb-viscous		Quadratic		
	μ_0	μ_1	μ_0	μ_1	μ_2
$T_1 = 150$ $A_1 = 15$	0.0350	0.0303	0.0390	0.0276	0.0002
$T_2 = 127$ $A_2 = 12$	0.0374	0.0293	0.0376	0.0291	0
$T_3 = 114$ $A_3 = 9$	0.0350	0.0306	0.0432	0.0225	0.0012
$T_4 = 97$ $A_4 = 6$	0.0374	0.0294	0.0456	0.0180	0.0025
$T_5 = 47$ $A_5 = 3$	0.0433	0.0242	0.0370	0.0406	-0.0067

Table 6. Coulomb-viscous and quadratic constants computed, corresponding to steel/steel lubricated with glycerol at 22°C with a normal load of 0.05N

Figure 35 shows the Coulomb-viscous law, determined at all the 5 parts and the quadratic friction law, determined at part 1, for the system studied. It is shown that the Coulomb-viscous law is slightly the same for all amplitudes. Moreover, the quadratic friction model seems to be similar to that of the Coulomb-viscous. Thus, one can conclude that for this studied system, the Coulomb-viscous friction law can be sufficiently used to model the system.

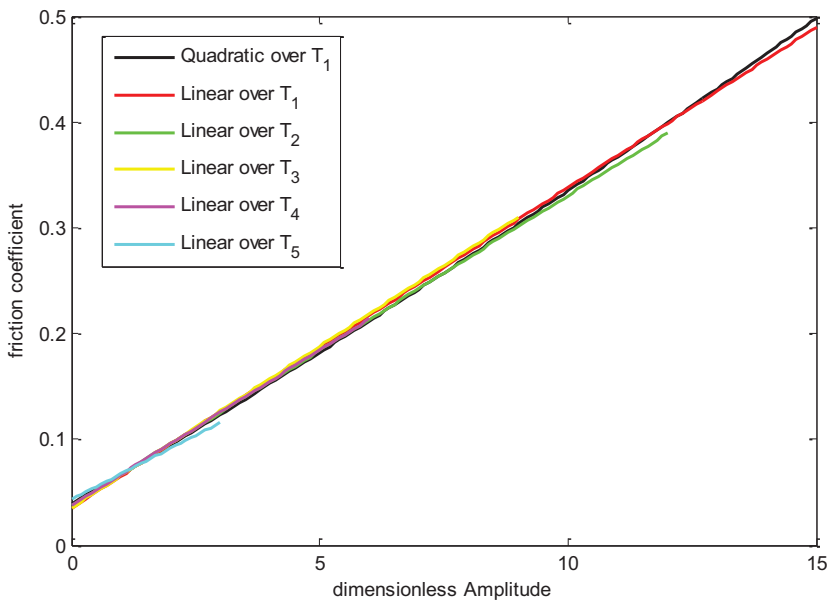

Figure 35. Friction coefficient as a function of the dimensionless amplitude.

Figures 36 (a) and (b) present the evaluated constants corresponding to the Coulomb-viscous and quadratic friction laws respectively. We can clearly observe that the constants μ_n corresponding to these two friction laws vary slightly with the amplitude although the

Coulomb-viscous and quadratic friction laws are similar to each other even at different amplitudes (as seen in Figure 35).

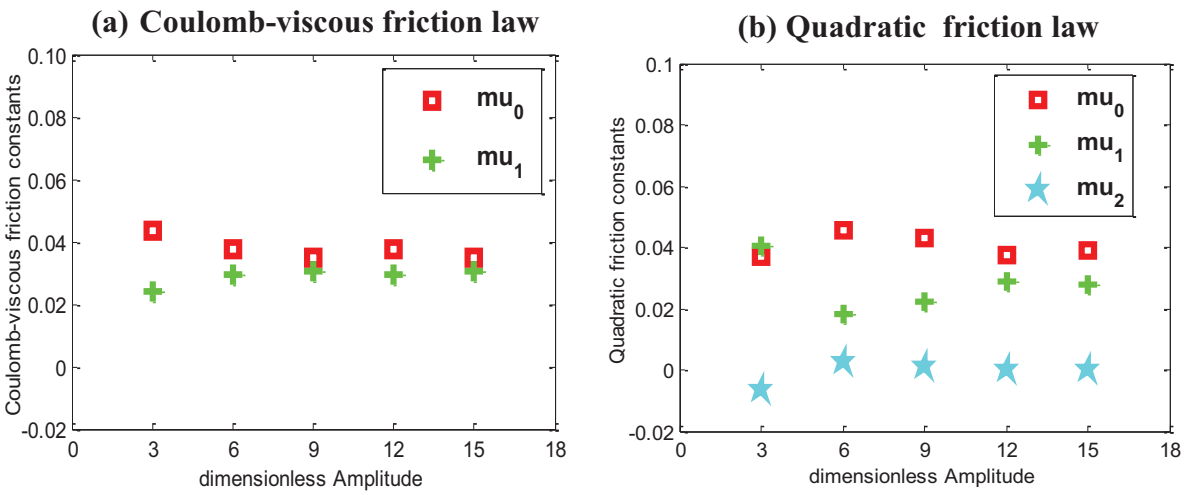

Figure 36. Evaluated friction constants (a) Coulomb-viscous friction law, (b) Quadratic friction law.

The above figure (Figure 37) presents the dimensionless velocity response of a steel/steel contact lubricated with pure glycerol having a normal load of 0.05 N at a temperature of 61°C. The decaying envelope of the corresponding response is described by a combination of both convex and concave. The oscillatory response is divided over 4 time sequences, denoted by T_1 to T_4. For each temporal sequence, one can associate the starting amplitude, denoted by A_1 to A_4. The 4 temporal sequences are represented in the above Figure 34.

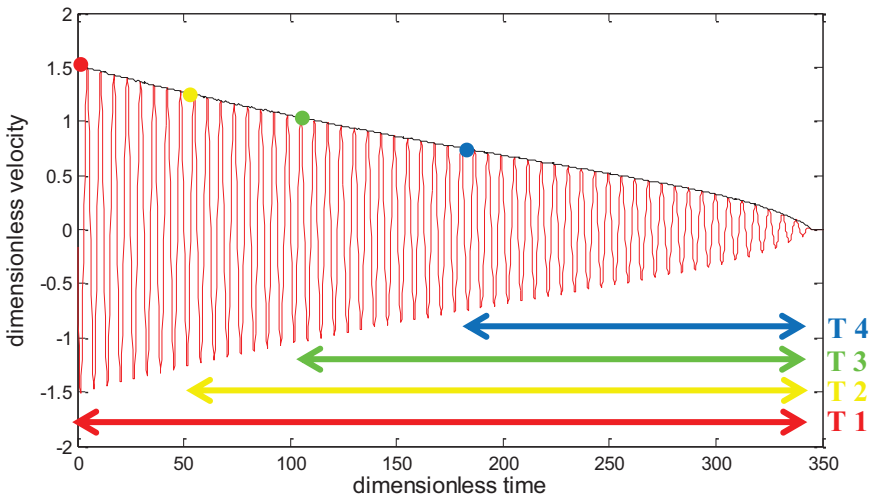

Figure 37. Dimensionless velocity time-response corresponding to a steel/steel contact lubricated with pure glycerol having a normal load of 0.05 N at 61°C.

Table 7 presents the values of the friction computed constants corresponding to the 4 different parts.

Parts	Coulomb-viscous		Quadratic		
	μ_0	μ_1	μ_0	μ_1	μ_2
$T_1 = 340$ $A_1 = 1.5$	0.0054	0.0017	0.011	-0.0184	0.0138
$T_2 = 284$ $A_2 = 1.25$	0.0067	-0.0009	0.0119	-0.0229	0.0180
$T_3 = 230$ $A_3 = 1$	0.0081	-0.0041	0.0131	-0.0299	0.0258
$T_4 = 170$ $A_4 = 0.75]$	0.0103	-0.0104	0.0133	-0.0310	0.0272

Table 7. Friction contribution constants of temporal sequences 1, 2, 3 and 4 of the velocity response (Figure 34) corresponding to Coulomb-viscous and quadratic friction laws.

Figures 38 and 39 present the friction coefficient at different temporal sequences of the response.

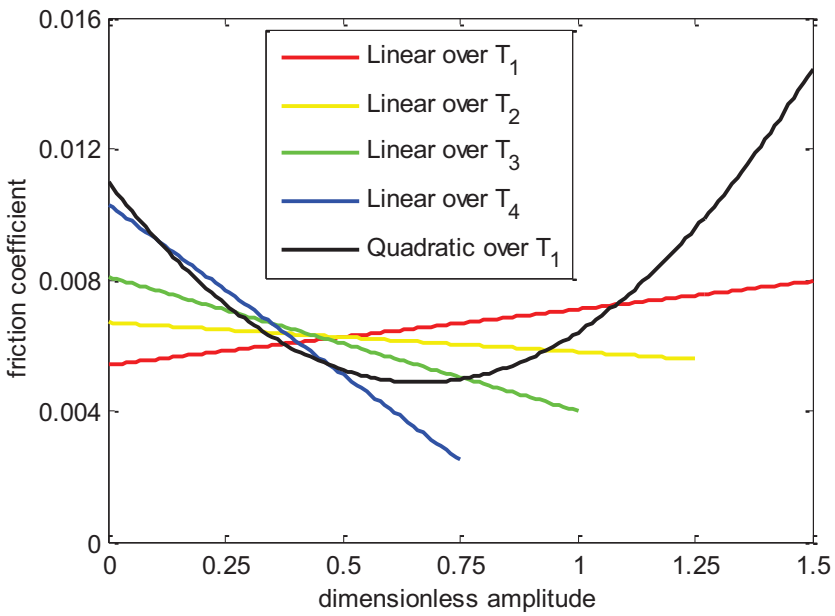

Figure 38. Friction coefficient described by a Coulomb-viscous law as a function of the dimensionless velocity at different temporal sequences of the response and also by a quadratic friction law corresponding to part 1 of the response.

The above figure shows that both the Coulomb-viscous and quadratic friction laws, found from the response, are not similar. Moreover, the Coulomb-viscous model varies with the initial amplitudes.

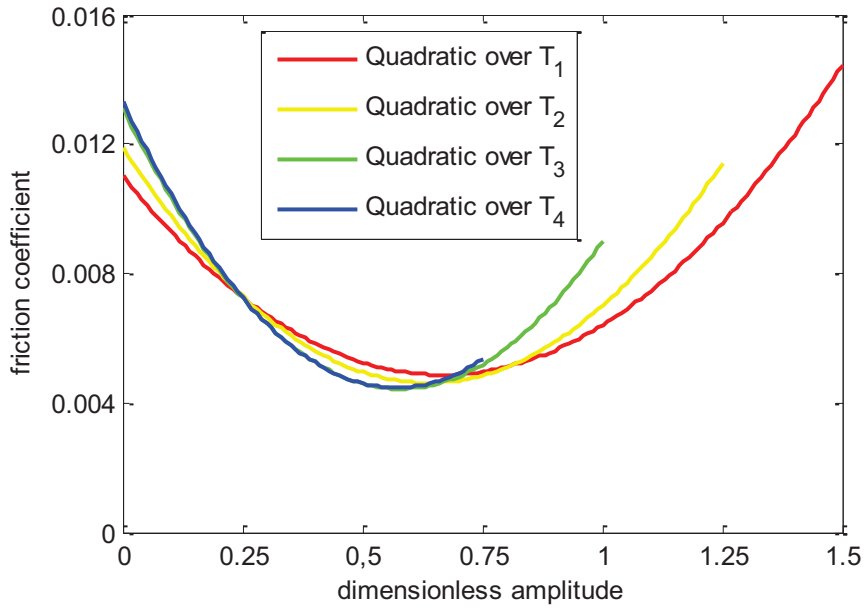

Figure 39. Friction coefficient described by a quadratic law as a function of the dimensionless velocity.

Figure 39 show that the quadratic friction models at different amplitudes are slightly similar. Thus, quadratic friction law may be sufficient friction model for some systems. One can also conclude that a Coulomb-viscous friction is not a sufficient law to model an oscillating dynamic system.

Figures 40 (a) and (b) present the evaluated constants corresponding to the Coulomb-viscous and quadratic friction laws respectively corresponding to steel/steel contact lubricated with pure glycerol having a normal load of 0.05 N at a temperature of 61°C.

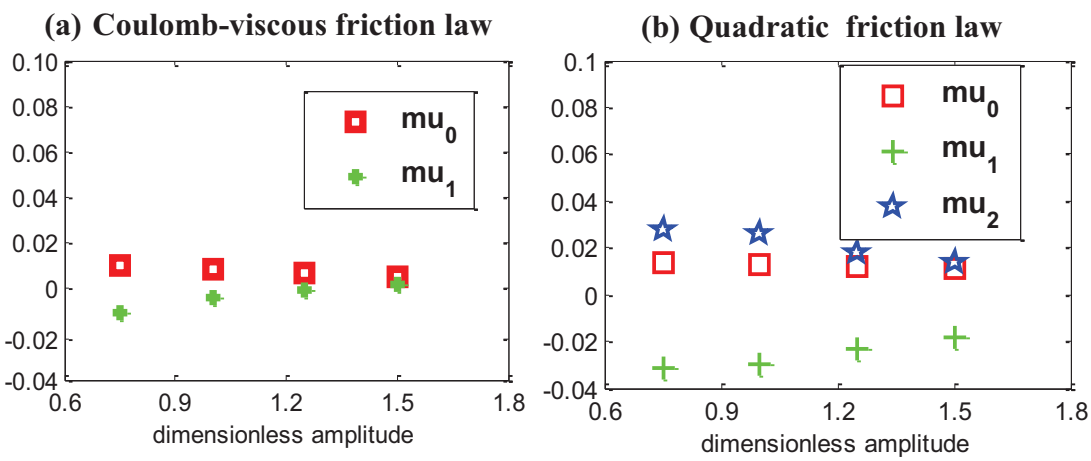

Figure 40. Evaluated friction constants (a) Coulomb-viscous friction law, (b) Quadratic friction law.

We can clearly observe that the constants μ_n corresponding to these two friction laws vary slightly with the amplitude although the quadratic friction laws are slightly similar to each other even at different amplitudes (as seen in Figure 39).

Moreover if only a pseudo-polynomial friction model is available, one can evaluate the polynomial friction law that can better model the system. Figure 41 presents the envelope corresponding to the response of the system presented before (see Figure 37). The envelope in red represented the experimentally measured envelope; however, the blue one is represented in blue defined by the following equation: $A_{fitted} = (-1 * 10^{-12})\tau^5 + (7 * 10^{-10})\tau^4 + (-2 * 10^{-7})\tau^3 + (3 * 10^{-5})\tau^2 + (-0.0062)\tau + 1.5273$.

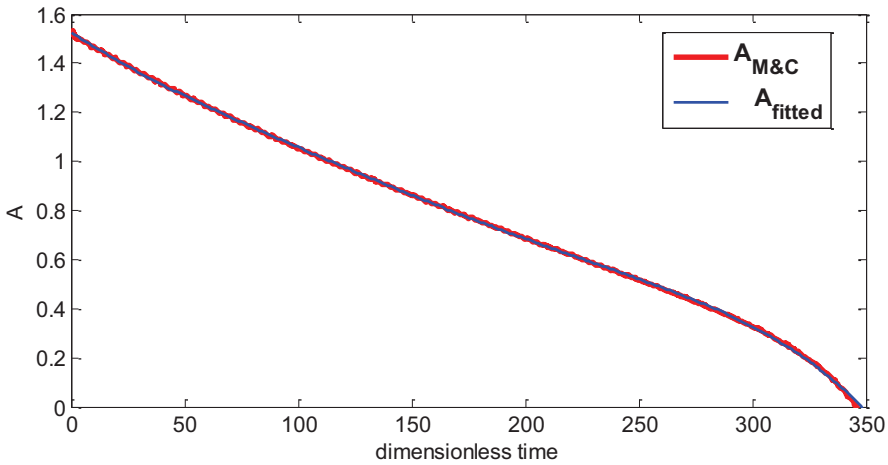

Figure 41. Envelope response corresponding to a steel/steel contact lubricated with pure glycerol having a normal load of 0.05 N at 61°C.

Its corresponding function $F(A)$ is found to be as follows: $F(A) = -0.0012A^4 + 0.0018A^3 + 0.0074A^2 - 0.0139A + 0.0096$ and represented in Figure 42.

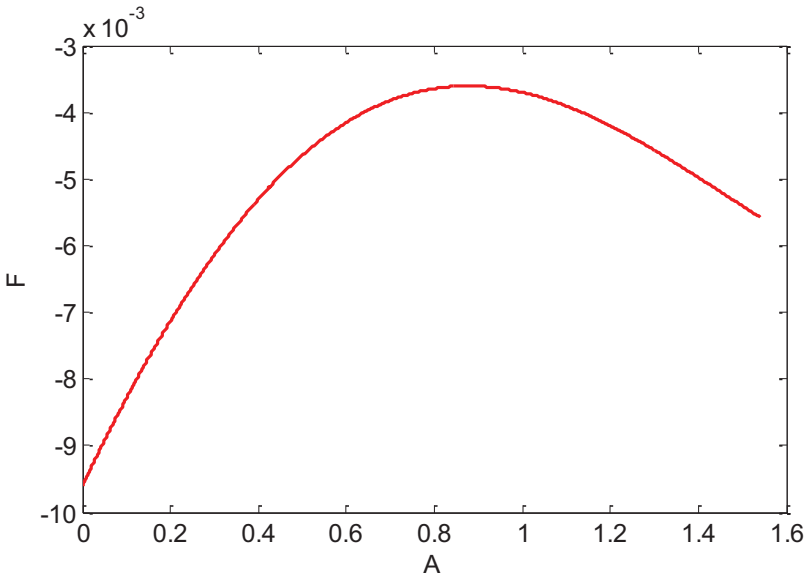

Figure 42. F as a function of A.

The function $F(A)$ is defined by theses constants: $a_4 = 0.0012, a_3 = -0.0018, a_2 = -0.0074, a_1 = 0.0139, a_0 = -0.0096$. Thus, using equations (27) and (28), one can find the friction law characterized by a 4th order polynomial friction law defined as: $\mu(A) = -0.0040A^4 + 0.0048A^3 + 0.0174A^2 - 0.0278A + 0.0151$. Figure 43 demonstrates the 4th order polynomial friction coefficient as a function of the dimensionless amplitude, A.

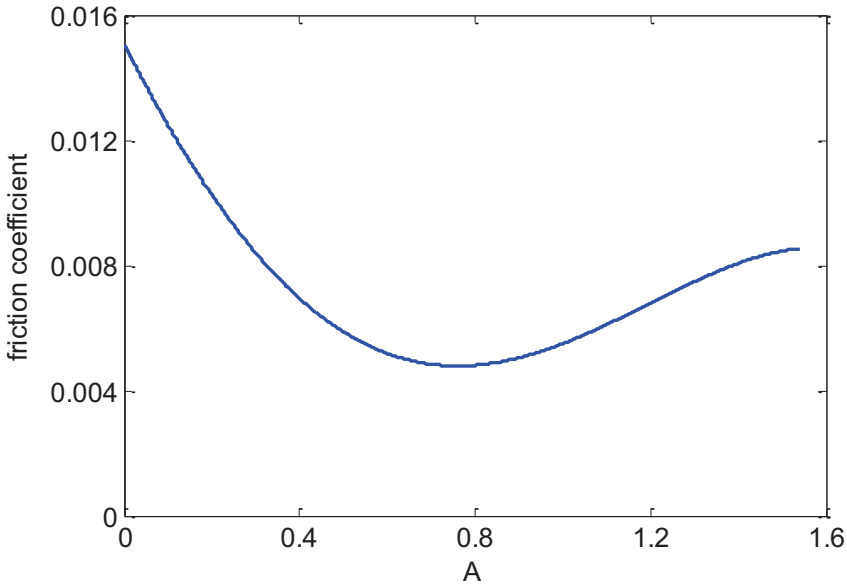

Figure 43. Friction coefficient as a function of A.

This latter example shows that a simple friction law, i.e. Coulomb-viscous and quadratic friction laws, cannot be always a sufficient model for a dynamic system, as seen in this chapter.

3.8 Conclusion

This chapter studies a mass-spring oscillator system described by a pseudo-polynomial kinematic friction model. The dimensionless equation of motion is set up in order to highlight the properties of the mechanical system. Thus, the oscillating free responses are determined numerically using the Runge-Kutta method of order 4. Moreover, the amplitude evolutions corresponding to the free responses are determined numerically either by using the definition of Crandall and Mark or by Hilbert Transform. Thus, Hilbert transform can better represent the envelope of the displacement-time response than that of the velocity. Depending on the friction constants, described by μ_{2n} and μ_{2n+1}, the analytical solution of the decaying amplitude can be determined.

Moreover, by determining the second derivative of the amplitude with respect to the time constant, we are able to determine the form of the envelop corresponding to an oscillating free response. Thus, we are able to know the friction model corresponding to each oscillating mechanical system. Four different forms of the envelopes are discussed numerically: straight,

convex, concave and a combination of both concave and convex. Thanks to our experimental apparatus, we are able to measure the displacement and velocity-time responses. Also, the different forms of the envelopes corresponding to the time responses are shown experimentally. It is shown that an experimental response described by a straight, convex or concave may be modeled using a linear friction law (for example a Coulomb-viscous friction); however, when the experimental oscillating response is described by both concave and convex, only a non-linear friction law (for example a quadratic friction law) can model the system. We examine that the non-linear friction law is always a successful model for all observed cases. This can be explained by the reason behind that all real life mechanical applications are characterized by their nonlinear behavior.

Beyond that all, the most important conclusion is that we are able to get valuable information of the behavior of the friction μ from the decaying form of the oscillatory free responses. Moreover, it is very significant to determine the friction laws at different initial amplitudes of the oscillatory dynamic system in order to successfully model the system.

Finally, we show a satisfactory agreement between the experimental, numerical and analytical results.

References

[1] Awrejcewicz, J. and Olejnik, P., Analysis of dynamic systems with various friction laws. Applied Mechanics Reviews 58, pp. 389-411, 2005.

[2] Ko, P.L., Taponat, M.-C. and Pfaifer, R., Friction-induced vibration – with and without external disturbance. Tribology International 34, pp. 7-24, 2001.

[3] Fredman, M. and Braun, S., Identification of nonlinear system parameters via the instantaneous frequency: Application of the Hilbert transform and Wigner-Ville Techniques. Sem proceedings, pp.637-642, 1995.

[4] Nayak, R., Contact Vibrations. Journal of Sound and Vibration 22 (3), pp. 297-322, 1972.

[5] Hess, D. and Soom, A., Normal vibrations and friction under harmonic loads. Part1-Hertzian contact. ASME Journal of Tribology 113, p.p. 80-86, 1991.

[6] Rigaud, E. and Perret-Liaudet, J., Experiments and numerical results on non-linear vibrations of an impacting Hertzian contact. Part 1: harmonic excitation. Journal of Sound and Vibration 265 (2), p.p. 289-307, 2003.

[7] Perret-Liaudet and Rigaud, E., J., Experiments and numerical results on non-linear vibrations of an impacting Hertzian contact. Part 2: random excitation. Journal of Sound and Vibration 265 (2), p.p. 309-327, 2003.

[8] Butcher, J. C., The numerical analysis of ordinary differential equations: Runge-Kutta and general linear methods. Wiley-Interscience New York, NY. Pub. 1987.

[9] Langley, R. S., On various definition of the envelope of a random process. Journal of Sound and Vibration. 105(3), pp. 503-1512, 1986.

[10] Feldman, M, Non-linear system vibration analysis using Hilbert transform-I. Free vibration analysis method 'FREEVIB', Mechanical System and Signal Processing 8 (2), pp. 119-127, 1994.

[11] Nayfeh, A.H. and Mook, D.T., Nonlinear Oscillations. Wiley-Interscience Pub. 1979.

[12] Majdoub, F., Belin, M., Martin, J.M., Perert-Liaudet, J., Kano, M. and Yoshida,K., Exploring low friction of lubricated DLC coatings in no-wear conditions with a new relaxation tribometer. Tribology International 65, 2013, pp. 278-285.

[13] Levenberg, K., A method for the solution of certain problems in least squares. Quart. Appl. Math. 2, p.p. 164-168, 1944.

[14] Marquardt, D., An algorithm for least-squares estimation of nonlinear parameters. SIAM J. Appl. Math. 11, pp. 431-441, 1963.

[15] Rigaud, E., Perret-Liaudet, J., Belin, M., Joly-Pottuz, L. and Martin, J.M., An original dynamic tribotest to discriminate friction and viscous damping. Tribology Internation 431 (2), pp. 320-329, 2010.

Appendix A: Runge-Kutta Method

In order to solve directly the equation of motion numerically, the known Runge Kutta (RK) integration time scheme of the 4th order is used. Thus, RK is followed to determine the solution of the non-linear different equation defined as:

$$\dot{\boldsymbol{Y}} = \boldsymbol{F}(\boldsymbol{Y}) \qquad \text{(A.1)}$$

with

$$\boldsymbol{Y}^T = \langle y_i, \dot{y}_i \rangle \qquad \text{(A.2)}$$

$\boldsymbol{F}$ is defined as the flow of the first order differential equation.

This method is based on several steps as will be shown in the following. Let assume:

$$\boldsymbol{X_i} = \langle y_i \quad \dot{y}_i \rangle \text{ where } i = 0,1, \dots, N \qquad \text{(A.2)}$$

and

$$\boldsymbol{X_i}^T = \langle \langle y_i \rangle, \langle \dot{y}_i \rangle \rangle \qquad \text{(A.3)}$$

with $y_i = y(t)$and $\dot{y}_i = \dot{y}_i(t)$.

Thus, the non-dimensionless displacement and velocity time responses are determined to be:

$$\boldsymbol{X} = \boldsymbol{X} + \frac{\boldsymbol{dt}}{\boldsymbol{6}}(\boldsymbol{k_1} + \boldsymbol{2k_2} + \boldsymbol{2k_3} + \boldsymbol{k_4}) \qquad \text{(A.4)}$$

having

$$[\boldsymbol{k_1}] = \boldsymbol{F}(\boldsymbol{X}) \qquad \text{(A.5)}$$

$$[\boldsymbol{k_2}] = \boldsymbol{F}(\boldsymbol{X} + \boldsymbol{dt}\frac{\boldsymbol{k_1}}{\boldsymbol{2}}) \qquad \text{(A.6)}$$

$$[\boldsymbol{k_3}] = \boldsymbol{F}(\boldsymbol{X} + \boldsymbol{dt}\frac{\boldsymbol{k_2}}{\boldsymbol{2}}) \qquad \text{(A.7)}$$

$$[\boldsymbol{k_4}] = \boldsymbol{F}(\boldsymbol{X} + \boldsymbol{dt}\ \boldsymbol{k_3}) \qquad \text{(A.8)}$$

k_1 is defined as the increment based on the slope at the beginning of the interval using X, k_2 is the increment based at the midpoint of the interval using $X + dt\frac{k_1}{2}$, k_3 is the increment based at the midpoint of the interval using $X + dt\frac{k_2}{2}$ and finally k_4 is the increment based on the slope at the end of the interval $X + dt\ k_3$.

Appendix B: Hilbert Transform Method

The Hilbert transform is defined as a filter which simply shifts the frequency input by a phase of $\pi/2$ radians. The functions $\tilde{y}(\tau)$ and $\widetilde{y'}(\tau)$ are defined as the Hilbert transform of the non-dimensionless displacement $y(\tau)$ and velocity $y'(\tau)$ respectively.

$$H[y(\tau)] = \hat{y}(\tau) = \frac{1}{\pi\,\tau} y(\tau) = \frac{1}{\pi} \int_{-\infty}^{+\infty} \frac{y(T)}{\tau - T} dT \qquad \text{(B.1)}$$

$$H[\dot{y}(\tau)] = \hat{\dot{y}}(\tau) = \frac{1}{\pi\,\tau} \dot{y}(\tau) = \frac{1}{\pi} \int_{-\infty}^{+\infty} \frac{\dot{y}(T)}{\tau - T} dT \qquad \text{(B.2)}$$

The Hilbert transform has a complex form as follows:

$$H[y(\tau)] = \hat{y}(\tau) = Y_1(\tau) + iY_2(\tau) \qquad \text{(B.3)}$$

$$H[\dot{y}(\tau)] = \hat{\dot{y}}(\tau) = \dot{Y}_1(\tau) + i\dot{Y}_2(\tau) \qquad \text{(B.4)}$$

Appendix C: Calculation of the coefficients

The constant a_n corresponding to the first order derivative $F(A)$ can be written as a function of the friction constants μ_n as follows:

$$a_n = -\frac{\mu_n}{\pi}\int_0^{\pi} \sin^{n+1}\varphi \, d\varphi, n \in \mathbb{N} \qquad \text{(C.1)}$$

$$\int \sin^{p+2}\varphi \, d\varphi = -\frac{1}{p+2}\sin^{p+1}\varphi \cos\varphi + \frac{p+1}{p+2}\int \sin^{p}\varphi \, d\varphi, p \in \mathbb{N} \qquad \text{(C.2)}$$

$$\int_0^{\pi} \sin^{p+2}\varphi \, d\varphi = \frac{p+1}{p+2}\int \sin^{p}\varphi \, d\varphi \qquad \text{(C.3)}$$

$$I_{p+2} = \int_0^{\pi} \sin^{p+2}\varphi \, d\varphi = \frac{p+1}{p+2} I_p \qquad \text{(C.4)}$$

$$I_0 = \int_0^{\pi} d\varphi = \pi \qquad \text{(C.5)}$$

$$I_1 = \int_0^{\pi} sin\varphi \, d\varphi = 2 \qquad \text{(C.6)}$$

$$I_{2k} = \frac{2k-1}{2k} I_{2k-2} = \frac{(2k-1)(2k-3)(2k-5)\ldots(1)}{2k(2k-2)(2k-4)\ldots(2)} I_0 = \prod_{j=1}^{j=k} \frac{2j-1}{2j} I_0 \qquad \text{(C.7)}$$

$$I_{2k+1} = \frac{2k}{2k+1} I_{2k-2} = \frac{2k(2k-2)(2k-4)\ldots(2)}{(2k+1)(2k-1)(2k-3)\ldots(3)} I_1 = \prod_{j=1}^{j=k} \frac{2j}{2j+1} I_1 \qquad \text{(C.8)}$$

$$I_{2k} = \prod_{j=1}^{j=k} \frac{2j-1}{2j}\pi \qquad \text{(C.9)}$$

$$I_{2k+1} = \prod_{j=1}^{j=k} \frac{2j}{2j+1} 2 \qquad \text{(C.10)}$$

$$a_{2k} = -\frac{\mu_{2k}}{\pi} I_{2k+1} = -\frac{2\mu_{2k}}{\pi}\prod_{j=1}^{j=k} \frac{2j}{2j+1} \qquad \text{(C.11)}$$

$$a_{2k+1} = -\frac{\mu_{2k+1}}{\pi} I_{2k+2} = -\mu_{2k+1}\prod_{j=1}^{j=k+1} \frac{2j-1}{2j} \qquad \text{(C.12)}$$

$$-\frac{a_{2k}}{\mu_{2k}} = \frac{2}{\pi}\prod_{j=1}^{j=k} \frac{2j}{2j+1} \qquad \text{(C.13)}$$

$$-\frac{a_{2k+1}}{\mu_{2k+1}} = \prod_{j=1}^{j=k+1} \frac{2j-1}{2j} \qquad \text{(C.14)}$$

$k \in \mathbb{N}$

Appendix D: Analytical equation of the amplitude for quadratic friction model

The decaying envelope for the quadratic friction model is determined analytically by performing the following integration process:

$$\tau - \tau_0 = \int_{A_0}^{A} \frac{dA}{a_2 A^2 + a_1 A + a_0} \qquad \text{(D.1)}$$

The above integration equation can be solved analytically as follows depending on the sign of Δ^2.

<u>Case 1</u>: $\Delta^2 < 0$

$$\tau - \tau_0 = \frac{2}{|\Delta|} \tan^{-1} \frac{2a_2 A + a_1}{|\Delta|} \Big]_{A_0}^{A} \qquad \text{(D.2)}$$

$$\tan\left(\frac{|\Delta|}{2}\tau + \tan^{-1}\frac{2a_2 A_0 + a_1}{|\Delta|}\right) = \frac{2a_2 A + a_1}{|\Delta|} \qquad \text{(D.3)}$$

$$\frac{2a_2 A}{|\Delta|} = \tan\left(\frac{|\Delta|}{2}\tau + \tan^{-1}\frac{2a_2 A_0 + a_1}{|\Delta|}\right) - \frac{a_1}{|\Delta|} \qquad \text{(D.4)}$$

<u>Case 2</u>: $\Delta^2 = 0$

$$\tau - \tau_0 = \frac{-2}{2a_2 A + a_1} \Big]_{A_0}^{A} \qquad \text{(D.5)}$$

$$\frac{2a_2 A + a_1}{2} = \frac{1}{\frac{2}{2a_2 A_0 + a_1} - \tau} \qquad \text{(D.6)}$$

$$a_2 A = \frac{1}{\frac{2}{2a_2 A_0 + a_1} - \tau} - \frac{a_1}{2} \qquad \text{(D.7)}$$

<u>Case 3</u>: $\Delta^2 > 0$

<u>Case 3.1</u>: $A_1 < 0$ and $A_2 > 0$.

$$a_2(\tau - \tau_0) = \frac{1}{A_2 - A_1} \ln\left|\frac{-A_2 + A}{-A_1 + A}\right| \Big]_{A_0}^{A} \qquad \text{(D.8)}$$

$A - A_1 > 0$ and $A - A_2 < 0$ since $A_1 < A < A_2$

$$a_2(A_2 - A_1)\tau = \ln\frac{A_2 - A}{A - A_1} - \ln\frac{A_2 - A_0}{A_0 - A_1} \qquad \text{(D.9)}$$

$$\text{Let } \alpha = a_2(A_2 - A_1) \text{ and } \beta = \frac{A_2 - A_0}{A_0 - A_1} \qquad \text{(D.10)}$$

$$\alpha\tau + \ln\beta = \ln\frac{A_2 - A}{A - A_1} \qquad \text{(D.11)}$$

$$\beta e^{\alpha\tau} = \frac{A_2 - A}{A - A_1} \qquad \text{(D.12)}$$

<u>Case 3.2</u>: $A_1 > 0$ and $A_2 > 0$.

$$a_2(\tau - \tau_0) = \frac{1}{A_2 - A_1}\ln\left|\frac{-A_2 + A}{-A_1 + A}\right|\Bigg]_{A_0}^{A} \qquad \text{(D.13)}$$

$A - A_1 < 0$ and $A - A_2 < 0$ since A$< A_1 < A_2$

$$a_2(A_2 - A_1)\tau = \ln\frac{A_2 - A}{A_1 - A} - \ln\frac{A_2 - A_0}{A_1 - A_0} \qquad \text{(D.14)}$$

Let $\alpha = a_2(A_2 - A_1)$ and $\beta = \frac{A_2 - A_0}{A_1 - A_0}$

$$\alpha\tau + \ln\beta = \ln\frac{A_2 - A}{A_1 - A} \qquad \text{(D.15)}$$

$$\beta e^{\alpha\tau} = \frac{A_2 - A}{A_1 - A} \qquad \text{(D.16)}$$

4 HYSTERESIS EFFECT OF THE FRICTION FORCE

4 Hysteresis Effect of the Friction Force

Chapter 4: Hysteresis Effect of the Friction Force

4.1 Introduction

Friction is a natural phenomenon that occurs in many engineering systems. In cases where the effect of friction cannot be ignored, a good friction model is necessary for the design and analysis of the system. Although the concept of friction is easily understood, it is notoriously difficult to model and simulate. Many friction models contain a variety of nonlinear features such as discontinuities, hysteresis, internal dynamics and other complications. These properties cause the friction models to be numerically stiff and therefore computationally cumbersome. Therefore, in this context we are interested to efficiently simulate a model that captures a significant key of the friction behavior and its effect on the mechanical system.

In literature, many researchers have faced some difficulties in the issues concerning simulating frictional systems (see for example [1] and [2]). Classical models of friction, derived from Coulomb law, suggest that the friction force changes discontinuously when the direction of the sliding velocity changes. Figure 1 presents the friction force F as a function of the sliding velocity $\dot{x}$ of some classical friction laws. It is obvious that for these classical friction models, the friction force spends intermittent and finite periods of time at zero sliding velocities. Therefore, one can say that the friction law is discontinuous.

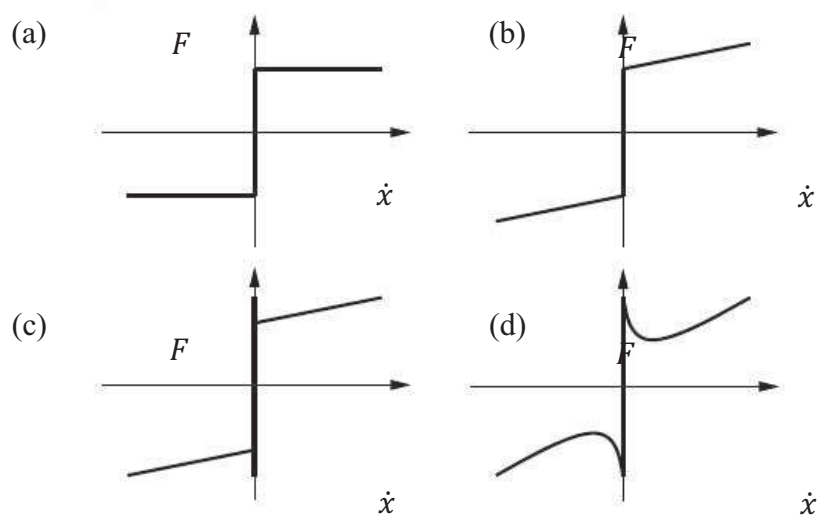

Figure 1. Examples of different classical friction laws. The friction force is given as a function of the sliding velocity. (a) Constant friction. (b) Coulomb and viscous friction. (c) Stiction Coulomb and viscous friction .(c) Stribeck friction law. [3]

Chapter 4 will revisit a bunch of some experimental results presented in the preceding chapters. These results contain the logarithmic scale of the electrical resistance as a function of time, the tangential friction force response and the tangential friction force as a function of both the displacement and the velocity. Then, the concluding remarks of these measurements will introduce the LuGre friction model. Thus, a single degree-of-freedom oscillating system will be studied in the spot of the LuGre friction law. Last but not least, some simulated results will be presented. Finally, a general conclusion of this latter chapter will end this study.

4.2 Friction force phenomenon

Friction force is a reaction in the tangential direction between a contact of two surfaces. The friction phenomenon can be produced as a result of many factors i.e. physical properties of the surfaces material, chemical properties of the lubricant between the two surfaces, relative velocity, geometrical configuration of the mechanical system, etc. There exist two different groups for the dynamical behavior of friction. The first description of the friction force dynamical behavior was formulated by Coulomb in 1785 [4]. This friction law describes the friction as a constant value or in other words, independent of the velocity. However in the earliest of the twentieth century, some friction laws show nonlinear dependence on the relative velocity [5 and 6]. Figure 2 presents an example for a Stribeck curve by presenting the friction force as a function of the velocity.

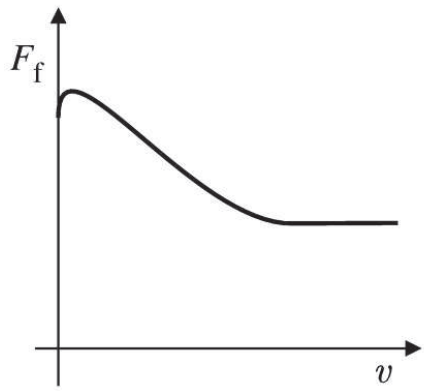

Figure 2. Friction force F_f as a function of the velocity v for a Stribeck curve.

The second category of friction features is the hysteresis effect accompanying the frictional behavior. One of them can appear during the stick and slip phenomenon. This latter is caused by the spring-like behavior of the friction force before the actual sliding. This microscopic motion phenomenon, also called pre-sliding displacement, is affected by the tangential stiffness of the two contacting surfaces [7, 8 and 9]. A pre-sliding motion is represented by a narrow hysteresis around the relative zero velocity (see Figure 3a). Another hysteresis effect can appear can appear during the oscillatory motion of macroscopic sliding. Such phenomenon has been first reported by Hess and Soom [10] during their experiments with a periodic relative velocity of unidirectional motion. Figure 3b presents the friction force of this latter phenomenon as a function of the relative velocity. Thus, a hysteresis frictional behavior

was observed as the velocity varies. The friction force is lower for decreasing velocities than that of increasing ones. Moreover, some analytical and experimental studies confirm the existence of different slopes of the friction force as a function of the velocity [11]. This is known as the non-reversibility of friction force [12]. The friction force-velocity relation, presented in Figure 3c, shows an example of the non-reversibility friction characteristic.

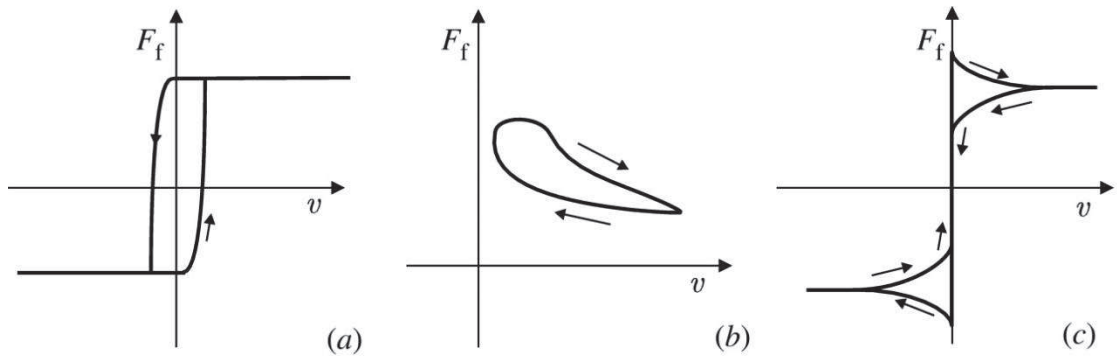

Figure 3. Friction force F_f as a function of the velocity v having hysteresis effect.

4.3 Friction force measurement

The oscillating dynamic tribometer presented in chapter 2 and in [13- 14-15] enables us to also measure the tangential friction force using the experimental rig thanks to a piezo-electric force transducer. The force transducer is implemented in the deformable mechanical sub-system with a high stiffness; so that it permits the measurement of the lateral force caused by the interface's shearing. Once a normal load, N is applied on the pin-on-plane contact, the spherical pin starts to oscillate, where the flat plane is fixed, allowing the system to vibrate. Due to the system's oscillatory movement, the elastic steel blade starts to vibrate horizontally. This latter motion causes the piezo-electric transducer to move horizontally, knowing that the mechanical stiffness of the elastic steel blade k_b is much smaller than that of the piezoelectric transducer K_t ($k_b \ll K_t$). Thus, the tangential friction fore is measured. The electric charges are collected by an amplifier (Kistler 5015A), then they are filtered using a Low-Pass filter having a bandwidth frequency of 300 Hz. Finally, the analog signals are converted to numerical data by using a 16-bits resolution analog/digital converter (DAQ NI USB 6221). As expected, the lower the friction force is detected, the lower the signal to noise ratio. Nevertheless, we notice some noise in the tangential force signals. This latter may be due to some irregularities in the mechanical system. The above figure (Figure 4) shows a schematic representation of the friction force measurement in the experimental apparatus used.

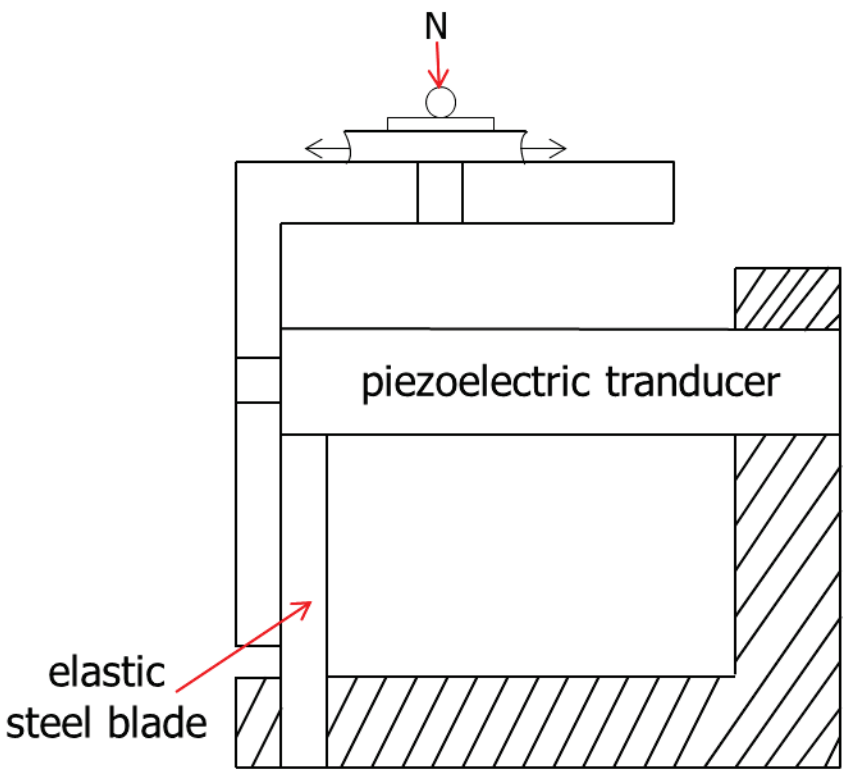

Figure 4. Schematic representation of the tangential friction force implemented in the experimental apparatus.

4.4 Experimental Results

In this section, we will show some experimental results concerning the tangential friction force measurements obtained by oscillating a spherical pin on a flat plane using the dynamic oscillating tribometer presented in Chapter 2 and [13, 14 and 15].

In the following, the tangential friction force response will be presented corresponding to some tribological systems tested. Moreover, we will present the relation of the tangential frictional force with the relative velocity.

A steel-on-steel sphere-on-plane contact is tested. Glycerol is used as a lubricant and a normal load of 0.05 N is applied. The test is performed at room temperature. Using the oscillating tribometer, the responses are measured.

Figure 5 presents a part of the dimensionless velocity response (in red) with its corresponding envelope (in blue) represented using Hilbert transform method. The envelope is described by a convex form. Figure 6 shows the corresponding dimensionless tangential friction force response measured.

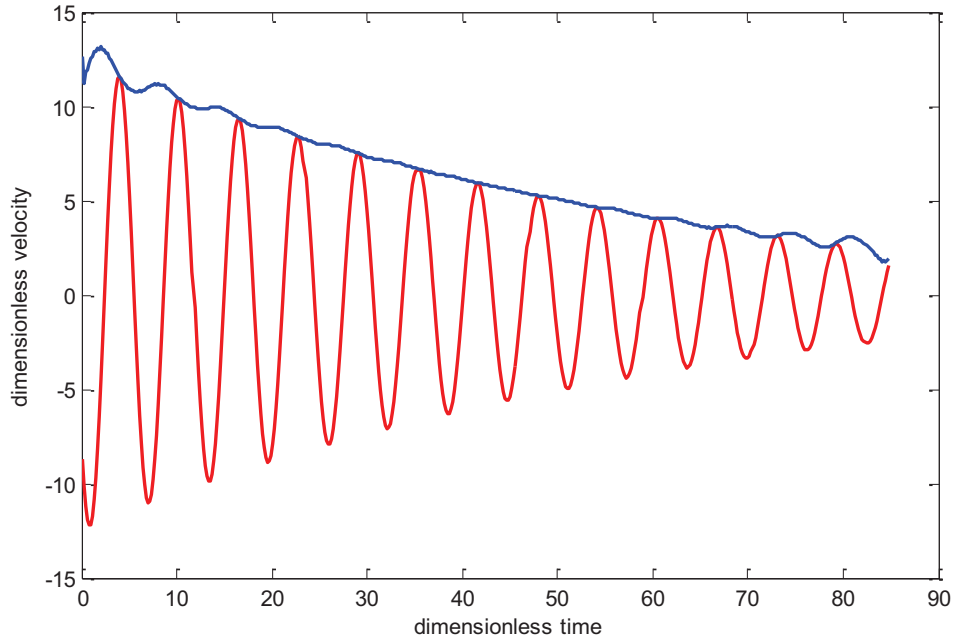

Figure 5. Dimensionless velocity-time response corresponding to a steel-on-steel pin-on-plane contact lubricated by pure glycerol having a normal load of 0.05 N at room temperature.

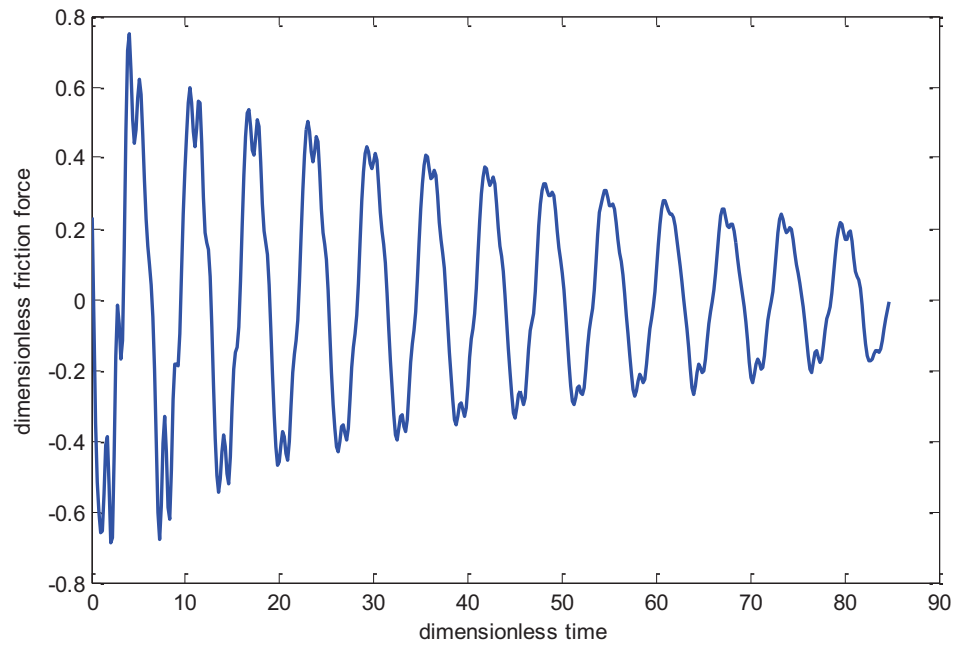

Figure 6. Dimensionless tangential friction force response corresponding to a steel-on-steel pin-on-plane contact lubricated by pure glycerol having a normal load of 0.05 N at room temperature.

We can clearly observe from the above Figure 6 that the friction force peaks increase with time. This latter is seen when the velocity response is described by a convex decaying envelope. Moreover, we notice from the above figure that both the velocity and friction force do not pass through zero at exactly the same time due to a small time-lag between the two

responses (about 0.003 sec). The peaks of the friction force represent the double frequency. Moreover, it is observed that when the system stops ($v = 0$), the friction force does not reach directly to zero. This can be understood by the fact that at the end of the experimental test, the lubricant film may cause some friction even if the system is not sliding anymore. This shows the effect of the solid friction when the system is at rest.

Later on, the friction coefficients corresponding to the partial measured responses (Figures 5-6) are computed (see Appendix C, Chapter 3) for linear (or Coulomb-viscous) and quadratic friction laws.

System	Linear friction law	Quadratic friction law
steel/steel		$\mu_0 = 0.0625$
pure glycerol	$\mu_0 = 0.0274$	$\mu_1 = 0.0179$
0.05 N	$\mu_1 = 0.0323$	$\mu_2 = 0.0012$
22 °C		

Table 1. Friction coefficients computed corresponding to linear and quadratic friction laws.

In Chapter 3, we showed that both the linear and quadratic friction laws may be used to model this system. Thus, we will compare these friction laws to the measured friction force. The figure below presents the tangential friction force as a function of the velocity in its dimensionless form, measured experimentally (in red) and simulated using both the linear (in green) and quadratic friction laws.

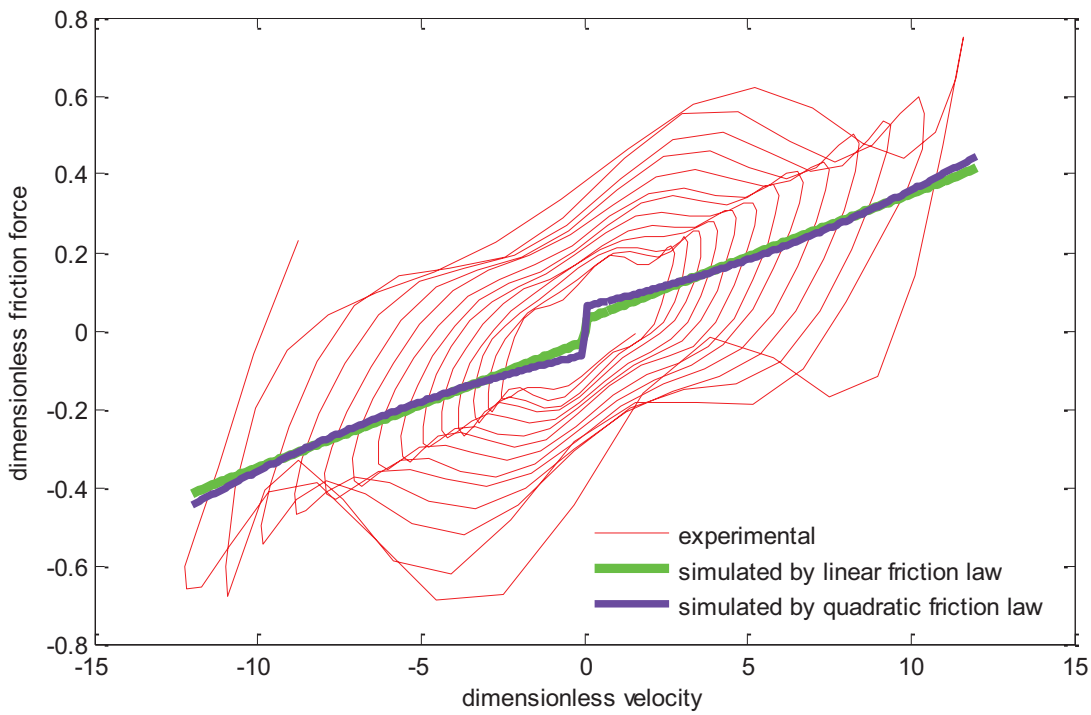

Figure 7. Dimensionless tangential friction force as a function of the dimensionless relative velocity corresponding to a steel-on-steel pin-on-plane contact lubricated by pure glycerol having a normal load of 0.05 N at room temperature.

As the tangential friction force is measured, a new dynamic behavior of friction is defined. This behavior is defined by the hysteresis effect studied previously in the literature. We are also able to see that lag effect that was seen previously by many scholars. According to the friction force-velocity relation, one can notice that the friction force is higher as the relative velocity increases. This latter confirms what was observed by Hess and Soom in 1990 [10]. Moreover, the hysteresis loop gets narrower as the relative velocity decreases.

Another steel-on-steel sphere-on-flat plane contact is lubricated with base oil 150NS. The test is performed at room temperature with an applied normal load of 0.10 N. The time-responses corresponding to this system are measured using the oscillating dynamic tribometer.

A part of the dimensionless velocity response measured for the latter system and its corresponding decaying envelope are presented in Figure 8. The decaying envelope, represented using Hilbert transform method, has a concave form. Moreover, a part of the measured friction force response is shown in Figure 9 in its dimensionless form.

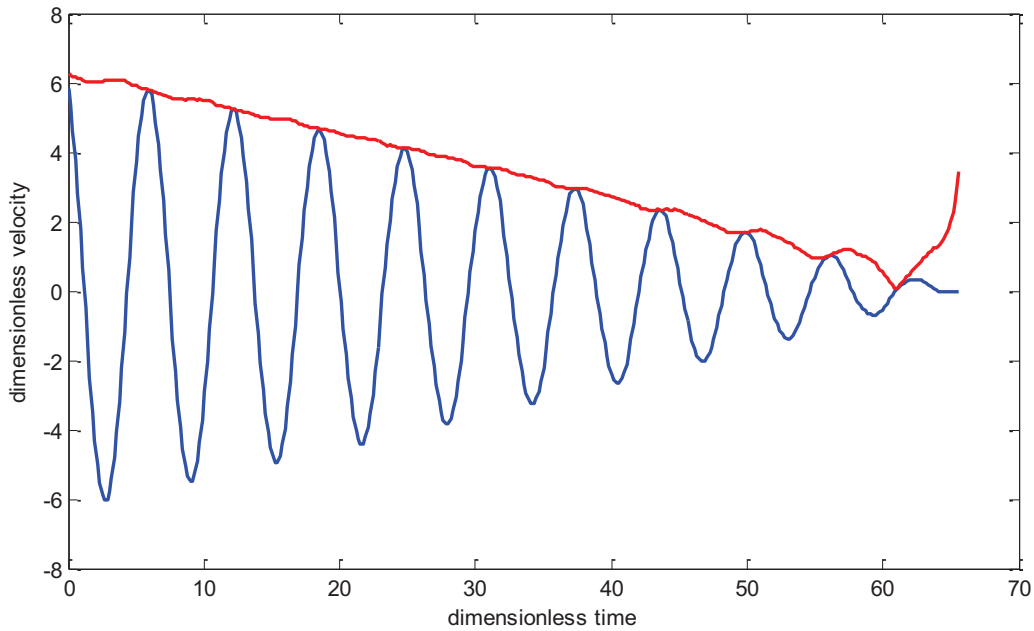

Figure 8. Dimensionless velocity-time response corresponding to a steel-on-steel pin-on-plane contact lubricated by pure 150 NS base oil having a normal load of 0.10 N at a temperature of 42°C.

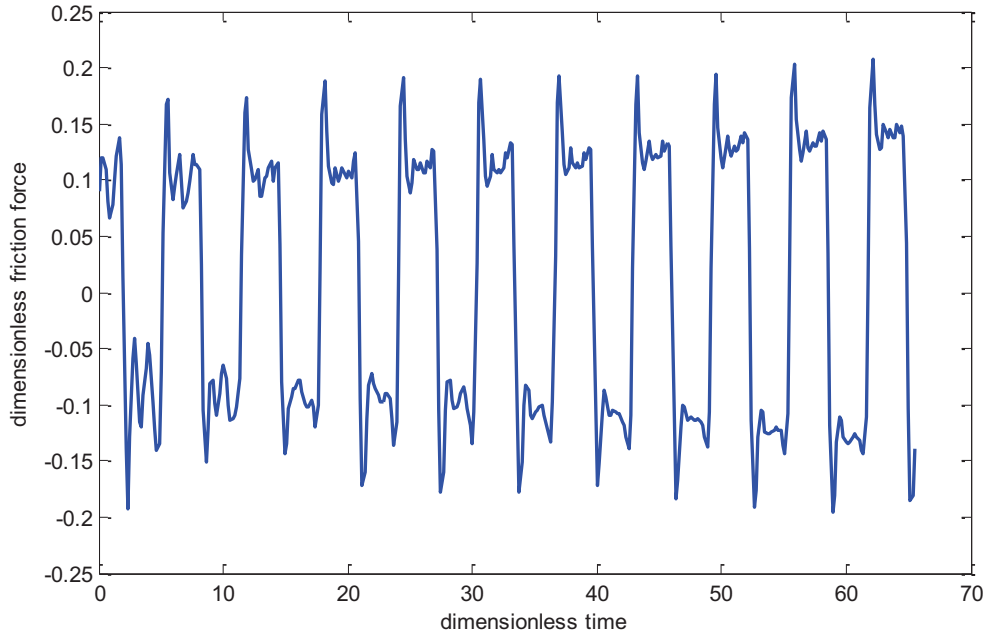

Figure 9. Dimensionless tangential friction force corresponding to a steel-on-steel pin-on-plane contact lubricated by pure 150 NS base oil having a normal load of 0.10 N at room temperature.

The system shows that the measured tangential friction force peaks increase with time. This latter corresponds to the case where the velocity envelope is described by a concave form. As we zoom on a part of the response, we can observe that when the velocity changes direction or in other words passes through zero, the velocity does not overlap with the friction force. This is mainly due to a time-lag (about 0.003 sec).

Table 2 shows the computed friction coefficients corresponding to the partial measured responses (Figures 8 & 9) for both linear and quadratic friction laws.

System	Linear friction law	Quadratic friction law
steel/steel		$\mu_0 = 0.0305$
pure 150NS	$\mu_0 = 0.1327$	$\mu_1 = 0.0884$
0.10 N	$\mu_1 = 0.0020$	$\mu_2 = -0.0139$
42 °C		

Table 2. Computed friction coefficients corresponding to both linear and quadratic friction laws.

In Chapter 3, we showed that both the linear and quadratic friction laws may be used to model such a system. Figure 10 presents the measured tangential friction force as a function of the relative velocity in a dimensionless from. Moreover, the simulated linear and quadratic friction laws are plotted in Figure 9 in order to compare the two latter friction laws computed with that measured.

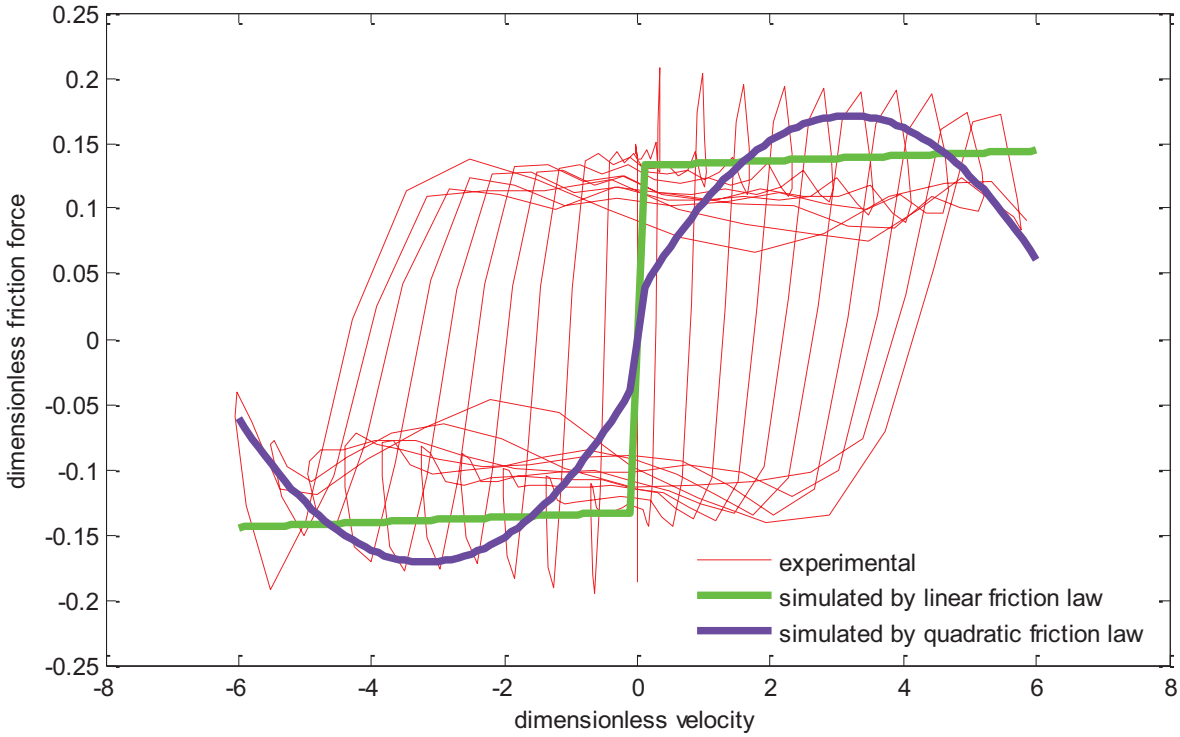

Figure 10. Dimensionless tangential friction force as a function of the dimensionless relative velocity corresponding to a steel-on-steel pin-on-plane contact lubricated by pure 150 NS base oil having a normal load of 0.10 N at a temperature of 42°C.

The friction force-velocity relationship, represented in Figure 10, presents a hysteresis effect. It also shows clearly that unlike the previous example there is not any proportional relationship between the tangential friction force and its corresponding velocity. We notice as well that the hysteresis loop minimizes as the relative velocity decreases.

In our research, the tangential friction forces measured using the oscillating dynamic tribometer are described by both hysteresis and lag effect. These two effects lead us to think about LuGre friction law. However, this law is used for dry friction unlike that of our systems measured. Nevertheless, we will study these effects in the following section by simulating a mass-spring dynamic oscillating system induced by a LuGre friction model will be studied.

4.5 Single Degree-of-Freedom Oscillating System Induced by a LuGre Friction Model

In the following section, we will present an oscillating mechanical system induced by LuGre friction model. Thus, the frictional behavior of this latter will be discussed. Although LuGre friction law is used to model systems described by dry contacts, our aim in this part of the thesis is to study a model exhibiting both hysteresis and time-lag effects. In this context,

LuGre friction model allows us to take these two effects into consideration and to introduce as well a variable-state, defined by the bristle deformation.

In the first sub-section, the single degree-of-freedom (SDOF) induced by a LuGre friction model is defined with its friction law. Later, we will show the steady-state conditions for this latter dynamic model. Then, some parameters will be assumed in order to set the dynamic system in its dimensionless form. Finally, some simulated results of the SDOF oscillating system induced by a LuGre friction model are presented

4.5.1 The dynamic model

The studied dynamic system is described by a single degree-of-freedom mass-spring oscillating system. Figure 11 presents the dynamic oscillating system. The mass m is restrained by a linear spring of stiffness k. Thus, the system can freely oscillate with respect to the lower fixed plane as shown in Figure 11. A constant normal load N is applied to the contact interface resulting in a tangential friction force F_T.

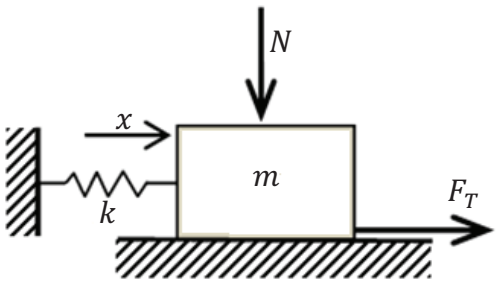

Figure 11. Mass-spring SDOF oscillating system.

The out of static equilibrium equation of motion which governs the free oscillating response of the studied dynamic system is written as follows:

$$m\frac{d^2x}{dt^2} + kx = -F_T \qquad (1)$$

where x is the displacement of the system and $\frac{d^2x}{dt^2}$ is the acceleration corresponding to the system. The dynamic oscillating system is induced by a LuGre friction law.

The LuGre friction law is a model that results in a friction force as an algebraic function of other state variables [16]. The variable is denoted by z.This friction low has also a relationship with the sliding velocity of the system [17]. The LuGre friction law is described by hysteresis behavior and time-lag effect. Moreover, this law is used to model systems with dry contacts. These systems have irregular surfaces at the microscopic level and they form a contact at a certain number of asperities. When a tangential force is applied, the bristles deflect acting like a spring and end up in a friction force. Figure 12 represents the friction interface between the contacts of two bristles.

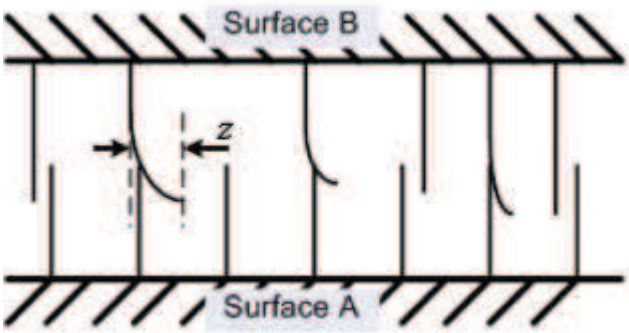

Figure 12. The deflection of the bristle of the LuGre friction model at the friction interface between 2 surfaces [18].

The tangential friction force is described as follows:

$$F_T = \sigma_0 z + \sigma_1 \frac{dz}{dt} + \sigma_2 v \qquad (2)$$

σ_0 is the stiffness which parameterize the presliding displacement, σ_1 is the internal viscous frictional damping coefficient and σ_2 is the viscous damping coefficient due to the relative velocity. The first two terms, $\sigma_0 z + \sigma_1 \frac{dz}{dt}$, represent the friction force generated from the bending of the bristles. However, the last term, $\sigma_2 v$, is added in order to account for the viscous friction. Moreover, the function, $\sigma_0 z + \sigma_2 v$, can be determined by measuring the steady-state friction force when the velocity is held constant. The variable $v = \frac{dx}{dt}$ is the sliding velocity of the system and z is an internal variable known as the deflection of the bristles, in which the LuGre friction model is based on. It is modeled as follows:

$$\frac{dz}{dt} = v - \frac{|v|}{g(v)} z \qquad (3)$$

The function $g(v)$ is positive and depends on a variety of functions such as material properties, temperature and lubrication. It also describes the behavior of the Stribeck curve and can be written as follows:

$$g(v) = F_c + (F_s + F_c) e^{-(v/v_s)^a} \qquad (4)$$

where F_c is the Coulomb friction level, F_s is the stiction force level and v_s is the Stribeck velocity.

4.5.2 Steady-state conditions

The condition of steady state is defined when:

$$\frac{dz_{ss}}{dt} = 0 \qquad (5)$$

Thus, the deflection of the bristles at steady state is easily found to be:

$$z_{ss} = \frac{v}{|v|} g(v) = g(v) sgn(v) \qquad (6)$$

Using the equation (2), the relation between the velocity and the friction force for steady-state motion is described by:

$$F_{ss}(v) = F_c sgn(v) + (F_s - F_c) e^{-\left(\frac{v}{v_s}\right)^a} sgn(v) + \sigma_2 v \qquad (7)$$

4.5.3 Modeling of the dynamic system in its dimensionless form

It is useful to nondimensionalize the equation of motion of the SDOF dynamic oscillating system governing the mass, spring stiffness as well as the tangential frictional force described by LuGre friction law by introducing the following terms:

$$\tau = \Omega t, \qquad \Omega = \sqrt{\frac{k}{m}} \qquad (8)$$

$$y_1 = \frac{k}{F_c} x, \qquad y_2 = \frac{\dot{x}}{v_s}, \qquad y_3 = \frac{\sigma_0}{F_c} z \qquad (9)$$

$$\alpha = \frac{k v_s}{\Omega F_c}, \qquad \gamma = \frac{F_s - F_c}{F_c}, \qquad \epsilon = \frac{k}{\sigma_0} \qquad (10)$$

$$s_1 = \frac{\sigma_1 v_s}{F_c}, \qquad s_2 = \frac{\sigma_2 v_s}{F_c} \qquad (11)$$

where τ is the dimensionless time, Ω is the undamped circular natural frequency, y_1 is the dimensionless displacement, y_2 is the dimensionless sliding velocity and y_3 is the deflection of bristles in its dimensionless form.

The dimensionless equation of motion governing to the SDOF spring-mass dynamic is represented in the following form:

$$y_2' = -\frac{y_1 + f_T}{\alpha} \qquad (12)$$

where $'$ denotes a derivative with respect to the dimensionless time τ, $y_2{}'$ is the dimensionless acceleration of the system and f_T is the dimensionless tangential friction force of the system.

The dimensionless tangential frictional force f_T can be written in the following form:

$$f_T = y_3 + s_1 \left(y_2 - \frac{|y_2|}{g(y_2)} y_3 \right) + s_2 y_2 \qquad (13)$$

The function $g(y_2)$ is represented as a function of the dimensionless sliding velocity y_2 as follows:

$$g(y_2) = 1 + \gamma e^{-|y_2|^a} \qquad (14)$$

The overall dimensionless equation of motion is written in the following form:

$$y_2' = -\frac{1}{\alpha}\left[y_1 + y_3 + s_1\left(y_2 - \frac{|y_2|}{g(y_2)}y_3\right) + s_2 y_2\right] \qquad (15)$$

The first derivative of the dimensionless of the bristles deflection as a function dimensionless time can be represented as follows:

$$y_3' = \frac{dy_3}{d\tau} = \frac{\alpha}{\epsilon}\left(y_2 - \frac{|y_2|}{g(y_2)}y_3\right) \qquad (16)$$

4.5.4 Numerical simulated results

Our system, presented above, is simulated using the MATLAB function *odeset*. The *odeset* function is based on an explicit Runge-Kutta formula, the Dormand-Prince pair [19-20].The routine a variable time step, based on a specified tolerances described by relative tolerance *RelTol* and absolute tolerance *AbsTol*. Table 1 presents the values used for the LuGre friction law in our system.

Parameters	Values
σ_0	$1\ N.m^{-1}$
σ_1	$0.1\ N.sec.m^{-1}$
σ_2	$0.0004\ N.sec.m^{-1}$
F_c	$1\ N$
F_s	$1.5\ N$
v_s	$0.1\ m.sec^{-1}$
a	1

Table 3. LuGre friction model parameters.

Note that for our simulated model, the system is described by a mass, m, of $0.2\ kg$ and a spring having a stiffness, k, of $225.591\ N.m^{-1}$. The initial conditions of the dimensionless displacement, velocity and bristles deflection are respectively $y_1(0) = 225.591$, $y_2(0) = 0$ and $y_3(0) = 0$.

Figure 13 and 14 denote respectively the dimensionless displacement, y_1 and velocity, y_2 as a function of the dimensionless time, τ.

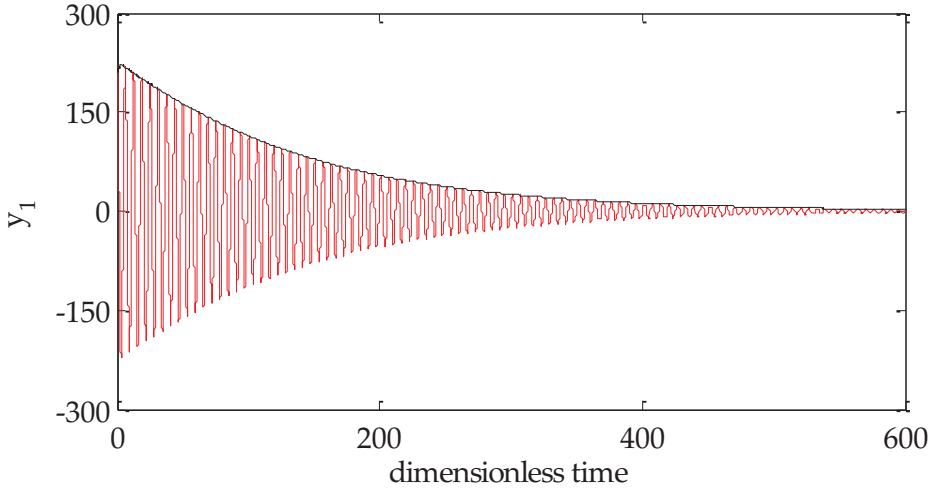

Figure 13. Dimensionless displacement as a function of the dimensionless time $y_1(\tau)$ for a system having a mass m of $0.2\ kg$ and a spring of stiffness $k = 225.591\ N.m^{-1}$. Initial conditions: $y_1(0) = 225.591$, $y_2(0) = 0$ and $y_3(0) = 0$.

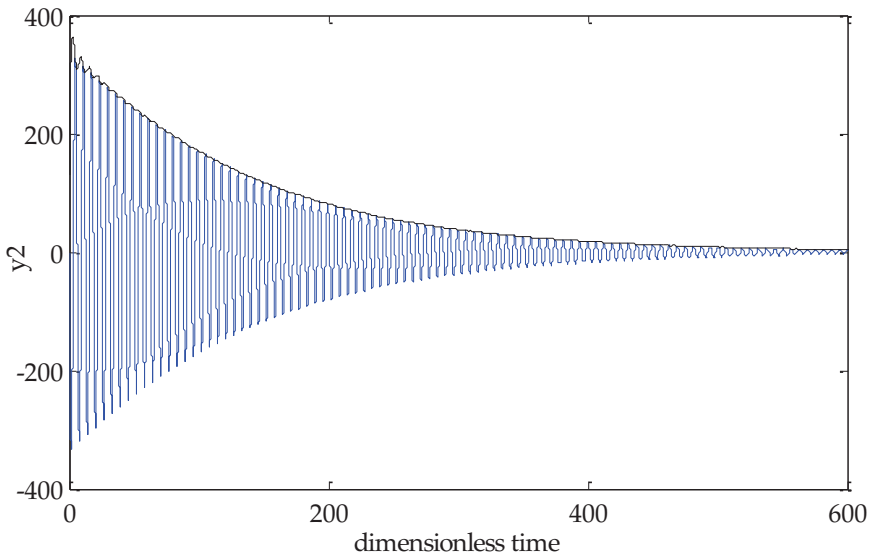

Figure 14. Dimensionless velocity as a function of the dimensionless time $y_2(\tau)$ for a system having a mass m of $0.2\ kg$ and a spring of stiffness $k = 225.591\ N.m^{-1}$. Initial conditions: $y_1(0) = 225.591$, $y_2(0) = 0$ and $y_3(0) = 0$.

These latter responses, $y_1(\tau)$ and $y_2(\tau)$, are described by oscillatory motion. Moreover, their corresponding envelope shows that the amplitude evolution of both the dimensionless displacement and velocity responses has a convex form.

Then, the dimensionless friction force, f_T described by a LuGre friction law is plotted as a function of the dimensionless time τ (see Figure 15).

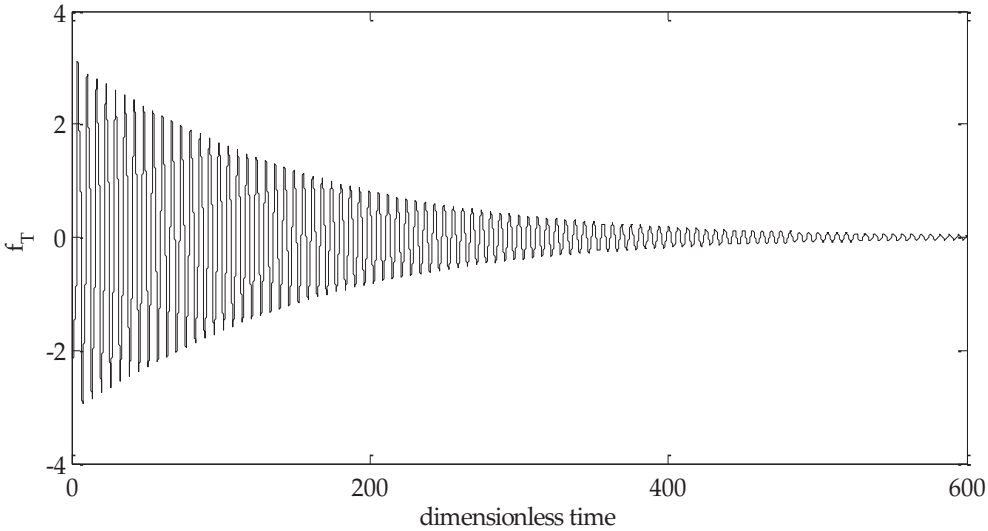

Figure 15. Dimensionless friction force as a function of the dimensionless velocity $f_T(y_2)$ for a system having a mass m of $0.2\ kg$ and a spring of stiffness $k = 225.591\ N.m^{-1}$. Initial conditions: $y_1(0) = 225.591$, $y_2(0) = 0$ and $y_3(0) = 0$.

The dimensionless friction force response is also described by an oscillatory motion. As we observe the amplitude evolution of friction force, one can conclude that the friction force is characterized by a decaying amplitude. This latter corresponds to the displacement and velocity responses which have a convex form envelope. This conclusion is coherent to the experimental results presented in the previous section.

The friction force, f_T is shown in the below figure (Figures 16) as a function of the displacement in a dimensionless form..

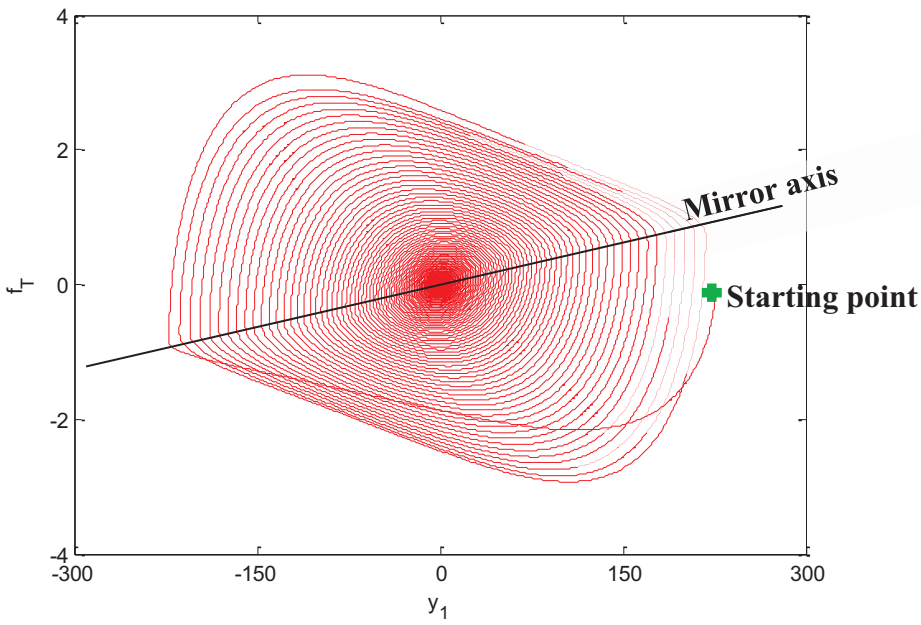

Figure 16. Dimensionless tangential frictional force as a function of the dimensionless displacement $f_T(y_1)$ for a system having a mass m of $0.2\ kg$ and a spring of stiffness $k = 225.591\ N.m^{-1}$. Initial conditions: $y_1(0) = 225.591$, $y_2(0) = 0$ and $y_3(0) = 0$.

The starting point is denoted by (225.591,0). The above dimensionless friction force-displacement is described by a hysteresis loop that gets narrower as the amplitude of the displacement response decreases until both the dimensionless friction force, f_T and displacement y_1 reach a negligible value. Moreover, we observe that the hysteresis loop has a mirror axis.

Figure 17 demonstrates the dimensionless friction force, f_T as a function of the dimensionless sliding velocity, y_2.

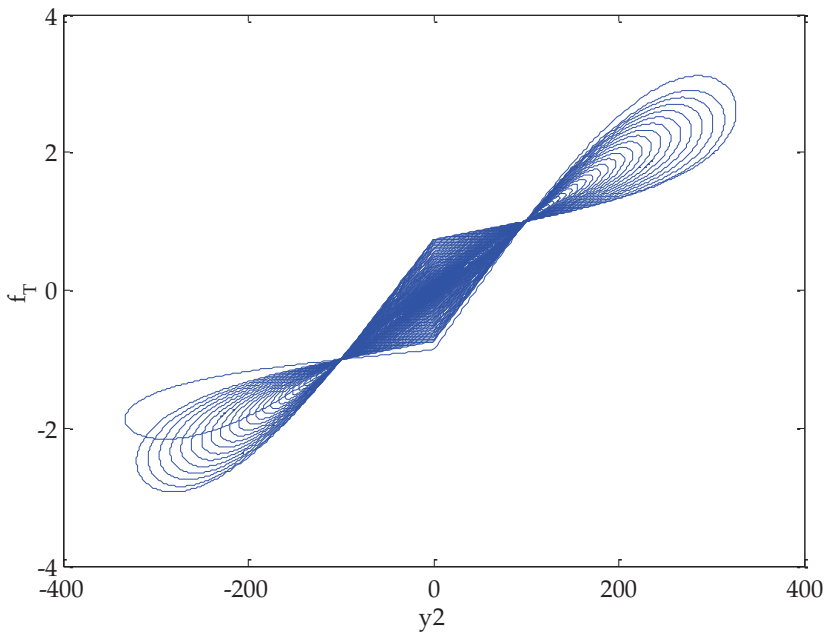

Figure 17. Dimensionless tangential frictional force as a function of the dimensionless velocity $f_T(y_2)$ for a system having a mass m of $0.2\ kg$ and a spring of stiffness $k = 225.591\ N.m^{-1}$. Initial conditions: $y_1(0) = 225.591$, $y_2(0) = 0$ and $y_3(0) = 0$.

We find that there is a hysteresis in the relation between the friction force and the relative velocity. The friction force is lower for decreasing velocities than for increasing ones. The hysteresis becomes wider at higher rates of the relative velocity. This cannot be explained in the classical friction laws, where the friction is unique for every non-zero velocity.

4.6 Conclusions and Perspectives

Chapter 4 studies the hysteresis effect of the frictional behavior experimentally and numerically. We started with a brief explanation of the different friction phenomena. Then, the results of the tangential friction measured experimentally are shown. Finally, a mass-

spring system is simulated using a LuGre friction law where the numerical results are presented.

We examined from the tangential friction force measurements that the friction behavior is described by a hysteresis effect. Unlike the classical friction models, this friction force described by hysteresis effect is not unique for every non-zero velocity. This latter is known as the frictional lag phenomenon. Thus, the pseudo-polynomial friction law, proposed in Chapter 3, is not sufficient to model the systems tested during our research. It is also insufficient to use a simple friction law in order to model vibrational oscillating nonlinear dynamic systems.

Moreover, we can conclude that the LuGre friction law is able to capture many friction phenomena which have been seen experimentally by using the dynamic oscillating tribometer. However, there will be some difficulties to apply such friction models like LuGre friction law to practical machines and devices, since one should definitely know enough information about the friction or the system dynamic characteristics to apply such models. Moreover, we cannot model our systems with LuGre friction law since this model is used for dry contacts applications.

The simulation study shows promising results for future work. In this context, it may be interesting to propose a new model that contains a variable state, i.e. film thickness.

References

[1] Armstrong-Hélouvry, B., Dupont, P. and Canudas de Wit, C., A survey of models, analysis, tools and compensation methods for the control of machines with friction. Automatica 30 (7), pp. 1083-1138, 1994.

[2] Mitiguy, P. C. and Banerjee, A. K., Efficient simulations of motion involving Coulomb friction. J. Guid. Control Dyn. 22 (1), pp. 78-86, 1999.

[3] Thesis of Henrik Olsson, Control Systems with Friction. Lund, 1996.

[4] Coulomb, C. A., *Théorie des machines simples*, vol. 10. Mémoires de Mathématique et de Physique de l'Academie des Sciences, pp. 161–331, 1785.

[5] Rabinowicz, E., The nature of the static and kinetic coefficients of friction. J. Appl. Phys. 22, 1373–1379, 1951, doi:10.1063/1.1699869.

[6] Stribeck, R., Die wesentlichen Eigenschaften der Gleitund Rollenlager—the key qualities of sliding and roller bearings. In *Zeitschrift des Vereines Deutscher Ingenieure*, no. 46(38,39), pp. 1342–1348, 1432–1437, 1902.

[7] Courtney-Pratt, J.S and Eisner, E., The effect of a tangential force on the contact of metallic bodies. Proc. R. Soc. A. 238, 529–550, 1956, doi:10.1098/rspa.1957.0016.

[8] Harnoy, A, and Friedland, B., Modeling and simulation of elastic and friction forces in lubricated bearings for precise motion control. Wear 172,155–165, 1994, doi:10.1016/0043-1648(94)90283-6.

[9] Liang, J.-W. and Feeny, B. F., Identifying Coulomb and viscous friction from free-vibration decrements. Nonlin. Dynam. 16, pp. 337–347, 1998b.

[10] Hess, D.P. and Soom, A., Friction at a lubricated line contact operating at oscillating sliding velocities. Journal of Tribology 112 (1), pp.147-152, 1990.

[11] Den Hartog J.P., Forced vibrations with combined Coulomb and viscous friction. Trans. ASME. 53, 107–115, 1931.

[12] Powell, J., Wiercigroch, M., Influence of non-reversible Coulomb characteristics on the response of a harmonically excited linear oscillator. Mach. Vib. 1, 94–104, 1992.

[13] Rigaud, E., Perret-Liaudet, J., Belin, M., Joly-Pottuz, L. and Martin, J.M., An original dynamic tribotest to discriminate friction and viscous damping. Tribology Internation 431 (2), pp. 320-329, 2010.

[14] Majdoub, F., Belin, M., Martin, J.M., Perert-Liaudet, J., Kano, M. and Yoshida,K., Exploring low friction of lubricated DLC coatings in no-wear conditions with a new relaxation tribometer. Tribology International, 2013, In Press.

[15] Belin, M. and Kakizawa, M., Rigaud, E. and Martin, J.M., Dual characterization of boundary friction thanks to the harmonic tribometer: Identification of viscous and solid friction contributions. Journal of Physics: Conference Series, 258: 012008, 2010.

[16] Hoffmann, N. P., Linear stability of steady sliding in point contacts with velocity dependent and LuGre type friction. Journal of Sound and Vibration 301, pp. 1023-1034, 2007.

[17] Canudas de Wit, C., Aström, K. J. and Lischinsky, P., A new model for control of systems with friction. IEEE Transactions onAutomatic Control 40 (3), pp. 419- 425, 2005.

[18] Kim, H. M., Park, S. H. and Han, S. I., Precise friction control for the nonlinear friction system using the friction state observer and sliding mode control with recurrent fuzzy neural networks. Mechatronics 19 (6), pp. 805-815, Sept. 2009.

[19] Kahaner, D., Moler, C. and Nash, S., *Numerical Methods and Software*. Prentice-Hall, Eaglewood Cliffs, NJ, 1989.

[20] Forthythe, G., Malcolm, M. and Moler, C., *Computer Methods for Mathematical Computations*. Prentice-Hall, Eaglewood Cliffs, NJ, 1997.

GENERAL CONCLUSION

General Conclusion

The objective behind this research was to better investigate a novel experimental technique, explored in this thesis. This experimental setup is described by a mass-spring-damper single degree-of-freedom (SDOF) oscillator mechanical system. The experimental measurements are performed at the contact of a spherical pin oscillating on a fixed flat plane. This apparatus allows us to measure the decaying displacement and velocity free responses thanks to a laser vibrometer. Then, the friction coefficient can be evaluated from these latter decaying free responses. A piezo-electric force transducer allows us as well to study the frictional behavior of the system by measuring the tangential friction force. Moreover, the electrical contact resistance (ECR) between the two counterparts can be measured. This latter is significant to present some information regarding the film thickness.

Some tribological contacts have been tested. As preliminary results, a first order polynomial friction model was induced to the system. Thus, both the transient friction contribution at zero speed μ_0 and the viscous damping friction contribution μ_1 were evaluated from the SDOF oscillating free responses corresponding to these contacts. Moreover, we were able to precise the lubrication regime for each tribological contact tested by measuring the electrical contact resistance.

Different steel/steel contacts lubricated with oleic acid and pure glycerol (green lubricants) were tested using this experimental technique. Some surfaces were coated with diamond-like-carbon (ta-C and a-C:H). These sets of experiments permitted us to compare the two different lubricants (pure glycerol and oleic acid) and understand as well the effect of diamond-like-carbon coatings steel surfaces. The ta-C/ta-C coated contact presents the lowest friction when tested by both the dynamic oscillating tribometer and the reciprocating tribometer. However, their corresponding friction coefficients are not comparable since the operating conditions differ between both tribometers. Then, a test of steel/steel contacts lubricated with three different lubricants (pure glycerol, base oil 150NS and poly-alpha-olefin PAO4) was carried out. Also, three different additives (oleic, linoleic and stearic acids) were added in PAO4 lubricant. These experiments were performed at different temperatures. Therefore, the task behind this experimental test was to study the effect of temperature on lubricated steel/steel contacts and the different additives in PAO4 and to compare as well between the 3 different pure lubricants using the dynamic tribometer. It is concluded from this set of experiments that the tendency of our friction results is in satisfactory agreement with those measured by the linear tribometer. From all the measured velocity and displacement free responses, we recognized different envelopes forms of the decreasing damping responses: linear, convex and concave. Moreover, our experimental tests were the first to show free responses described by a concave envelope form using this dynamic tribometer.

Unlike the classical tribometer, this novel apparatus is interesting since we are able to bring a new insight by understanding the overall friction. This latter allows us to interpret the friction through both the velocity-independent and velocity-dependent friction contributions. This dynamic apparatus is considered closer to real life applications since most of the mechanical

systems are described by an oscillatory motion. Moreover, the decaying envelope corresponding to the measured free responses can be described from the friction contributions. It is also recognized that the results of friction using the oscillating tribometer are coherent to that of the classical alternative uni-directional tribometer. Nevertheless, the values are not comparable since the conditions and parameters defined using the new techniques differ than that of the classical tribometer. Although, the linear friction can be a sufficient model for some systems; however, we should be careful since it is not valid for other systems. This is recognized when the decaying envelope corresponding to the measured free response is described by both a convex and concave form.

For this reason, we aimed to better understand and study the decreasing damping free oscillations. Therefore, a general friction law was introduced, defined by a polynomial friction model. The free responses of a SDOF oscillator mechanical system induced by a pseudo-polynomial friction model were found numerically using Runge-Kutta method. One can conclude that a quadratic friction law is able to describe correctly the envelopes seen in our experimental tests: straight, convex, concave and a combination of both convex and concave. From our measured displacement and velocity oscillating free responses, we also observed the existence of the four different envelope forms. After evaluating the friction constants corresponding to zero, first and second order polynomial friction laws, we showed that an experimental free response, described by a straight, convex or concave envelope form, can be modeled by a linear friction model (i.e. Coulomb-viscous or first-order polynomial friction law); however, a free response, having both convex and concave envelope form, can only be modeled by a non-linear friction model (i.e. second-order polynomial friction law). It is also significant to study the friction coefficient as a function of the amplitude in order to check the validity of the friction law.

In order to go further in our study, a particular attention was given to the measured tangential friction force. The experimental friction force presented a hysteresis behavior as a function of the velocity. Moreover, frictional lag phenomenon was observed in the tangential friction force measured. We have seen also that the amplitude evolutions of the tangential friction force showed a correlation with the results presented previously regarding the different envelop form of the displacement and velocity free responses. Thus, as the amplitude of the friction force decays with time, then the envelope has a convex form. Nevertheless, when the tangential friction force increases with time, then its corresponding free response envelope is described by a concave form. Finally, a mass-spring single degree-of-freedom mechanical system, induced by a friction law described by a hysteresis frictional behavior, is studied. In this study, the LuGre friction law has been chosen since it is described by both hysteresis and lag effect which have been seen experimentally by using the dynamic oscillating tribometer. However, this friction law cannot be used to model our systems since this model is used for dry contacts applications.

This research showed promising results; thus, leading to many interrogations and ideas for perspective work. One of the objectives was to couple the measurements performed by the conventional tribometer and those by the dynamic oscillatory. The system that is able to perform experiments with both stationary motion and oscillatory motion has been recently

implemented. As a perspective, it would be interesting to test our systems in order to compare the results under both stationary and oscillatory motions for the same conditions. These measurements can be immediately launched. The experimental tangential friction forces presented are interesting to be investigated since they can permit us to better understand the frictional behavior of the system. The sensor can be modified in a way that it permits us to measure both the tangential and normal forces. Moreover, it is significant to measure instantaneously the lubricant film of the tested systems. This latter can be performed by using either a high-speed camera for flow visualization process under a longer test period or a triple axes accelerometer. It is also important to improve the dynamics of the electrical contact resistance measurements; however, this latter cannot be easily attained. We can also measure tribosystems that allows us to detect superlubricity using the new apparatus. This idea was the initial objective behind developing the dynamic oscillating tribometer. On the other hand, it would be interesting to introduce a new friction law that can describe both the hysteresis frictional effect and lag phenomenon for wet contacts. A numerical study is ongoing that insist of developing a new friction law depending not only on the sliding velocity of the system but also on other state variables.

Scientific Production

Publications:

1. **F. Majdoub**, J.M. Martin, M. Belin, J. Perret-Liaudet and R. Iovine. "Effect of temperature on lubricated steel/steel systems with or without saturated fatty acids additives with an original tribometer". Tribology Letters (In Press), DOI : 10.1007/s11249-014-0323-2, 2014.

2. **F. Majdoub**, M. Belin, J.M. Martin, J. Perret-Liaudet, M. Kano and K. Yoshida. "Exploring low friction of lubricated coatings in no-wear conditions with a new relaxation tribometer". International Tribology 65, pp. 278-285, 2013.

3. **F. Majdoub**, J. Perret-Liaudet, M. Belin and J-M. Martin. "Nonlinear free dynamic response of a one degree-of-freedom oscillator induced by a quadratic velocity dependent model of friction". Proc. ASME (1), pp 513-520, 2012.

Communications:

Internationals

1. M. Belin, H. Miki and **F. Majdoub**. "Detailed characterization of microcrystalling diamond coatings thanks to the relaxation tribometer technique". 5th World Tribology Congress (WTC 2013), 8-13 Sept. 2013, Oral presentation.

2. **F. Majdoub**, J. Perret-Liaudet, M. Belin and J-M. Martin. "Free oscillations of a sliding SDOF system: Effect of a polynomial friction model". MEDYNA 2013: 1st Euro-Mediterranean Conference on Structural Dynamics and Vibroacoustics, 23-25 Apr. 2013, Marrakech, Morocco, Oral presentation.

3. **F. Majdoub**, M. Belin, J-M. Martin J. Perret-Liaudet, M. Kano and K. Yoshida. "Understanding low friction of DLC coatings using a novel technique". 39th Leeds-Lyon Symposium on Tribology , 4-7 Sept. 2012, Leeds, England, Oral presentation.

4. **F. Majdoub**, J. Perret-Liaudet, J-M. Martin and M. Belin. "Nonlinear free dynamic response of one degree-of-freedom oscillator induced by a quadratic velocity-dependent model of friction". ASME 2012 International Design Engineering Technical Conferences (IDETC 2012) , 12-15 August 2012, Chicago, IL., USA, Oral presentation.

5. **F. Majdoub**, J. Perret-Liaudet, J-M. Martin and M. Belin. "Free dynamic response of a damped oscillator mechanical system induced by a 2nd order polynomial velocity-dependent model of friction". 19th International Congress on Sound and Vibration, 8-12 July 2012, Vilnius, Lithuania, Oral presentation.

6. **F. Majdoub**, M. Belin and J-M. Martin and J. Perret-Liaudet. "A new technique for measuring low friction-Application to DLC Coatings". Society of Tribologists and Lubrication Engineers , 6-10 May. 2012, St. Louis, Missouri, USA, Poster Presentation.

7. C. Matta, J.M. Martin, K.Yoshida,M. Kano, M.I. De Barros Bouchet, **F. Majdoub** and M. Belin. "Lubrication of DLC coatings with oleic acid". ASME/STLE 2011 International Joint Tribology Conference (IJTC 2011), 24-26 Oct. 2011, Los Angeles, California, USA, Oral presentation.

National

1. **F. Majdoub**, M. Belin and J-M. Martin and J. Perret-Liaudet. "Mesure innovante des frottementsfaibles, à partir de la réponse d'un systeme frottant soumis à des oscillations de relaxation ".Jornée Internationale Francophone de Tribologie (JIFT 2011), 11-13 May. 2011, Obernai, France, Poster Presentation.

Distinctions:

1. **Poster Award**, Society of Tribologists and Lubrication Engineers, 6-10 May. 2012, St. Louis, Missouri, USA.

2. **Best Poster Award** , Journée Internationale Francophone de Tribologie (JIFT 2011), 11-13 May 2011, Obernai, France.

3. **Article**. "A new Insight in low friction characterization-application to DLC coatings". Tribology and Lubrication Technology TLT magazine, Feb. 2013, pp. 15-17. http://d27vj430nutdmd.cloudfront.net/5716/143463/bd4da55be91431078b940dd599a6aa34c192ee5c.pdf

Abstract

Controlling friction is a one of the most significant challenges in the field of tribology. Its major purpose is directed towards the reduction of energy in real mechanical systems, especially in the area of transportation. In response to this necessity, the automobile industries are emphasizing on minimizing the consumption of energy by selecting the appropriate lubricants and materials on one hand and mechanical system with high performance on the other hand. DLC (Diamond-like carbon) coated surfaces are considered one of the solutions thanks to their physical and tribological properties in reducing friction and wear. In this study, we have been interested in investigating the friction behavior of both amorphous hydrogenated (a-C:H) and hydrogen-free tetrahedral amorphous carbon (ta-C) DLC coatings. Furthermore, some "green lubricants" and additives are tested which play a role in reducing friction and wear. These latter tests are performed at different operating conditions using a new experimental methodology, known as the dynamic oscillating tribometer. This original tribometer, developed at the Laboratory of Tribology and System Dynamics (LTDS), is able to measure the oscillatory motion corresponding to various tribosystems having low friction. This technique has the ability to quantify with remarkable precision and without any force transducer, low friction values (in the range of 10^{-5} to10^{-2}) and also to evaluate different friction contributions from the displacement and velocity-time responses of a mass-spring-damper oscillating system. First, a linear friction law has been used for the systems tested in order to calculate two contributions of friction. The first one, μ_0 is the transient friction coefficient at zero speed and the second one (Coulomb-type fiction), $\mu_1$is a velocity-dependent friction coefficient. Then, a numerical study is carried out in order to better understand the dynamic aspect of the oscillatory vibratory free responses. A quadratic friction law is used to model on the mechanical system of the apparatus. This allows us to study numerically the behavior of the decreasing amplitudes of the damping responses which are determined using the Averaging method. Furthermore, we are interested in studying the various forms of these oscillations' envelop in relation with the polynomial expansion of the friction model. Also, numerical and experimental results are compared using both the linear and quadratic friction models. In addition, a particular attention is given to the measured tangential forces corresponding to our tribosystems. Finally, we study numerically a damped mass-spring single degree-of-freedom mechanical system, induced by LuGre friction law described by both hysteresis and lag effect which have been detected experimentally. Results show that friction tests performed with the oscillating tribometer can be qualitatively compared to those obtained with a conventional tribometer. Moreover, ta-C/ta-C surfaces reveal the lowest friction μ_0 when tested by both oscillating and reciprocating tribometers. Also, both numerical and experimental results are found to be of good agreement. This study shows that a quadratic friction law is able to describe correctly the envelopes observed in our experimental tests: straight, convex, concave and a combination of both convex and concave.

Keywords: tribology, mechanical systems, friction, diamond-like carbon coatings, "green lubricants", additives, friction law, free responses, tangential force, LuGre friction law, hysteresis.

Résumé

Réduire l'énergie générée par le frottement et dissipée dans les systèmes mécaniques réels est un des challenges actuels en tribologie. Ce point représente une importance toute particulière dans le domaine des transports terrestres. En réponse à cette nécessité, les constructeurs automobiles se concentrent sur la réduction de la consommation d'énergie en sélectionnant des lubrifiants et des matériaux appropriés d'une part et les systèmes mécaniques performants d'autre part. Grâce à leurs propriétés physiques et tribologiques en termes de réduction de la friction et de l'usure, les couches minces de DLC (Diamond-like Carbon) sont considérées comme l'une des solutions. Le comportement tribologique de couches minces de ta-C (carbone amorphe très dur dépourvu d'hydrogène) et de a-C:H (carbone amorphe hydrogéné) est ici exploré. D'autre part, des "lubrifiants verts" et des additifs participant aussi à la réduction du frottement et de l'usure sont testés. Ces essais sont effectués dans différentes conditions en utilisant une nouvelle méthodologie expérimentale. Le tribomètre dynamique oscillant développé au LTDS possède la capacité de quantifier avec une très grande précision et sans recourir à une quelconque mesure de force, des niveaux de frottement faibles (dans la gamme 10^{-5} à 10^{-2}), et permet en plus d'identifier différentes contributions du frottement. Dans un premier temps, une loi de frottement linéaire a été utilisée afin d'évaluer deux contributions de frottement. La première, μ_0, est le coefficient transitoire de frottement quand la vitesse s'annule au changement de direction (du type frottement de Coulomb). La seconde, μ_1, est une contribution dépendante de la vitesse de glissement. Ensuite, une étude numérique a été réalisée en appliquant une loi de frottement quadratique afin de mieux comprendre l'aspect dynamique des réponses libres. Cela nous a permis d'étudier numériquement la décroissance d'amplitude des oscillations déterminée grâce à la méthode de moindres carrés. Nous nous intéressons aussi à l'étude des formes de l'enveloppe de ces oscillations en relation avec le modèle de frottement. Les résultats numériques et expérimentaux pour les lois de frottement linéaire et quadratique sont ensuite comparés. En complément, nous avons mesuré la force tangentielle correspondant aux tribosystèmes testés. Finalement, nous avons étudié numériquement un système dynamique masse-ressort à un degré de liberté, modelisé par la loi de frottement LuGre. Cette loi est décrite par le phénomène d'hystérésis et l'effet de décalage de temps qui ont été détectés expérimentalement. Les résultats expérimentaux obtenus avec le tribomètre oscillant montrent qu'ils sont qualitativement comparables à ceux obtenus en configuration classique cylindre-plan, travaillant à vitesse de glissement constante. Dans tous les cas, les résultats montrent la supériorité du tribosystème ta-C/ta-C dans la réduction du frottement μ_0. De plus, les résultats numériques et expérimentaux sont cohérents. Cette étude montre qu'une loi de frottement quadratique est capable de décrire correctement toutes les formes d'enveloppes obtenues expérimentalement : droite, convexe, concave et une combinaison des formes convexe et concave.

Mots-clés : tribologie, système mécanique, friction, couches minces DLC, "lubrifiants verts", additifs, loi de frottement, réponses libres, force tangentielle, loi de frottement LuGre, hystérésis.